2003

Studies of solute transport through fractured till in Iowa

Martin Frederick Helmke
Iowa State University

Studies of solute transport through fractured till in Iowa

by

Martin Frederick Helmke

A dissertation submitted to the graduate faculty

in partial fulfillment of the requirements for the degree of

DOCTOR OF PHILOSOPHY

Co-majors: Geology; Water Resources

Program of Study Committee:
William Simpkins, Co-major Professor
Michael Burkart, Co-major Professor
Carl Jacobson
Thomas Moorman
Lee Burras

Iowa State University

Ames, Iowa

2003

ProQuest Information and Learning Company
300 North Zeeb Road
P.O. Box 1346
Ann Arbor, MI 48106-1346

Graduate College
Iowa State University

This is to certify that the doctoral dissertation of

Martin Frederick Helmke

has met the dissertation requirements of Iowa State University

Signature was redacted for privacy.

Committee Member

Signature was redacted for privacy.

Co-major Professor

Signature was redacted for privacy.

Co-major Professor

Signature was redacted for privacy.

For the Co-major Program

Signature was redacted for privacy.

For the Co-major Program

TABLE OF CONTENTS

LIST OF FIGURES

FRACTURE-DOMINATED TRANSPORT OF NITRATE AND ATRAZINE THROUGH TILL IN IOWA

COMPARISON OF THREE FORWARD-MODE MODELING APPROACHES TO SIMULATE SOLUTE TRANSPORT THROUGH FRACTURED TILL

SIMULATION OF SOLUTE TRANSPORT THROUGH FRACTURED TILL USING A STOCHASTIC, 3-DIMENSIONAL, DISCRETE FRACTURE MODEL

MEASUREMENT OF EFFECTIVE DIFFUSION PARAMETERS IN FRACTURED SOILS

EFFECT OF FRACTURES ON HYDRAULIC CONDUCTIVITY OF TILL UNITS IN IOWA

LIST OF TABLES

ABSTRACT

Fractures may provide pathways for agricultural chemicals to reach aquifers through till units that have traditionally been considered effective barriers to contaminant transport. Till units were studied at three sites in Iowa that represented three landform regions, till ages from 12.5 to >730 ka, and depths from 1 to 27.5 m. Fractures were present at all study locations and at all depths, including one site where fractures intersected an aquifer at 30 m depth. Laboratory experiments using eight large (0.40 to 0.45 m in length and 0.43 m in diameter), undisturbed columns of till showed K_b ranging from 7.7×10^{-10} to 3.8×10^{-5} m/s, which is generally greater than the matrix hydraulic conductivity reported in the literature. Laboratory experiments with KBr, PFBA, PIPES, KNO_3, and atrazine as tracers were used to produce breakthrough curves (BTCs). First arrival velocities of Br ranged from 0.004 to 64.8 m/d – 10 to 100 times faster than predicted using the equivalent porous medium (EPM) assumption. Similar velocities of NO_3 and atrazine were observed for columns collected from depths of less than 3 m. In deeper columns, sorption (atrazine) and degradation (NO_3 and atrazine) retarded transport. Tracers were not affected significantly by fracture origin or orientation. Separation of conservative tracers with different aqueous diffusion coefficients was observed during the rising and tailing limbs of BTCs, which indicates that matrix diffusion was a controlling process. Laboratory BTCs were compared against model-simulated BTCs using three approaches: the Mobile-Immobile Model (MIM), the Parallel-plate Discrete Fracture Model (PDFM), and a 3-Dimentional Discrete Fracture Model (3-D DFM). All three model approaches were reasonable predictors of the BTCs (goodness-of-fit statistic d_I ranged from 0.751 to 0.959).

The results of this study demonstrate that fractures may have a controlling influence on solute transport through till units in Iowa. Contaminants may be transported rapidly through thin aquitards of fractured till, but non-conservative compounds are likely to be retarded or degraded in thicker till units. Fractures should be considered in groundwater studies in glaciated regions and in assessments of aquifer vulnerability to non-point source pollution.

GENERAL INTRODUCTION

In glaciated regions, till protects aquifers from the downward migration of contaminants. This is the case in Iowa, where groundwater is threatened at the surface by agricultural fertilizers and herbicides, landfill leachate, effluent from Concentrated Animal Feeding Operations (CAFOs), and toxic compounds from hazardous waste sites. Till units of Pre-Illinoian through late Wisconsinan age comprise the predominant surficial material in Iowa and have been assumed by consultants and regulators to be an adequate barrier to downward migration of contaminants. However, Iowa's aquifers show evidence of contamination despite this protective layer of till (Kross et al., 1990; U.S. EPA, 1994).

Preferential flow through fracture networks is a well-documented mechanism for rapid migration of contaminants vertically and horizontally through till. Fractures have been documented in Iowa till units (Lee, 1991; Kemmis et al., 1992; Helmke et al., 1998; Eidem et al., 1999) and are ubiquitous features. They have also been observed at the till-bedrock contact at depths of 30 m (Kemmis et al., 1992; Helmke et al., 1998). Fractures in till have been reported elsewhere in the United States (see Connell, 1984; Mickelson and Simpkins, 1991; Brockman and Szabo, 2000), in Canada (see Keller et. al, 1988; Ruland et al., 1991; McKay and Fredericia, 1995), and in Denmark (see Fredericia, 1990; Jørgensen and Fredericia, 1992; Klint and Gravensen, 1999).

Fractures play an influential role in the hydrogeology of till. Bulk hydraulic conductivity (K_b) of fractured till in Iowa is one to two orders of magnitude greater than the hydraulic conductivity of the till matrix (K_m) (Seo, 1996; Bruner and Lutenegger, 1993). Similar observations have been reported elsewhere (Keller et al., 1989; Simpkins and

Bradbury, 1992; McKay and Fredericia, 1995). Although there is general agreement that fractures increase hydraulic conductivity, how fractures influence contaminant transport has not been quantified in Iowa. Moreover, appropriate methods for predicting solute transport through fractured till need to be identified.

Despite general agreement that fractures control solute transport through till, only a few studies in Denmark and Canada have included fractures when simulating solute transport in this environment (Grisak and Pickens, 1980; McKay et al. 1993b; Jørgensen et al., 1998). The lack of simulation efforts is puzzling and may be due to the burden of obtaining input parameters for such models, or a lack of knowledge about or understanding of the models. The benefits of these models extend beyond being a predictive tool for solute transport in fractured till—they may also be used to determine which solute transport processes are dominant in fractured systems.

Purpose and Scope

The hypothesis posed by this dissertation is that fractures in till may be the primary pathway for contaminant transport, and that they increase the velocity of contaminants above that expected for low permeability units. Coupled with this hypothesis is the premise that the geometry of fracture networks affects transport processes, and that knowledge of these characteristics may help in the prediction of contaminant transport through till.

To evaluate how fractures influence solute transport through till, eight large columns of intact till were collected for laboratory tracer experiments. The columns were collected from three study sites, each representing a different landform region of Iowa. These sites

represented a wide spectrum of till units in Iowa, ranging in age from 12.5 to >730 ka and depths between 1 and 27.5 m. Fractures were mapped at each site to document their presence and to determine their density and orientation.

Laboratory experiments were conducted using potassium bromide (KBr), pentafluorobenzoate (PFBA), 1,4-piperazinediethanesulfonate (PIPES), potassium nitrate (KNO_3), and 2-chloro-4-(ethylamino)-6-(isopropylamino)-s-triazine (atrazine) as tracers. The conservative compounds Br, PFBA, and PIPES were chosen because they would be the most likely to migrate rapidly through fractured till, and because differences in the effective diffusion coefficients (D_e) would cause their breakthrough curves (BTCs) to separate in the presence of matrix diffusion. Nitrate (a nutrient) and atrazine (a broadleaf herbicide) were chosen as tracers because they are agricultural chemicals of environmental concern that frequently occur beneath fields in Iowa.

To determine that fractures were hydraulically conductive, a dye (FD&C Blue no. 1) was passed through one of the columns. Upon dissection, the flow path of the dye was mapped and compared to the fractures.

Results from the tracer experiments were compared to BTCs simulated by computer models. The objectives of the computer modeling were a) to determine transport parameters using a variety of simulation techniques that had not previously been applied to fractured till, and b) to determine if it is necessary to incorporate complex fracture geometry and orientation within these models. The models evaluated included the Mobile-Immobile Model (MIM), the Parallel-plate Discrete Fracture Model, and the Three-Dimensional Discrete

Fracture Model (3-D DFM). These models were run in the forward mode using parameters that were determined independent of the tracer tests.

The results from the field mapping, solute transport experiments, dye-trace experiments, and fracture-flow simulations were all used to verify that fracture flow exists and controls transport in these till units.

Dissertation Organization

This dissertation entitled "Studies of solute transport through fractured till in Iowa" is composed of five papers for future submission to scientific journals. The first paper is entitled "Fracture-dominated transport of nitrate and atrazine through till in Iowa", which will be submitted to the *Journal of Environmental Quality*. The second paper, "Comparison of forward modeling approaches to simulate solute transport through fractured till", will be submitted to the scientific journal *Ground Water*. The third paper is entitled "Simulation of solute transport through fractured till using a stochastic, 3-dimensional, discrete-fracture model", and will be submitted to the journal *Water Resources Research*. The fourth paper, "Laboratory measurement of effective diffusion parameters in fractured soil", will be submitted to the journal *Soil Science*. The fifth and final paper will be submitted to the journal *Environmental and Engineering Geoscience* and is entitled "Effect of fractures on hydraulic conductivity of till units in Iowa". The format and reference style of each paper is in accordance with each journal. A general summary follows the five papers. Data compiled by this study are included as appendices following the general summary. References cited in the General Introduction follow the appendices.

FRACTURE-DOMINATED TRANSPORT OF NITRATE AND ATRAZINE THROUGH TILL IN IOWA

A paper to be submitted to the *Journal of Environmental Quality*

Martin F. Helmke, William W. Simpkins, and Robert Horton

Abstract

Fractures may provide pathways for agricultural chemicals to reach aquifers through till units that have traditionally been considered effective barriers to contaminant transport. The objectives of this study are to determine whether till fractures transmit nitrate and atrazine at velocities greater than till matrix and to quantify till solute transport parameters. Laboratory experiments were conducted using eight large (0.4 to 0.45 m in length and 0.43 m in diameter), undisturbed columns of till to evaluate the potential transport of nitrate and atrazine in fractured till. The till units came from three locations in Iowa, ranged in age from 13.5 to > 730 ka, and were recovered from depths of 1 to 30 m. Fractures of different origin and orientation were present at all study locations and at all depths. A tracer test using FD&C Blue dye no.1 demonstrated that water and dye flowed exclusively through the fracture network in the till column. Experiments with KBr, PFBA, PIPES, KNO_3, and atrazine as tracers showed first arrival velocities of Br from 0.004 to 64.8 m/d – 10 to 100 times faster than predicted using the equivalent porous medium (EPM) assumption. Similar velocities of NO_3 and atrazine were observed for columns taken from depths of less than 3 m. In deeper columns, sorption (atrazine) and degradation (NO_3 and atrazine) retarded transport. Tracers were not affected by fracture origin or orientation in the till. Separation of conservative tracers with different aqueous diffusion coefficients (D_0) was observed during the rising and tailing limbs of breakthrough curves, BTCs, which indicates that matrix

diffusion is a controlling process in the till units. Inverse modeling using the Mobile-Immobile Model (MIM) produced BTCs that matched the observed data and provided further evidence of a dual-porosity system. From the model, first-order exchange coefficients (α) ranged from 1 x 10^{-8} to 1.7 x 10^{-2} 1/s, sorption coefficients (K_d) ranged from 2.6 x 10^{-5} to 1 x 10^{-3} m^3/kg, and degradation half-life was between 0.24 to 67 days for NO_3 and 1.6 to 277 days for atrazine. Results of this study indicate that NO_3 and atrazine may be transported rapidly through thin, fractured till aquitards, but are retarded or degraded in thicker till units. Fracture control of NO_3 and atrazine should be incorporated in groundwater studies of these contaminants and considered in general assessments of aquifer vulnerability to non-point source pollution.

Introduction

Till units of Pre-Illinoian through late Wisconsinan age protect aquifers in Iowa from surficial contaminants. In Iowa, like other states in the Midwestern U.S., contaminant sources include nutrients and herbicides applied to fields, landfill leachate, effluent from swine manure lagoons, and toxic compounds from hazardous waste sites. Consultants and regulators have traditionally assumed that till acts as a barrier to contaminant migration, particularly nonpoint source contaminants. However, recent evidence suggests that this assumption may not be valid.

Studies in Iowa indicate that widespread nitrate and herbicide contamination of aquifers has occurred despite being overlain by till. A sampling of 686 rural wells in Iowa revealed that 35 percent of the state's shallow wells were contaminated by NO_3-N above the US EPA Maximum Contaminant Level (MCL) of 10 mg/L NO_3-N, and 18 percent contained

detectable concentrations of herbicides (Kross et al., 1990). Contamination of till-confined aquifers by non-point sources has also been documented in Canada (McKay and Fredericia, 1995) and Denmark (Jørgensen and Fredericia, 1992; Jørgensen and Spliid, 1992). Point-source contamination of till has been demonstrated by contaminant plumes in till downgradient of landfills (D'Astous et al., 1989; Herzog et al., 1989; McKay et al., 1998), and earthen manure-storage structures (Simpkins et al., 2002). Rapid transport of contaminants through fractures in till has been reported in Canada (Freeze and Cherry, 1979; Grisak and Pickens, 1980; McKay et al., 1993b) and Denmark (Jørgensen and Spliid, 1992). Fractures are well documented in till and have been reported in studies conducted in the U.S. (Connell, 1984; Kemmis et al., 1992; Simpkins and Bradbury, 1992; Brockman and Szabo, 2000; Helmke and Simpkins, 2003), Canada (Keller et al., 1988; McKay et al., 1993a), and Denmark (Klint and Gravensen, 1999).

That fractures increase solute transport velocity is also well documented. Fractures increase bulk hydraulic conductivity (K_b) and reduce effective porosity (θ_e). The K_b of a fractured till is typically one to 3 orders of magnitude greater than K_b for an unfractured till (Freeze and Cherry, 1979; Keller et al., 1989). Fracture porosity (θ_f) is often one to 4 orders of magnitude less than the total porosity (θ_T) of till (McKay et al., 1993a; Jørgensen et al., 1998). Advective velocity of solutes may be estimated using the average linear velocity equation

$$v = \frac{K_b i}{\theta_e} \tag{1}$$

where v is velocity, and i is the hydraulic gradient. By Eq. (1), the combined effects of increased K_b and decreased θ_e result in a great increase in velocity. Using this equation, fluid velocities up to 200 m/day have been calculated for fractured till (Jørgensen et al., 1998). Typically, the processes of matrix diffusion, sorption, and degradation retard contaminants as they pass through fractured till, allowing only a small percentage of a solute to travel at velocities calculated by Eq. (1) (Freeze and Cherry, 1979).

Although fractures have been identified in Iowa till units for some time, research into their influence on the transport of non-point source contaminants such as NO_3 and atrazine has been lacking. Our hypothesis is that NO_3 and atrazine can be transported rapidly and without degradation through the till units of Iowa and into adjacent streams, lakes, or underlying aquifers. The objectives of this paper are: a) to determine whether fractures can transmit nitrate and atrazine at velocities greater than predicted for the matrix, and b) to quantify solute transport parameters for till.

Materials and Methods

Study Sites

Three study sites, each representing a different till unit and a different Iowa landform region were investigated (Figure 1). The sites were chosen because they represent some of Iowa's youngest and oldest till units (ranging in age from 12.5 to >730 ka), because they allowed access to depths up to 30 m, and because previous studies had established the glacial stratigraphy and hydrogeology at each site. The three sites were named after their respective landform regions: the Des Moines Lobe site (DML), the Iowan Erosion Surface site (IES), and the Southern Iowa Drift Plain site (SIDP), as identified by Prior (1991).

The DML site is located within the Walnut Creek watershed, 7 km south of Ames, Iowa. The Quaternary stratigraphy and hydrogeology of the Walnut Creek Watershed was previously investigated as part of the Management Systems Evaluation Area (MSEA) program (Seo, 1996; Eidem et al., 1999). The surficial deposit at the DML site is the Alden Member till of the Dows Formation, deposited 14 to 12.5 ka during the late Wisconsinan (Prior, 1991; Eidem et al., 1999). The Alden Member is a massive, basal till with a bulk density of approximately 1,700 kg/m^3 (Eidem et al., 1999). The texture of the Alden Member is approximately 40 percent sand, 45 percent silt, and 15 percent clay and is classified as a loam; and unlike older tills in Iowa, the Alden Member has a high smectite content (69 percent, Kemmis et al., 1981).

The IES site is located 6 km southwest of Nashua, Iowa. Previous studies established the glacial stratigraphy and hydrogeology at the site (Weis and Simpkins, 1996). The surficial deposit (c-horizon) at the site is a 1.09-m thick section of late Wisconsinan to Holocene age pedisediment above the Hickory Hills Member till of the Wolf Creek Formation, which is Pre-Illinoian in age (approximately 500 ka, Kemmis et al., 1992). Thus, at this site, the top-half of the uppermost column was collected from material that is not strictly till, but instead reworked till and slopewash sediment. The Hickory Hill Member is a loam with 45 percent sand, 35 percent silt, and 20 percent clay and a bulk density ranging from 1,760 to 1,880 kg/m^3 (Kemmis et al., 1992).

The third site (the SIDP site) is near Coralville, Iowa. At the SIDP site, a 30 m sequence of unlithified deposits had recently been removed to provide quarry access to limestone. Stratigraphic studies at the site (Kemmis et al., 1992) reported the presence of the Hickory Hills, Aurora, and Winthrop till Members of the Wolf Creek Formation (500 to 730

ka), and the Alburnett Formation till (>730 ka). The till units are loams with 30 to 50 percent sand, 30 to 45 percent silt, and 20 to 25 percent clay. Bulk densities range from 1,760 to 2,110 kg/m^3. The deepest and oldest till is the Alburnett, which has a higher bulk density (1,970 to 2,110 kg/m^3, Kemmis at al., 1992).

Fracture Mapping

Fractures were mapped at each site to document their occurrence and density. A backhoe was used to excavate soil pits at the DML and IES sites, which were 3.9 and 2.3 m deep, respectively. Active quarry operations at the SIDP site allowed convenient access to fresh till faces to a depth of 30 m. The walls of the excavation pits were constructed using a bench and tier system, which increased the stability of the walls and provided multiple dihedral faces for mapping fractures and collecting samples. Till exposures were further prepared using a hand trowel and putty knife to ensure that exposed till was fresh and undisturbed by backhoe excavation. Fractures were identified by iron-stained halos or evidence of leaching along fracture surfaces. Fractures from both horizontal and vertical faces were traced onto sheets of clear acetate and later digitized. Average fracture spacing ($2B$) was measured in the field using a measuring tape.

Column Preparation

Till was removed from benches in the soil pits using hand trowels and putty knives to exhume free-standing columns of intact soil, 43 cm in diameter and approximately 50 cm in length. The columns were collected from depths between 1.0 and 27.5 m (Table 1). Each column was kept cylindrical by using a level and a section of polyvinyl chloride (PVC) pipe

as a guide. A 61-cm-long piece of PVC with an interior diameter (ID) of 46 cm was placed over each column, leaving a 1-cm void between the column and the pipe. This annulus between the till and the casing was sealed with paraffin wax, a technique that has been demonstrated to prevent sidewall flow (Grisąk et al., 1980; Kluitenberg et al., 1991). After the wax cooled (approximately 8 hours), a putty knife was used to separate each column from its in-situ base, after which each column was lifted from the excavation trench. Disks made of high-density polyethylene (HDPE) with a thickness of 3 mm were placed at the column ends and sealed with wax to prevent moisture loss during transport to the laboratory.

Laboratory Methods

After being transported to the laboratory, the column ends were carefully scraped with a putty knife to minimize smearing of the till. Ottawa sand was placed in 5-mm-thick layers at the column ends and held in place by the HDPE disks. Perforated HDPE tubes of 3-mm ID were pressed into the sand to provide fluid access to the sand packs. Pistons of 19-mm-thick plywood were added to the column ends and sealed with silicone caulking. The ends and the walls of the columns were mechanically compressed to a pressure approximately equal to in-situ lithostatic conditions. A pressure of 60 kPa, or a depth of approximately 3.5 m, was the maximum pressure that could be obtained by this method. Although great care was exercised to minimize desaturation of the columns, it is possible that some of the larger pores drained during excavation and transport. Each column was slowly re-saturated from beneath by upward flow during a period of at least 7 days to reduce the chance of entrapped air within pores.

Groundwater collected from each site was induced to flow through each column under a constant upward gradient. A unit hydraulic gradient was applied to the ALT, BEM, H1, H2, AO, AT, and ALB columns. A gradient of 0.021 was applied to the ALG column (the most conductive column collected) to reduce the flow rate from 330 mL/min to 6.93 mL/min. Although an upward gradient was applied (to prevent desaturation at the column base), groundwater flow was, in effect, downward because each column was inverted in the laboratory. Column temperature was maintained at a constant 12°C to simulate *in-situ* conditions. Flow rates were monitored and K_b was calculated using the Darcy equation.

Soil texture was determined using the sieve and pipette method (Walter et al., 1978). Sand, silt, and clay particle sizes used in this study were 2 to 0.063 mm, 0.063 to 0.002 mm, and <0.002 mm, respectively. Bulk density (ρ_b) was determined by collecting samples in cylinders of known volume and weighing them after being dried for 24 hours at 104°C. Total porosity was determined gravimetrically by weighing saturated samples, oven-drying them, dividing the difference by the density of water, then dividing this by the original volume of each sample. Pore volume (PV) was determined as the product of θ_T and the volume of each column.

Five compounds were used as tracers: potassium bromide (KBr), pentafluorobenzoate (PFBA), 1,4-piperazinediethanesulfonate (PIPES), potassium nitrate (KNO_3), and 2-chloro-4-(ethylamino)-6-(isopropylamino)-s-triazine (atrazine). The aqueous diffusion coefficients (D_0) of Br, PFBA, PIPES, NO_3, and atrazine are 1.8×10^{-9}, 7.6×10^{-10}, 4.1×10^{-10}, 1.6×10^{-9}, and 6.6×10^{-10} m^2/s, respectively (National Research Council, 1929; Scott and Phillips, 1973; Bowman and Gibbons, 1992; Helmke et al., 2003). Conservative compounds with different

D_0 values (Br, PFBA, and PIPES) were selected because differences in the morphology of their breakthrough curves, BTCs, would indicate matrix diffusion, thereby providing evidence of fracture flow. Nitrate (a nutrient) and atrazine (a broadleaf herbicide) were chosen as tracers because they are agricultural chemicals frequently occurring in groundwater in agricultural areas.

An influent tracer concentration (C_0) of 0.5 mM was used for KBr, PFBA, PIPES, and KNO_3, which is equivalent to 39.95 mg/L Br, 106.04 mg/L PFBA, 167.69 mg/L PIPES, and 7.00 mg/L NO_3-N, respectively. The C_0 of atrazine was 4.64 μM (1 mg/L). The concentration of NO_3-N was chosen because it is similar to the MCL of 10 mg/L NO_3-N. The molar concentrations of Br, PFBA, and PIPES were then set to equal that of NO_3. The resulting concentration of PFBA was similar to the 101.3 mg/L concentration used in previous studies of fluorobenzoate transport through shallow soil in Iowa (Jaynes, 1993). The concentration of atrazine was chosen to reduce the amount of waste atrazine produced, while still providing a sufficient concentration to ensure instrument detection.

The tracer solution was introduced to each column under a constant hydraulic gradient using a Mariotte bottle. The shallow column experiments (ALG, H1, H2, and ALT) lasted 3.0, 0.5, 1.4, and 2.0 days, respectively. The tracer solution for these experiments was applied for 1.0, 0.167, 0.47, and 0.67 days, respectively, then rinsed until the end of the experiment. Deep column experiments (BEM, AO, AT, and ALB) lasted for 70, 117, 90, and 145 days, respectively. The deeper columns were not rinsed due to time constraints.

Effluent samples were passed through a 0.2 μm filter immediately upon collection and stored at 4°C until analyzed at the end of each experiment. Br, PFBA, PIPES, and NO_3 concentrations were determined by ion chromatography. Atrazine concentrations were

analyzed by HPLC at the ARS-National Soil Tilth Laboratory in Ames, Iowa. Analytical precision (95 percent confidence limit) was determined for Br (0.63 mg/L), PFBA (1.14 mg/L), PIPES (2.65 mg/L), NO_3 (0.10 mg/L), and atrazine (0.01 mg/L) by analyzing replicates of spiked samples using Student's t distribution (Harris, 1991).

After the end of the tracer experiment, a 1 g/L solution of FD&C Blue dye no. 1 was introduced to the BEM column for 24 hours under a gradient of 3. The column was then dissected to determine if the dye followed fracture flow-paths. FD&C Blue dye no. 1 is a popular tracer among soil scientists because its bright blue color is easily distinguishable from the brown color of most soils, and because it is considered non-toxic (Flury and Flühler, 1995). Once drained, the column was dissected into 5-cm slices. Both iron-stained fractures and the regions of blue-stained soil were mapped onto sheets of clear acetate and later digitized.

Estimation of Transport Parameters

Solute transport and fate parameters were estimated by fitting the mobile-immobile model (MIM) to the BTCs. The MIM simulates a dual porosity medium as two regions: one in which fluid is moving (the fractures), and the other where fluid is stagnant (the soil matrix). The MIM simulates exchange between the mobile and immobile regions (matrix diffusion) as a first-order process (Coats and Smith, 1964). The MIM has been widely used by soil physicists to simulate solute transport through soil containing macropores. Because of the great density of macropores within the top meter of soil, the MIM does not require explicit knowledge of pore geometry. An added benefit of the simplicity of the model is the MIM's computational efficiency, which allows it to be used in the inverse mode to predict

input parameters from experimental data (van Genuchten, 1981; Parker and van Genuchten, 1984; Gaber et al., 1995).

The MIM was first developed by Coats and Smith (1964). It was later modified to include solute sorption (van Genuchten and Wierenga, 1976) and degradation (van Genuchten and Wagenet, 1989). The MIM includes two governing equations for the mobile (Equation 2) and immobile (Equation 3) regions (van Genuchten and Wagenet, 1989):

$$(\theta_m + f\rho_b K_d)\frac{\partial c_m}{\partial t} = \theta_m D_m \frac{\partial^2 c_m}{\partial x^2} - J_w \frac{\partial c_m}{\partial x} - \alpha(c_m - c_{im}) - (\theta_m \mu + f\rho_b K_d \mu)c_m \qquad (2)$$

$$[\theta_{im} + (1-f)\rho_b K_d]\frac{\partial c_{im}}{\partial t} = \alpha(c_m - c_{im}) - [\theta_{im}\mu + (1-f)\rho_b K_d \mu]c_{im} \qquad (3)$$

where c_m and c_{im} are solute concentrations in the mobile and immobile regions, θ_m and θ_{im} are the mobile and immobile region porosities, t is time, D_m is the dispersion coefficient for the mobile region, x is distance along the flowpath, J_w is the volumetric flux (specific discharge), α is the first-order kinetic rate coefficient, K_d is the equilibrium-sorption coefficient, f is the fraction of adsorption sites in the mobile region, and μ us the degradation coefficient. A semi-analytical solution to Equations 2 and 3 was developed by van Genuchten and Wagenet (1989), and was later included in the computer program CXTFIT 2.1 (Toride et al., 1999). CXTFIT 2.1 solves the problem in the inverse mode using a non-linear method of least squares (Marquardt, 1963).

The MIM is not strictly a fracture-flow model, because it does not incorporate an actual fracture geometry. However, by substituting θ_f for θ_m, the MIM has been shown to reproduce BTCs generated by discrete-fracture models (Sudicky, 1990). Following this

approach, θ_m was calculated by representing the fractures as equally-spaced, vertical, and orthogonal plates. In this case, θ_m can be estimated by (Sudicky, 1990):

$$\theta_m = 2\frac{2b}{2B} \tag{4}$$

where $2b$ is fracture aperture. Fracture aperture was estimated using the cubic law (Snow, 1969):

$$2b = \left(\frac{K_b 6\mu 2B}{\rho g}\right)^{\frac{1}{3}} \tag{5}$$

where μ is fluid viscosity, ρ is fluid density, and g is the acceleration due to gravity. In this fashion, θ_m was calculated from field and laboratory measurements and entered as an input parameter for the MIM simulations.

Model goodness-of-fit was evaluated using the modified index of agreement, d_1 (Willmott et al., 1985). The parameter d_1 is given by

$$d_1 = 1.0 - \frac{\sum_{i=1}^{N}|O_i - P_i|}{\sum_{i=1}^{N}\left(|P_i - \overline{O}| + |O_i - \overline{O}|\right)} \tag{6}$$

where O and P are the observed and model-simulated data, respectively, and N is the number of observations. The value of d_1 varies from 0 to 1, with 1 indicating a perfect fit between the simulated and observed data. Therefore, d_1 may be interpreted in a fashion similar to coefficient of determination (R^2). The quantity d_1 is considered superior to R^2 because it is less sensitive to outliers than R^2 and because d_1 is sensitive to additive and proportional

differences (unlike R^2). The utility of d_1 has been demonstrated through the validation of hydrologic models (Legates and McCabe, 1999).

Results and Discussion

Fracture Mapping

Fractures were encountered at all three study sites and at each of the depths evaluated, although the fracture patterns and the density of fractures were different at the sites. The deepest fractures were observed in the Alburnett Formation at the SIDP site (30 m depth) where they intersected the till/limestone contact.

The fractures observed near the base of the DML excavation trench were dense, subvertical, and oriented in a northeast/southwest pattern (Figure 2a). The average fracture spacing at this site was 4.3 cm at a depth of 3.3 m with a fracture density of 260 fractures/m^2. In contrast to the fractures observed at the DML site, fractures at the IES site did not have a preferred orientation (Figure 2b). Fracture spacing at the 1.6 m depth at the IES site was 3.8 cm and fracture density was 145 fractures/m^2. The fractures at the SIDP site consisted of widely spaced, distinct polygons (Figure 2c). At the sample depth of 27.5 m, average fracture spacing was 10.4 cm and fracture density was 221 fractures/m^2. The observed fracture spacing of less than 5 cm at shallow depths (< 2 m) is consistent with studies in Canada (McKay et al., 1993a) and Denmark (Klint and Gravensen, 1999). However, these studies reported large fracture spacing (between 20 cm and >8 m) at depths below 4 m (Helmke and Simpkins, 2003).

Column Experiments

Breakthrough curves produced during the laboratory experiments demonstrate that contaminant transport is controlled by fractures (Figures 3 and 4). In the absence of fractures, breakthrough would have occurred after one pore volume (PV) had passed through each column as though it were an equivalent porous medium (EPM). Contrary to this, the BTCs were characterized by early times of first arrival. In all eight experiments, the conservative tracers (Br, PFBA, and PIPES) appeared in the column effluent ($C/C_0 > 0.02$; the instrument detection limit) at least 10 times faster than 1 PV (Figure 5). This suggests that preferential flow paths (i.e., fractures) allow the advancing solute front to move rapidly through the columns. We will define the time of first arrival here using the velocity of Br, or V_{Br}. Observed V_{Br} ranged from 0.004 to 64.8 m/d, versus 0.0002 to 1.97 m/d as calculated using the EPM approach (V_{EPM}) (Figure 5). Similar results have been reported in the literature. The V_{Br} reported from a tracer test conducted in a fractured till in Ontario, Canada was 0.05 m/d, versus an average V_{EPM} of 0.006 m/d under a gradient of 0.24 (McKay et al., 1993b). Research of fractured till in Denmark reported an initial chloride velocity of 2.8 m/d for a 4 m deep column under a unit hydraulic gradient (Jørgensen et al., 1998) where calculated V_{EPM} was 0.2 m/d.

Differences of BTC morphology between the three conservative tracers (Br, PFBA, and PIPES) provide additional evidence that transport is dominated by fractures. Matrix diffusion (a process that would only occur if fractures or macropores are present) should retard solutes as they pass through the column. Therefore, the rate at which solutes increase in concentration during the rising limbs of BTCs should be inversely proportional to their respective D_0 values (i.e. PIPES will appear first, followed by PFBA and then Br) if matrix

diffusion is a governing process. By the same process, there should be a separation of solutes during the falling limbs, or tails, of the BTCs. This phenomenon is displayed by the BTCs, although it is more pronounced in the slower experiments (ALG, BEM, AO, and AT columns). A similar separation of Br, PFBA, and PIPES BTCs was observed during solute transport studies of a column of fractured saprolite in Tennessee (Moline et al., 1997; Gwo et al., 1998). As in this paper, the authors concluded that the separation of these compounds provided evidence of fracture-dominated transport. Further evidence of matrix diffusion is the elongated tails observed when the shallow columns were rinsed. Even when rinsed for twice the time of injection, low concentrations of solutes continued to emerge from the columns. Mass balance calculations indicate that 15 to 35 percent of the conservative solutes remained in the shallow columns after rinsing. Hence, rinsing of the columns was only 65 to 85 percent effective in removing these contaminants.

Nitrate behaved as a conservative tracer during short-term experiments (fewer than 3 days) and in a non-conservative manner during longer-term experiments. The NO_3 BTCs from the ALG, H1, H2, and ALT column experiments appear almost identical to the Br BTCs (Figure 3). This was not the case for the BEM column, where the relative concentration of NO_3 remained below 0.05 for the duration of the experiment (Figure 4). Nitrate was not detected in effluent during the AO, AT, or ALB column experiments, indicating that nitrate degraded (presumably by denitrification) quickly in these deeper till units.

Atrazine behaved as a non-conservative solute in experiments of all eight columns. In the rapid experiments (ALG, H1, H2, and ALT columns; Figure 3), atrazine breakthrough was delayed by a factor of approximately 2 with respect to the conservative tracers (Br,

PFBA, and PIPES). In addition, the maximum concentration of atrazine was 80 percent of the concentrations of the conservative tracers during the rising limb of these BTCs. On the falling limb of the four shallow-column BTCs, atrazine exceeded the concentration of the conservative tracers. This prolonged tailing suggests that sorption, rather than degradation, caused the non-ideal nature of the atrazine BTCs. This effect was more pronounced in the longer-term experiments (Figure 4). In the BEM BTC, atrazine reached an equilibrium concentration of approximately 30 percent of the conservative-tracer BTCs after a period of 30 days. In a similar fashion, atrazine reached equilibrium at a C/C_0 of 0.07 during the AO column experiment after 40 days. Atrazine was not detected in outflow during the AT or ALB experiments, suggesting that atrazine sorption coupled with the low K_b of these deeper till units increases residence time, enough for atrazine degradation to occur.

Inverse Modeling and Estimation of Transport Parameters

The BTCs simulated by the MIM were in close agreement with those generated by the column experiments (Figures 3 and 4). Resulting d_1 values had a median of 0.93, a minimum of 0.50, and a maximum of 0.98 (Table 2). Eighty percent of the d_1 values were 0.90 or greater, indicating that the model fit the data well. In cases where concentrations were low during the entire BTC (less than a relative concentration of 0.1), d_1 dropped below 0.8, indicating a poorer goodness-of-fit. The ability of the MIM to fit the BTCs with the specified θ_f provides additional evidence that solute transport through the columns was controlled by fractures.

Estimates of α provided by the MIM simulations demonstrate that matrix diffusion was a controlling process. The range of α estimates spanned six orders of magnitude, from 1

x 10^{-8} to 1.7 x 10^{-2} 1/s (Table 2). Because α was non-zero for all compounds, we conclude that matrix diffusion was a controlling process, and that a model ignoring fractures would be inappropriate for these materials. Caution should be exercised when using the inverse method to estimate parameters such as α, however. Non-unique combinations of parameters could produce similar BTCs, and this effect is likely to increase with the number of parameters estimated (Parker and van Genuchten, 1984). Both D and α cause curvature in BTCs, so a non-unique solution is expected for these parameters. Independent estimates of α for Br, PFBA, and PIPES were determined for the same till samples using the radial diffusion method (Helmke et al., 2003). Independent estimates of α from this method were 1- to 2-orders of magnitude less than those estimated by fitting the MIM to BTCs. Moreover, estimates of α should increase as a function of D_0 (i.e., PIPES should be lowest, followed by PFBA, then Br); however, such an increase was absent in the model-fitted estimates of α. Nonetheless, even if α were less than predicted by the MIM, it would still have a controlling influence on the shape of the BTCs.

Estimates of K_d from the MIM model indicate that sorption retards atrazine in these till units. Estimates of K_d ranged from 2.6 x 10^{-5} to 1 x 10^{-3} m^3/kg (Table 2). Sorption of atrazine was determined for the same till units at similar depths using batch-equilibrium experiments (Moorman et al., 2001). Sorption coefficients using the Freundlich isotherm (which may be compared to K_d because 1/n was close to 1.0) reported by this study were 3.1 x 10^{-4} to 2 x 10^{-3} m^3/kg. These independent estimates of K_d were similar (within a factor of ten) to those estimated by inverse modeling. Values of R calculated from estimated K_d

values range from 1.2 to 6.8, indicating that sorption retards atrazine as it passes through these till units.

Estimates of μ from inverse modeling indicate that degradation is rapid enough to cause measurable loss of both atrazine and NO_3 as they pass through the till. Estimates of μ ranged from 1.2×10^{-7} to 3.4×10^{-5} 1/s for NO_3, and from 2.9×10^{-8} to 5.1×10^{-6} 1/s for atrazine (Table 2). These values of μ equate to half-lives between 0.24 and 67 days for NO_3, and 1.6 and 277 days for atrazine. These values are somewhat greater than those derived from laboratory batch experiments in the literature. Time-concentration plots of NO_3 in microcosms of unoxidized till in Iowa (Cambardella et al. 1999) suggested a half-life of NO_3 degradation to be approximately 225 days. First-order degradation coefficients have not been independently determined for atrazine in till in Iowa. However, estimated half-lives of atrazine degradation in this study are similar to those reported in the literature (20 to 200 days; Jury et al., 1987). At these degradation rates, it is unlikely that NO_3 or atrazine would persist in these deeper (greater than 3 m) till units for more than a few months or years. However, the rapid velocities observed in the shallow till units suggest that both compounds could travel laterally or vertically at rates great enough to contaminate shallow aquifers before the contaminants could be degraded.

Dye Trace Study

Results of the dye trace study provide further evidence that fractures control flow and transport through the till units. Upon dissection of the BEM column, dye was present in approximately 60 percent of the iron-stained fractures (Figure 6), and absent in areas of the matrix where there were no fractures. Because dye was absent from some fractures, it

appears that some fractures were more conductive. Perhaps, if given enough time, the dye would have entered all fractures. It is likely, however, that if the experiment had been allowed to progress for more time, the haloes surrounding each fracture would have converged and obscured the results of the experiment. A similar dye-trace experiment was conducted by Jorgensen et al. (1998), who injected fluorescent dye into large columns of fractured till from Denmark. In these columns, between 80 and 100 percent of the fractures contained dye upon dissection.

Conclusions

Results of this study indicate that transport of solutes such as NO_3 and atrazine through till in Iowa is fracture-dominated. Fractures were encountered in till at the three study sites and at all depths evaluated (from ground surface to 30 m depth). The fracture networks were dense, with fracture spacing ranging from 3.4 to 17.8 cm. The abundance of fractures at each site suggests that these fractures are ubiquitous features of till units in Iowa. The dye-trace test through the BEM column demonstrated that water and dye flowed exclusively through the fracture network.

Additional evidence of preferential flow was indicated by early times of first arrival and the characteristic morphology of BTCs. First-arrival velocities of Br ranged from 0.004 to 64.8 m/d, which were between 10 and 100 times faster than calculated using the EPM assumption. Similar velocities of NO_3 and atrazine were observed during the shallow column experiments (less than 3 m depth). The rate of separation of conservative solutes during the rising and tailing limbs of BTCs was inversely proportional to their respective D_0 values, which demonstrated that matrix diffusion is a controlling process. Further evidence

of matrix diffusion was indicated by the long tails of BTCs. Rinsing the columns for twice the time of injection removed only 65 to 85 percent of the conservative solutes as a result of matrix storage.

Nitrate and atrazine BTCs displayed evidence of sorption (in the case of atrazine) and degradation (both NO_3 and atrazine). Atrazine BTCs were characterized by delayed rising limbs and increased tails with respect to the conservative-tracer BTCs, indicating retardation by sorption. Effluent concentrations of NO_3 and atrazine during the deeper column experiments were diminished compared to the conservative tracers, and indicated degradation. Nitrate and atrazine were not detected in the effluent during the two deepest column experiments (AT and ALB columns), suggesting that degradation and/or sorption were capable of preventing these contaminants from passing through the columns.

Inverse modeling demonstrated that the mobile-immobile model could produce BTCs that closely matched those from the laboratory. The model simulations fit the data well, with d_1 values ranging from 0.50 to 0.98 with a median of 0.93. Model estimates of α (ranging from 1×10^{-8} to 1.7×10^{-2} 1/s) indicated that matrix diffusion is a controlling process. Estimates of K_d from the model simulations for atrazine (2.6×10^{-5} to 1×10^{-3} m^3/kg) are similar to those reported in the literature for samples from identical till units. Half-lives ranged from 0.24 to 67 days for NO_3 and from 1.6 to 277 days for atrazine.

The implications of this study are that fractures have the ability to rapidly transmit nitrate and atrazine through till aquitards in Iowa, either laterally or vertically in cases where aquitards are thin (less than 3 m). At the SIDP site, fractures extended from ground surface through the aquitard and into an aquifer, demonstrating that a fracture network and a flow path could exist in the till from the ground surface to 31 m depth. Fractures in till may play a

dominant role in the transport of NO_3 and atrazine in glaciated regions, and should be considered in studies of both point and non-point pollution and assessments of aquifer vulnerability.

Acknowledgements

This research was funded by grants from the American Geophysical Union (Horton Grant), the Association of Ground Water Scientists and Engineers, the Geological Society of America, Sigma Xi, and the USEPA through an Interagency Agreement DW12036252 to the Agricultural Research Service. We thank T. Moorman, B. Douglas, and A. Reungsang at the National Soil Tilth Laboratory for their analysis of atrazine samples. We thank P. Jardine and G. Moline for the suggestion of using PIPES as a tracer.

References

Bowman, R. S. and J. S. Gibbens. 1992. Difluorobenzoates as nonreactive tracers in soil and ground water. Ground Water. v. 30, pp. 8-14.

Brockman, C. S. and J. P. Szabo. 2000. Fractures and their distribution in the tills of Ohio. Ohio Journal of Science. v. 100, n. 3/4, pp. 39-55.

Cambardella, C. A, T. B. Moorman, D. B. Jaynes, J. L. Hatfield, T. B. Parkin, W. W. Simpkins, and D. L. Karlen. 1999. Water quality in Walnut Creek Watershed: Nitrate-ntogen in soils, subsurface drainage water, and shallow groundwater. Journal of Environmental Quality. v. 28, pp. 25-34.

Coats, K. H. and B. D. Smith. 1964. Dead-end pore volume and dispersion in porous media. Society of Petroleum Engineers Journal. v. 4, pp. 73-84.

Connell, D. E. 1984. Distribution, characteristics, and genesis of joints in fine-grained till and lacustrine sediments, eastern and northwestern Wisconsin. Master's Thesis, University of Wisconsin, Madison. 443 p.

D'Astous, A. Y., W. W. Ruland, J. R. G. Bruce, J. A. Cherry, and R. W. Gillham. Fracture effects in the shallow groundwater zone in weathered Sarnia-area clay. Canadian Geotechnical Journal. v. 26, pp. 43-56.

Eidem, J. M., W. W. Simpkins, and M. R. Burkart. 1999. Geology, groundwater flow, and water quality in the Walnut Creek watershed. Journal of Environmental Quality. v. 28, pp. 60-69.

Flury, M. and H. Flühler. 1995. Tracer characteristics of Brilliant Blue FCF. Soil Science Society of America Journal, v. 59, pp. 22-27.

Fredericia, J. 1990. Saturated hydraulic conductivity of clayey tills and the role of fractures. Nordic Hydrology. v. 21, pp. 119-132.

Freeze, R. A. and J. A. Cherry. 1979. Groundwater. Prentice Hall Pub. 604 p.

Gaber, H. M., W. P. Inskeep, S. D. Comfort, and J. M. Wraith. 1995. Nonequilibrium transport of atrazine through large intact soil cores. Soil Science of America Journal. v. 59, pp. 60-67.

Grisak, G. E. and J. F. Pickens. 1980. Solute transport through fractured media: 1. The effect of matrix diffusion. Water Resources Research. v. 16, pp. 719-730.

Grisak, G. E., J. F. Pickens, and J. A. Cherry. 1980. Solute transport through fractured media: 2. Column study of fractured till. Water Resources Research. v. 16, pp. 731-739.

Gwo, J. P., R. O'Brien, and P. M. Jardine. 1998. Mass transfer in structured porous media: embedding mesoscale structure and microscale hydrodynamics in a two-region model. Journal of Hydrology. v. 208, pp. 204-222.

Harris, D. C. 1991. *Quantitative Chemical Analysis, Third Ed.*, W. H. Freeman and Company, 782 p.

Helmke, M. F. and W. W. Simpkins. 2003. Chapter 5: Effect of fractures on hydraulic conductivity of till units in Iowa. In unpub. Ph.D. dissertation, Iowa State University, pp. 144-167.

Helmke, M. F., W. W. Simpkins, and R. Horton. 2003. Chapter 4: Laboratory measurement of effective diffusion parameters in fractured soil. In unpub. Ph.D. dissertation, Iowa State University, pp. 119-143.

Herzog, B. L., R. A. Griffin, C. J. Stohr, L. R. Follmer, W. J. Morse, and W. J. Su. 1989. Ground Water Monitoring and Review. v. 9, pp. 82-89.

Jaynes, D. B. 1993. Evaluation of fluorobenzoate tracers in surface soils. Ground Water. v. 32, pp. 532-538.

Jørgensen, P. R. and J. Fredericia. 1992. Migration of nutrients, pesticides and heavy metals in fractured clayey till. Geotechnique. v. 42, pp. 67-77.

Jørgensen, P. R., L. D. McKay, and N. ZH. Spliid. 1998. Evaluation of chloride and pesticide transport in a fractured clayey till using large undisturbed columns and numerical modeling. Water Resources Research. v. 34, pp. 539-553.

Jørgensen, P. R. and N. H. Spliid. 1992. Mechanisms and rates of pesticide leaching in shallow clayey till. European Conference on Integrated Research for Soil and Sediment Protection and Remediation. MECC, Maastricht, the Netherlands. 11 p.

Jury, W. A., D. D. Focht, and W. J. Farmer. 1987. Evaluation of pesticide groundwater pollution potential from standard indices of soil-chemical adsorption and biodegradation. Journal of Environmental Quality, v. 16, pp. 422-428.

Keller, C. K., G. van der Kamp, and J. A. Cherry. 1988. Hydrogeology of two Saskatchewan tills, I. Fractures, bulk permeability, and special variability of downward flow. Journal of Hydrology. v. 101, pp. 97-121.

Keller, C. K., G. van der Kamp, and J. A. Cherry. 1989. A multiscale study of the permeability of a thick clayey till. Water Resources Research. v. 25, n. 11. pp. 2299-2317.

Kemmis, T. J., E. A. Bettis III, and G. R. Hallberg. 1992. Quaternary geology of Conklin Quarry. Guidebook Series no. 13. Iowa Department of Natural Resources. 41 p.

Kemmis, T. J., G. R. Hallberg, and A. J. Lutenegger. 1981. Depositional environments of glacial sediments and landforms on the Des Moines Lobe, Iowa. Guidebook Series no. 6. Iowa Department of Natural Resources. 132 p.

Klint, K. E. S. and P. Gravensen. 1999. Fractures and biopores in Weichselian clayey till Aquitards at Flakkebjerg, Denmark. Nordic Hydrology. v. 30, n. 4/5, pp. 267-284.

Kluitenberg, G. L., J. R. Bilskie, and R. Horton. 1991. Rubberized asphalt for sealing cores of shrinking soil. Soil Science Society of America Journal. v. 55, pp. 1504-1507.

Kross, B. C., G. R. Hallberg, D. R. Bruner, R. D. Libra, K. D. Rex, L. M. B. Weih, M. E. Vermace, L. F. Burmeister, N. H. Hall, K. L. Cherryhomes, J. K. Johnson, M. I. Selim, B. K. Nations, L. S. Seigley, D. J. Quaide, A. G. Dudler, K. D. Sesker, M. A. Culp, C. F. Lynch, H. F. Nicholson, and J. Hughes. 1990. *The Iowa State-Wide Rural Well-Water Survey, Water Quality Data: Initial Analysis*, Iowa Department of Natural Resources Technical Information Series 19, 142 p.

Legates, D. R. and G. J. McCabe Jr. 1999. Evaluating the use of "goodness-of-fit" measures in hydrologic and hydroclimatic model validation. Water Resources Research. v. 35, pp. 233-241.

Marquardt, D. W. 1963. An algorithm for least-squares estimation of nonlinear parameters. Journal of the Society of Industrial and Applied Mathematics. v. 11, n. 2, pp. 431-441.

McKay, L. D., J. A. Cherry, and R. W. Gillham. 1993a. Field experiments in a fractured clay till: 1. Hydraulic conductivity and fracture aperture. Water Resources Research. v. 29, pp. 1149-1162.

McKay, L. D., J. A. Cherry, and R. W. Gillham. 1993b. Field experiments in a fractured clay till: 2. Solute and colloid transport. Water Resources Research. v. 29, pp. 3879-3890.

McKay, L. D. and J. Fredericia. 1995. Distribution, origin, and hydraulic influence of fractures in a clay-rich glacial deposit. Canadian Journal of Technology. v. 32, pp. 957-975.

McKay, L. D., D. J. Balfour, and J. A. Cherry. 1998. Lateral chloride migration from a landfill in a fractured clay-rich glacial deposit. Ground Water. v. 36, pp. 988-999.

Moline, G. R., C. R. Knight, and R. Ketcham. 1997. Laboratory measurement of transport processes in a fractured limestone/shale saprolite using solute and colloid tracers. Abstracts with Programs, Geological Society of America. v. 29, n. 6, p. 370.

Moorman, T. B., K. Jayachandran, and A. Reungsang. 2001. Adsorption and desorption of atrazine in soils and subsurface sediments. Soil Science, v. 166, n. 12, pp. 921-929.

National Research Council. 1929. International critical tables of numerical data, physics, chemistry and technology v. 5; E. W. Washburn Ed.. McGraw-Hill Book Company, Inc. Pub. 470 p.

Parker, J. C. and M. Th. van Genuchten. 1984. Determining Transport Parameters from Laboratory and Field Tracer Experiments. Virginia Agricultural Experiment Station Bulletin. v. 84, pp. 1-97.

Prior, J. C. 1991. Landforms of Iowa. University of Iowa Press, Iowa City, Iowa. 154 p.

Scott, H. D., and R. E. Phillips. 1973. Self-diffusion coefficients of selected herbicides in water and estimates of their transmission factors in soil. . Soil Science Society of America Proceedings. v. 37, pp. 965-967.

Seo, H. H. 1996. Hydraulic properties of Quaternary stratigraphic units in the Walnut Creek watershed. Master's Thesis. Iowa State University. 145 p.

Simpkins, W. W. and K. R. Bradbury. 1992. Groundwater flow, velocity, and age in a thick, fine-grained till unit in southeastern Wisconsin. Journal of Hydrology. v. 132, pp. 283-319.

Simpkins, W. W., M. R. Burkart, M. F. Helmke, T. N. Twedt, D. E. James, R. J. Jaquis, and K. J. Cole. 2002. Potential impact of earthen waste storage structures on water resources in Iowa. Journal of the American Water Resources Association. v. 38, n. 3, pp. 759-771.

Snow, D. T. 1969. Anisotropic permeability of fractured media. Water Resources Research. v. 5, pp. 1273-1289.

Sudicky, E. A. 1990. The Laplace transform Galerkin technique for efficient time-continuous solution of solute transport in double-porosity media. Geoderma. v. 46, pp. 209-232.

Toride, N, F. J. Leij, and M. Th. van Genuchten. 1999. The CXTFIT code for estimating transport parameters from laboratory or field tracer experiments. *Research Report No. 137.* U. S. Salinity Lab., USDA, ARS, Riverside, CA, 121 p.

van Genuchten, M. Th. 1981. Non-equilibrium transport parameters from miscible displacement experiments. Research Report 119, U. S. Salinity Lab., USDA-ARS, Riverside, CA.

van Genuchten, M. Th. and R. J. Wagenet. 1989. Two-site/two-region models for pesticide transport and degradation: theoretical development and analytical solutions. Soil Science Society of America Journal. v. 53, pp. 1303-1310.

van Genuchten, M. Th. and P. J. Wierenga. 1976. Mass transfer studies in sorbing porous media, I, Analytical solutions. Soil Science Society of America Journal. v. 40, pp. 473-481.

Walter, N. F., Hallberg, G. R., and Fenton, T. E. 1978. Particle-size analysis by the Iowa State University Soil Survey Laboratory, in Hallberg, G. R. ed.: Standard procedures for evaluation of Quaternary materials in Iowa: Iowa Geological Survey, Technical Information Series, no. 8, p. 61-74.

Weis, M. R. and W. W. Simpkins. 1996. Nitrate and herbicide transport in groundwater within fractured, pre-Illinoian till units near Nashua, Iowa. Abstracts with Programs, Geological Society of America. v. 28, n. 6, pp. 70.

Willmott, C. J., S. G. Ackleson, R. E. Davis, J. J. Feddema, K. M. Klink, D. R. Legates, J. O'Donnell, and C. M. Rowe. 1985. Statistics for the evaluation and comparison of models. Journal of Geophysical Research. v. 90, pp. 8995-9005.

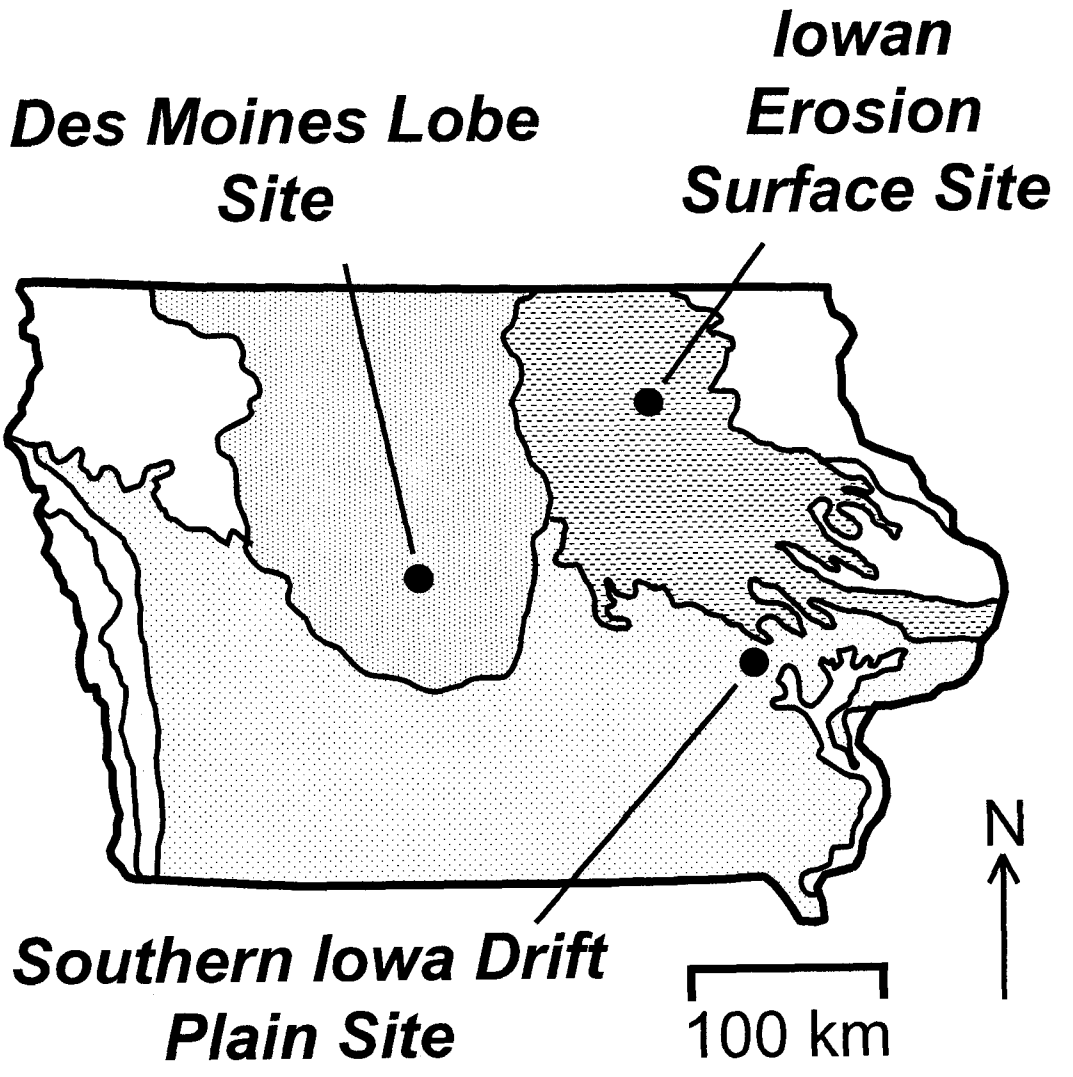

Figure 1. Map showing the locations of the three study sites on the Des Moines Lobe (DML), Iowan Erosion Surface (IES), and Southern Iowa Drift Plain (SIDP) landform regions of Iowa. Other landform regions given in Prior (1991).

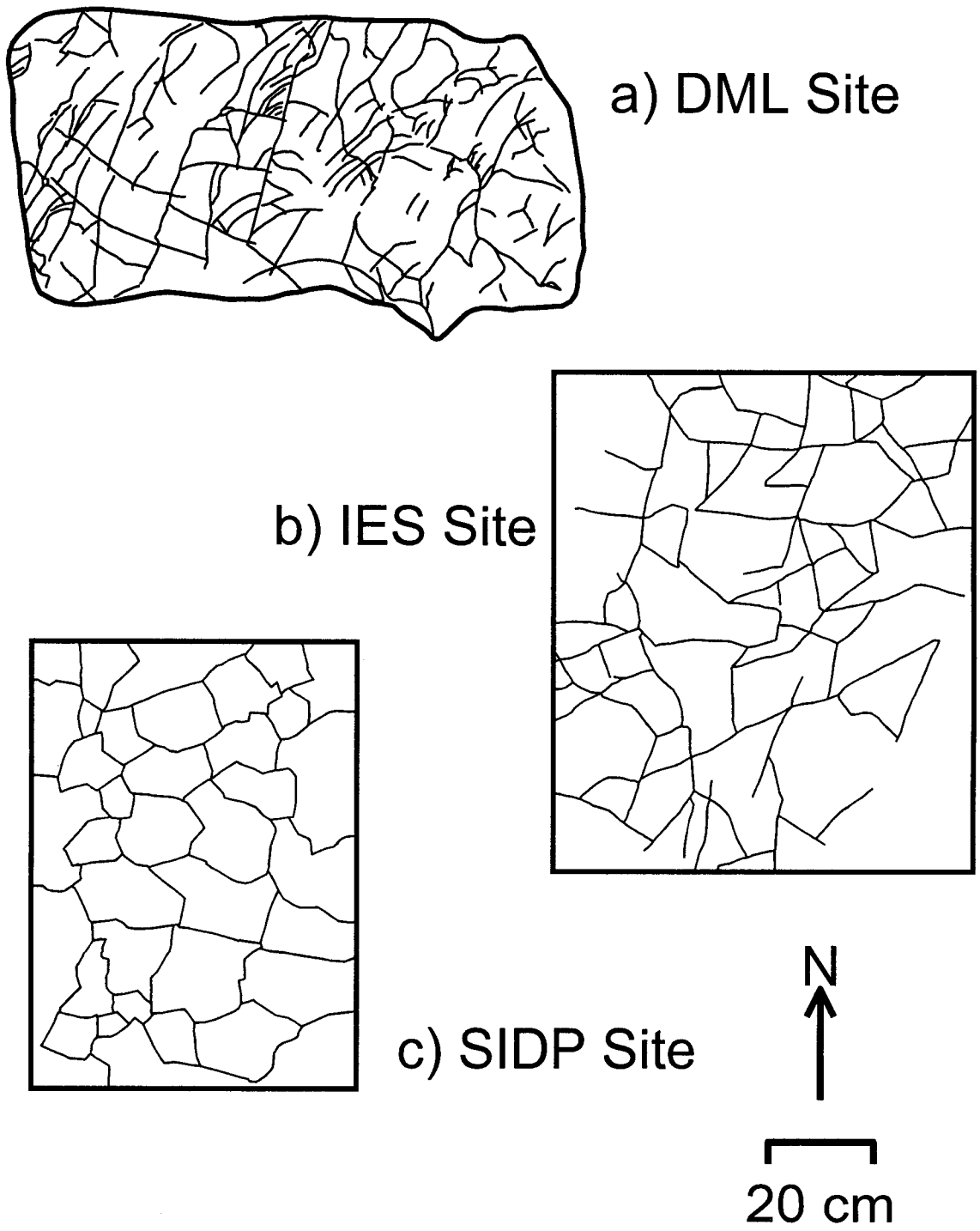

Figure 2. Plan-view fracture maps from the DML site (a), IES site (b), and SIDP site (c) at a depths of 3.3, 1.6, and 27.5 m, respectively.

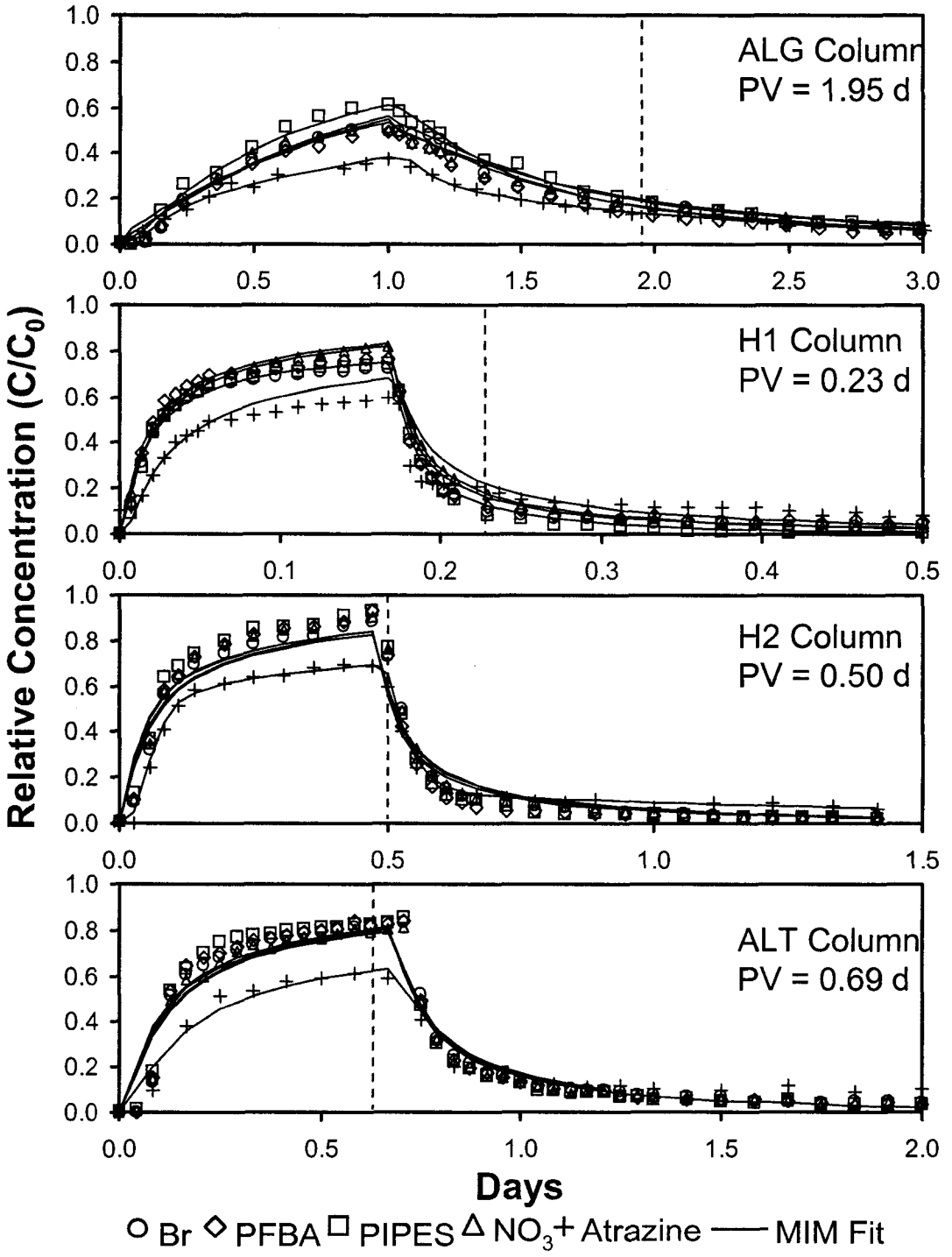

Figure 3. Breakthrough curves from the ALB, H1, H2, and ALT columns. Solid lines represent BTCs simulated by the Mobile-Immobile Model. Dashed lines indicate the time for one pore volume (PV) to pass through each column.

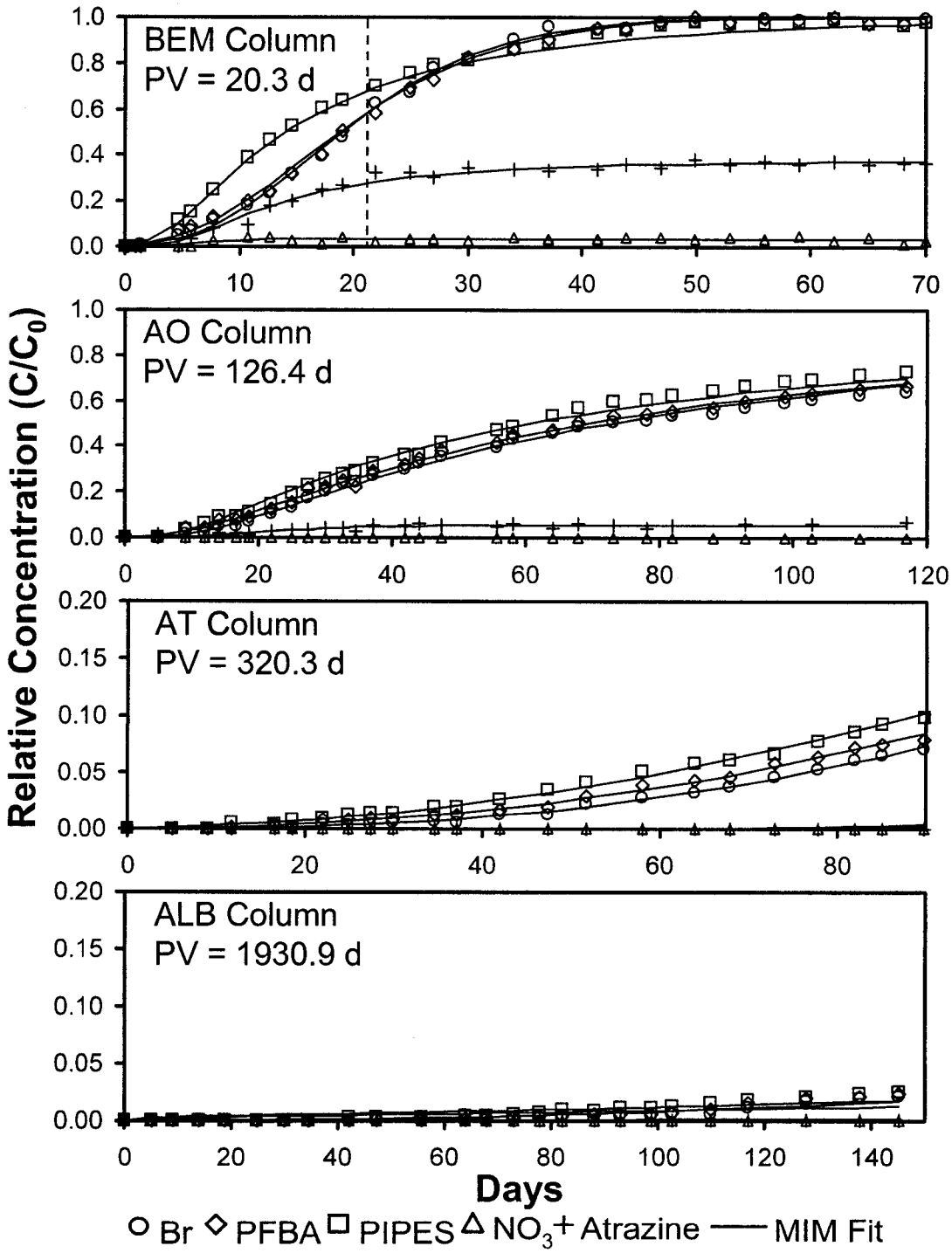

Figure 4. Breakthrough curves from the BEM, AO, AT, and ALB columns. Solid lines represent BTCs simulated by the Mobile-Immobile Model. Dashed lines indicate the time for one pore volume (PV) to pass through each column (off scale for AO, AT, and ALB columns).

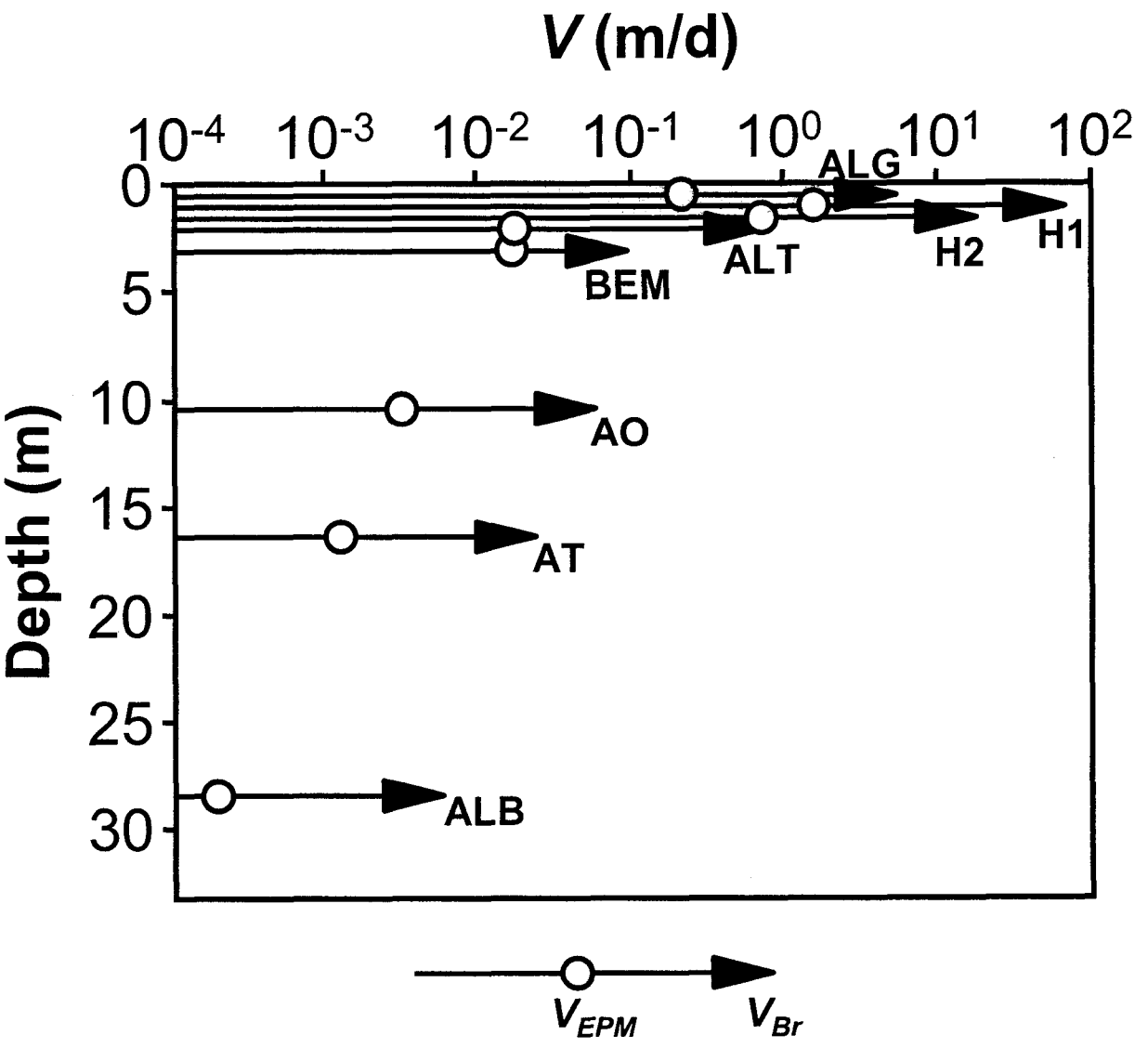

Figure 5. Plot of bromide velocity (V_{Br}, filled arrows) and velocity calculated using the equivalent porous medium (EPM) assumption (V_{EPM}, open arrows). Velocity is plotted on a log scale.

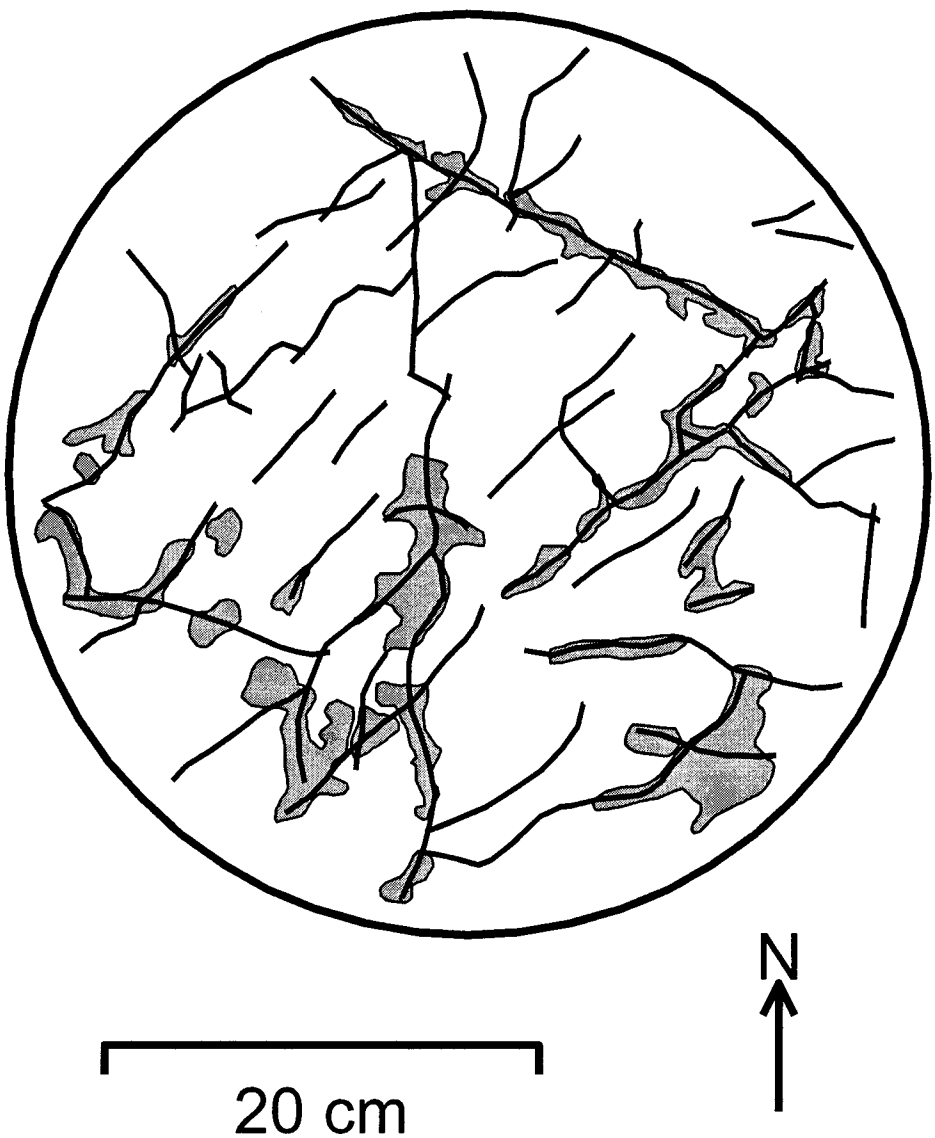

Figure 6. Map of fractures (dark lines) and presence of FD&C Blue no. 1 dye (gray zones) in the BEM column after dissection. The slice represents till at a depth of 3.65 m after 24 hours of dye injection.

Table 1. Location, depth, stratigraphic classification, status of till weathering, bulk density (ρ_b), total porosity (θ_T), and texture of the eight columns collected for this study.

Column name	Site†	Sample Depth (m)	Formation	Member	Status of till weathering	ρ_b (kg/m^3)	θ_T (percent)	Sand (percent)	Silt (percent)	Clay (percent)
ALG	DML	1.0 to 1.45	Dows	Alden	weathered	1,670	29.8	46.8	37.8	15.5
ALT	DML	2.0 to 2.45	Dows	Alden	weathered	1,840	30.5	49.6	36.0	14.4
BEM	DML	3.3 to 3.7	Dows	Alden	partially weathered	1,830	29.6	48.2	37.0	14.8
H1	IES	1.25 to 1.7	Wolf Creek	Hickory Hills	weathered	1,820	31.2	38.7	33.8	27.5
H2	IES	1.5 to 1.9	Wolf Creek	Hickory Hills	weathered	1,860	30.7	44.1	33.2	22.8
AO	SIDP	10.5 to 10.95	Wolf Creek	Aurora	weathered	1,820	30.5	37.4	38.1	24.6
AT	SIDP	16.5 to 16.95	Wolf Creek	Aurora	partially weathered	1,890	28.8	31.0	41.6	27.4
ALB	SIDP	27.5 to 27.95	Alburnett	N/A	unweathered	2,010	28.6	31.0	45.6	23.4

† DML = Des Moines Lobe; IES = Iowan Erosion Surface; SIDP = Southern Iowa Drift Plain

Table 2. Dispersion coefficient (D), mass-exchange coefficient (α), sorption coefficient (K_d), and degradation coefficient (μ) estimated by the mobile-immobile model (MIM) from breakthrough curves. The modified index of agreement (d_1) is also provided as a measure of goodness-of-fit.

Column name	Compound	D (m^2/s)	α (1/s)	K_d (m^3/kg)	μ (1/s)	d_1
ALG	Br	1.9×10^{-6}	4.8×10^{-5}	NE	NE	0.907
	PFBA	1.7×10^{-6}	3.0×10^{-5}	NE	NE	0.837
	PIPES	2.5×10^{-6}	1.4×10^{-4}	NE	NE	0.941
	NO_3	1.9×10^{-6}	4.8×10^{-5}	NE	1.4×10^{-6}	0.921
	Atrazine	1.2×10^{-6}	7.2×10^{-6}	7.2×10^{-5}	2.8×10^{-6}	0.949
ALT	Br	1.4×10^{-5}	2.2×10^{-3}	NE	NE	0.924
	PFBA	1.5×10^{-5}	4.8×10^{-3}	NE	NE	0.922
	PIPES	1.6×10^{-5}	4.1×10^{-3}	NE	NE	0.919
	NO_3	1.3×10^{-5}	4.8×10^{-5}	NE	5.4×10^{-7}	0.929
	Atrazine	2.4×10^{-5}	1.8×10^{-3}	3.3×10^{-4}	5.1×10^{-6}	0.908
BEM	Br	1.8×10^{-9}	1.5×10^{-6}	NE	NE	0.981
	PFBA	1.4×10^{-9}	1.2×10^{-6}	NE	NE	0.979
	PIPES	4.3×10^{-8}	1.5×10^{-5}	NE	NE	0.971
	NO_3	2.1×10^{-8}	4.2×10^{-5}	NE	3.4×10^{-6}	0.722
	Atrazine	6.1×10^{-8}	6.5×10^{-5}	1.5×10^{-4}	4.7×10^{-7}	0.958
H1	Br	8.8×10^{-5}	8.5×10^{-3}	NE	NE	0.947
	PFBA	1.0×10^{-4}	9.8×10^{-3}	NE	NE	0.943
	PIPES	1.0×10^{-4}	9.8×10^{-3}	NE	NE	0.943
	NO_3	8.7×10^{-5}	1.7×10^{-2}	NE	3.4×10^{-5}	0.967
	Atrazine	2.7×10^{-4}	4.5×10^{-5}	1.0×10^{-3}	2.7×10^{-7}	0.857
H2	Br	2.2×10^{-5}	2.3×10^{-3}	NE	NE	0.917
	PFBA	2.7×10^{-5}	4.1×10^{-3}	NE	NE	0.905
	PIPES	2.8×10^{-5}	9.0×10^{-3}	NE	NE	0.903
	NO_3	2.3×10^{-5}	2.7×10^{-3}	NE	1.2×10^{-7}	0.915
	Atrazine	7.3×10^{-7}	4.2×10^{-6}	2.6×10^{-5}	2.9×10^{-8}	0.964
AO	Br	1.5×10^{-8}	4.6×10^{-6}	NE	NE	0.968
	PFBA	1.6×10^{-8}	2.7×10^{-6}	NE	NE	0.974
	PIPES	2.1×10^{-8}	1.1×10^{-5}	NE	NE	0.958
	NO_3	NE	NE	NE	NE	NE
	Atrazine	4.7×10^{-8}	5.2×10^{-6}	2.8×10^{-4}	8.4×10^{-7}	0.764
AT	Br	1.6×10^{-9}	3.5×10^{-7}	NE	NE	0.975
	PFBA	1.6×10^{-9}	2.6×10^{-7}	NE	NE	0.965
	PIPES	1.8×10^{-9}	2.2×10^{-7}	NE	NE	0.963
	NO_3	NE	NE	NE	NE	NE
	Atrazine	NE	NE	NE	NE	NE
ALB	Br	7.9×10^{-10}	1.3×10^{-7}	NE	NE	0.777
	PFBA	8.7×10^{-10}	1.0×10^{-8}	NE	NE	0.504
	PIPES	2.0×10^{-10}	2.0×10^{-8}	NE	NE	0.663
	NO_3	NE	NE	NE	NE	NE
	Atrazine	NE	NE	NE	NE	NE

K_d and μ were not estimated (NE) for non-sorbing and non-degrading compounds, respectively. Parameters were not estimated for experiments in which solutes were not detected.

COMPARISON OF FORWARD MODELING APPROACHES TO SIMULATE SOLUTE TRANSPORT THROUGH FRACTURED TILL

A paper to be submitted to *Ground Water*

Martin F. Helmke, William W. Simpkins, and Robert Horton

Abstract

Despite general agreement that fractures control solute transport through till, only a few studies have included fractures when simulating solute transport in this material. The purpose of this study is to demonstrate three different approaches, the Mobile-Immobile Model (MIM), the Parallel-plate Discrete Fracture Model (PDFM), and a 3-Dimensional Discrete Fracture Model (3-D DFM) to simulate solute transport in a large-diameter column of fractured till.

Model results were tested statistically against breakthrough curves (BTCs) generated from solute transport experiments in the columns using KBr, PFBA, and PIPES. Each model was run in the forward mode using input parameters determined from independent field and laboratory methods. All three models were reasonable predictors of the BTCs (goodness-of-fit stastistic d_1 ranged from 0.751 to 0.959). Model predictions of Br BTCs were not significantly different ($\alpha = 0.05$); however, the 3-D DFM was more accurate than the MIM or PDFM when predicting PFBA and PIPES transport. The MIM was the poorest predictor of PIPES transport ($d_1 = 0.751$).

Results of the study show that fractures may be readily incorporated into any of the solute-transport models and that the more elaborate models do not necessarily produce results that are more accurate. The MIM and PDFM models were the simplest to construct and the most computationally efficient (less than 3 seconds). The 3-D DFM model was the most data

intensive and required approximately 14 hours for a simulation. The 3-D DFM is the only one that is capable of simulating realistic fracture geometry. This is particularly important because our results suggest that fracture orientation and geometry may have an influence on BTCs for compounds with small effective diffusion coefficients (D_e) and that first-order approximations (MIM) of matrix diffusion may be inappropriate under these conditions. At large scales, the MIM and PDFM will likely prove more practical than the 3-D DFM due to the computational effort required to simulate many fractures. Where fracture spacing is large with respect to the investigation scale, or during very short time scales, discrete fracture models are likely to produce superior results than the simplified MIM or PDFM approaches. Models incorporating fractures should provide more reliable predictions of solute transport through fractured till than the traditional equivalent porous medium, EPM, approach and should be used routinely.

Introduction

Previous Work

Hydrogeologists have long suspected that fractures in till act as preferential flow paths and facilitate rapid transport of contaminants. Fractures are well documented in till throughout the U.S., Canada, and Denmark, and appear to be a ubiquitous feature of these deposits. In the U.S., till fractures have been documented in Iowa (Kemmis et al., 1992; Helmke and Simpkins, 2003), Wisconsin (Connell, 1984), and Ohio (Brockman and Szabo, 2000). Fractures in till have also been reported throughout Canada (Keller et al., 1988; McKay et al., 1993a) and Denmark (Klint and Gravensen, 1999). The potential for fractures

to rapidly transmit chemical contaminants through till is also well documented (Freeze and Cherry, 1979; Grisak and Pickens, 1980; Jørgensen and Spliid, 1992; McKay et al., 1993b).

The bulk hydraulic conductivity (K_b) of fractured till is commonly 1 to 3 orders of magnitude greater than the hydraulic conductivity of the till matrix (K_m) (Freeze and Cherry, 1979; Helmke and Simpkins, 2003). Fracture porosity (n_f) is frequently 1 to 4 orders of magnitude less than the total porosity (n_T) of the till (Jørgensen and Spliid, 1992; McKay et al., 1993a). The combined effects of increased K_b and decreased effective porosity (n_e, n_f in a fractured medium) may result in calculated fluid velocities up to 200 m/day under a unit hydraulic gradient (Jørgensen and Spliid, 1992; McKay et al., 1993a).

Despite general agreement that fractures control solute transport through till, only a few studies in Denmark and Canada have included fractures when simulating solute transport in this environment (Grisak and Pickens, 1980; McKay et al. 1993b; Jørgensen et al., 1998). We propose that the lack of use of these models may be due to the burden of obtaining input parameters for such models, or a lack of knowledge about or understanding of the models. The purpose of this paper is to demonstrate three different approaches, the Mobile-Immobile Model (MIM), the Parallel-plate Discrete Fracture Model (PDFM), and a 3-Dimensional Discrete Fracture Model (3-D DFM) to simulate solute transport in a large-diameter column of fractured till and to discuss their applicability to investigations of solute transport at various scales.

Existing Models

Models that simulate solute transport through fractured media differ from equivalent porous medium (EPM) models for two reasons: 1) water flow through a fracture is typically

orders of magnitude faster than within the matrix, and 2) solute storage is far greater in the matrix than in the fracture. Therefore, most fracture models simulate advection in the fractures and diffusive exchange between the fractures and the matrix. Beyond these similarities, fracture transport models differ by how they represent the geometry of the fracture system and how they solve the problem mathematically. Some models specify fracture geometry explicitly by simulating 3-dimensional sets of fractures (e.g. FracMan/MAFIC, Dershowitz et al., 1994 or Frac3DVS, Therrien et al., 2000), whereas other models disregard fracture geometry (e.g. CXTFIT, Toride et al., 1999). Still other models represent fracture networks using a simplified geometry, such as orthogonal or parallel plates (e.g. FRACTRAN, Sudicky and McLaren, 1998). The more realistic fracture models are more difficult for the user to construct, and may take hundreds or thousands of times longer to produce results with a computer. These three classes of models are discussed below.

Mobile-Immobile Model (MIM)

The MIM simulates a dual porosity medium as two regions: one in which fluid is moving and the other where fluid is stagnant (Coats and Smith, 1964). When applied to a fractured medium, the MIM represents fractures as the mobile region and the matrix as the immobile region. Using this approach, advection and dispersion occur exclusively in the mobile region and the immobile region is treated as a sink that stores solute. The MIM simulates exchange between the mobile and immobile regions (matrix diffusion) as a first-order process (Coats and Smith, 1964).

The MIM was first introduced by petroleum engineers in the 1960s (Coats and Smith, 1964). The model is referred to as the MIM by Jury et al. (1991), but is also known as the dual-porosity model (Brusseau et al., 1994), the two-phase model (Skopp and Warrick, 1974), the two-site/two-region model (van Genuchten and Wierenga, 1976), and the double-porosity model (Sudicky, 1990; Sudicky and McLaren, 1998). Early versions of the MIM included advection and dispersion in the mobile region and first-order exchange between the mobile and immobile regions. The MIM was later expanded to include sorption (van Genuchten and Wagenet, 1989) and first-order degradation and production (Toride et al., 1993). In this paper, sorption and degradation will not be considered because only conservative solutes will be discussed.

The MIM has been used widely by soil physicists to model solute transport through soil containing macropores. Because of the great density of macropores within the top meter of soil, the MIM has become the standard model for soil scientists because it does not require explicit knowledge of pore geometry. An added benefit of the simplicity of the model is the MIM's computational efficiency, which allows it to be used in the inverse mode to predict input parameters from experimental data (van Genuchten, 1981; Parker and van Genuchten, 1984; Gaber et al., 1995).

The MIM includes two governing equations for the mobile (Equation 1) and immobile (Equation 2) regions (Coats and Smith, 1964):

$$n_m \frac{\partial c_m}{\partial t} = n_m D_m \frac{\partial^2 c_m}{\partial x^2} - J_w \frac{\partial c_m}{\partial x} - \alpha(c_m - c_{im}) \tag{1}$$

$$n_{im} \frac{\partial c_{im}}{\partial t} = \alpha(c_m - c_{im}) \tag{2}$$

where c_m and c_{im} are solute concentrations in the mobile and immobile regions, n_m and n_{im} are the mobile and immobile region porosities, t is time, D_m is the mobile region dispersion coefficient, x is the location along the flowpath, J_w is the volumetric flux density, and α is the first-order mass-transfer coefficient. Semi-analytical solutions to Equations 1 and 2 were developed by van Genuchten and Wagenet (1989), and Toride et al. (1993) for one-dimensional flow. Numerical solutions of the MIM have also been presented in 2- and 3-dimensions using finite-element (Sudicky and McLaren, 1998; Therrien et al., 2000) and finite-difference methods (Zheng and Wang, 1999). The computer program CXTFIT Version 2.1 (Toride et al., 1999) was used to simulate the MIM BTCs in this paper.

Parallel-plate Discrete Fracture Model (PDFM)

The PDFM represents a fractured medium as a system of equally spaced, parallel plates. The geometry of the system causes matrix diffusion to be symmetrical about each fracture, which allows the entire system of fractures to be modeled as a single fracture with one-half of a matrix block on each side (Sudicky and Frind, 1982). This simplified system results in a computationally efficient model and minimizes the number of required input parameters.

For the few studies that have simulated solute transport through fractured till, the PDFM is the most widely used. The PDFM was used to simulate chloride BTCs from a fractured till column in Canada (Grisak et al., 1980) and chloride and pesticide transport through large columns in Denmark (Jørgensen et al., 1998). These studies demonstrated that the PDFM produced simulated BTCs that closely resembled laboratory-derived BTCs.

Moreover, the PDFM BTCs were superior to those produced using the EPM approach in both of these studies. The PDFM was also used to simulate chloride BTCs in a trench-to-trench test in Canada (McKay et al., 1993a, b). Most of these simulations, however, required some adjustment of parameters to make the model fit the observed BTCs.

Similar to the MIM, the PDFM requires governing equations for the fracture (Equation 3) and the till matrix (Equation 4), respectively:

$$\frac{\partial c}{\partial t} + v\frac{\partial c}{\partial z} - D\frac{\partial^2 c}{\partial z^2} + \frac{q}{b} = 0 \tag{3}$$

$$\frac{\partial c'}{\partial t} - D'\frac{\partial^2 c'}{\partial x^2} = 0 \tag{4}$$

where c and c' are solute concentration in the fracture and matrix; z and x are distances along the fracture and into the matrix normal to the fracture, respectively; q is specific discharge; v is the advective velocity in the fracture; D is the dispersion coefficient in the fracture; and D' is the effective diffusion coefficient in the matrix (Sudicky and Frind, 1982). The PDFM treats matrix diffusion as a second-order, Fickian process that may be more accurate than the first-order approach (i.e. MIM) for short times and/or larger fracture spacing (Harrison et al., 1992).

Solutions to Equations 3 and 4 have been derived using semi-analytical (Sudicky and Frind, 1982) and finite element (Sudicky, 1989; Sudicky, 1990; Sudicky and McLaren, 1998) methods. In this paper, FRACTRAN version 5.01 (Sudicky and McLaren, 1998) was used to simulate BTCs.

Three-Dimensional Discrete Fracture Model (3-D DFM)

Models of groundwater flow and solute transport through fractured rock typically represent fractures as 3-dimensional, discrete, planar features. These models have been used for development of groundwater well fields in fractured media (Jones et al., 1999), oil and gas reservoir engineering (Dershowitz et al., 1994), and evaluation of sites for disposal of high-level nuclear waste (Anna, 1998). Three-dimensional DFMs are well suited for simulating flow through fractured rocks because of the large contrast in K between fractures and the rock matrix and the low fracture densities frequently encountered in rock.

Water and solute transport through the DFM was simulated using the MAFIC (MAtrix/Fracture Interaction Code) program (Miller et al., 1997). For this paper, MAFIC was used to simulate steady-state fluid flow and transient solute transport. The equation for 2-D fluid flow at steady state through a triangular element is:

$$q = -T\nabla^2 h \tag{5}$$

where T is transmissivity, h is hydraulic head and ∇ is the two-dimensional Laplace Operator. Using the Galerkin finite element solution technique, Equation 5 may be approximated for an entire system of elements by

$$\sum_{m=1}^{N}\left[\int_R (T_{nm}\nabla\xi_n \bullet \nabla\xi_m dR)h_m\right] = \int_R q\xi_n dR \quad n = 1,2,...N \tag{6}$$

where R is element area and ξ is the linear basis function (Miller et al., 1997). Using this approximation and specified boundary conditions, MAFIC constructs a global finite element

matrix and solves it using a pre-conditioned, incomplete Choleskii conjugate gradient solver (Meijerink and van der Vorst, 1977).

MAFIC simulates solute transport through the discrete fracture network using particle tracking. The concentration (C) of solute in an element is calculated by

$$C = \frac{M_p}{\rho_w A_e 2b_e} \tag{7}$$

where M_p is the mass of the particles in an element, ρ_w is the fluid density, A_e is the element area, and $2b_e$ is the element aperture. Advection is simulated by moving each particle according to the flow velocity vector during each time step.

Matrix diffusion is treated as a stochastic retardation process by MAFIC. At the end of each time step, the particle travel time ($\Delta t_{f,i}$) is re-calculated to include the portion of time it spends in the matrix by the equation (Miller, 1997):

$$\Delta t_{f,i} = \left(\frac{b}{b + n_{De}B}\right)\Delta t_i - \left(\frac{b+B}{b+n_{De}B}\right) - \left(\frac{2(b+B)^2}{\pi^4 D^* b/(b+B)}\right) \tag{8}$$
$$\bullet \sum_{n=1}^{\infty} \frac{1}{n^4} \sin^2\left(n\pi b/(b+B)\right)\left[\exp\left(-n^2\pi^2 \frac{D_e t_{i+1}}{(b+B)^2}\right) - \exp\left(-n^2\pi^2 \frac{D_e t_i}{(b+B)^2}\right)\right]$$

The principal advantage of the particle tracking approach is that it is relatively simple to program. Verification studies in the fractured rock literature have shown that at least 50,000 particles are required to produce realistic BTCs (Herbert et al., 1992). Therefore, the method may be computationally inefficient.

Methods

Location of Study

The study site is located within the Walnut Creek watershed, 6 km south of Ames, Iowa on the Des Moines Lobe landform region (Figure 1). The Quaternary stratigraphy and hydrogeology of the Walnut Creek Watershed was previously investigated as part of the Management Systems Evaluation Area (MSEA) program (Seo, 1996; Eidem et al., 1999). The surficial deposit at the site is the Alden Member till of the Dows Formation, deposited 14 to 12.5 ka during the late Wisconsinan (Prior, 1991; Eidem et al., 1999). The Alden Member is a massive, basal till with a bulk density (ρ_b) of approximately 1,700 kg/m^3. The Alden Member is classified as a loam, containing approximately 40 percent sand, 45 percent silt, and 15 percent clay. Unlike older tills in Iowa, the Alden Member has a high smectite content (approximately 69 percent, Kemmis et al., 1981). Previous investigations at the site revealed that the till is fractured (Eidem et al., 1999). Pumping and slug tests performed on a nest of piezometers 10 m north of the sampling location also suggest that fractures increase K_b in this till (Seo, 1996).

Column Preparation

A 4-m-deep trench was excavated using a backhoe to provide access to the till. The excavation trench was carved using a bench and tier method to provide multiple faces for fracture mapping and to ease column collection. Fractures were identified as planes with iron-oxide staining, or as leached zones in the till. Fractures were mapped using sheets of clear acetate on both vertical and horizontal faces in the trench, and fracture strike and dip was measured using a Brunton compass.

An intact column of till, 43 cm in diameter and 45 cm in length, was carved from the basal step of the excavation trench from a depth of 3.3 to 3.75 m using a shovel and putty knife (Figure 2). This column was one of eight collected as part of a larger study of fractured till in Iowa (Helmke et al., 2003a). The column was kept cylindrical by using a level and a section of polyvinyl chloride (PVC) pipe as a guide. A 61-cm-long piece of PVC with an interior diameter (ID) of 45.7 cm was placed over the column, leaving a 1-cm void between the column and the pipe. This annulus between the till and the casing was sealed using paraffin wax, a technique which has been demonstrated to prevent side-wall flow (Grisak et al., 1980; Kluitenberg et al., 1991). After the wax cooled (approximately 8 hours), a putty knife was used to separate the column from its base. The column was then winched from the trench and disks of high-density polyethylene (HDPE) (3-mm-thick) were placed at the column ends to prevent moisture loss during transport to the laboratory.

Laboratory Setup

In the laboratory, the ends of the column were carefully scraped with a putty knife to eliminate smear zones. The resulting length of the column was 40 cm. A 5-mm-thick layer of Ottawa Sand was placed at each end of the column and held in place by the HDPE disks. Perforated tubes (3-mm-ID HDPE) were fed through the sand to provide fluid access to the sand packs. Plywood pistons (19-mm-thick and 43-cm-diameter) were added to each end and sealed with silicone caulking. The ends and the walls of the column were mechanically compressed to 60 kPa to approximate the lithostatic stress at 3.5 m. Although care was exercised to minimize desaturation of the column, it is possible that some of the larger pores

drained during excavation and transport. To reduce the chances of entrapped air in these pores, the column was slowly re-saturated by upward flow for 7 days.

Three compounds were used as tracers for the solute transport experiment: potassium bromide, pentafluorobenzoate (PFBA), and disodium-1,4-piperazinediethane sulfonate (PIPES). These compounds do not sorb readily nor do they undergo biodegradation, so they are considered conservative tracers (Jaynes, 1993; Moline et al., 1997). The diffusion coefficients in pure aqueous solution (D_0) of Br and PFBA at 25°C are 1.8×10^{-9} and 7.6×10^{-10} m^2/s, respectively (Bowman and Gibbons, 1992). The D_0 of PIPES has not been determined experimentally, however the calculated D_0 using the Stokes-Einstein equation is 4.1×10^{-10} m^2/s (Helmke et al., 2003c). Conservative compounds with different D_0 values were selected because differences in the morphology of their BTCs would indicate matrix diffusion, thereby providing evidence of fracture flow. In-situ groundwater spiked with a 0.5 mM concentration (C_0) of the tracers was passed through the column for a period of 70 days. Although an upward gradient was applied (to prevent desaturation at the column base), groundwater flow was, in effect, downward because the column was inverted in the laboratory. The temperature of the column was maintained at a constant 12°C to simulate in-situ conditions. The flow rate was measured using a graduated cylinder and a stopwatch.

Effluent samples were passed through a 0.2 μm filter immediately upon collection and stored at 4°C until analyzed at the end of the experiment. Concentrations of Br, PFBA, and PIPES were determined by ion chromatography. Analytical precision (95 percent confidence limit) was determined for Br (0.63 mg/L), PFBA (1.14 mg/L), and PIPES (2.65 mg/L), by analyzing replicates of spiked samples using Student's t distribution (Harris, 1991).

Soil texture was determined using the sieve and pipette method (Walter et al., 1978). Sand, silt, and clay particle sizes used in this study were 2 to 0.063 mm, 0.063 to 0.002 mm, and <0.002 mm, respectively. Total porosity was determined gravimetrically by weighing a saturated soil sample, oven-drying it, dividing the difference by the density of water, then dividing this by the original volume of the sample. Pore volume (PV) was determined as the product of n_T and the volume of the column.

Models

Model Implementation

MIM Model

The input parameters required by the MIM in this paper were measured or estimated using both field and laboratory methods. Fluid flux (J_w) was calculated from the flow rate (Q) and cross-sectional area (A) of the column. Bulk hydraulic conductivity was calculated from J_w and hydraulic gradient (i) using Darcy's Law. Mobile porosity was calculated assuming that the mobile pores (fractures) may be represented as a series of parallel and orthogonal plates. In this case, n_m can be estimated by n_f (Sudicky, 1990):

$$n_f = 2\frac{2b}{2B} \tag{9}$$

where $2b$ is the fracture aperture and $2B$ is the fracture spacing. Fracture aperture may be estimated by the cubic law (Snow, 1969):

$$2b = \left(\frac{K_b 6\mu 2B}{\rho g}\right)^{\frac{1}{3}} \tag{10}$$

where K_b is bulk hydraulic conductivity, μ is fluid viscosity, ρ is water density, and g is the acceleration due to gravity.

When the velocity of a solute in a fracture is large and the flow path is short, the effect of longitudinal dispersion along the fracture axis is negligible (Tang et al., 1981; Sudicky and Frind, 1982; Sudicky, 1990). Moreover, the total dispersion coefficient D may be related to D_m by:

$$D = \frac{D_m n_{im}}{\theta_T} \tag{11}$$

Because the ratio of n_{im}/n_m is a very small quantity for a fractured medium, D is likely to be extremely small. Thus, D was set equal to the D_0 of each compound for the simulations.

Estimates of α were calculated using the relation

$$\alpha = \frac{aD_e n_{im}}{l^2} \tag{12}$$

where a is a shape factor, D_e is the effective diffusion coefficient, n_{im} is the immobile porosity, and l is a characteristic length (Parker and Valocchi, 1986; Sudicky, 1990). D_e was determined for each compound using the radial diffusion cell method (Novakowski and van der Kamp, 1996; Helmke et al., 2003c). This method also produced estimates of the effective diffusive porosity (n_{De}), which were used as an approximation of n_{im} in Equation 12. This equation has been shown to work well for a system of equally-spaced, parallel fractures (Sudicky, 1990) and for spherical soil aggregates (Rao et al., 1980). For the purposes of this

paper, the matrix blocks were assumed to be prismatic slabs of width equal to fracture spacing ($2B$). Therefore, a and l were set to 3 and B (obtained from field measurements in Helmke and Simpkins, 2003), respectively.

PDFM Model

The input requirements for the PDFM are essentially the same as for the MIM. Velocity in the fractures was estimated using the average linear velocity equation

$$v = \frac{q}{n_f} \tag{13}$$

where q is specific discharge, and n_f is the fracture porosity (see Equation 9). Aqueous diffusion coefficients were used for D in Equation 3, and the effective matrix diffusion coefficients obtained from radial diffusion cell experiments (Helmke et al., 2003c) were used for D' in Equation 4 corrected for temperature.

3-D DFM Model

A 3-D DFM requires that the location, size, and orientation of each fracture be placed explicitly into the model. This modeled network of fractures is referred to as a Discrete Fracture Network (DFN). Actual geometry of all fractures at the field scale is rarely obtainable, so sets of statistically similar fractures are commonly used to represent fractures surveyed in the field (Doe, 1997). To properly characterize a DFN, stochastic distributions of fracture location, intensity, orientation, and size must be determined.

The first step in creating a DFN is to decide how the fractures will be placed into the model. The method used for this paper was to place each fracture randomly in space (a Poisson point process), and then expand each fracture sequentially in the appropriate orientation to the desired size. Fractures that intersect are truncated at a frequency equal to the termination percentage. This approach is referred to as the Enhanced Baecher Model (Baecher et al., 1977; Dershowitz et al., 1994).

Perhaps the most important information regarding a fracture network is fracture intensity. Fracture intensity reflects the degree of fracturing in a medium. Fracture intensity may be described by several parameters, including the number of fractures per distance (P_{10}; the inverse of fracture spacing, 2B), the number of fractures per area (P_{20}), the length of fractures per area (P_{21}), the number of fractures per volume (P_{30}), and the surface area of fractures per volume (P_{32}). In this study, P_{10}, P_{20}, and P_{21} were obtained directly from field measurements and maps. P_{30} and P_{32} were estimated by creating virtual sets of 3-D fractures using FracMan, then slicing them until the simulated P_{21} matched the observed value (Helmke et al., 2003b). Of all the measures of fracture intensity, P_{32} is the most useful because it increases as a linear function with scale (Baecher et al., 1977), allowing models to be expanded in size.

The stochastic distribution of fracture orientation was determined by fitting a Fisher distribution to fracture poles plotted on a stereonet. This was achieved by using the ISIS module provided in the FracMan software package, which also calculates the level of statistical significance using the Kolmogorov-Smirnov method (Conover, 1980). The fracture length distribution was obtained by fitting a log-normal distribution to the fracture length data collected during mapping. Fracture termination data was obtained from the

fracture trace map. The FracMan software package (Dershowitz et al., 1994) was used to generate the stochastic DFN after the stochastic distribution of the fractures was established.

Methods for determining transmissivity of individual fractures in till are not available at this time. Therefore, fracture transmissivity was adjusted in the model until the simulated K_b equaled the observed K. A log-normal T distribution with a standard deviation of 0.5 was employed (Dershowitz et al., 1994). Fracture aperture was calculated from the T of each fracture using the Cubic Law (Snow, 1969). The effective properties of the matrix (D_e and n_{De}) were determined in the laboratory using radial diffusion cells (Helmke et al., 2003c). BTCs were simulated by particle tracking within the program MAFIC (Lee et al., 1994).

Statistical Evaluation

Model goodness-of-fit was evaluated using the modified index of agreement (d_1) (Willmott et al., 1985) as well as the better-known root mean squared error (RMSE) and coefficient of determination (R^2). The parameter d_1 is given by

$$d_1 = 1.0 - \frac{\sum_{i=1}^{N} |O_i - P_i|}{\sum_{i=1}^{N} \left(|P_i - \overline{O}| + |O_i - \overline{O}| \right)} \tag{14}$$

where O and P are the observed and modeled simulated data, and N is the number of observations. Values of d_1 vary from 0 to 1, with 1 indicating a perfect fit between the simulated and observed data. Therefore, d_1 may be interpreted in a fashion similar to R^2. The quantity d_1 is considered superior to R^2 and RMSE because it is less sensitive to outliers than R^2 and RMSE and because d_1 is sensitive to additive and proportional differences

(unlike R^2). The utility of d_1 has been demonstrated in the validation of hydrologic models (Legates and McCabe, 1999).

There is uncertainty associated with goodness-of-fit parameters such as d_1, RMSE, and R^2. Unfortunately, statistical techniques for establishing confidence intervals for these parameters have not been established, so numerical procedures such as the bootstrap method must be employed (Efron, 1981; Legates and McCabe, 1999). For the purposes of this study, a computer program was developed to sample and re-sample random pairs of observed/simulated data to generate a population of 1,000 goodness-of-fit estimates. Boxplots of d_1 were then generated to compare the goodness-of-fit data for each BTC. Confidence intervals of mean d_1, RMSE, and R^2 were calculated using Student's t distribution (Walpole, 2001). The Kruskal-Wallace and Mann-Whitney tests were used to determine the level of statistical difference between the modeling approaches for each compound (Conover, 1980).

Results

Estimation of Input Parameters

Excavation revealed that the till contained numerous sub-horizontal and sub-vertical fractures from ground surface to the base of the soil pit (a depth of 4 m). Fracture spacing ranged from < 2 cm near the surface to approximately 4.6 cm at 4 m depth. The most prominent fractures were observed below 3 m depth where the till was in a transition zone (partially oxidized) between weathered (oxidized) and unweathered (unoxidized) till. At this depth, the fractures were stained reddish brown (10 YR 5/8) in contrast to the olive-brown

(2.5 Y 5/4) till matrix. The column carved from a depth of 3.3 to 3.7 m shows the prominent iron-stained fractures (Figure 2).

The fractures mapped at a depth of 3.3 m were dense and were preferentially oriented (Figure 3). Measures of fracture intensity at this depth were 23.2 fractures/m (P_{10}), 23.3 m/m^2 (P_{21}), 643 fractures/m^3 (P_{30}), and 24.4 m^2/m^3 (P_{32}) (Table 3). Analysis of fracture strike and dip revealed the presence of two fracture sets - both predominantly vertical and striking northeast-southwest. The first fracture set followed a Fisher distribution with a trend of 326.0°, plunge of 16.1°, and Fisher dispersion (k) of 6.13 (Kolmogorov-Smirnov (K.S.) confidence of 98.4 percent that the distribution fit the data). The second fracture set displayed a trend of 124.5°, plunge of 10.1°, and a k of 4.85 (K.S. 98.8 percent).

The physical properties of the till column were consistent with previous studies of the Alden Member till. The (ρ_b) of the till column was 1,830 kg/m^3. Soil texture was a loam, with 48.2 percent sand, 37.0 percent silt, and 14.8 percent clay. The n_T was 29.6 percent, resulting in a calculated PV of 0.0172 m^3. The K_b of the column was 6.8 x 10^{-8} m/s. Measurements of D_e (D' for the PDFM) at 23°C were 5.8 x 10^{-10}, 3.5 x 10^{-10}, and 1.7 x 10^{-10} m^2/s^2 for Br, PFBA, and PIPES, respectively (Helmke et al., 2003c). These values of D_e were modified by the Stokes-Einstein equation to correct for the temperature difference between 23°C and 12°C. The resulting values of D_e were 4.3 x 10^{-10}, 2.6 x 10^{-10}, and 1.3 x 10^{-10} m^2/s, respectively (Tables 1, 2, and 4). Effective diffusive porosities (n_{De}, n_{im} for the MIM, and n_{mat} for the PDFM) were 26.8, 25.2, and 21.4 percent for Br, PFBA, and PIPES.

Breakthrough Curves

Detectable concentrations ($C/C_0 > 0.02$) of the three tracers were observed in the column effluent after 4.7 days, resulting in a first-arrival velocity of at least 0.085 m/day (Figure 4). Breakthrough for Br, PFBA, and PIPES was achieved after 13.8, 18.9, and 19.2 days, respectively. The center-of-mass velocities ($C/C_0 = 0.5$) calculated from these breakthrough times are 0.029, 0.021, and 0.021 m/day, respectively. All three solutes resulted in breakthrough times earlier than the time for one PV (19.9 days), providing evidence that preferential flow paths (presumably fractures) influenced the BTCs.

Separation of the three tracers indicated that matrix diffusion was a controlling process in the till. The concentration of PIPES increased more rapidly than Br or PFBA during the first 30 days of the experiment, resulting in a separation between the BTCs. This separation was likely due to the lower D_e of PIPES compared to Br and PFBA, and provides evidence that matrix diffusion was a controlling mechanism as the solutes passed through the column. A similar separation of PIPES and Br was observed in BTCs produced from a column of fractured saprolite from Tennessee (Moline et al., 1997). Likewise, Grisak et al. (1980) observed that calcium increased in concentration more rapidly than chloride during a laboratory experiment using an intact column of fractured till from Canada. The authors attributed the separation of calcium and chloride to differences in D_e (5×10^{-11} and 1.9×10^{-11} m^2/s, respectively).

The solutes reached a C/C_0 of 0.98 or greater after a period of 50 days, indicating that the concentration between the fractures and the matrix were not at equilibrium for the majority of the test. Using the EPM approach with advection only (i.e. plug flow), the predicted time for C/C_0 to equal 1 would be 19.9 days (1 PV). Using fracture velocity

calculated by the cubic law (9.6 m/day), C/C_0 would equal 1 after only 1 hour. Clearly, a process such as matrix diffusion is serving to retard mass as it flows through the column. Therefore, use of the EPM (that assumes fractures are at equilibrium with the matrix) would be inappropriate for these till units at the flow rates and timescales of this study. Over long timescales and low flow rates, fractured till could behave as an EPM if the fractures were at equilibrium with the matrix, as has been documented by McKay et al. (1998). However, the transient nature of hydraulic head and contaminant sources at the field scale is unlikely to allow equilibrium to occur.

Model Simulations

The MIM was successful at simulating some, but not all the BTCs accurately (Figure 4a). The simulated Br BTC closely matched the observed data (d_1 = 0.947, Table 5). The PFBA and PIPES simulations, however, over predicted solute concentration during the initial phase of the experiment (d_1 = 0.884 and 0.751, respectively). The simulated PFBA and PIPES BTCs appear to instantly rise to a C/C_0 of 0.1 and 0.38, respectively. However, closer inspection reveals that these concentrations were predicted after 1 hour; which corresponds to the calculated fracture velocity of 9.6 m/day. However, it is likely that the MIM's inability to accurately simulate BTCs at short timescales for solutes with low D_e values is a result of the first-order approximation of matrix diffusion. This effect would be more pronounced for systems with large fracture spacing under short timescales using tracers with small D_e values. Despite its limitations, the MIM reproduced the overall morphology of the three BTCs, and would likely be applicable at the field scale where transport distances are large with respect to fracture spacing. In addition, the model's disadvantages should be weighed against the

few input parameters required and the model's computational efficiency (CXTFIT 2.1 simulated each BTC in less than 2 CPU seconds).

The morphology of the BTCs produced by the PDFM simulations resembled the observed data better than the MIM (Figure 4b). The model, like the MIM, predicted the Br BTC well (d_1 = 0.932); and less well in the case of PFBA and PIPES (d_1 = 0.881 and 0.836, respectively). The PDFM simulations of Br, PFBA, and PIPES, however, over-predicted concentration during the first 30 days of the experiment. Unlike the MIM simulations, predicted concentration rose gradually, similar to the observed BTCs. The PDFM was used to simulate Br BTCs for a trench-to-trench test in Canada (McKay et al., 1993b). In that study, the model successfully simulated the observed BTCs, and only minor adjustment of $2b$ and $2B$ were necessary to improve model fit. Favorable results were also obtained using the PDFM in a study in Denmark using large columns of fractured till in the forward mode (Jørgensen et al., 1998). Using FRACTRAN, the PDFM was more difficult to assemble than the MIM because it required specifying the spatial location of the fracture explicitly within the model. Once constructed, however, simulations required only 3 CPU seconds to complete.

The stochastic DFN created during the 3-D DFM simulation illustrates the density of the fracture network in the till. In a cube only 40 cm on a side, 103 fractures were required to produce the fracture intensity of 24.4 m^2/m^3. Triangulation of the fractures generated a finite element mesh of 1884 elements. Ten million particles were required to generate the relatively smooth BTCs in this study. This process required approximately 14 hours on a standard 400 MHz PC. The 3-D DFM produced BTCs that most closely matched the observed BTCs of the three models (d_1 = 0.937, 0.939, and 0.958 for Br, PFBA, and PIPES).

However, the breakthrough times were approximately 5 to 10 percent faster than observed. Although the BTCs appear "choppy" because of their stochastic nature, the 3-D DFM is the most accurate of the three modeling approaches.

Statistical Evaluation

The goodness-of-fit analysis demonstrated that all three modeling approaches were reasonable predictors of the BTCs (Figure 5 and Table 5), yet reflected the apparent differences between the model predictions (Figure 4). The RMSE ranged between 0.036 and 0.168 for the three solutes and three models. The highest RMSE was for the MIM prediction of the PIPES BTC, which is not surprising given the unlikely rapid increase of concentration during the initial phase of the simulation. The MIM, PDFM, and 3-D DFM all fit the Br BTC well, with d_1 values ranging from 0.932 to 0.947. The 3-D DFM also predicted the PFBA and PIPES BTCs with relative accuracy, as indicated by the high d_1 statistics (0.939 and 0.942, respectively). The MIM and PDFM, on the other hand, predicted PFBA and PIPES BTCs that were inferior to the 3-D DFM fits. The d_1 value for the MIM prediction of the PIPES BTC was 0.751, which, although not a low number (i.e. greater than 0.5), was the poorest of all the d_1 statistics. The R^2 values for the predicted BTCs were greater than 0.9. This value would suggest that all models fit the data exceptionally well, however visual inspection of the BTCs and results from RMSE and d_1 indicate otherwise. It is also interesting to note that the R^2 statistic for the poorest fitting BTC (the MIM prediction of PIPES) was relatively high (0.949). Clearly, the R^2 statistic is insensitive to consistent differences between the BTC and the model, and provides an example of the limitation of using a correlation parameter to indicate goodness-of-fit (see Willmott et al., 1985). Most

researchers choose not to quantify model performance with a goodness-of-fit measure. One notable exception is the application of the MIM, where it is common to report R^2 (e.g. Gaber et al., 1995; Toride et al., 1999). However, as pointed out in this paper, R^2 may not always provide the best indicator of model performance.

A more rigorous comparison of model goodness-of-fit is provided by statistical analysis of d_1. Boxplots of the d_1 populations were generated from 1,000 bootstrap iterations (Figure 5). Visual inspection of the overlap of the 25th and 75th percentiles of the populations (boxes) and 1.5 interquartile ranges (whiskers) indicates that the three models predicted the Br BTC with certainty, and less so for PFBA and PIPES. The Kruskal-Wallis test confirmed that differences between the MIM, PDFM, and 3-D DFM predictions of the Br BTC were not statistically significant at the $\alpha = 0.05$ level. Pair-wise comparison of the MIM and PDFM predictions of the PFBA BTC by the Mann-Whitney test revealed a lack of statistical difference at the $\alpha = 0.05$ level. The remaining model predictions of the PFBA and PIPES BTCs were all statistically significant by the Mann-Whitney test ($\alpha < 0.01$).

The lack of statistical difference between the model simulations of Br transport suggests that features unique to each modeling approach do not significantly affect the results for this compound. Differences between models become more pronounced for compounds with lower D_e values (most notably PIPES). It is likely that the first-order approximation of matrix diffusion employed by the MIM may fail in cases were D_e is small or fracture spacing is large. A second-order approach should be used in these cases (Sudicky, 1990). Moreover, in cases where matrix diffusion governs the shape of a BTC (as in the Br BTC), matrix diffusion may obscure the comparatively minor affect of fracture geometry and orientation. For compounds that are less susceptible to matrix diffusion (i.e. PFBA and PIPES), the

oversimplification of the fracture network may result in rapid transport times that are unrealistic.

Conclusions

Three modeling approaches (the MIM, PDFM, and 3-D DFM) were used to simulate solute transport through fractures in till and compared to laboratory BTCs. The goodness-of-fit analysis demonstrated that all three modeling approaches were reasonable predictors of the BTCs (d_I ranged from 0.751 to 0.959), yet reflected the apparent differences between the model predictions. Statistical analyses indicated that differences between the three methods were not significant ($\alpha = 0.05$) when simulating Br transport. Thus, models that are more elaborate do not necessarily produce results that are more accurate. Simulations of PFBA and PIPES, on the other hand, revealed that the 3-D DFM fit was superior to the MIM and PDFM ($\alpha = 0.01$). This difference was largely due to the MIM and PDFM predicting more rapid transport of PFBA and PIPES than observed during the initial portions of the experiment. The difference in predicted BTCs appears to be a function of the D_e of each compound. If the rate of diffusion is low (as in the case of PFBA and PIPES), the first-order approximation of diffusion employed by the MIM may produce inaccurate results, indicating that a second-order approach should be used (i.e. the PDFM and 3-D DFM). This effect would likely be more pronounced in cases where fracture spacing is large and/or timescales are small.

In cases where D_e is particularly small (e.g. PIPES), differences between the modeling approaches might also be a result of how the models incorporate fracture orientation and geometry. This effect would likely be obscured by matrix diffusion if D_e is

large. The MIM and PDFM assume that fractures provide flow-paths oriented in the direction of groundwater flow, which may be overly simplistic. The more accurate orientation and geometry of fractures in the 3-D DFM produce flow-paths that are slightly longer than those predicted using a simplified geometry, which would serve to increase residence time (Helmke et al., 2003b). However, this effect is likely to be small for this till due to the small spacing (4.3 cm) and great density (643 fractures/m^3) of the fracture network.

The MIM and PDFM methods had the advantage of requiring fewer input parameters and were computationally efficient (run times less than 3 seconds). The 3-D DFM may be a more compelling model because it is capable of representing realistic fracture orientation and geometry, however it is a difficult model to construct and is computationally less efficient than the MIM or PDFM (run times greater than 14 hours per BTC).

Further investigations are required to test and compare these methods to see if they apply to the field scale. At large scales, the MIM and PDFM will likely prove more practical than the 3-D DFM due to the greater computational effort required by simulating large numbers of fractures. On the other hand, in cases where fracture spacing is large with respect to the investigation scale, or during very short time scales, discrete fracture models are likely to produce superior results than the simplified MIM or PDFM approaches. It is for this reason that 3-D DFMs have been favored for simulations of solute transport through fractured rock (Doe, 1997).

Regardless of the simulation approach, fractures should be incorporated into solute transport models in glaciated terrain. Recent advances in computer codes and hardware, and the development of independent methods for obtaining input parameters make this approach

much easier than it has been in the past. Proper representation of fractures offers distinct advantages over the traditional EPM approach, and should provide more reliable predictions of solute transport through fractured till.

Acknowledgements

This research was funded by grants from the American Geophysical Union (Horton Grant), the Association of Ground Water Scientists and Engineers, the Geological Society of America, Sigma Xi, and the USEPA through an Interagency Agreement DW12036252 to the Agricultural Research Service. The authors wish to thank E. A. Sudicky and R. McLaren at the University of Waterloo for the use of FRACTRAN, and T. Doe and W. Dershowitz at Golder Associates for access to the FracMan/MAFIC software package. We thank P. Jardine and G. Moline for the suggestion of using PIPES as a tracer.

References

Anna, L. O. 1998. Preliminary three-dimensional discrete fracture model of the Topopah Spring Tuff in the Exploratory Studies Facility, Yucca Mountain Area, Nye County, Nevada. U.S. Geological Survey Open-File Report 97-834, Denver, Colorado. 41 p.

Baecher, G. B., N. A. Laney, H. H. Einstein. 1977. Statistical description of rock properties and sampling. Proceedings of the 18th U.S. Symposium on Rock Mechanics, American Institute of Mining Engineers. pp. 5C1-8.

Bowman, R. S. and J. S. Gibbens. 1992. Difluorobenzoates as nonreactive tracers in soil and ground water. Ground Water. v. 30, pp. 8-14.

Brockman, C. S. and J. P. Szabo. 2000. Fractures and their distribution in the tills of Ohio. Ohio Journal of Science. v. 100, n. 3/4, pp. 39-55.

Brusseau, M. L., Z. Gerstl, D. Augustijn, and P. S. C. Rao. 1994. Simulating solute transport in an aggregated soil with the dual-porosity model: measured and optimized parameter values. Journal of Hydrology. v. 163, pp. 187-193.

Coats, K. H. and B. D. Smith. 1964. Dead-end pore volume and dispersion in porous media. Soc. Pet. Eng. J. v. 4, pp. 73-84.

Connell, D. E. 1984. Distribution, characteristics, and genesis of joints in fine-grained till and lacustrine sediments, eastern and northwestern Wisconsin. Master's Thesis, University of Wisconsin, Madison. 443 p.

Conover, W. J. 1980. Practical Nonparametric Statistics (Second Edition). John Wiley and Sons, New York, New York, 493 pp.

Doe, T. 1997. Understanding and solving fracture flow problems. Water Engineering Management. v. 144, pp. 36-43.

Dershowitz, W., G. Lee, J. Geier, S. Hitchcock, and P. R. La Plointe. 1994. FracMan version 2.4 – Interactive discrete feature data analysis, geometric modeling and exploration simulation. Golder Associates, Inc., Redmond, Washington. 171 p.

Efron, B. 1981. Nonparametric estimates of standard error: The jackknife, the bootstrap, and other methods. Biometrica. v. 68, pp. 589-599.

Eidem, J. M., W. W. Simpkins, and M. R. Burkart. 1999. Geology, groundwater flow, and water quality in the Walnut Creek watershed. Journal of Environmental Quality. v. 28, pp. 60-69.

Freeze, R. A. and J. A. Cherry. 1979. Groundwater. Prentice Hall Pub. 604 p.

Gaber, H. M., W. P. Inskeep, S. D. Comfort, and J. M. Wraith. 1995. Nonequilibrium transport of atrazine through large intact soil cores. Soil Science of America Journal. v. 59, pp. 60-67.

Grisak, G. E. and J. F. Pickens. 1980. Solute transport through fractured media: 1. The effect of matrix diffusion. Water Resources Research. v. 16, pp. 719-730.

Grisak, G. E., J. F. Pickens, and J. A. Cherry. 1980. Solute transport through fractured media: 2. Column study of fractured till. Water Resources Research. v. 16, pp. 731-739.

Harris, D. C. 1991. *Quantitative Chemical Analysis, Third Ed.*, W. H. Freeman and Company, 782 p.

Harrison, B., E. A. Sudicky, and J. A. Cherry. 1992. Numerical analysis of solute migration through fractured clayey deposits into underlying aquifers. Water Resources Research. v. 28, pp. 515-526.

Helmke, M. F. and W. W. Simpkins. 2003. Chapter 5: Effect of fractures on hydraulic conductivity of till units in Iowa. In unpub. Ph.D. dissertation, Iowa State University, pp. 144-167.

Helmke, M. F., W. W. Simpkins, and R. Horton. 2003a. Chapter 1: Fracture dominated transport of nitrate and atrazine through till in Iowa. In unpub. Ph.D. dissertation, Iowa State University, pp. 5-37.

Helmke, M. F., W. W. Simpkins, and R. Horton. 2003b. Chapter 3: Simulation of solute transport through fractured till using a stochastic, three-dimensional, discrete-fracture model. In unpub. Ph.D. dissertation, Iowa State University, pp. 80-118.

Helmke, M. F., W. W. Simpkins, and R. Horton. 2003c. Chapter 4: Laboratory measurement of effective diffusion parameters in fractured soil. In unpub. Ph.D. dissertation, Iowa State University, pp. 119-143.

Herbert, A. W., G. W. Lanyon, J. E. Gale, and R. MacLeod. 1992. Discrete fracture network modelling for phase 3 of the Stripa project using NAPSAC. In Situ Experiments at the Stripa Mine, OECD Nuclear Energy Agency and Swedish Nuclear Fuel and Waste Management Company. pp. 219-235.

Jaynes, D. B. 1993. Evaluation of fluorobenzoate tracers in surface soils. Ground Water. v. 32, pp. 532-538.

Jones, M. A., A. B. Pringle, I. M. Fulton, and S. O'Neill. 1999. Discrete fracture network modeling applied to groundwater resource exploitation in southwest Ireland. In: McCaffey, K. J. W., L. Lonegran, and J. J. Wilkinson (eds) Fractures, Fluid Flow and Mineralization. Geological Society, London, Special Publications. v. 155, pp. 83-103.

Jørgensen, P. R., L. D. McKay, and N. ZH. Spliid. 1998. Evaluation of chloride and pesticide transport in a fractured clayey till using large undisturbed columns and numerical modeling. Water Resources Research. v. 34, pp. 539-553.

Jørgensen. P. R. and N. H. Spliid. 1992. Mechanisms and rates of pesticide leaching in shallow clayey till. European Conference on Integrated Research for Soil and Sediment Protection and Remediation. MECC, Maastricht, the Netherlands. 11 p.

Jury, W. A., W. R. Gardner, and W. H. Gardner. 1991. Soil Physics, Fifth Edition. John Wiley and Sons, Pub. 328 p.

Keller, C. K., G. van der Kamp, and J. A. Cherry. 1988. Hydrogeology of two Saskatchewan tills, I. Fractures, bulk permeability, and special variability of downward flow. Journal of Hydrology. v. 101, pp. 97-121.

Kemmis, T. J., E. A. Bettis III, and G. R. Hallberg. 1992. Quaternary geology of Conklin Quarry. Guidebook Series no. 13. Iowa Department of Natural Resources. 41 p.

Kemmis, T. J., G. R. Hallberg, and A. J. Lutenegger. 1981. Depositional environments of glacial sediments and landforms on the Des Moines Lobe, Iowa. Guidebook Series no. 6. Iowa Department of Natural Resources. 132 p.

Klint, K. E. S. and P. Gravensen. 1999. Fractures and biopores in Weichselian clayey till Aquitards at Flakkebjerg, Denmark. Nordic Hydrology. v. 30, n. 4/5, pp. 267-284.

Kluitenberg, G. L., J. R. Bilskie, and R. Horton. 1991. Rubberized asphalt for sealing cores of shrinking soil. Soil Science Society of America Journal. v. 55, pp. 1504-1507.

Legates, D. R. and G. J. McCabe Jr. 1999. Evaluating the use of "goodness-of-fit" measures in hydrologic and hydroclimatic model validation. Water Resources Research. v. 35, pp. 233-241.

McKay, L. D., D. J. Balfour, and J. A. Cherry. 1998. Lateral chloride migration from a landfill in a fractured clay-rich glacial deposit. Ground Water. v. 36, pp. 988-999.

McKay, L. D., J. A. Cherry, and R. W. Gillham. 1993a. Field experiments in a fractured clay till: 1. Hydraulic conductivity and fracture aperture. Water Resources Research. v. 29, pp. 1149-1162.

McKay, L. D., J. A. Cherry, and R. W. Gillham. 1993b. Field experiments in a fractured clay till: 2. Solute and colloid transport. Water Resources Research. v. 29, pp. 3879-3890.

Meijerink, J. A., and H. A. van der Vorst. 1977. An iterative solution method for linear systems of which the coefficient matrix is a symmetric M-matrix. Mathematics of Computation. v. 31, n. 137, pp. 148-168.

Miller, I., G. Lee, and W. Dershowitz. 1997. MAFIC version 1.6 – matrix/fracture interaction code with heat and solute transport. Golder Associates, Inc., Redmond, Washington. 87 pp.

Moline, G. R., C. R. Knight, and R. Ketcham. 1997. Laboratory measurement of transport processes in a fractured limestone/shale saprolite using solute and colloid tracers. Abstracts with Programs, Geological Society of America. v. 29, n. 6, p. 370.

Novakowski, K. S. and G. van der Kamp. 1996. The radial diffusion method 2. A semianalytical model for the determination of effective diffusion coefficients, porosity, and adsorption. Water Resources Research. v. 32, pp. 1823-1830.

Parker, J. C. and A. J. Valocchi. 1986. Constraints on validity of equilibrium and first-order kinetic transport models in structural soils. Water Resources Research. v. 22, pp. 399-407.

Parker, J. C. and M. Th. van Genuchten. 1984. Determining Transport Parameters from Laboratory and Field Tracer Experiments. Virginia Agricultural Experiment Station Bulletin. v. 84, pp. 1-97.

Prior, J. C. 1991. Landforms of Iowa. University of Iowa Press, Iowa City, Iowa. 154 p.

Rao, P. S. C., D. E. Rolston, R. E. Jessup, and J. M. Davidson. 1980. Solute transport in aggregated porous media: theoretical and experimental evaluation. Soil Science Society of America Journal. v. 44, pp. 1139-1146.

Seo, H. H. 1996. Hydraulic properties of Quaternary stratigraphic units in the Walnut Creek watershed. Master's Thesis. Iowa State University. 145 p.

Skopp, J. and A. W. Warrick. 1974. A two-phase model for the miscible displacement of reactive solutes in soils. Soil Science Society of America Proceedings. v. 38, pp. 545-550.

Snow, D. T. 1969. Anisotropic permeability of fractured media. Water Resources Research. v. 5, pp. 1273-1289.

Sudicky, E. A. 1989. The Laplace transform Galerkin technique: a time-continuous finite element theory and application to mass transport in groundwater. Water Resources Research. v. 25, pp. 1833-1846.

Sudicky, E. A. 1990. The Laplace transform Galerkin technique for efficient time-continuous solution of solute transport in double-porosity media. Geoderma. v. 46, pp. 209-232.

Sudicky, E. A. and E. O. Frind. 1982. Contaminant transport in fractured porous media: Analytical solutions for a system of parallel fractures. Water Resources Research. v. 18, pp. 1634-1642.

Sudicky, E. A. and R. G. McLaren. 1998. FRACTRAN User's Guide. An efficient simulator for two-dimensional, saturated groundwater flow and solute transport in porous or discretely-fractured porous formations. Groundwater Simulations Group, Waterloo Centre for Groundwater Research. University of Waterloo, Ontario, Canada. 97 p.

Tang, D. H., E. O. Frind, and E. A. Sudicky. 1981. Contaminant transport in fractured porous media: Analytical solution for a single fracture. Water Resources Research. v. 17 n. 3, pp. 555-564.

Therrien, R., E. A. Sudicky, and R. G. McLaren. 2000. User's guide for NP 3.49. A preprocessor for FRAC3DVS 3.49: an efficient simulator for three-dimensional, saturated-unsaturated groundwater flow and chain-decay solute transport in porous or discretely-fractured porous formations. Groundwater Simulations Group, Waterloo Centre for Groundwater Research. University of Waterloo, Ontario, Canada. 90 p.

Toride, N, F. J. Leij, and M. Th. van Genuchten. 1999. The CXTFIT code for estimating transport parameters from laboratory or field tracer experiments version 2.1. Research Report No. 137. U. S. Salinity Lab., USDA, ARS, Riverside, CA, 119 p.

Toride, N., F., F. J. Leij, and M. Th. van Genuchten. 1993. A comprehensive set of analytical solutions for nonequilibrium solute transport with first-order decay and zero-order production. Water Resources Research. v. 29, pp. 2167-2182.

van Genuchten, M. Th. 1981. Non-equilibrium transport parameters from miscible displacement experiments. Research Report 119, U. S. Salinity Lab., USDA-ARS, Riverside, CA.

van Genuchten, M. Th. and P. J. Wierenga. 1976. Mass transfer studies in sorbing porous media, I, Analytical solutions. Soil Science Society of America Journal. v. 40, pp. 473-481.

van Genuchten, M. Th. and R. J. Wagenet. 1989. Two-site/two-region models for pesticide transport and degradation: theoretical development and analytical solutions. Soil Science Society of America Journal. v. 53, pp. 1303-1310.

Walpole, R. E., R. H. Myers, S. L. Myers, and K. Ye. 2001. Probability and Statistics for Engineers and Scientists, 7th Ed. Pearson Education. 752 pp.

Walter, N. F., Hallberg, G. R., and Fenton, T. E. 1978. Particle-size analysis by the Iowa State University Soil Survey Laboratory, in Hallberg, G. R. ed.: Standard procedures for evaluation of Quaternary materials in Iowa: Iowa Geological Survey, Technical Information Series, no. 8, p. 61-74.

Willmott, C. J., S. G. Ackleson, R. E. Davis, J. J. Feddema, K. M. Klink, D. R. Legates, J. O'Donnell, and C. M. Rowe. 1985. Statistics for the evaluation and comparison of models. Journal of Geophysical Research. v. 90, pp. 8995-9005.

Zheng, C. and P. P. Wang. 1999. MT3DMS: A modular three-dimensional multispecies model for simulation of advection, dispersion and chemical reactions of contaminants in groundwater systems; Documentation and User's Guide. Contract Report SERDP-99-1. U.S. Army Engineer Research and Development Center, Vicksburg, MS.

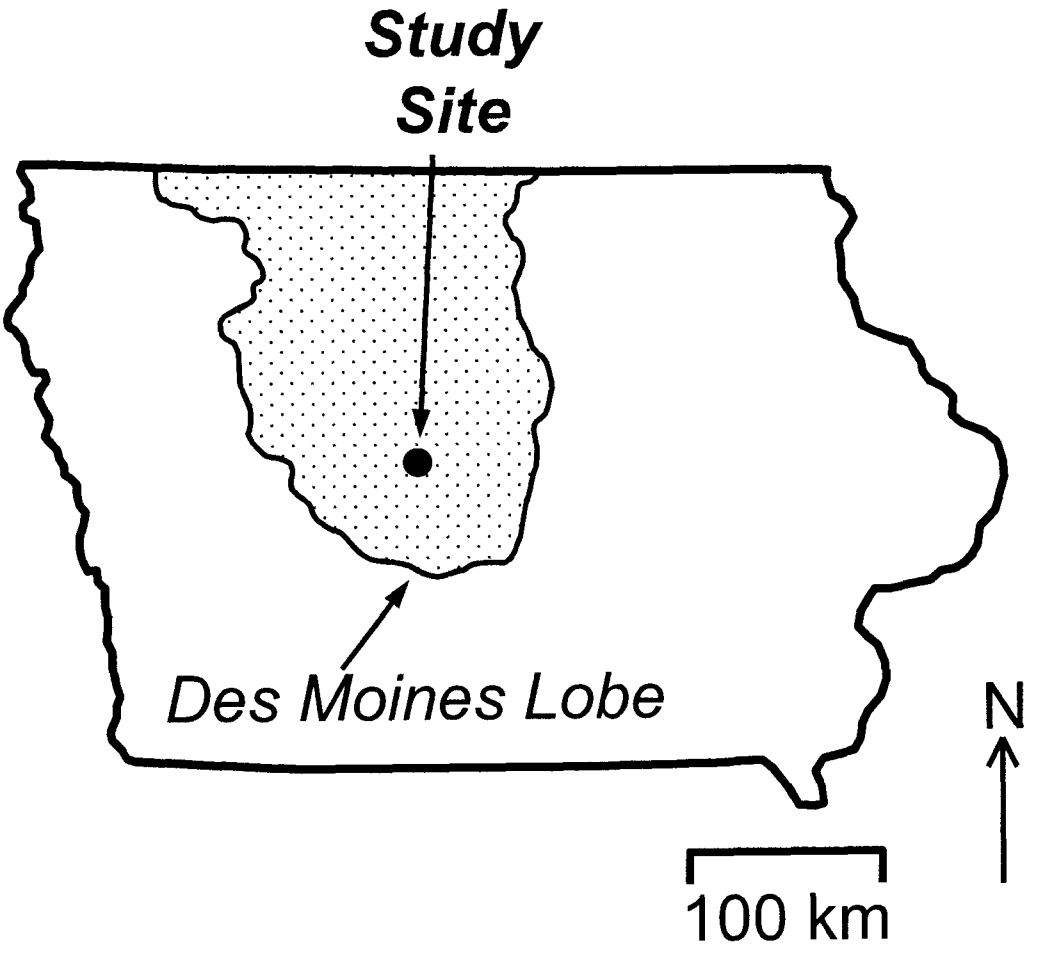

Figure 1. Map of Iowa showing the location of the study site within the Des Moines Lobe landform region (after Prior, 1991).

Figure 2. Photograph of the till column (43-cm diameter and 45-cm length) in the field prior to encasement in the field. Note sub-vertical, iron-stained fractures. Putty knife for scale.

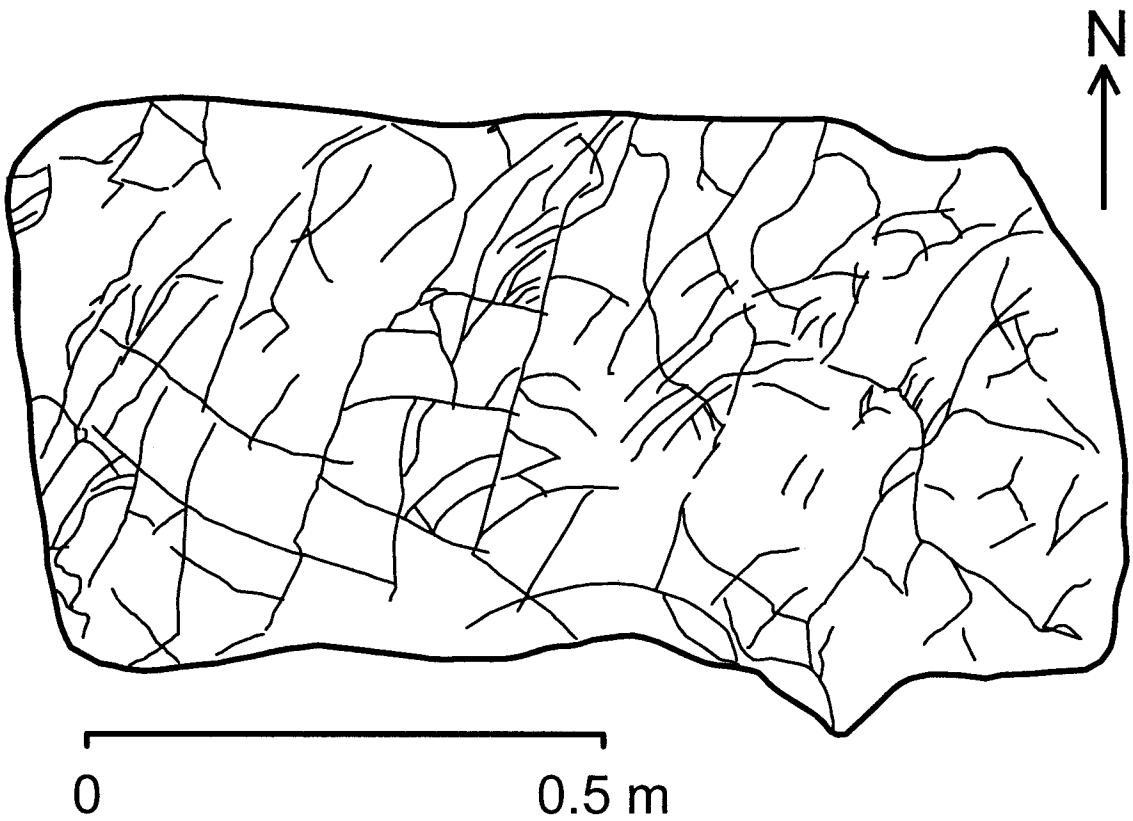

Figure 3. Plan-view map of fractures observed at a depth of 3.3 m at the site. Fractures predominantly sub-vertical in orientation at this depth. Trend of predominant fractures is from northeast to southwest.

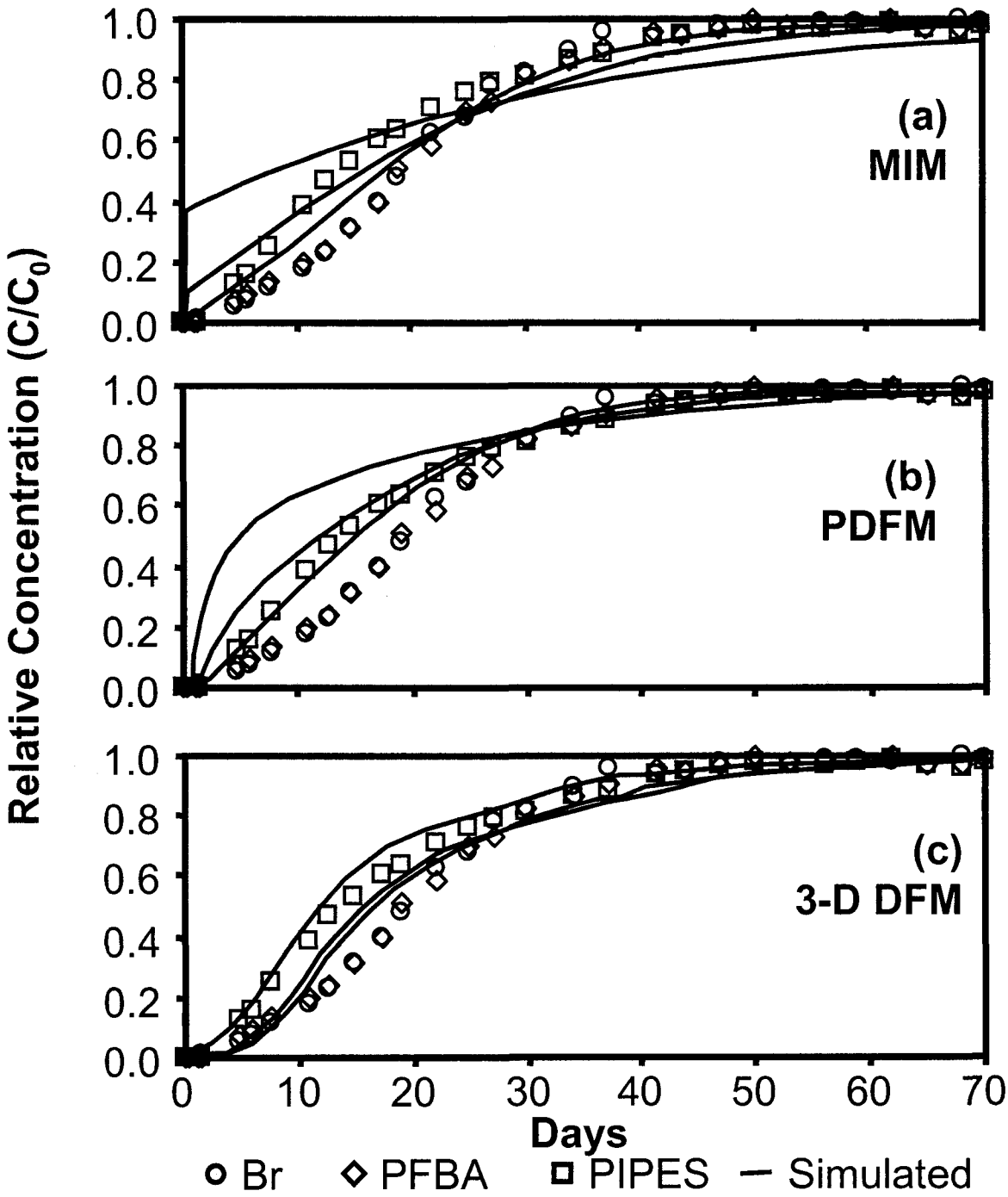

Figure 4. Breakthrough curves for Br, PFBA, and PIPES from column tracer tests. Breakthrough curves simulated by the Mobile-Immobile Model (MIM), Parallel-plate Discrete Fracture Model (PDFM), and Three-Dimensional Discrete Fracture Model (3DDFM) are shown in (a), (b), and (c), respectively.

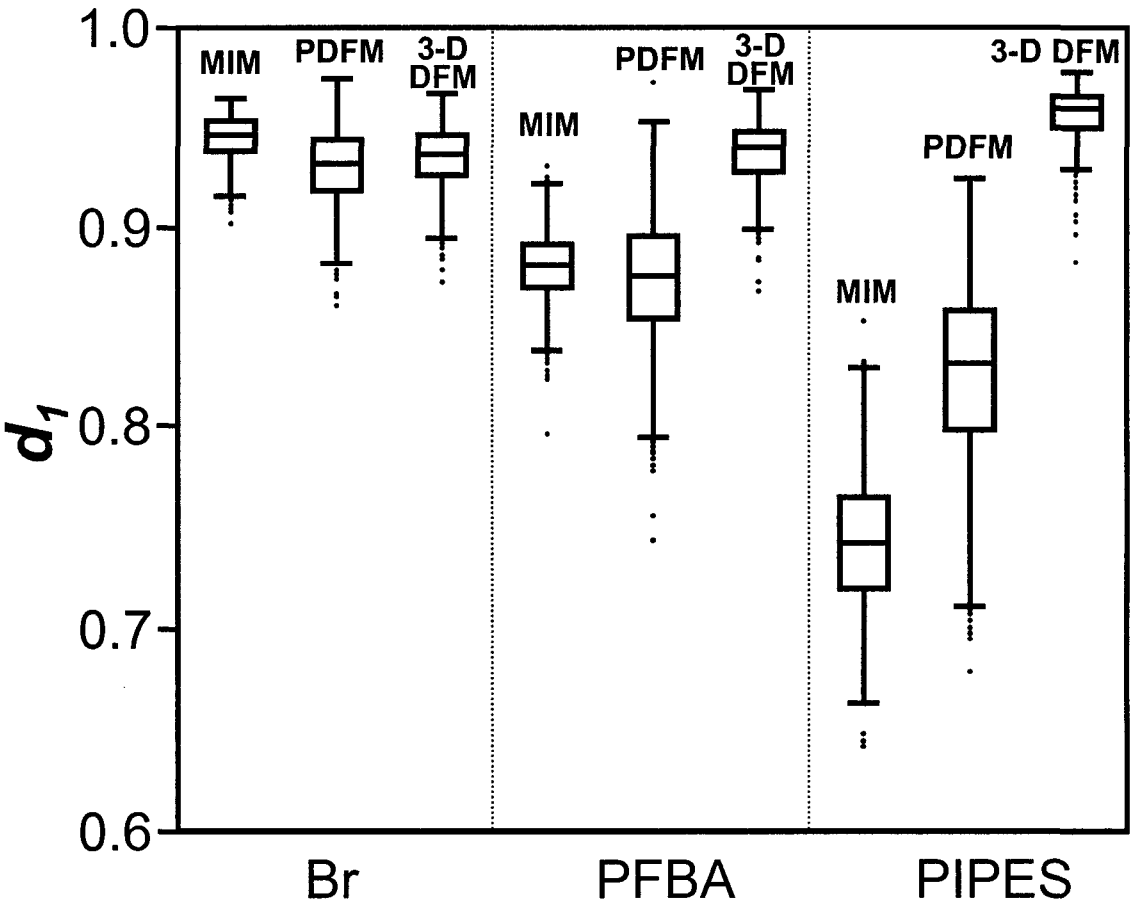

Figure 5. Boxplots showing modified index of agreement (d_1) as a measure of goodness-of-fit for the Mobile-Immobile Model (MIM), Parallel-plate Diescrete Fracture Model (PDFM), and Three-Dimensional Discrete Fracture Model (3-D DFM). Boxes represent 25th and 75th percentiles, whiskers indicate 1.5 interquartile ranges of the bootstrapped distributions (n = 1,000), and dots indicate outliers.

Table 1. Input parameters used for the Mobile-Immobile Model (MIM) simulations.

Parameter	Value	Source
Mobile porosity, n_m	0.061 percent	Equation 9
Bulk hydraulic conductivity, K_b	6.8 x 10^{-8} m/s	Darcy's Law
Hydraulic gradient, i	1.0	Applied
Exchange coefficient, $\alpha^{\dagger}$		
Br	7.5 x 10^{-7} 1/s	Helmke et al., 2003c
PFBA	4.3 x 10^{-7} 1/s	Helmke et al., 2003c
PIPES	1.7 x 10^{-7} 1/s	Helmke et al., 2003c
Immobile porosity, n_{im}		
Br	26.8 percent	Helmke et al., 2003c
PFBA	25.2 percent	Helmke et al., 2003c
PIPES	21.4 percent	Helmke et al., 2003c

† Converted from 23°C to 12°C using the Stokes-Einstein equation.

Table 2. Input parameters used for the Parallel-plate Discrete Fracture Model (PDFM) simulations.

Parameter	Value	Source
Fracture spacing, $2B$	0.043 m	Field measurements
Fracture aperture, $2b$	1.3×10^{-5} m	Equation 6
Fracture porosity, n_f	0.061 percent	Equation 5
Fracture velocity, v	8.1×10^{-5} m/s	Equation 9
Hydraulic gradient, i	1.0	Applied
Effective diffusion coefficient, D_e†		
Br	4.3×10^{-10} m^2/s	Helmke et al., 2003c
PFBA	2.6×10^{-10} m^2/s	Helmke et al., 2003c
PIPES	1.3×10^{-10} m^2/s	Helmke et al., 2003c
Matrix porosity, n_{mat}		
Br	26.8 percent	Helmke et al., 2003c
PFBA	25.2 percent	Helmke et al., 2003c
PIPES	21.4 percent	Helmke et al., 2003c

† Converted from 23°C to 12°C using the Stokes-Einstein equation.

Table 3. Fracture network parameters required for the Three-Dimensional Discrete Fracture Model (3-D DFM) simulations.

Parameter	Value	Source
Fracture intensity		
Length of fractures per unit area, P_{21}	23.3 m/m^2	Fracture maps
Number of fractures per unit volume, P_{30}	643 $fractures/m^3$	FracMan
Area of fractures per unit volume, P_{32}	24.4 m^2/m^3	FracMan
Fracture orientation		
Set 1	trend 326.0°, plunge 16.1°, Fisher *k* 6.13 Fisher distribution	ISIS
Set 2	trend 124.5°, plunge 10.1°, Fisher *k* 4.65 Fisher distribution	ISIS
Fracture size		
radius	mean (μ) 7.9 cm, std. dev. (σ) 5.7 cm Log-normal distribution	Fracture maps
termination	35.5 percent	Fracture maps

Table 4. Fracture transport parameters required for the Three-Dimensional Discrete Fracture Model (3-D DFM) simulations.

Parameter	Value	Source
Transmissivity		
T	mean (μ) 6.6 x 10^{-9} m^2/s, std. dev. (σ) 2.0 x 10^{-8} m^2/s Log-normal distribution	Calculated from K_b
Aperture		
2b	mean (μ) 1.8 x 10^{-5} m, std. dev. (σ) 1.9 x 10^{-5} m Log-normal distribution	Equation 6
Effective diffusion coefficient, D_e†		
Br	4.3 x 10^{-10} m^2/s	Helmke et al., 2003c
PFBA	2.6 x 10^{-10} m^2/s	Helmke et al., 2003c
PIPES	1.3 x 10^{-10} m^2/s	Helmke et al., 2003c
Effective Diffusive Porosity, n_{De}		
Br	26.8 percent	Helmke et al., 2003c
PFBA	25.2 percent	Helmke et al., 2003c
PIPES	21.4 percent	Helmke et al., 2003c

† Converted from 23°C to 12°C using the Stokes-Einstein equation.

Table 5. Goodness-of-fit statistics for the Mobile-Immobile Model (MIM), Parallel-plate Discrete Fracture Model (PDFM), and Three-Dimensional Discrete Fracture Model (3-D DFM) simulations, ordered by solute (Br, PFBA, and PIPES). Statistics include the root mean squared error (RMSE), the coefficient of determination (R^2), and the modified index of agreement (d_1). Ninety-five percent confidence intervals of the mean are given in parentheses.

Model	RMSE	R^2	d_1
Br			
MIM	0.049	0.996	0.947
	(0.044 to 0.051)	(0.989 to 0.992)	(0.935 to 0.948)
PDFM	0.076	0.977	0.932
	(0.066 to 0.080)	(0.973 to 0.980)	(0.913 to 0.935)
3-D DFM	0.057	0.982	0.937
	(0.051 to 0.059)	(0.977 to 0.984)	(0.921 to 0.938)
PFBA			
MIM	0.091	0.990	0.884
	(0.083 to 0.094)	(0.975 to 0.982)	(0.864 to 0.885)
PDFM	0.122	0.941	0.881
	(0.106 to 0.128)	(0.931 to 0.948)	(0.846 to 0.885)
3-D DFM	0.053	0.984	0.939
	(0.049 to 0.058)	(0.976 to 0.983)	(0.923 to 0.940)
PIPES			
MIM	0.168	0.949	0.751
	(0.148 to 0.176)	(0.897 to 0.932)	(0.719 to 0.757)
PDFM	0.145	0.900	0.836
	(0.124 to 0.152)	(0.889 to 0.919)	(0.792 to 0.841)
3-D DFM	0.036	0.994	0.958
	(0.032 to 0.037)	(0.993 to 0.995)	(0.942 to 0.959)

SIMULATION OF SOLUTE TRANSPORT THROUGH FRACTURED TILL USING A STOCHASTIC, THREE-DIMENSIONAL, DISCRETE-FRACTURE MODEL

A paper to be submitted to *Water Resources Research*

Martin F. Helmke, William W. Simpkins, and Robert Horton

Abstract

Fractures are important pathways that enable rapid chemical transport through soils and geologic materials. The purpose of this study was to use a three-dimensional, discrete-fracture model (3-D DFM) to simulate solute transport in a large (0.45 m in length and 0.43 m in diameter) column of fractured till from central Iowa. Model results were tested statistically against breakthrough curves (BTCs) generated from solute transport experiments in the laboratory using the conservative tracers KBr, PFBA, and PIPES. For the stochastic 3-D DFM model, distributions of fracture orientation, geometry, and location obtained from fracture maps and field orientation measurements were used to create a discrete fracture network (DFN) similar statistically to the fractures observed in the field. In addition, a model composed of explicitly measured fractures that were mapped during column dissection, termed the "reconstructed" column, was compared to the results from the stochastic 3-D DFM.

The results demonstrate that realistic fracture geometry in till may be represented by a stochastic 3-D DFM using standard field measurements. A goodness-of-fit statistic, d_1, ranged from 0.937 to 0.958 for the stochastic DFM and 0.905 to 0.953 for the reconstructed DFM. In contrast to the more traditional "parallel-plate" approach, this method allows for realistic fracture location, intensity, geometry, and size. However, both models required nearly 14 hours per single BTC simulation, and the input data requirements required

intensive field work (~300 person hours). Computation power may also constrain this method to relatively small sites. The 3-D DFM probably shows the most promise for solute transport prediction at the field scale, where heterogeneity exerts a greater influence and where groundwater flow is three-dimensional.

Introduction

In glaciated regions, till protects aquifers from the downward migration of contaminants. This is the case in Iowa where groundwater is threatened by agricultural fertilizers and herbicides, landfill leachate, effluent from Concentrated Animal Feeding Operations (CAFOs), and toxic compounds from hazardous waste sites. Till units of Pre-Illinoian through late Wisconsinan age comprise the predominant surficial material in Iowa and have been assumed by consultants and regulators to be an adequate barrier to downward migration of contaminants. However, Iowa's aquifers show evidence of contamination despite this protective layer of till (Kross et al., 1990; U.S. EPA, 1994).

Preferential flow through fracture networks is a potential mechanism for rapid migration of contaminants vertically and horizontally through till. Fractures have been documented in Iowa till units (Lee, 1991; Kemmis et al., 1992; Eidem et al., 1999; Helmke and Simpkins, 2003) and are ubiquitous features. They have also been observed at the till-bedrock contact at depths of 30 m (Kemmis et al., 1992; Helmke and Simpkins, 2003). Fractures in till have been reported elsewhere in the United States (see Connell, 1984; Mickelson and Simpkins, 1991; Brockman and Szabo, 2000), in Canada (see Keller et. al, 1988; Ruland et al., 1991; McKay and Fredericia, 1995), and in Denmark (see Fredericia, 1990; Jørgensen and Fredericia, 1992; Klint and Gravensen, 1999).

Fractures play an influential role in the hydrogeology of till. Bulk hydraulic conductivity (K_b) of fractured till in Iowa is one to two orders of magnitude greater than the hydraulic conductivity of the till matrix (K_m) (Bruner and Lutenegger, 1993; Seo, 1996; Helmke and Simpkins, 2003). Similar observations have been reported elsewhere (Keller et al., 1989; Simpkins and Bradbury, 1992; McKay and Fredericia, 1995). Although there is general agreement that groundwater flow and contaminant transport through till is controlled by fractures, including fractures in models has been limited. Most modeling studies have represented till fractures as networks of vertical, parallel or orthogonal plates (see Grisak et al., 1980; McKay et al., 1993b; Jørgensen et al., 1998; McKay et al., 1999). This approach fails to reflect the complex, 3-dimensional nature of fractures as they are observed in the field (Connell, 1984; Helmke and Simpkins, 2003).

We hypothesize that the 3-D DFM could also be applied successfully in a fractured till setting. The purpose of this paper is to apply the 3-D DFM for simulation of water and solute transport in a column of till using fracture geometries observed and measured in the field. Two DFMs were created. The first employed stochastic methods borrowed from the fractured rock industry to create a Discrete Fracture Network (DFN) statistically similar to fractures measured in the field. A second model was created by dissecting a large till column, mapping each fracture in 3-dimensions, and placing each into the model explicitly to create a "reconstructed column". Breakthrough curves (BTCs) produced by the models were then compared against BTCs produced from laboratory experiments using the large till column.

Previous Work

Discrete fracture models have been used to simulate solute transport through fractured till during the past two decades. Grisak et al. (1980) used a finite element model to simulate BTCs through fractured till from Manitoba, Canada. The model assumed that the fractures could be represented by vertical, equally-spaced, and parallel plates. The model results were then compared to Ca and Cl BTCs collected from a large column of fractured till in the laboratory (Grisak and Pickens, 1980). The simulations matched the observed BTCs only when the effective matrix diffusion coefficient (D_e) and sorption coefficient (K_d) were adjusted to make the model fit. A similar study using Cl, mecoprop, and simazine as tracers was conducted in Denmark (Jorgensen et al., 1998). The BTCs were simulated using sets of vertical, equally-spaced, orthogonal fractures within the finite element model FRACTRAN (Sudicky and McLaren, 1998). In this case, the simulated BTCs in the study predicted the observed BTCs without adjustment of input parameters. Discrete fracture models have also been used at the field scale. McKay et al. (1993a; 1993b) used a parallel-plate DFM to simulate Br transport and compared the results against trench-to-trench tracer tests. The model fit the data, but only when fracture aperture ($2b$) and fracture dispersivity (α) were optimized. None of the above models included actual fracture orientation or size as input parameters to the model.

More elaborate DFMs have been used to simulate the movement of water, oil, and solutes through fractured bedrock. These models have been employed to predict mine stability (Elsworth and Mase, 1993), improve extraction of oil from fractured reservoirs (LaPointe and Dershowitz, 1994), and simulate radioisotope transport from proposed nuclear storage facilities (Anna, 1998). In most of these studies, aerial maps, borehole logs, tunnel

studies, and outcrop measurements were used to identify stochastic distributions of fracture density, orientation, and size. This information was then used to create DFNs. Hydraulic properties of fractures and chemical properties of the contaminants were used to model the system with the 3-D DFM.

Solute Transport Model

Water and solute transport through the DFM was simulated using the MAFIC (MAtrix/Fracture Interaction Code) program (Miller et al., 1997). For this paper, MAFIC was used to simulate steady-state fluid flow and transient solute transport. The equation for 2-D fluid flow at steady state through a triangular element is

$$q = -T\nabla^2 h \tag{1}$$

where q is fluid flux, T is transmissivity, ∇ is the two-dimensional Laplace Operator, and h is hydraulic head. Using the Galerkin finite element solution technique, Equation 1 may be approximated for an entire system of elements by

$$\sum_{m=1}^{N}\left[\int_R (T_{nm}\nabla\xi_n \bullet \nabla\xi_m dR)h_m\right] = \int_R q\xi_n dR \quad n = 1,2,...N \tag{2}$$

where R is element area and ξ is the linear basis function (Miller et al., 1997). Using this approximation and specified boundary conditions, MAFIC constructs a global finite element matrix and solves it using a pre-conditioned, incomplete Choleskii conjugate gradient solver (Meijerink and van der Vorst, 1977).

MAFIC simulates solute transport through the discrete fracture network using particle tracking. The concentration (C) of solute in an element is calculated by

$$C = \frac{M_p}{\rho_w A_e 2b_e} \tag{3}$$

where M_p is the mass of the particles in an element, ρ_w is the fluid density, A_e is the element area, and $2b_e$ is the element aperture. Advection is simulated by moving each particle according to the flow velocity vector during each time step.

Matrix diffusion is treated as a stochastic retardation process by MAFIC. At the end of each time step, the particle travel time ($\Delta t_{f,i}$) is re-calculated to include the portion of time it spends in the matrix by the equation (Miller, 1997):

$$\Delta t_{f,i} = \left(\frac{b}{b+\theta_{De}B}\right)\Delta t_i - \left(\frac{b+B}{b+\theta_{De}B}\right) - \left(\frac{2(b+B)^2}{\pi^4 D^* b/(b+B)}\right) \tag{4}$$
$$\bullet \sum_{n=1}^{\infty} \frac{1}{n^4} \sin^2\left(n\pi b/(b+B)\right)\left[\exp\left(-n^2\pi^2 \frac{D_e t_{i+1}}{(b+B)^2}\right) - \exp\left(-n^2\pi^2 \frac{D_e t_i}{(b+B)^2}\right)\right]$$

where $2B$ is fracture spacing. The principal advantage of the particle tracking approach is that it is relatively simple to program. The simplicity of the model comes with a price; simulation of thousands or even millions of particles required to produce BTCs is computationally inefficient.

Methods

Location of Study

The study site is located within the Walnut Creek watershed, 6 km south of Ames, Iowa on the Des Moines Lobe landform region (Figure 1). The Quaternary stratigraphy and hydrogeology of the Walnut Creek Watershed was previously investigated as part of the Management Systems Evaluation Area (MSEA) program (Seo, 1996; Eidem et al., 1999). The surficial deposit at the site is the Alden Member till of the Dows Formation, deposited 14 to 12.5 ka during the late Wisconsinan (Prior, 1991; Eidem et al., 1999). The Alden Member is a massive, basal till with a bulk density (ρ_b) of approximately 1,700 kg/m^3. The Alden Member is classified as a loam, containing approximately 40 percent sand, 45 percent silt, and 15 percent clay. Unlike older tills in Iowa, the Alden Member has a high smectite content (approximately 69 percent, Kemmis et al., 1981). Previous investigations at the site revealed that the till is fractured (Eidem et al., 1999). Pumping and slug tests performed on a nest of piezometers 10 m north of the sampling location also suggest that fractures increase K_b in this till (Seo, 1996).

Column Preparation

A 4-m-deep trench was excavated using a backhoe to provide access to the till. The excavation trench was carved using a bench and tier method to provide multiple faces for fracture mapping and to ease column collection. Fractures were identified as planes with iron-oxide staining, or as leached zones in the till. Fractures were mapped using sheets of clear acetate on both vertical and horizontal faces in the trench, and fracture strike and dip was measured using a Brunton compass.

An intact column of till, 43 cm in diameter and 45 cm in length, was carved from the basal step of the excavation trench from a depth of 3.3 to 3.75 m using a shovel and putty knife (Figure 2). This column was one of eight collected as part of a larger study of fractured till in Iowa (Helmke et al., 2003a). The column was kept cylindrical by using a level and a section of polyvinyl chloride (PVC) pipe as a guide. A 61-cm-long piece of PVC with an interior diameter (ID) of 45.7 cm was placed over the column, leaving a 1.35-cm void between the column and the pipe. This annulus between the till and the casing was sealed using paraffin wax, a technique which has been demonstrated to prevent side-wall flow (Grisak et al., 1980; Kluitenberg et al., 1991). After the wax cooled (approximately 8 hours), a putty knife was used to separate the column from its base. The column was then winched from the trench and disks of high-density polyethylene (HDPE) (3-mm-thick) were placed at the column ends to prevent moisture loss during transport to the laboratory.

Laboratory Setup

In the laboratory, the ends of the column were carefully scraped with a putty knife to eliminate smear zones. The resulting length of the column was 40 cm. A 5-mm-thick layer of Ottawa Sand was placed at each end of the column and held in place by the HDPE disks. Perforated tubes (3-mm-ID HDPE) were fed through the sand to provide fluid access to the sand packs. Plywood pistons (19-mm-thick and 43-cm-diameter) were added to each end and sealed with silicone caulking. The ends and the walls of the column were mechanically compressed to 60 kPa to approximate the lithostatic stress at 3.5 m. Although care was exercised to minimize desaturation of the column, it is possible that some of the larger pores

drained during excavation and transport. To reduce the chances of entrapped air in these pores, the column was slowly re-saturated by upward flow for 7 days.

Three compounds were used as tracers for the solute transport experiment: potassium bromide, pentafluorobenzoate (PFBA), and disodium-1,4-piperazinediethane sulfonate (PIPES). These compounds do not sorb readily nor do they undergo biodegradation, so they are considered conservative tracers (Jaynes, 1993; Moline et al., 1997). The diffusion coefficients in pure aqueous solution (D_0) of Br and PFBA at 25°C are 1.8×10^{-9}, 7.6×10^{-10} m^2/s, respectively (Bowman and Gibbons, 1992). The D_0 of PIPES has not been determined experimentally, however the calculated D_0 using the Stokes-Einstein equation is 4.1×10^{-10} m^2/s (Helmke et al., 2003c). Conservative compounds with different D_0 values were selected because differences in the morphology of their BTCs would indicate matrix diffusion, thereby providing evidence of fracture flow. In-situ groundwater spiked with a 0.5 mM concentration (C_0) of the tracers was passed through the column for a period of 70 days. Although an upward gradient was applied (to prevent desaturation at the column base), groundwater flow was, in effect, downward because the column was inverted in the laboratory. The temperature of the column was maintained at a constant 12°C to simulate in-situ conditions. The flow rate was measured using a graduated cylinder and a stopwatch.

Effluent samples were passed through a 0.2 μm filter immediately upon collection and stored at 4°C until analyzed at the end of the experiment. Concentrations of Br, PFBA, and PIPES were determined by ion chromatography. Analytical precision (95 percent confidence limit) was determined for Br (0.63 mg/L), PFBA (1.14 mg/L), and PIPES (2.65 mg/L) by analyzing replicates of spiked samples using Student's t distribution (Harris, 1991).

Soil texture was determined using the sieve and pipette method (Walter et al., 1978).

Sand, silt, and clay particle sizes used in this study were 2 to 0.063 mm, 0.063 to 0.002 mm, and <0.002 mm, respectively. The resulting texture of the column was 48.2 percent sand, 37.0 percent silt, and 14.8 percent clay. Total porosity (θ_T) was 29.6 percent as determined gravimetrically by weighing a saturated soil sample, oven-drying it, dividing the difference by the density of water, then dividing this by the original volume of the sample. Pore volume (PV) as determined by the product of θ_T and the volume of the column was 0.017 m^3.

Stochastic DFN

A stochastic DFN was constructed because a) it is the most practical method for creating realistic fracture networks, and b) it is the method most often used by the fractured rock industry (Doe, 1997). The construction of a DFN requires that the location, orientation, size, and shape of each fracture be specified before it may be placed into the model. In most field applications, it is impractical to map all fractures in 3-dimensions. An alternative approach is to determine the stochastic distributions of fracture properties by a relatively few measurements in the field, then create virtual (yet statistically similar) fracture sets to construct the DFN. This study provides a unique opportunity to compare a stochastic DFN with a reconstructed DFN.

For the purposes of this study, fractures were traced onto sheets of clear acetate to create a plan-view map (Figure 3a). The strike and dip of 47 of these fractures were also recorded. The fracture poles from these measurements are shown in Figure 3b as an equal-area stereonet. The statistical information recorded by these fracture measurements were used to construct DFNs on the computer.

The first step in creating a DFN is to decide how the fractures will be placed in the model. The simplest method is to place each fracture randomly in space (a Poisson point process), then expand each sequentially to the desired size and according to the appropriate orientation. This approach is referred to as the Enhanced Baecher Model (Baecher et al., 1977; Dershowitz et al., 1994). To determine if this model was appropriate for the fracture pattern shown in Figure 3a, a fractal algorithm (Baecher et al., 1977) was used to show that the fracture locations are, in fact, random. The results of this analysis provided a χ^2 of 9.9 (p = 95.7 percent confidence that the distribution was random), which demonstrates that the fractures were randomly located and that the Enhanced Baecher model is appropriate.

Perhaps the most important information about a fracture network is fracture intensity, which quantifies the degree of fracturing in a medium. There are 127 fractures represented by the fracture map in Figure 3a. This translates to a fracture intensity of 258.2 fractures/m^2 (P_{20}). By summing the lengths of all the fractures, the resulting fracture intensity is 23.3 m of fracture/m^2 (P_{21}). More useful measures of fracture intensity include the number of fractures per volume (P_{30}) and the surface area of fractures per volume (P_{32}). These parameters increase as a linear function of scale, and may be used to apply results from bench-scale tests to the field scale (Baecher et al., 1977). To estimate P_{32}, numerous DFNs were created with various P_{32}s until fracture maps made from slices of the DFNs matched the P_{21} observed in the field. This inverse method is referred to as iterative sampling, and is a standard method employed by FracMan (Dershowitz et al., 1994). The resulting P_{30} and P_{32} values were 643 fractures/m^3 and 24.4 m^2/m^3, respectively (Table 1). Fracture intensity for till has not been reported previously. However, these estimates of fracture intensity are high

compared to fractured rock, where typical values of P_{32} range from 0.02 to 1.89 m^2/m^3 (Anna, 1998; Jones et al., 1999).

The fracture orientation data indicate that two fracture sets are present. These were identified using a pattern recognition algorithm within FracMan (Dershowitz et al., 1994). Both fracture sets follow Fisher distributions (Fisher, 1953), which is equivalent to a normal distribution in polar space. This was achieved by using the ISIS module provided in the FracMan software package, which also calculates the level of statistical significance using the Kolmogorov-Smirnov method (Conover, 1980). The first fracture set had a trend of 326.0°, a plunge of 16.1°, and a Fisher *k* of 6.13 (K.S. = 98.4 percent confidence of fit). The second fracture set had a trend of 124.5°, a plunge of 10.1°, and a Fisher *k* of 4.65 (K.S. = 98.9 percent confidence of fit). A random number generator was used to extract fracture orientations from the Fisher distributions and place them into the DFN.

Distribution of fracture length was calculated from the fractures mapped in Figure 3a. The distribution was lognormal with a log-mean length of 7.9 cm and a standard deviation of 5.7 cm (Table 1). Mean fracture length was used to represent fracture diameter in the model. Although fracture diameter may be larger than fracture length, the difference between the two is likely to be insignificant for fracture networks of high density (Herbert et al., 1992). To simplify the creation of the finite element mesh, the fractures were represented as hexagons in the DFN. Fracture termination (the percentage of fractures that end when they contact adjacent fractures) obtained from the fracture map was 35.5 percent. As the DFN was assembled, fractures that intersected were terminated at a frequency of 35.5 percent.

DFN of Reconstructed Column

The large till column was dissected destructively after the laboratory experiments were completed. Fractures were mapped at 5-cm intervals onto sheets of clear acetate and later digitized. The nine digitized maps are shown in Figure 4. The distinct fracture patterns and the vertical nature of the fractures allowed them to be traced between each consecutive layer. By this method, the fractures were converted into triangular elements oriented in 3-dimensions using the drafting program AutoCAD (Autodesk, 1997). This process required approximately 300 hours of labor. The resulting "reconstructed column" included 2077 triangular elements and 1360 nodes.

One of the disadvantages of particle tracking in this model is the large number of particles required to produce BTCs. Smith and Schwartz (1984) used 500 particles to simulate BTCs in a model with a theoretical set of orthogonal fractures. The results produced BTCs with four-separate segments instead of smooth curves. Hull et al. (1987) used 6,000 particles to compare 2-D DFM-simulations with laboratory results. The particle tracking produced BTCs that appeared similar to the laboratory model BTCs; however, the particle tracking "curves" contained frequent spikes, making direct comparison difficult. Three-dimensional studies require even more particles. A 3-D DFM used to predict radionuclide transport in Sweden required 450,000 particles (Herbert et al., 1992). Based on the previous research and wishing to err conservatively to produce realistic BTCs, we used 10 million particles to generate each BTC.

Fracture and Solute Transport Parameters

MAFIC requires fracture and matrix physical properties and solute specific properties to be added to a DFN before a DFM may be constructed. These properties include T, $2b$, $2B$, and α for each fracture/matrix block, and D_e and θ_{De} for each solute (Table 2).

The traditional approach to determine the T distribution in fractured rock is to use packers to isolate single fractures in boreholes (Doe, 1997). Due to the small size of the fractures in till, however, this approach is impractical. Instead, a distribution of log-normal T was assumed based on distributions of fracture T reported in the literature (Dershowitz, 1994). Transmissivity was adjusted until the DFM simulated K value matched the observed K_b of the column (6.8 x 10^{-8} m/s). This resulted in a mean T of 6.6 x 10^{-9} m^2/s with a standard deviation of 2.0 x 10^{-8} m^2/s for the stochastic DFM, and a mean T of 5.2 x 10^{-9} m^2/s with a standard deviation of 1.6 x 10^{-8} m^2/s for the reconstructed DFM.

For each fracture placed into the models, a T value was specified using a random number generator of log-normal values. Once each T was specified, the aperture for each fracture was calculated using the Cubic Law:

$$2b = \left(\frac{12\mu T}{\rho g} \right)^{1/3} \tag{5}$$

(Snow, 1969), where μ is fluid viscosity, and g is the acceleration due to gravity. This approach assumes that fluid flowing through each fracture element may be represented by smooth, parallel plates (McKay et al., 1993b; Jørgensen et al., 1998). Based on Equation 5, the stochastic DFM had a mean $2b$ of 1.8 x 10^{-5} m and a standard deviation of 1.9 x 10^{-5} m,

and the reconstructed column DFM had a mean $2b$ of 1.6 x 10^{-5} m with a standard deviation of 1.7 x 10^{-5} m (Table 2).

Dispersivity (α) was set to zero for the model simulations. It was assumed that a hydrodynamic dispersion coefficient (D) could be ignored because macroscopic dispersion would be a natural result of the geometry, connectivity, and T distribution of the DFN. The validity of this approach has been demonstrated by 2-dimensional simulations (Smith and Schwarz, 1984). The value of D was set equal to the aqueous diffusion coefficient (D_0) for each compound to specify a lower limit of D.

The radial diffusion cell method (Novakowski and van der Kamp, 1996; van der Kamp et al., 1996; Helmke et al., 2003c) was used to determine the D_e and θ_{De} for the three compounds used. Mean values of D_e from triplicate experiments were 5.8 x 10^{-10}, 3.5 x 10^{-10}, and 1.7 x 10^{-10} m^2/s for Br, PFBA, and PIPES. These values of D_e were modified by the Stokes-Einstein equation to correct for the temperature difference between 23°C and 12°C. The resulting values of D_e were 4.3 x 10^{-10}, 2.6 x 10^{-10}, and 1.3 x 10^{-10} m^2/s, respectively (Table 2). Effective diffusive porosity, the portion of soil that a diffusing solute may occupy, was also considered in this analysis. Effective diffusive porosity (θ_{De}) may be less than total porosity due to anion exclusion and pore occlusion (Oscarson et al., 1992; van der Kamp et al., 1996;). Estimates of θ_{De} obtained from the radial diffusion cell experiments were 26.8, 25.2, and 21.4 percent for Br, PFBA, and PIPES, respectively.

Statistical Evaluation

Model goodness-of-fit was evaluated using the modified index of agreement (d_1) (Willmott et al., 1985) as well as the better-known root mean squared error (RMSE) and coefficient of determination (R^2). The parameter d_1 is given by

$$d_1 = 1.0 - \frac{\sum_{i=1}^{N} |O_i - P_i|}{\sum_{i=1}^{N} \left(|P_i - \overline{O}| + |O_i - \overline{O}| \right)} \tag{6}$$

where O and P are the observed and modeled simulated data, respectively, and N is the number of observations. d_1 varies from 0 to 1, with 1 indicating a perfect fit between the simulated and observed data. Therefore, d_1 may be interpreted in a fashion similar to R^2. d_1 is considered superior to R^2 and RMSE because d_1 is less sensitive to outliers than R^2 and RMSE and because d_1 is sensitive to additive and proportional differences (unlike R^2). The utility of d_1 has been demonstrated in the validation of hydrologic models (Legates and McCabe, 1999).

There is uncertainty associated with goodness-of-fit parameters such as d_1, RMSE, and R^2. Unfortunately, statistical techniques for establishing confidence intervals for these parameters have not been established, so numerical procedures such as the bootstrap method must be employed (Efron, 1981; Legates and McCabe, 1999). For the purposes of this study, a simple computer program was developed to sample and re-sample random pairs of observed/simulated data to generate a population of 1,000 goodness-of-fit estimates. Box plots of d_1 were then generated to compare the goodness-of-fit data for each BTC. Confidence intervals of mean d_1, RMSE, and R^2 were calculated using Student's t

distribution (Walpole, 2001). The Mann-Whitney test was used to determine the level of statistical difference between the two models for each compound (Conover, 1980).

Results and Discussion

Tracer Experiment

The breakthrough curves were characterized by rapid first arrival, indicating that flow was fracture-dominated. Detectable concentrations ($C/C_0 > 0.02$) of the three tracers were observed in the column effluent after 4.7 days, resulting in a first-arrival velocity of at least 0.085 m/day (Figure 5). Breakthrough for Br, PFBA, and PIPES was achieved after 13.8, 18.9, and 19.2 days, respectively. The center-of-mass ($C/C_0 = 0.5$) velocities calculated from these breakthrough times are 0.029, 0.021, and 0.021 m/day, respectively. All three solutes resulted in breakthrough times earlier than the time for one PV (19.9 days), providing evidence that preferential flow paths (presumably fractures) influenced the BTCs.

Separation of the three tracers indicated that matrix diffusion was a controlling process in the till. The concentration of PIPES increased more rapidly than Br or PFBA during the first 30 days of the experiment, resulting in a separation between the BTCs. This separation was likely due to the lower D_e of PIPES compared to Br and PFBA, and provides evidence that matrix diffusion was a controlling mechanism as the solutes passed through the column. A similar separation of PIPES and Br was observed in BTCs produced from a column of fractured saprolite from Tennessee (Moline et al., 1997). Likewise, Grisak et al. (1980) observed that calcium increased in concentration more rapidly than chloride during a laboratory experiment using an intact column of fractured till from Canada. The authors

attributed the separation of calcium and chloride to differences in D_e (5×10^{-11} and 1.9×10^{-11} m^2/s, respectively).

Stochastic Simulation

The stochastic DFN included a dense and well-interconnected network of fractures. The stochastic DFN contained 103 fractures, which were triangulated into a mesh of 1884 finite elements (Figure 6). The BTCs generated from MAFIC simulations using the stochastic DFM closely approximated the observed data (Figure 7). The distinct properties of the compounds tested the hypothesis that the 3-D DFM could simulate the solute transport processes in a till. The shape and distinct separation of the BTCs belonging to the three tracers corresponds with the shape and separation of the observed data, suggesting that the model quantifies both rapid fracture transport and matrix diffusion. Similar success was achieved in Sweden when stochastic DFM simulations were compared against tracer experiments in fractured rock at the Stripa Mine (Herbert et al., 1992). Relative error in that study ranged from 5 to 75 percent.

Reconstructed Column Simulation

The DFN for the reconstructed column is probably the best representation of the actual fracture network present in the till (Figure 8). The 2077 finite elements (3-D triangles) that comprise the DFN indicate the high degree of interconnection that exists between the fractures as was observed in the column. It also illustrates why vertical, equally spaced, parallel plates do not accurately represent the fracture network. Similar to the stochastic 3-D DFM, shape and distinct separation of the BTCs for the reconstructed column corresponds to

the shape and separation of the observed data, suggesting that this model also quantifies matrix diffusion (Figure 10).

Statistical Evaluation

The results of the goodness-of-fit analysis demonstrated that the stochastic and reconstructed column models predicted the BTCs with accuracy. Estimates of d_1 for both models demonstrated excellent goodness-of-fit, ranging from 0.937 to 0.958 for the stochastic DFM and 0.905 to 0.953 for the reconstructed DFM (Table 3). RMSE was low (0.036 to 0.085) and R^2 was close to 1 (0.969 to 0.994) for both model simulations, providing additional evidence that both models predicted the data well. Boxplots of the d_1 populations generated from 1,000 bootstrap iterations demonstrate visually that differences between the simulations are small (Figure 10). The Mann-Whitney tests revealed that differences of mean d_1 were insignificant for Br between the two models ($\alpha = 0.05$ level). In the case of PFBA, however, mean d_1 of the stochastic DFM was statistically smaller than reconstructed DFM ($p = 0.004$). Conversely, the stochastic DFM simulation of PIPES was statistically superior to the reconstructed DFM ($p < 0.001$). Considering that both models fit the data well (d_1 greater than 0.9) and the distributions of d_1 coincide, we conclude that although the models are statistically different for PFBA and PIPES, the differences are minor.

Conclusions

The results of this study demonstrate field-derived fracture geometry can be used as input to a flow and solute transport model which accurately simulates BTCs generated by column experiments in fractured till. Simulated BTCs from the stochastic 3-D DFM

compared closely with laboratory column BTCs (d_1 from 0.937 to 0.958), as did BTCs from the simulations of the "reconstructed column" (d_1 from 0.905 to 0.953). In contrast to the more traditional "parallel-plate" approach, this method allows for realistic fracture location, intensity, geometry, and size. However, both models shown here required nearly 14 hours per single BTC simulation, and the input data requirements required intensive field work (~ 300 person hours) which may not be possible under normal conditions. Computation power may also constrain this method to relatively small sites. Comparisons of alternative 1- and 2-D models for fracture flow and contaminant transport (Helmke et al., 2003b) suggest that the effort needed to obtain the data for a model of this type may not yield necessarily a better simulation than a 1-D or 2-D model. The 3-D DFM probably shows the most promise for solute transport prediction at the field scale, where heterogeneity exerts a greater influence and where flow is three-dimensional.

Acknowledgements

This research was funded by grants from the American Geophysical Union (Horton Grant), the Association of Ground Water Scientists and Engineers, the Geological Society of America, Sigma Xi, and the USEPA through an Interagency Agreement DW12036252 to the Agricultural Research Service. The authors wish to thank T. Doe and W. Dershowitz at Golder Associates for providing access to the FracMan/MAFIC software package. We thank P. Jardine and G. Moline for the suggestion of using PIPES as a tracer.

References

Anna, L. O. 1998. Preliminary three-dimensional discrete fracture model of the Topopah Spring Tuff in the Exploratory Studies Facility, Yucca Mountain Area, Nye County, Nevada. U.S. Geological Survey Open-File Report 97-834, Denver, Colorado. 41 p.

Autodesk. 1997. AutoCAD release 14 user's guide. Autodesk, Inc. San Rafael,California. 805 p.

Baecher, G. B., N. A. Laney, H. H. Einstein. 1977. Statistical description of rock properties and sampling. Proceedings of the 18th U.S. Symposium on Rock Mechanics, American Institute of Mining Engineers. pp. 5C1-8.

Bowman, R. S. and J. S. Gibbens. 1992. Difluorobenzoates as nonreactive tracers in soil and ground water. Ground Water. v. 30, pp. 8-14.

Brockman, C. S. and J. P. Szabo. 2000. Fractures and their distribution in the tills of Ohio. Ohio Journal of Science. v. 100, n. 3/4, pp. 39-55.

Bruner, D. R. and A. J. Lutenegger. 1993. Measurement of saturated hydraulic conductivity in fine-grained glacial tills in Iowa: Comparison of in situ and laboratory methods. Hydraulic Conductivity and Waste Contaminant Transport in Soils, ASTM STP 1142, David E. Daniel and Stephen J. Trautwein, Eds., American Society for Testing and Materials, Philadelphia.

Connell, D. E. 1984. Distribution, characteristics, and genesis of joints in fine-grained till and lacustrine sediments, eastern and northwestern Wisconsin. Master's Thesis, University of Wisconsin, Madison. 443 p.

Conover, W. J. 1980. Practical Nonparametric Statistics (Second Edition). John Wiley and Sons, New York, New York, 493 pp.

Dershowitz, W., G. Lee, J. Geier, S. Hitchcock, and P. R. La Pointe. 1994. FracMan version 2.4 – Interactive discrete feature data analysis, geometric modeling and exploration simulation. Golder Associates, Inc., Redmond, Washington. 171 p.

Doe, T. 1997. Understanding and solving fracture flow problems. Water Engineering Management. v. 144, pp. 36-43.

Eidem, J. M., W. W. Simpkins, and M. R. Burkart. 1999. Geology, groundwater flow, and water quality in the Walnut Creek watershed. Journal of Environmental Quality. v. 28, pp. 60-69.

Fisher, R. A. 1953. Dispersion on a sphere. Proceedings fromt the Royal Society of London. A217, pp. 295-305.

Efron, B. 1981. Nonparametric estimates of standard error: The jackknife, the bootstrap, and other methods. Biometrica. v. 68, pp. 589-599.

Elsworth, D. and C. R. Mase. 1993. Groundwater in Rock Engineering. *Comprehensive Rock Engineering*, v. 1, pp. 201-226.

Fredericia, J. 1990. Saturated hydraulic conductivity of clayey tills and the role of fractures. Nordic Hydrology. v. 21, pp. 119-132.

Grisak, G. E. and J. F. Pickens. 1980. Solute transport through fractured media: 1. The effect of matrix diffusion. Water Resources Research. v. 16, pp. 719-730.

Grisak, G. E., J. F. Pickens, and J. A. Cherry. 1980. Solute transport through fractured media: 2. Column study of fractured till. Water Resources Research. v. 16, pp. 731-739.

Harris, D. C. 1991. *Quantitative Chemical Analysis, Third Ed.*, W. H. Freeman and Company, 782 p.

Helmke, M. F. and W. W. Simpkins. 2003. Chapter 5: Effect of fractures on hydraulic conductivity of till units in Iowa. In unpub. Ph.D. dissertation, Iowa State University, pp. 144-167.

Helmke, M. F., W. W. Simpkins, and R. Horton. 2003a. Chapter 1: Fracture-dominated transport of nitrate and atrazine through till in Iowa. In unpub. Ph.D. dissertation, Iowa State University, pp. 5-37.

Helmke, M. F., W. W. Simpkins, and R. Horton. 2003b. Chapter 2: Comparison of forward modeling approaches to simulate solute transport through fractured till. In unpub. Ph.D. dissertation, Iowa State University, pp. 38-79.

Helmke, M. F., W. W. Simpkins, and R. Horton. 2003c. Chapter 4: Laboratory measurement of effective diffusion parameters in fractured soil. In unpub. Ph.D. dissertation, Iowa State University, pp. 119-143.

Herbert, A. W., G. W. Lanyon, J. E. Gale, and R. MacLeod. 1992. Discrete fracture network modelling for phase 3 of the Stripa project using NAPSAC. In Situ Experiments at the Stripa Mine, OECD Nuclear Energy Agency and Swedish Nuclear Fuel and Waste Management Company. pp. 219-235.

Hull, L. C., J. D. Miller, and T. M. Clemo. 1987. Laboratory and simulation studies of solute transport in fracture networks. Water Resources Research. v. 23, n. 8, pp. 1505-1513.

Jaynes, D. B. 1993. Evaluation of fluorobenzoate tracers in surface soils. Ground Water. v. 32, pp. 532-538.

Jones, M. A., A. B. Pringle, I. M. Fulton, and S. O'Neill. 1999. Discrete fracture network modeling applied to groundwater resource exploitation in southwest Ireland. In: McCaffey, K. J. W., L. Lonegran, and J. J. Wilkinson (eds) Fractures, Fluid Flow and Mineralization. Geological Society, London, Special Publications. v. 155, pp. 83-103.

Jørgensen. P. R. and J. Fredericia. 1992. Migration of nutrients, pesticides and heavy metals in fractured clayey till. Geotechnique. v. 42, pp. 67-77.

Jørgensen, P. R., L. D. McKay, and N. ZH. Spliid. 1998. Evaluation of chloride and pesticide transport in a fractured clayey till using large undisturbed columns and numerical modeling. Water Resources Research. v. 34, pp. 539-553.

Keller, C. K., G. van der Kamp, and J. A. Cherry. 1988. Hydrogeology of two Saskatchewan tills, I. Fractures, bulk permeability, and special variability of downward flow. Journal of Hydrology. v. 101, pp. 97-121.

Keller, C. K., G. van der Kamp, and J. A. Cherry. 1989. A multiscale study of the permeability of a thick clayey till. Water Resources Research. v. 25, n. 11. pp. 2299-2317.

Kemmis, T. J., E. A. Bettis III, and G. R. Hallberg. 1992. Quaternary geology of Conklin Quarry. Guidebook Series no. 13. Iowa Department of Natural Resources. 41 p.

Kemmis, T. J., G. R. Hallberg, and A. J. Lutenegger. 1981. Depositional environments of glacial sediments and landforms on the Des Moines Lobe, Iowa. Guidebook Series no. 6. Iowa Department of Natural Resources. 132 p.

Klint, K. E. S. and P. Gravesen. Fractures and biopores in Weichselian clayey till Aquitards at Flakkebjerg, Denmark. Nordic Hydrology. v. 30, n. 3/4, pp. 267-284.

Kluitenberg, G. L., J. R. Bilskie, and R. Horton. 1991. Rubberized asphalt for sealing cores of shrinking soil. Soil Science Society of America Journal. v. 55, pp. 1504-1507.

Kross, B. C., G. R. Hallberg, D. R. Bruner, R. D. Libra, K. D. Rex, L. M. B. Weih, M. E. Vermace, L. F. Burmeister, N. H. Hall, K. L. Cherryhomes, J. K. Johnson, M. I. Selim, B. K. Nations, L. S. Seigley, D. J. Quaide, A. G. Dudler, K. D. Sesker, M. A. Culp, C. F. Lynch, H. F. Nicholson, and J. Hughes. 1990. The Iowa State-Wide Rural Well-Water Survey, Water Quality Data: Initial Analysis. Iowa Department of Natural Resources Technical Information Series 19. 142 p.

La Pointe, P. R., and W. S. Dershowitz. 1994. Discrete fracture approaches for oil and gas applications. Proceedings: 1st North American Rock Mechanics Symposium, The University of Texas at Austin, pp. 19-30.

Lee, S. H. 1991. Genesis and distribution of fractures in late-Wisconsinan till of the Des Moines Lobe in central Iowa.

Legates, D. R. and G. J. McCabe Jr. 1999. Evaluating the use of "goodness-of-fit" measures in hydrologic and hydroclimatic model validation. Water Resources Research. v. 35, pp. 233-241.

McKay, L. D., J. A. Cherry, and R. W. Gillham. 1993a. Field experiments in a fractured clay till: 1. Hydraulic conductivity and fracture aperture. Water Resources Research. v. 29, pp. 1149-1162.

McKay, L. D., J. A. Cherry, and R. W. Gillham. 1993b. Field experiments in a fractured clay till: 2. Solute and colloid transport. Water Resources Research. v. 29, pp. 3879-3890.

McKay, L. D. and J. Fredericia. 1995. Distribution, origin, and hydraulic influence of fractures in a clay-rich glacial deposit. Canadian Journal of Technology. v. 32, pp. 957-975.

McKay, L., J. Fredericia, M. Lenczewski, J. Morthorst, and K. E. S. Klint. 1999. Spatial variability of contaminant transport in a fractured till, Avedøre Denmark. Nordic Hydrology. v. 30, n. 4/5, pp. 333-360.

Meijerink, J. A. and H. A. van der Vorst. 1977. An iterative solution method for linear systems of which the coefficient matrix is a symmetric M-matrix. Mathematics of Computation. v. 31, n. 137, pp. 148-168.

Mickelson, D. M., and W. W. Simpkins. 1991. Observations on the origin of fractures in fine-grained lake sediment and till in the Midwestern and Eastern U.S. EOS. v. 72, n. 44, p. 166.

Miller, I., G. Lee, and W. Dershowitz. 1997. MAFIC version 1.6 – matrix/fracture interaction code with heat and solute transport. Golder Associates, Inc., Redmond, Washington. 87 pp.

Moline, G. R., C. R. Knight, and R. Ketcham. 1997. Laboratory measurement of transport processes in a fractured limestone/shale saprolite using solute and colloid tracers. Abstracts with Programs, Geological Society of America. v. 29, n. 6, p. 370.

Novakowski, K. S. and G. van der Kamp. 1996. The radial diffusion method 2. A semianalytical model for the determination of effective diffusion coefficients, porosity, and adsorption. Water Resources Research. v. 32, pp. 1823-1830.

Oscarson, D. W., H. B. Hume, N. G. Sawatsky, and S. C. H. Cheung. 1992. Diffusion of iodide in compacted bentonite. Soil Science Society of America Journal. v. 56, pp. 1400-1406.

Prior, J. C. 1991. Landforms of Iowa. University of Iowa Press, Iowa City, Iowa. 154 p.

Ruland, W. W., J. A. Cherry, and Stan Feenstra. 1991. The depth of fractures and active ground-water flow in a clayey till plain in southwestern Ontario. Ground Water. v. 29, n. 3, pp. 405-417.

Seo, H. H. 1996. Hydraulic properties of Quaternary stratigraphic units in the Walnut Creek watershed. Master's Thesis. Iowa State University. 145 p.

Simpkins, W. W. and K. R. Bradbury. 1992. Groundwater flow, velocity, and age in a thick, fine-grained till unit in southeastern Wisconsin. Journal of Hydrology. v. 132, pp. 283-319.

Smith, L. and F. W. Schwartz. 1984. An analysis of the influence of fracture geometry on mass transport in fractured media. Water Resources Research. v. 20, n. 9, pp. 1241-1252.

Snow, D. T. 1969. Anisotropic permeability of fractured media. Water Resources Research. v. 5, pp. 1273-1289.

Sudicky, E. A. and R. G. McLaren. 1998. FRACTRAN User's Guide. An efficient simulator for two-dimensional, saturated groundwater flow and solute transport in porous or discretely-fractured porous formations. Groundwater Simulations Group, Waterloo Centre for Groundwater Research. University of Waterloo, Ontario, Canada. 97 p.

U.S. Environmental Protection Agency. 1994. Progress at Region 7 National Priorities List (NPL) Superfund Sites, Iowa. Report published by EPA Region 7. 73 p.

van der Kamp, G., D. R. Van Stempvoort, and L. I. Wassenaar. 1996. The radial diffusion method 1. Using intact cores to determine isotopic composition, chemistry, and effective porosities for groundwater in aquitards. Water Resources Research. v. 32, pp. 1815-1822.

Walpole, R. E., R. H. Myers, S. L. Myers, and K. Ye. 2001. Probability and Statistics for Engineers and Scientists, 7th Ed. Pearson Education. 752 pp.

Walter, N. F., Hallberg, G. R., and Fenton, T. E. 1978. Particle-size analysis by the Iowa State University Soil Survey Laboratory, in Hallberg, G. R. ed.: Standard procedures for evaluation of Quaternary materials in Iowa: Iowa Geological Survey, Technical Information Series, no. 8, p. 61-74.

Willmott, C. J., S. G. Ackleson, R. E. Davis, J. J. Feddema, K. M. Klink, D. R. Legates, J. O'Donnell, and C. M. Rowe. Statistics for the evaluation and comparison of models. Journal of Geophysical Research. v. 90, pp. 8995-9005.

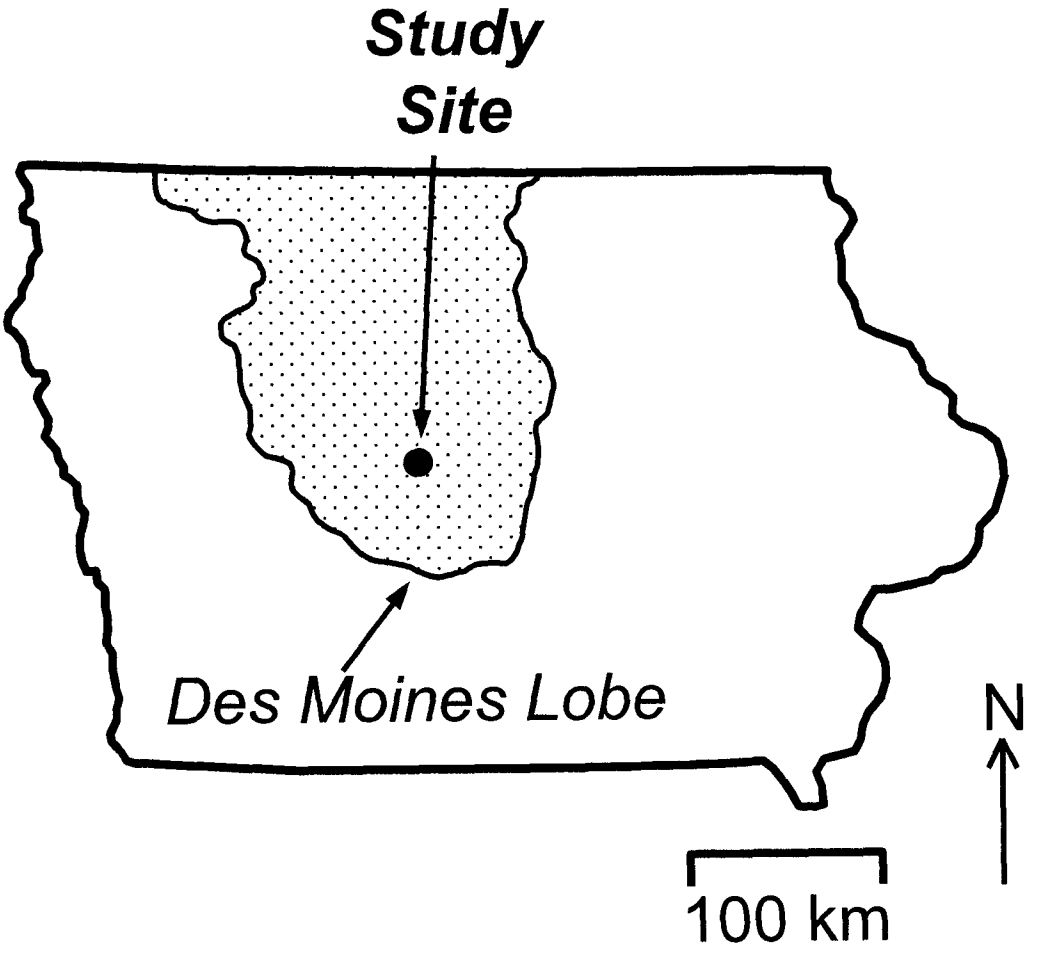

Figure 1. Map of Iowa showing the location of the study site within the Des Moines Lobe landform region (after Prior, 1991).

Figure 2. Photograph of till column (43-cm diameter and 45-cm length) prior to encasement in the field. Note sub-vertical, iron-stained fractures. Putty knife for scale.

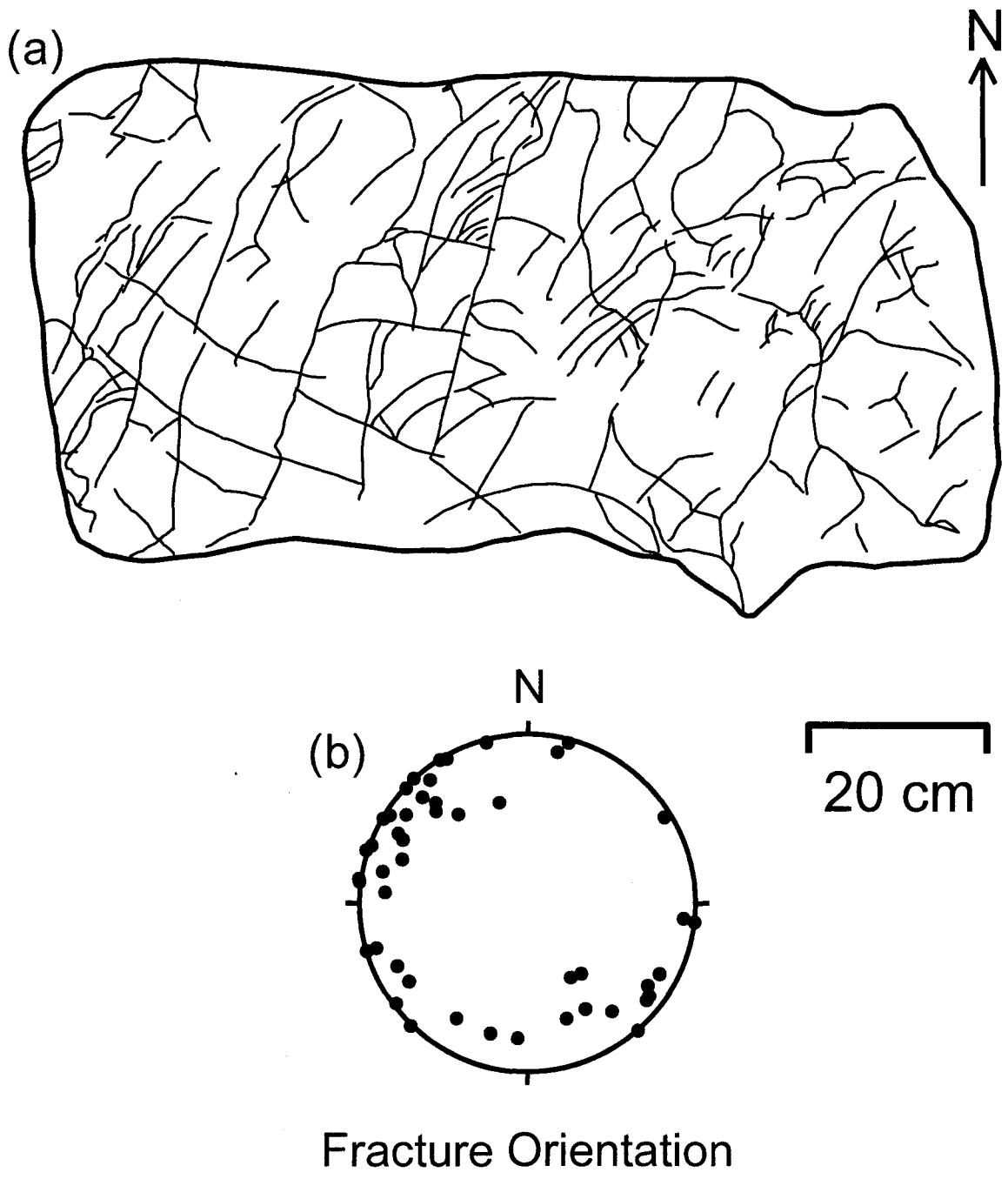

Figure 3. Plan-view map of fractures (a) and fracture orientation stereonet (b) recorded at a depth of 3.3 m. Two predominantly vertical fracture sets were observed at this depth: Set 1 with a trend of 326.0° and plunge of 16.1 °, and Set 2 with a trend of 124.5° and plunge of 10.1°.

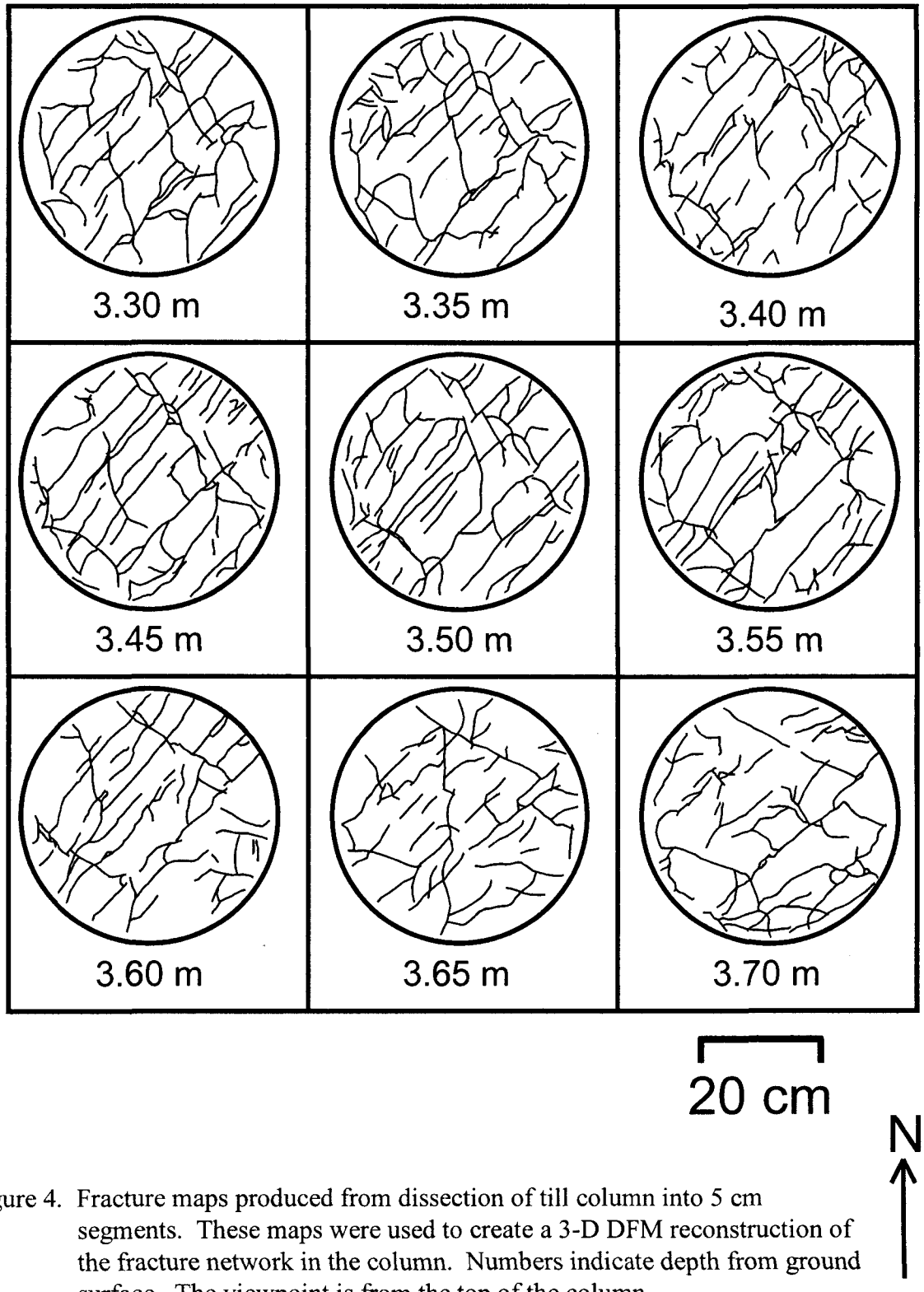

Figure 4. Fracture maps produced from dissection of till column into 5 cm segments. These maps were used to create a 3-D DFM reconstruction of the fracture network in the column. Numbers indicate depth from ground surface. The viewpoint is from the top of the column.

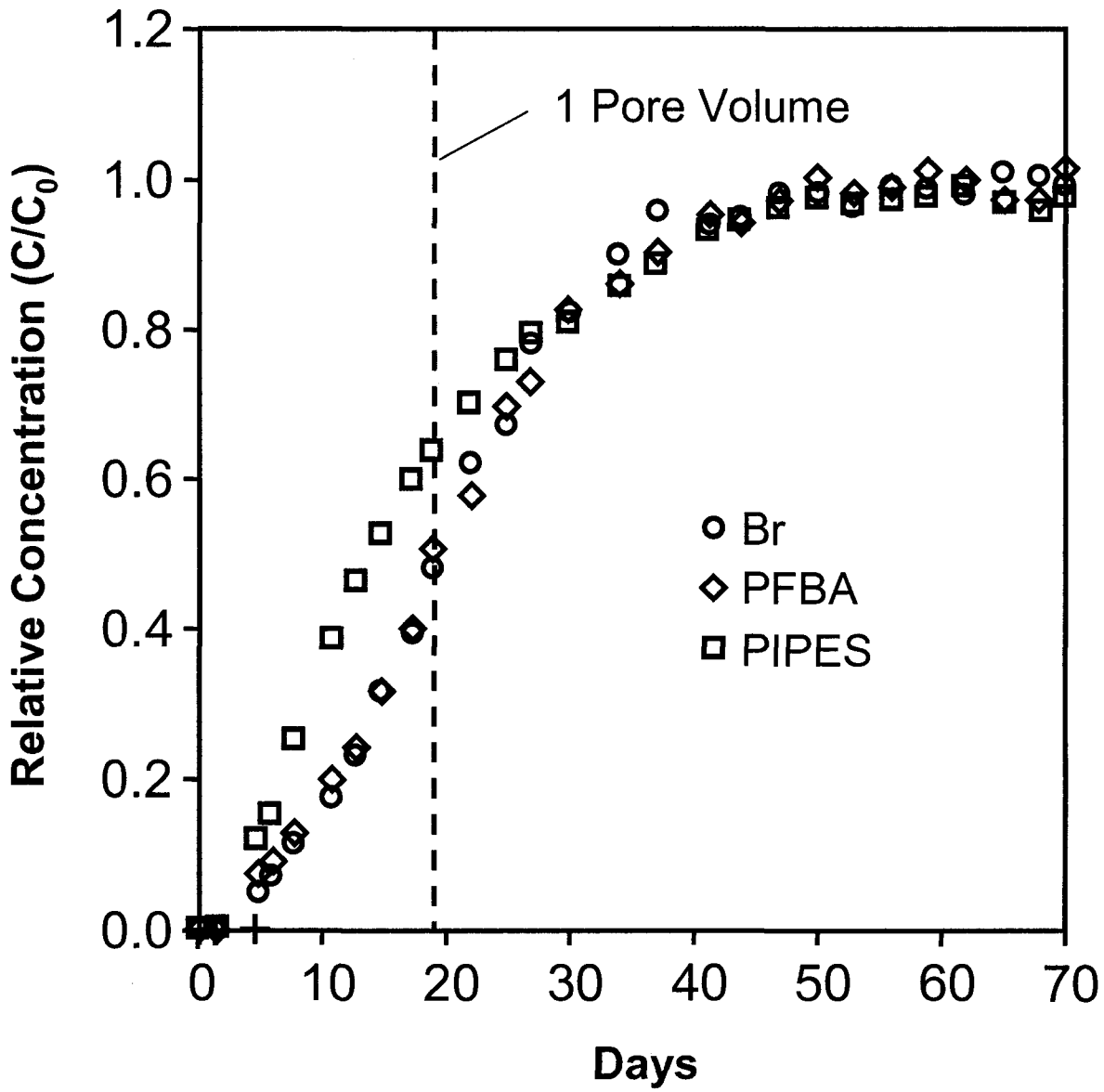

Figure 5. Breakthrough curves for Br, PFBA, and PIPES from column tracer tests. Dashed line indicates the time for 1 pore volume (19.9 days) to pass through the column.

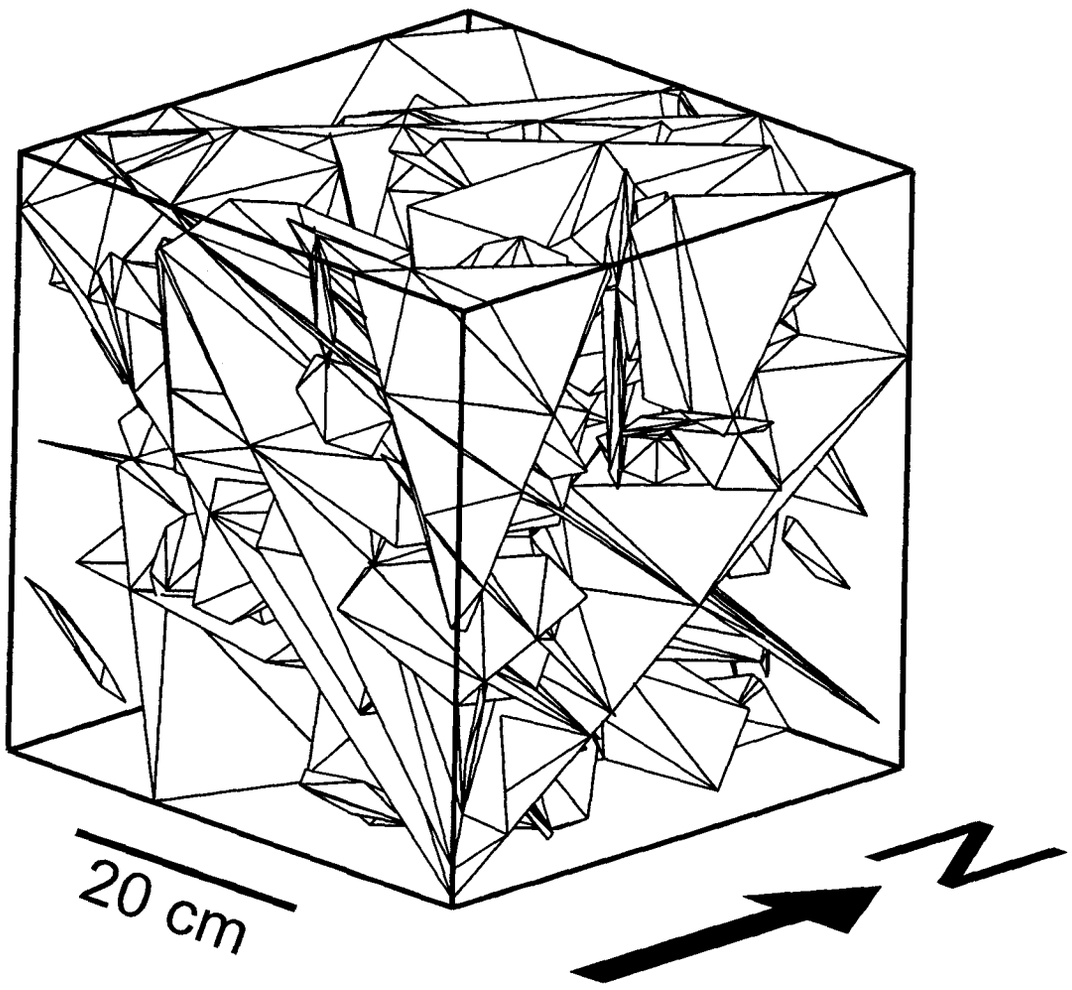

Figure 6. Discrete fracture network in the till core generated stochastically by FracMan (Dershowitz, 1994). Column contains 103 fractures and 1884 triangular elements.

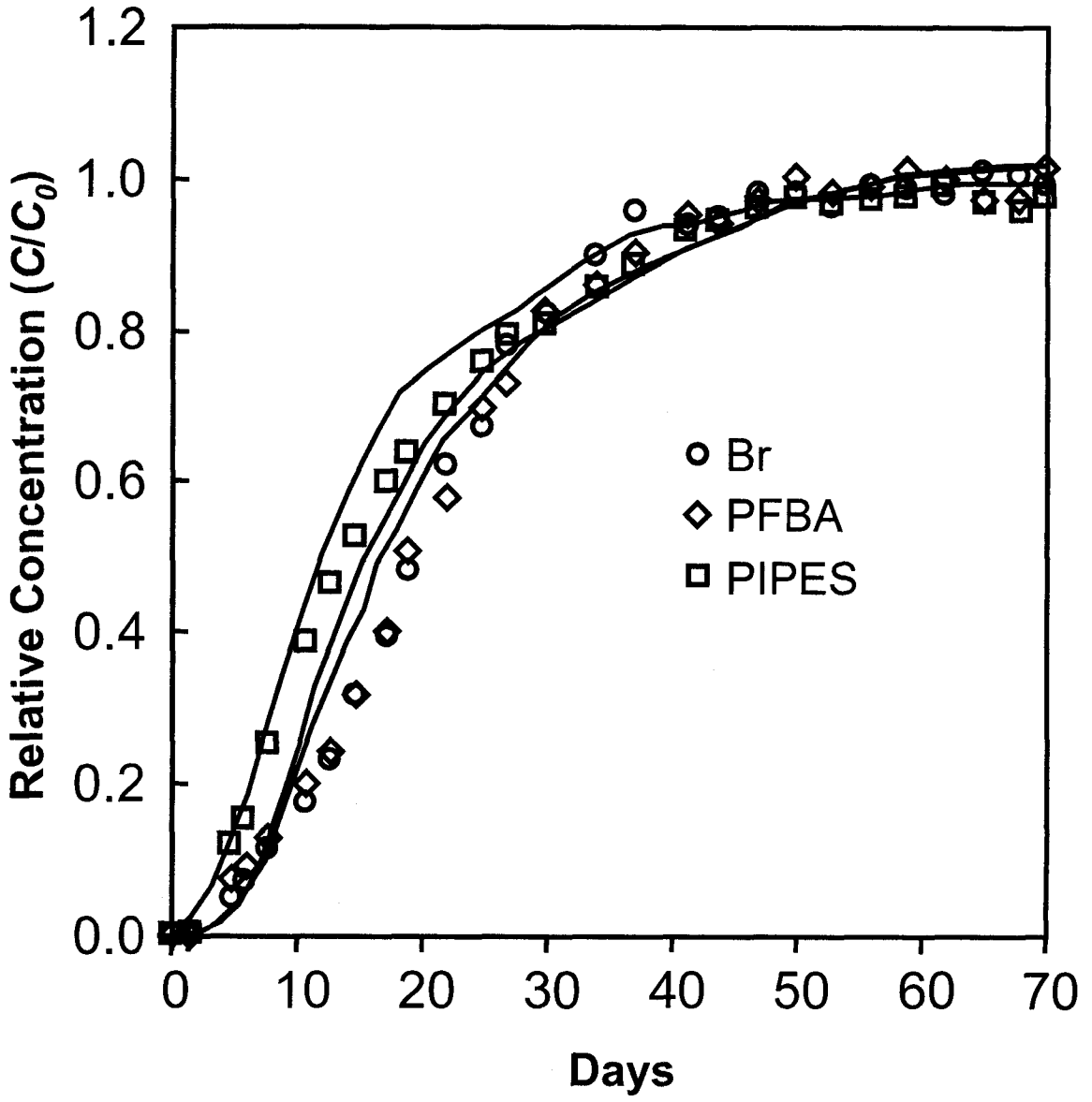

Figure 7. Simulated breakthrough curves (lines) produced by the stochastic discrete fracture model. Breakthrough curves for Br, PFBA, and PIPES from column tracer tests are shown as symbols.

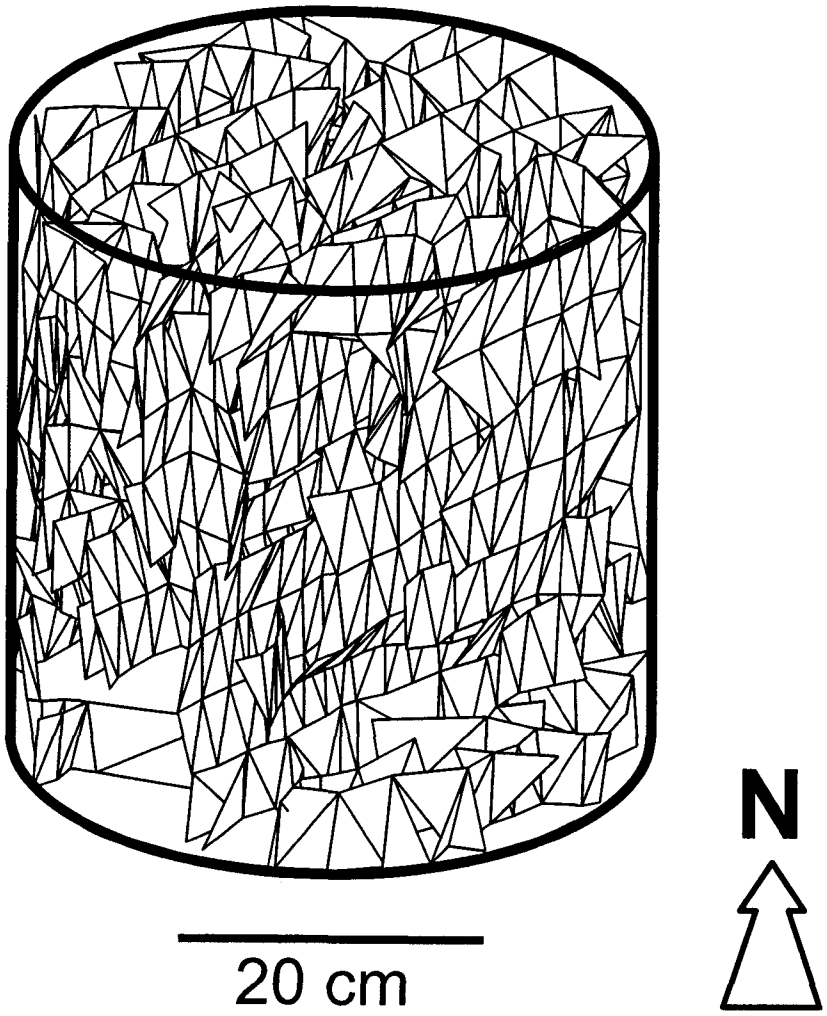

Figure 8. A discrete fracture network consisting of 2077 triangular finite elements that represents the fracture network from the dissected column. North is forward from this viewpoint.

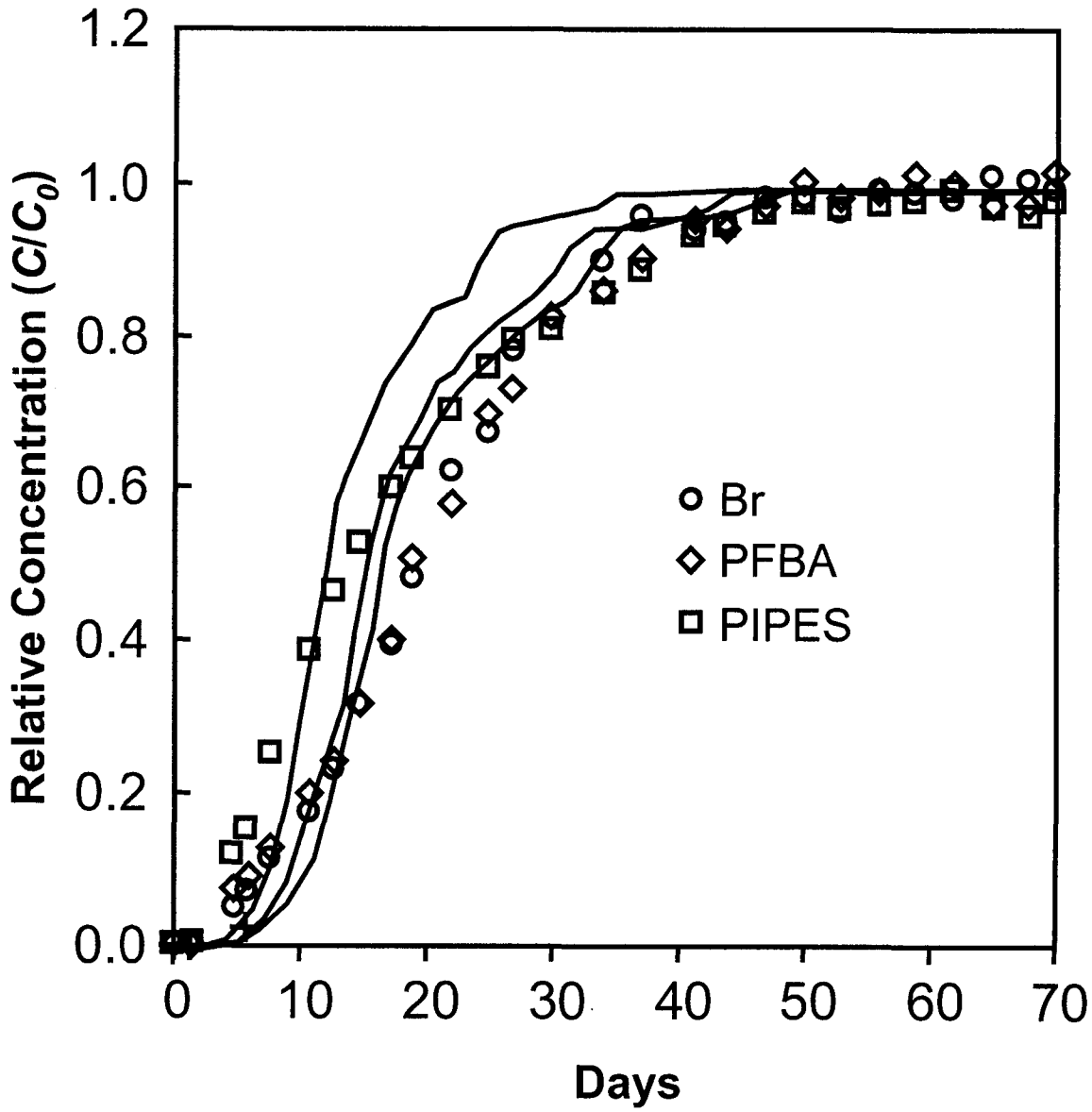

Figure 9. Simulated breakthrough curves (lines) produced by the reconstructed discrete fracture model. Breakthrough curves for Br, PFBA, and PIPES from column tracer tests are shown as symbols.

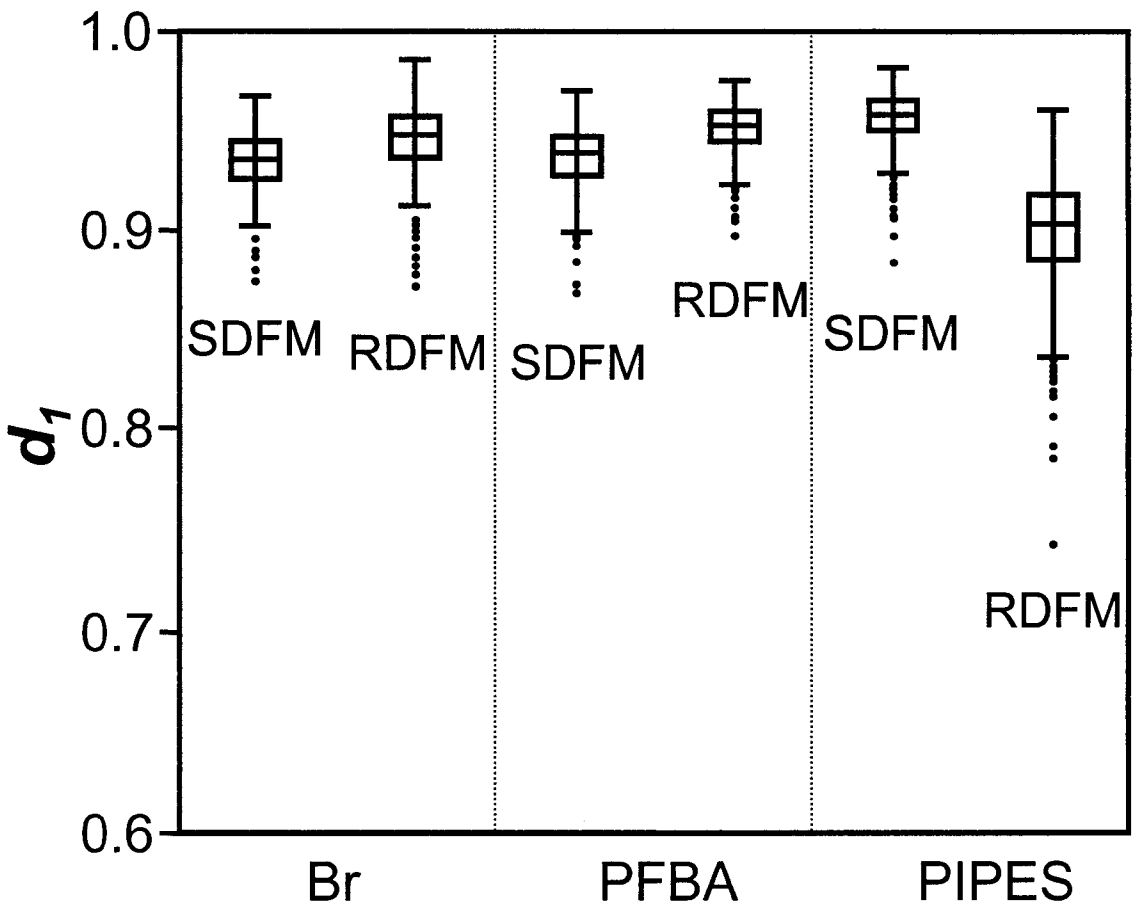

Figure 10. Boxplots showing modified index of agreement (d_1) as a measure of goodness-of-fit for the Stochastic Discrete Fracture Model (SDFM) and Reconstructed Discrete Fracture Model (RDFM). Boxes represent 25th and 75th percentiles, whiskers indicate 1.5 interquartile ranges of the bootstrapped distributions (n = 1,000), and dots indicate outliers.

Table 1. Parameters used as input for the stochastic fracture network (DFN).

Parameter	Value	Source
Fracture intensity		
Length of fractures per unit area, P_{21}	23.3 m/m^2	Fracture maps
Number of fractures per unit volume, P_{30}	643 $fractures/m^3$	FracMan
Area of fractures per unit volume, P_{32}	24.4 m^2/m^3	FracMan
Fracture orientation		
Set 1	trend 326.0°, plunge 16.1°, Fisher *k* 6.13 Fisher distribution	ISIS
Set 2	trend 124.5°, plunge 10.1°, Fisher *k* 4.65 Fisher distribution	ISIS
Fracture size		
Radius	mean (μ) 7.9 cm, std. dev. (σ) 5.7 cm Log-normal distribution	Fracture maps
Termination	35.5 percent	Fracture maps

Table 2. Fracture and solute transport parameters required by the Stochastic and Reconstructed Discrete Fracture Models (DFMs).

Parameter	Value	Source
Transmissivity		
T	mean (μ) 6.6 x 10^{-9} m^2/s, std. dev. (σ) 2.0 x 10^{-8} m^2/s Log-normal distribution	Calculated from K_b
Aperture		
Stochastic DFM 2b	mean (μ) 1.8 x 10^{-5} m, std. dev. (σ) 1.9 x 10^{-5} m Log-normal distribution	Equation 5
Reconstructed DFM 2b	mean (μ) 1.8 x 10^{-5} m, std. dev. (σ) 1.9 x 10^{-5} m Log-normal distribution	Equation 5
Effective diffusion coefficient, D_e†		
Br	4.3 x 10^{-10} m^2/s	Helmke et al., 2003c
PFBA	2.6 x 10^{-10} m^2/s	Helmke et al., 2003c
PIPES	1.3 x 10^{-10} m^2/s	Helmke et al., 2003c
Effective diffusive porosity, θ_{De}		
Br	26.8 percent	Helmke et al., 2003c
PFBA	25.2 percent	Helmke et al., 2003c
PIPES	21.4 percent	Helmke et al., 2003c

† Converted from 23°C to 12°C using the Stokes-Einstein equation.

Table 3. Goodness-of-fit statistics for the Stochastic and Reconstructed Discrete Fracture Models (DFMs) ordered by solute (Br, PFBA, and PIPES). Statistics include the root mean squared error (RMSE), the coefficient of determination (R^2), and the modified index of agreement (d_1). Ninety-five percent confidence intervals of the mean are given in parentheses.

Model	RMSE	R^2	d_1
Br			
Stochastic DFM	0.057 (0.051 to 0.059)	0.982 (0.977 to 0.984)	0.937 (0.921 to 0.938)
Reconstructed DFM	0.063 (0.052 to 0.066)	0.979 (0.971 to 0.982)	0.947 (0.929 to 0.949)
PFBA			
Stochastic DFM	0.053 (0.049 to 0.058)	0.984 (0.976 to 0.983)	0.939 (0.923 to 0.940)
Reconstructed DFM	0.050 (0.045 to 0.053)	0.986 (0.981 to 0.988)	0.953 (0.940 to 0.954)
PIPES			
Stochastic DFM	0.036 (0.032 to 0.037)	0.994 (0.993 to 0.995)	0.958 (0.942 to 0.959)
Reconstructed DFM	0.085 (0.077 to 0.089)	0.969 (0.957 to 0.971)	0.905 (0.871 to 0.906)

LABORATORY MEASUREMENT OF EFFECTIVE DIFFUSION PARAMETERS IN FRACTURED SOIL

A paper to be submitted to *Soil Science*

Martin F. Helmke, William W. Simpkins, and Robert Horton

Abstract

In soils where advection is small, diffusion can be the dominant mode of solute transport. This paper describes the application of a radial diffusion cell method to determine the effective diffusion coefficient (D_e) and effective diffusive porosity (θ_{De}) for three conservative solutes (Br, PFBA, and PIPES) in eight fractured till units. Twenty-four experiments (three replicates of each of the eight soils) were conducted for a period of 28 days. Estimated values of D_e ranged between 4.6×10^{-10} and 7.2×10^{-10} m^2/s, 1.7×10^{-10} and 3.7×10^{-10} m^2/s, and 7.5×10^{-11} and 2.0×10^{-10} m^2/s for Br, PFBA, and PIPES, respectively. Statistical analysis (using the Kruskal-Wallis and Student's t methods) revealed that D_e differed by compound but not by soil sample, and that each D_e was significantly different from the aqueous diffusion coefficient (D_0) of each compound ($\alpha = 0.05$). Results from the θ_{De} estimates indicated that θ_{De} for PIPES was statistically significantly less than the total porosity, θ_T. Statistical analysis of the difference between θ_{De} and θ_T for Br and PFBA indicated that the differences were statistically significant for only some of the soil samples. Estimates of the first-order exchange coefficient (α) that governs diffusive chemical exchange between fractures and matrix were calculated from D_e, θ_{De}, and fracture spacing as input for fracture solute transport models, and ranged from 1.3×10^{-8} to 1.4×10^{-6} 1/s. The results of this study indicate that effective diffusion parameters may be readily determined by

the radial diffusion cell method, and that effective parameters should be used to model solute transport in fractured soils.

Introduction

In soils where advection is minimal, diffusion may be the dominant mode of solute transport (e.g. Sawatsky et al., 1997); hence, quantification of solute diffusion may be critical. Diffusion may also have a strong influence on solute concentration within mobile pores in a dual porosity medium or in soil of low permeability containing fractures or macropores. In such a soil, small diffusive exchange of mass from the mobile to the immobile region (or vice versa) is likely to cause a large change in solute concentration within the mobile region (Coats and Smith, 1964).

Diffusion is a function not only of the solute but also of the porous medium. For example, the tortuosity of pore throats through which a solute diffuses can cause the effective diffusion coefficient (D_e) to be lower than the diffusion coefficient of a compound in water (D_0) (Rao et al., 1980). Moreover, exclusion of a solute from pores could reduce the effective diffusive porosity (θ_{De}) (van der Kamp et al., 1996). These effective parameters are likely to be specific to each soil/solute combination, and therefore require direct measurement of these properties for the material of interest.

Mathematical solutions to the diffusion problem are well established (e.g. Crank, 1957). In addition, a number of models are capable of simulating solute diffusion coupled with advection through both fractured and unfractured soils (Sudicky and McLaren, 1998; Toride et al., 1999). However, research into measurement of diffusion parameters is not as advanced. Several laboratory methods, including the half-cell, the reservoir-cell, and radial

diffusion cell, have been proposed for determination of D_e. The most widely used is the half-cell method, where two cells, one spiked with a solute, are pressed together allowing diffusion to take place (e.g. Li and Gregory, 1974; Robin et al., 1987). Work by van Rees et al. (1991), however, demonstrated that the process of sectioning a soil column might cause errors in D_e estimates. As an alternative, they proposed a reservoir-cell method, where a reservoir of water spiked with a solute is allowed to diffuse into an adjacent soil column. This method was shown to be more accurate and less labor intensive than the half-cell method. A modification of this method conducts the experiment in radial coordinates using a radial diffusion cell (Novakowski and van der Kamp, 1996; van der Kamp et al., 1996). The technique requires a small, cylindrical reservoir to be drilled into a soil core along its axis. The sample reservoir is filled with a solution of known tracer concentration, and the tracer concentration is monitored over time. The effective diffusion parameters D_e and θ_{De} may be estimated by fitting a radial diffusion model (Novakowski and van der Kamp, 1996) to the time-concentration curve generated from the experiment. Benefits of the method include: 1) ease of sample collection and preparation, 2) minimal sample disturbance, 3) an estimate of θ_{De} may be obtained, and 5) sectioning of the soil sample is unnecessary. Its main drawback is the requirement of saturated soil.

This paper describes the application of the radial diffusion cell method to estimate diffusion properties of eight fractured soils in Iowa. Diffusion parameters were required to simulate solute transport through fractured till as part of a larger study (Helmke et al., 2003). By evaluating a variety of soil samples and tracers, we were also able to determine an acceptable range of diffusion parameters for till and to identify any differences among the samples and tracers that were statistically significant.

Materials and Methods

Study Sites

Till samples were collected from three sites, each from a separate landform region of Iowa (Figure 1). The sites were chosen because they represent some of Iowa's youngest and oldest till units, allowed access to a variety of depths, and because previous studies had established the till stratigraphy and hydrogeology at each site. Site 1 (referred to as the DML site) is located within the Walnut Creek Watershed, 7 km south of Ames, Iowa on the Des Moines Lobe landform region. The Quaternary stratigraphy and hydrogeology of the Walnut Creek Watershed was previously investigated as part of the Management Systems Evaluation Area (MSEA) program (Seo, 1996; Eidem et al., 1999). The surficial deposit at the DML site (and hence the soil parent material) is the Alden Member till of the Dows Formation, deposited 14,000 to 12,500 yr ago during the late Wisconsinan (Prior, 1991; Eidem et al., 1999). The soil at the DML site is the Clarion, a Typic Hapludoll and member of the Clarion-Nicollet-Webster soil association.

The second site (the IES site) is located 6 km southwest of Nashua, Iowa and within the Iowan Erosion Surface landform region. The site was part of the MSEA program to evaluate agricultural impacts on water quality. Previous studies established the till stratigraphy and hydrogeology at the site (Weis and Simpkins, 1996). The soil at the IES site is the Kenyon, a Typic Hapludoll of the Kenyan-Floyd-Clyde soil association. The parent material of this soil is pedisediment from the Hickory Hills Member of the Wolf Creek Formation, which is Pre-Illinoian in age and approximately 500 ka old (Kemmis et al., 1992).

The third site (the SIDP site) is located in Coralville, Iowa on the Southern Iowa Drift Plain landform region. At the SIDP site, the entire 30 m sequence of unconsolidated deposits

had recently been removed to provide quarry access to limestone. Loess caps Pre-Illinoian till units at the site, therefore soil samples were not collected near the surface. Stratigraphic studies at the site (Kemmis et al., 1992) report the till of the Hickory Hills, Aurora, and Winthrop Members of the Wolf Creek Formation (500-730 ka), and till of the Alburnett Formation (>730 ka).

Soil Sampling and Preparation

Samples of till were collected from depths between 1 and 27.5 m at the three sites (Table 1). Soil trenches were excavated at the DML and IES sites to depths of 4 and 2.3 m, respectively to provide access for sample collection and fracture mapping. Only minimal excavation was required at the SIDP site to allow access to undisturbed till. Fractures in the till were mapped on sheets of clear acetate at each site to determine fracture spacing. Samples for diffusion experiments were collected in triplicate at each depth for statistical purposes. Care was taken to avoid collection of fractures within diffusion cell samples. To collect samples for the radial diffusion cell, the till was carved by hand in-situ to form vertical columns 6.7 cm in diameter and 7 cm in height. A 7-cm-long section of polyvinyl chloride (PVC) casing with an interior diameter (ID) of 7.65 cm was placed around each column, after which paraffin wax was poured into the annulus between the sample and the casing. Upon removal from the till in the excavation trench, each sample was sealed in paraffin wax and submerged in groundwater collected from each site to prevent disturbance and desaturation during transport to the laboratory.

In the laboratory, the ends of each sample were removed, reducing the length to 5 cm. Methods similar to those described by van der Kamp et al. (1996) were used to construct the

radial diffusion cells (Figure 2). The column ends were sealed with a 0.5 cm thick layer of paraffin wax. The base of each column was capped by an end plate of high-density polyethylene. A reservoir of diameter 1.2 cm was drilled by hand into the center of each sample. Stainless steel screens with a screen aperture of 1 mm were placed into the sample reservoirs to prevent sidewall collapse or expansion. The top of each sample was then capped by an end plate with a 2 mm diameter hole in the center to provide access to the sample reservoir. This access port was sealed by a removable rubber septum to reduce evaporation. The sample chambers were filled with groundwater (the reservoir fluid) collected from each site and allowed to equilibrate for 1 month prior to the experiment.

Diffusion Cell Experiments

Twenty-four experiments were conducted using the diffusion cells (three replicates of eight soil samples). Three compounds were added simultaneously during each experiment: potassium bromide (KBr), pentafluorobenzoate (PFBA), and 1,4-piperazinediethanesulfonate (PIPES) (Figure 3). Bromide has traditionally been used as a tracer because it reacts little with most soils, is rarely present in natural soil water, and may be readily analyzed by ion chromatography or by an ion-selective electrode. PFBA is another commonly used tracer because it has conservative properties similar to Br, yet can be distinguished from Br using ion chromatography (Bowman and Gibbons, 1992). PIPES is an organic buffer commonly used in microbiological studies. It has recently been used as a groundwater tracer because it is not likely to sorb to till at neutral pH, is not easily biodegraded, has an aqueous diffusion coefficient approximately one-fifth that of Br, and is readily analyzed by ion chromatography (Moline et al., 1997; Jardine, 1998). Br and PIPES have D_0 values reported in the literature

of 1.8 x 10^{-9} and 7.6 x 10^{-10} m^2/s (at 25°C), respectively (Bowman and Gibbons, 1992). To date, D_0 has not been determined for PIPES. Therefore, D_0 was calculated by the Stokes-Einstein equation (Einstein, 1905):

$$D_0 = \frac{kT}{6\pi\mu r} \tag{1}$$

where k is the Boltzman Constant, T is temperature, μ is viscosity, and r is the molecular radius (6.0 x 10^{-10} m for PIPES). Using this equation, the D_0 for PIPES at 25°C is 4.1 x 10^{-10} m^2/s.

A solution of groundwater spiked with 0.5 mM (C_0) of each of the three tracers was used to replace the reservoir fluid in the radial diffusion cells. The reservoirs were sampled nine times over a period of 28 days during the experiment. Sample removal volumes were kept small (0.1 mL) to minimize changes in reservoir concentration. After sampling, an equal volume of clean groundwater (0.1 mL) was returned to the sample reservoir.

Samples were stored at 4°C until analyzed at the end of the experiment. The concentration of Br, PFBA, and PIPES were were determined by ion chromatography. Analytical precision (95 percent confidence limit) was determined for Br (0.63 mg/L), PFBA (1.14 mg/L), and PIPES (2.65 mg/L) by analyzing replicates of spiked samples using Student's t distribution (Harris, 1991).

Estimation of Parameters

Effective diffusion parameters were estimated by fitting the radial diffusion model of Novakowski and van der Kamp (1996) to the results from the experiments. The solution

calculates solute concentration in the sample reservoir as a function of time, and includes diffusion, equilibrium adsorption, and first-order mass loss. The governing equation for radial diffusion is

$$\frac{\partial c}{\partial t} = \frac{D_e \partial^2 c}{R \partial r^2} + \frac{D_e \partial c}{R r \partial r} - \frac{\lambda}{R} c \tag{2}$$

where c is solute concentration, t is time, r is distance from the cell center, R is the retardation factor, and λ is the first-order degradation coefficient (Novakowski and van der Kamp, 1996). Given the boundary conditions of the radial diffusion cell, the solution for Equation 2 requires a Laplace inversion algorithm. For this study, the Stehfest (1970) algorithm was used to perform the Laplace inversion, and the Novakowski-van der Kamp solution was fit to the experimental results using the Levenberg-Marquardt algorithm (Marquardt, 1963). In theory, this approach provides estimates of D_e, θ_{De}, R, and λ. In practice, however, non-equilibrium sorption and degradation may produce non-unique estimates of D_e and θ_{De} (Novakowski and Van der Kamp, 1996). For this reason, only conservative compounds were chosen for this study. Therefore, the parameters estimated were D_e and θ_{De}.

Statistical Analysis

Confidence intervals of mean D_e, and θ_{De} were calculated using Student's t-distribution (Walpole et al., 2001) by:

$$\bar{x} \pm t_{(\alpha, n-1)} \frac{s}{\sqrt{n}} \tag{3}$$

where x is the sample mean, t is the Student's t statistic (two-tailed) with $\alpha = 0.05$ level of significance and n-1 degrees of freedom, s is the sample standard deviation, and n is the number of samples. The statistical difference between means was determined using both parametric and nonparametric techniques (Conover, 1980), which are commonly employed in the field of water resources (Helsel and Hirsch, 1992). The Kruskal-Wallis test (Kruskal and Wallis, 1952) was used to compare medians between more than two sets of independent data. In cases where the means of two sets of data were compared, the independent Student's t-test was employed.

Model goodness-of-fit was evaluated using the modified index of agreement, d_1 (Willmott et al., 1985). The parameter d_1 is given by

$$d_1 = 1.0 - \frac{\sum_{i=1}^{N} |O_i - P_i|}{\sum_{i=1}^{N} \left(|P_i - \overline{O}| + |O_i - \overline{O}| \right)} \tag{4}$$

where O and P are the observed and modeled simulated data, and N is the number of observations. d_1 varies from 0 to 1, with 1 indicating a perfect fit between the simulated and observed data. Therefore, d_1 may be interpreted in a fashion similar to coefficient of determination (R^2). d_1 is considered superior to R^2 because d_1 is less sensitive to outliers than R^2, and because d_1 is sensitive to additive and proportional differences (unlike R^2). The utility of d_1 has been demonstrated in the validation of hydrologic models (Legates and McCabe, 1999).

Results and Discussion

Concentrations of the three compounds declined with time and approached equilibrium near the end of the 28-day experiment (Figure 4). In all cases, diffusion of Br out of the reservoir was the most rapid, followed by PFBA, then PIPES. The rate of concentration decline was inversely proportional to the D_0 of each compound, as expected due to the differences in D_e. Br, PFBA, and PIPES reached a relative concentration of approximately 0.1 by the end of each experiment, at which time the solute concentration throughout the diffusion cell had reached a equilibrium. However, the equilibrium concentration of Br and PFBA was slightly lower than that of PIPES, suggesting that the θ_{De} may be lower for PIPES than for Br or PFBA. The radial diffusion model provided excellent fits to the observed data and d_I values ranged from 0.850 to 0.951 (Figure 4). We conclude from these results that diffusion is an active process in the soil, and that the model can simulate the process and therefore provide reasonable estimates of diffusion parameters.

Effective Diffusion Coefficient

The experiments allowed us to determine whether there were differences in D_e among the soils and among the compounds. Plots of mean D_e for each compound show that there is little difference in D_e between samples (Figure 5). Estimated values of D_e ranged between 4.6×10^{-10} and 7.2×10^{-10} m^2/s, 1.7×10^{-10} and 3.7×10^{-10} m^2/s, and 7.5×10^{-11} and 2.0×10^{-10} m^2/s for Br, PFBA, and PIPES, respectively. Results from the Kruskal-Wallis tests indicate that differences in D_e between soils were not statistically significant at the $\alpha = 0.05$ level. Previous studies (Mehta et al., 1995) have shown that soil type may have an effect on D_e (greater than 50 percent difference), but only when there is significant difference in pore

structure (such as between a sand and a clay soil, for example). The soils evaluated in this study all were similar in texture (all were loams) and porosity (θ_T varied by only 8 percent among the samples; Table 1). Although the Pre-Illinoian samples had a 10 percent greater clay content on average than the late Wisconsinan samples, this difference apparently had little or no effect on the value of D_e. However, differences in D_e were significant ($\alpha = 0.05$) when compared on a compound-to-compound basis. The Kruskal-Wallis test revealed that mean values of D_e among the three compounds were different ($p < 0.0001$). Moreover, the Mann-Whitney test demonstrated that mean D_e between Br and PFBA, PFBA and PIPES, and Br and PIPES were all different statistically ($p < 0.0001$). Another finding of this research was that mean D_e was less than D_0 for all compounds and for all soils (Kruskal-Wallis $p < 0.0001$).

Effective Diffusive Porosity

Results from the θ_{De} estimates indicate that θ_{De} may be slightly less than θ_T. Values of θ_{De} ranged from 17.4 to 32.0 percent with a mean of 25.5 percent (Table 2). On average, θ_{De} was 15 percent less than θ_T (28 percent less in the case of PIPES), which is a smaller difference than the 50 percent decrease reported by Meegoda and Gunaskera (1992) and van der Kamp et al. (1996). However, these earlier studies evaluated diffusion in clays and clay-rich tills, which would likely contain smaller pore throats and have a greater charge density. The authors attributed differences between θ_{De} and θ_T to isolated pores, bound water, and ion exclusion. Identifying the exact mechanism of reduction in θ_{De} is beyond the scope of this

paper; however, the lower θ_{De} is likely to affect model predictions of solute transport through fractured soils, and should therefore be considered.

Differences between θ_T and θ_{De} appear to be a function of both compound and soil. The results from the independent t-tests demonstrate that for all soil samples, θ_{De} for PIPES was statistically different ($\alpha = 0.05$) than θ_T ($p < 0.002$ that they were identical). Statistical comparisons between θ_{De} and θ_T were less conclusive for Br and PFBA, and varied by sample. In the case of Br, the ALG, ALT, H2, AO, and ALB estimates of θ_{De} were not statistically different from their respective θ_T values at the $\alpha = 0.05$ level. Likewise, estimated θ_{De} was not statistically different from θ_T for the ALG, ALT, H1, and AO samples for PFBA. Meegoda and Gunaskera (1992) reported that θ_{De} was lower for heavier compounds (propanol and glycerol) than lighter ones (acetone). Van der Kamp et al. (1996) reported a reduction in θ_{De} for chloride and sulfate, but not deuterium. The results from the earlier studies and from this paper suggest that properties of the compound may have an influence on θ_{De}, but further research is needed to quantify the underlying mechanism.

Calculation of α

Part of the motivation for this study was to determine solute transport properties for fractured soil experimentally without the aid of the parameter estimation techniques common in the literature. In particular, solute transport models that simulate diffusion as a second-order process require D_e and θ_{De} as input explicitly. Mobile-immobile models, such as those proposed by Coats and Smith (1964), Sudicky (1989); van Genuchten and Wagenet (1989), and Toride et al. (1993), require a first-order mass exchange coefficient (α) and the porosity

of the immobile region (θ_{im}). Our experiments allow direct estimates of α from D_e and θ_{De} through the equation:

$$\alpha = \frac{aD_e\theta_{im}}{l^2} \tag{5}$$

where a is a shape factor, θ_{im} is the immobile porosity (represented by θ_{De}), and l is a characteristic length (Parker and Valocchi, 1986; Sudicky, 1990). Equation 5 has been shown to work well for a system of equally spaced, parallel fractures (Sudicky, 1990) and for spherical soil aggregates (Rao et al., 1980). For the purposes of this study, the matrix blocks are assumed to be prismatic slabs of width equal to fracture spacing ($2B$). Therefore, a and l are equal to 3 and B in Equation 3, respectively. In contrast to D_e, calculated values of α range between 1.3 x 10^{-8} and 1.4 x 10^{-6} 1/s (Table 3). Calculated values of α are strongly influenced by fracture spacing because they increase as the inverse square of $2B$; thus, field measurements of this parameter are necessary to produce valid estimates of α.

Conclusions

Results from this study demonstrate that diffusion is an active process in fractured till. Concentration of Br, PFBA, and PIPES within the diffusion cell reservoirs rapidly diminished and approached equilibrium within the first week of the 28-day experiments. Estimates of D_e and θ_{De} were readily determined by fitting the radial diffusion model (Novakowski and van der Kamp, 1996) to the data. All D_e estimates were significantly less than D_0, indicating that D_e should be determined experimentally for soil. D_e was not a function of soil type, however the soils evaluated in this paper all had similar texture.

Estimates of θ_{De} were significantly less (28 percent less) than θ_T for PIPES. However, only some θ_{De} estimates were less than θ_T for Br and PFBA. Although differences between θ_{De} and θ_T may appear small, these differences may have a greater effect on diffusive transport than D_e because they determine concentration at equilibrium whereas D_e only influences transient concentrations. Whether diffusion is a controlling process depends on the presence of other solute transport mechanisms (e.g. advection and dispersion) that may mask the effect of diffusion. However, if diffusion is a controlling process, then effective diffusion parameters should be used.

This paper demonstrates that model input parameters of diffusion, such as α, may be calculated directly from D_e, θ_{De}, and field parameters (i.e. fracture spacing). As such, α is sensitive not only to effective diffusion parameters, but also to the internal geometry of the system. The results of this study indicate that the radial diffusion cell method is an accurate and efficient method for obtaining parameters of effective diffusion in fractured soils, and that these effective parameters should be used to model chemical transport in fractured soil.

Acknowledgements

This research was funded by grants from the American Geophysical Union (Horton Grant), the Association of Ground Water Scientists and Engineers, the Geological Society of America, Sigma Xi, and the USEPA through an Interagency Agreement DW12036252 to the Agricultural Research Service. We thank P. Jardine and G. Moline for the suggestion of using PIPES as a tracer, and G. van der Kamp for suggesting the use of the radial diffusion cell method.

References

Bowman, R. S. and J. S. Gibbens. 1992. Difluorobenzoates as nonreactive tracers in soil and ground water. Ground Water. v. 30, pp. 8-14.

Coats, K. H. and B. D. Smith. 1964. Dead-end pore volume and dispersion in porous media. Society of Petroleum Engineers Journal. v. 4, pp. 73-84.

Conover, W. J. 1980. Practical Nonparametric Statistics (Second Edition). John Wiley and Sons, New York, New York, 493 pp.

Crank, J. 1975. The Mathematics of Diffusion, Second Edition. Oxford University Press, 424 p.

Eidem, J. M., W. W. Simpkins, and M. R. Burkart. 1999. Geology, groundwater flow, and water quality in the Walnut Creek watershed. Journal of Environmental Quality. v. 28, pp. 60-69.

Einstein, A. 1905. On the movement of small particles suspended in a stationary liquid demanded by the molecular kinetics of heat. Ann Phys. v. 17, pp. 549-560.

Harris, D. C. 1991. *Quantitative Chemical Analysis, Third Ed.*, W. H. Freeman and Company, 782 p.

Helmke, M. F., W. W. Simpkins, and R. Horton. 2003. Chapter 1: Fracture-dominated transport of nitrate and atrazine through till in Iowa. In unpub. Ph.D. dissertation, Iowa State University, pp. 5-37.

Helsel, D. R. and R. M. Hirsch. 1992. Statistical Methods in Water Resources. Studies in Environmental Science 49, Elsevier, Amsterdam, The Netherlands. 522 p.

Jardine, P. 1998. Personal communication.

Kemmis, T. J., E. A. Bettis III, and G. R. Hallberg. 1992. Quaternary geology of Conklin Quarry. Guidebook Series no. 13. Iowa Department of Natural Resources. 41 p.

Legates, D. R. and G. J. McCabe Jr. 1999. Evaluating the use of "goodness-of-fit" measures in hydrologic and hydroclimatic model validation. Water Resources Research. v. 35, pp. 233-241.

Li, Y. and S. Gregory. 1974. Diffusion of ions in sea water and in deep-sea sediments. Geochemica et Cosmochemica Acta. v. 38, pp. 703-714.

Marquardt, D. W. 1963. An algorithm for least-squares estimation of nonlinear parameters. Journal of the Society of Industrial and Applied Mathematics. v. 11, n. 2, pp. 431-441.

Meegoda, N. J. and S. D. Gunasekera. A new method to measure effective porosity of clays. Geotechnical Testing Journal. v. 15, n. 4, pp. 340-351.

Mehta, B. K., S. Shiozawa, and M. Nakano. 1995. Measurement of molecular diffusion of salt in unsaturated soils. Soil Science. v. 159, n. 2, pp. 115-121.

Moline, G. R., C. R. Knight, and R. Ketcham. 1997. Laboratory measurement of transport processes in a fractured limestone/shale saprolite using solute and colloid tracers. Abstracts with Programs, Geological Society of America. v. 29, n. 6, p. 370.

Novakowski, K. S. and G. van der Kamp. 1996. The radial diffusion method 2. A semianalytical model for the determination of effective diffusion coefficients, porosity, and adsorption. Water Resources Research. v. 32, pp. 1823-1830.

Parker, J. C. and A. J. Valocchi. 1986. Constraints on validity of equilibrium and first-order kinetic transport models in structural soils. Water Resources Research. v. 22, pp. 399-407.

Prior, J. C. 1991. Landforms of Iowa. University of Iowa Press, Iowa City, Iowa. 154 p.

Rao, P. S. C., R. E. Jessup, D. E. Rolston, J. M. Davidson, and D. P. Kilcrease. 1980. Experimental and mathematical description of nonadsorbed solute transfer by diffusion in spherical aggregates. Soil Science Society of America Journal. v. 44, pp. 684-688.

Robin, M. J. L., R. W. Gillham, and D. W. Oscarson. 1987. Diffusion of strontium and chloride in compacted clay-based materials. Soil Science Society of America Journal. v. 51, pp. 1102-1108.

Sawatsky, N., Y. Feng, and M. J. Dudas. 1997. Diffusion of 1-naphthol and naphthalene through clay materials: measurement of apparent exclusion from the pore space. Journal of Contaminant Hydrology. v. 27, pp. 25-41.

Seo, H. H. 1996. Hydraulic properties of Quaternary stratigraphic units in the Walnut Creek watershed. Master's Thesis. Iowa State University. 145 p.

Stehfest, H. 1970. Algorithm 368, numerical inversion of Laplace transforms. Communications of the ACM. v. 13, n. 1, pp. 47-49.

Sudicky, E. A. 1989. The Laplace transform Galerkin technique: a time-continuous finite element theory and application to mass transport in groundwater. Water Resources Research. v. 25, pp. 1833-1846.

Sudicky, E. A. 1990. The Laplace transform Galerkin technique for efficient time-continuous solution of solute transport in double-porosity media. Geoderma. v. 46, pp. 209-232.

Sudicky, E. A. and R. G. McLaren. 1998. FRACTRAN User's Guide. An efficient simulator for two-dimensional, saturated groundwater flow and solute transport in porous or discretely-fractured porous formations. Groundwater Simulations Group, Waterloo Centre for Groundwater Research. University of Waterloo, Ontario, Canada. 97 p.

Toride, N, F. J. Leij, and M. Th. van Genuchten. 1999. The CXTFIT code for estimating transport parameters from laboratory or field tracer experiments. *Research Report No. 137.* U. S. Salinity Lab., USDA, ARS, Riverside, CA, 121 p.

van der Kamp, G., D. R. Van Stempvoort, and L. I. Wassenaar. 1996. The radial diffusion method 1. Using intact cores to determine isotopic composition, chemistry, and effective porosities for groundwater in aquitards. Water Resources Research. v. 32, n. 6, pp. 1815-1822.

van Genuchten, M. Th. and R. J. Wagenet. 1989. Two-site/two-region models for pesticide transport and degradation: theoretical development and analytical solutions. Soil Science Society of America Journal. v. 53, pp. 1303-1310.

van Rees, K. C. J., E. A. Sudicky, P. S. C. Rao, and R. Reddy. 1991. Evaluation of laboratory techniques for measuring diffusion coefficients in sediments. Environmental Science and Technology. v. 25, n. 9, pp. 1605-1611.

Walpole, R. E., R. H. Myers, S. L. Myers, and K. Ye. 2001. Probability and Statistics for Engineers and Scientists, 7th Ed. Pearson Education. 752 pp.

Weis, M. R. and W. W. Simpkins. 1996. Nitrate and herbicide transport in groundwater within fractured, pre-Illinoian till units near Nashua, Iowa. Abstracts with programs, Geological Society of America. v. 28, n. 6, pp. 70.

Willmott, C. J., S. G. Ackleson, R. E. Davis, J. J. Feddema, K. M. Klink, D. R. Legates, J. O'Donnell, and C. M. Rowe. 1985. Statistics for the evaluation and comparison of models. Journal of Geophysical Research. v. 90, pp. 8995-9005.

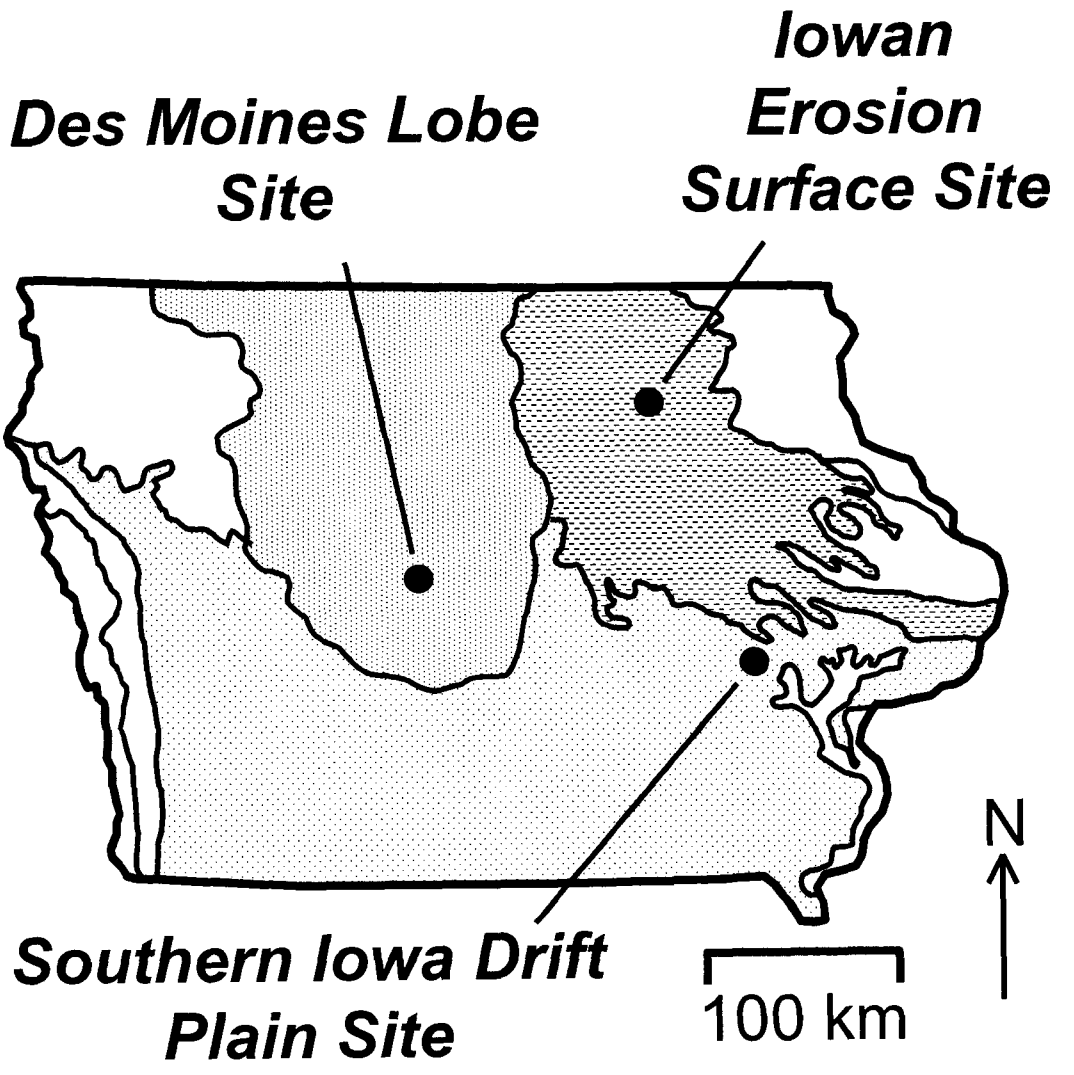

Figure 1. Map showing the locations of the three study sites on the Des Moines Lobe (DML), Iowan Erosion Surface (IES), and Southern Iowa Drift Plain (SIDP) landform regions of Iowa. Other landform regions given in Prior (1991)

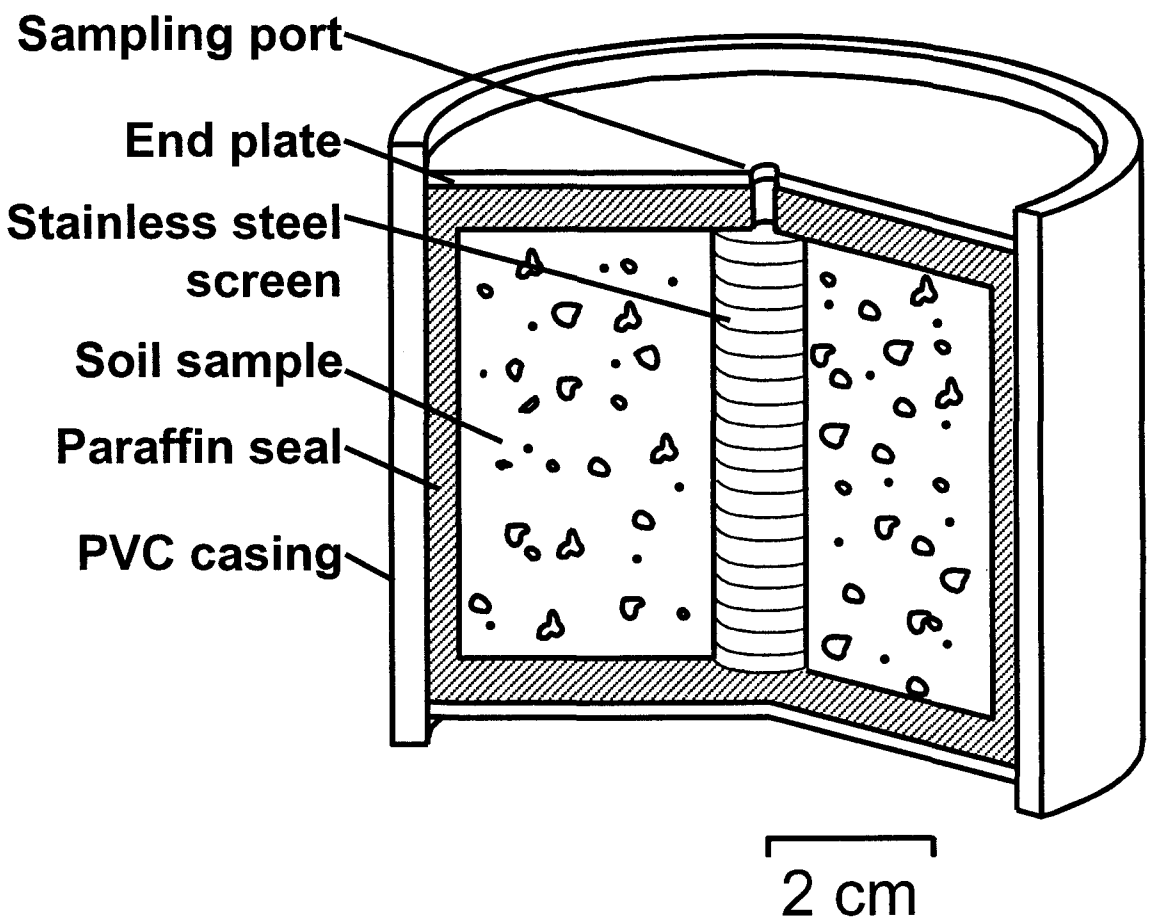

Figure 2. Schematic diagram of the diffusion cell apparatus.

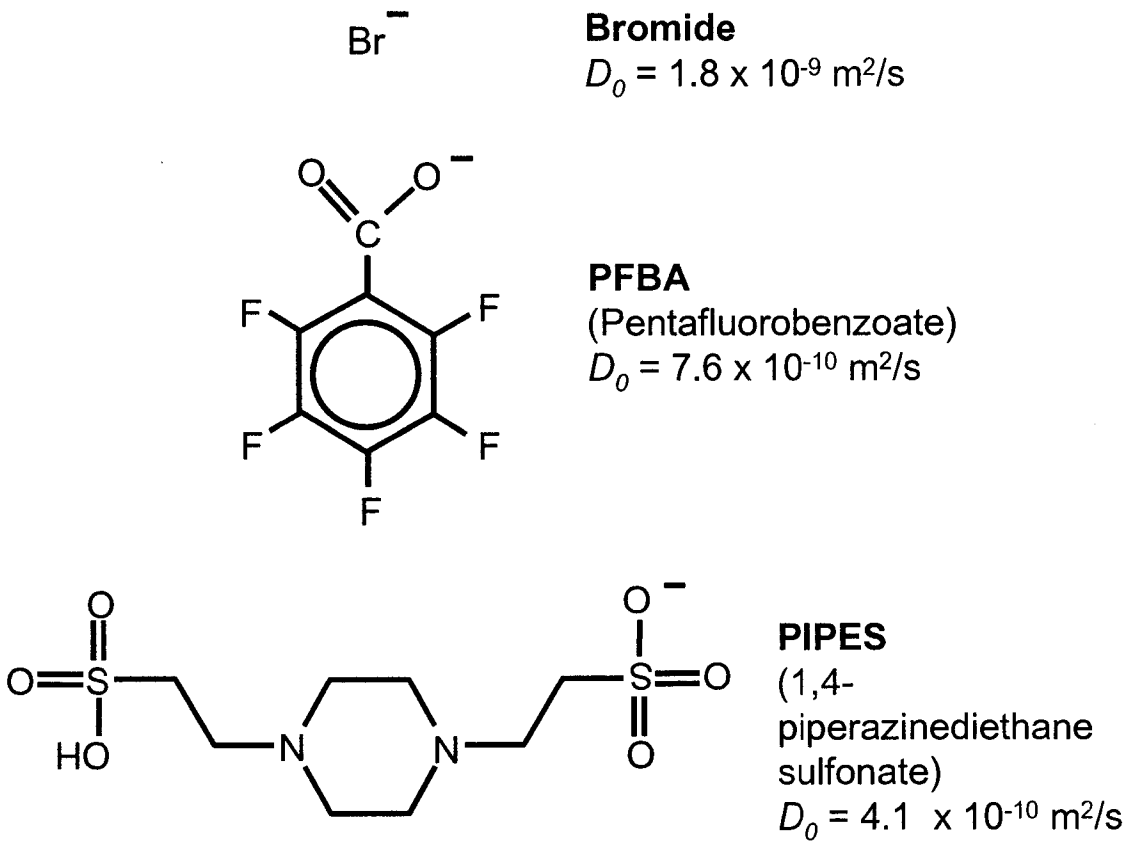

Figure 3. Molecular structure and aqueous diffusion coefficient (D_0) of bromide, PFBA, and PIPES.

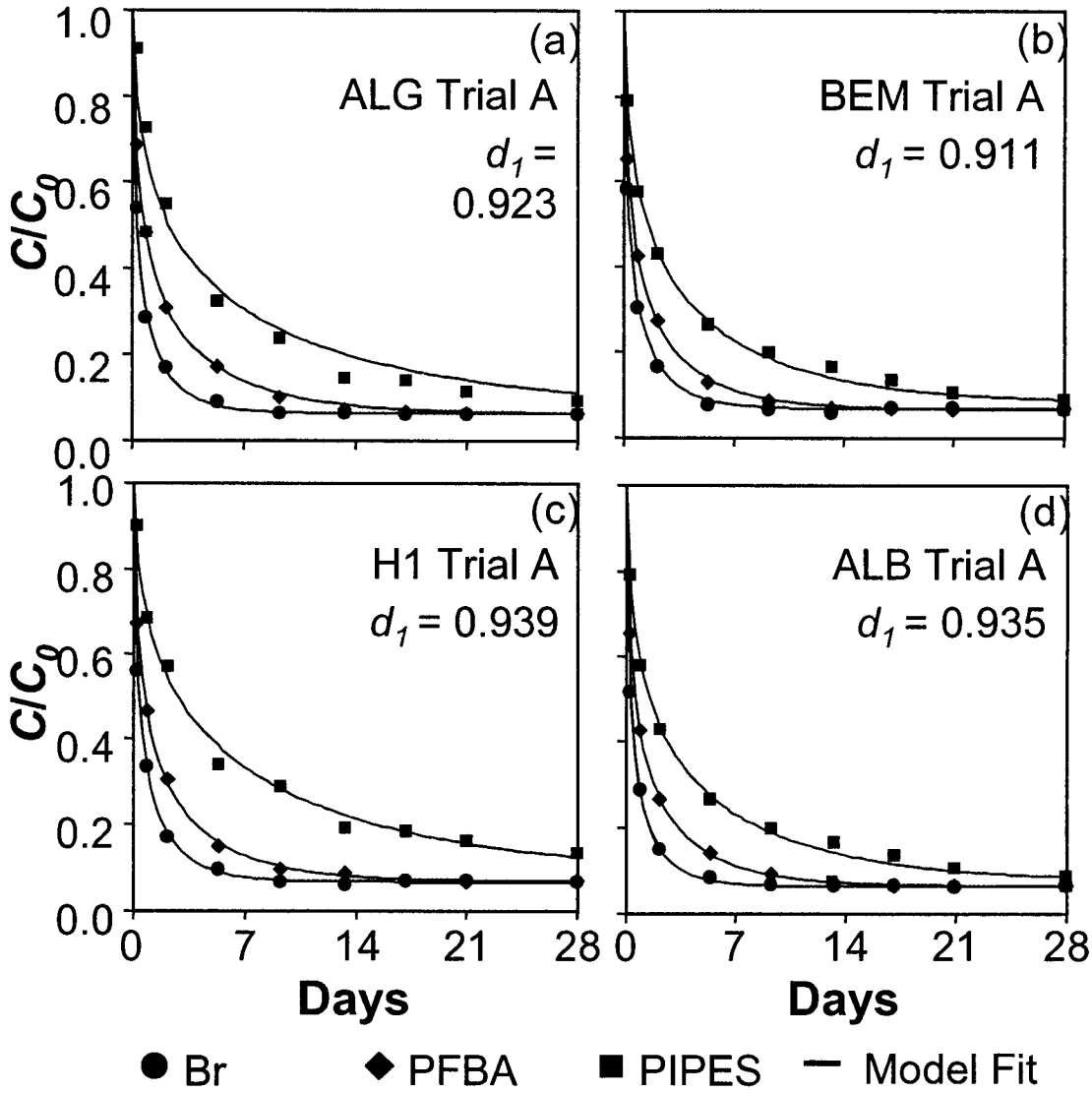

Figure 4. Time-concentration plots of Br, PFBA, and PIPES taken from four radial diffusion cell experiments. Lines represent the diffusion curves simulated by the radial diffusion model.

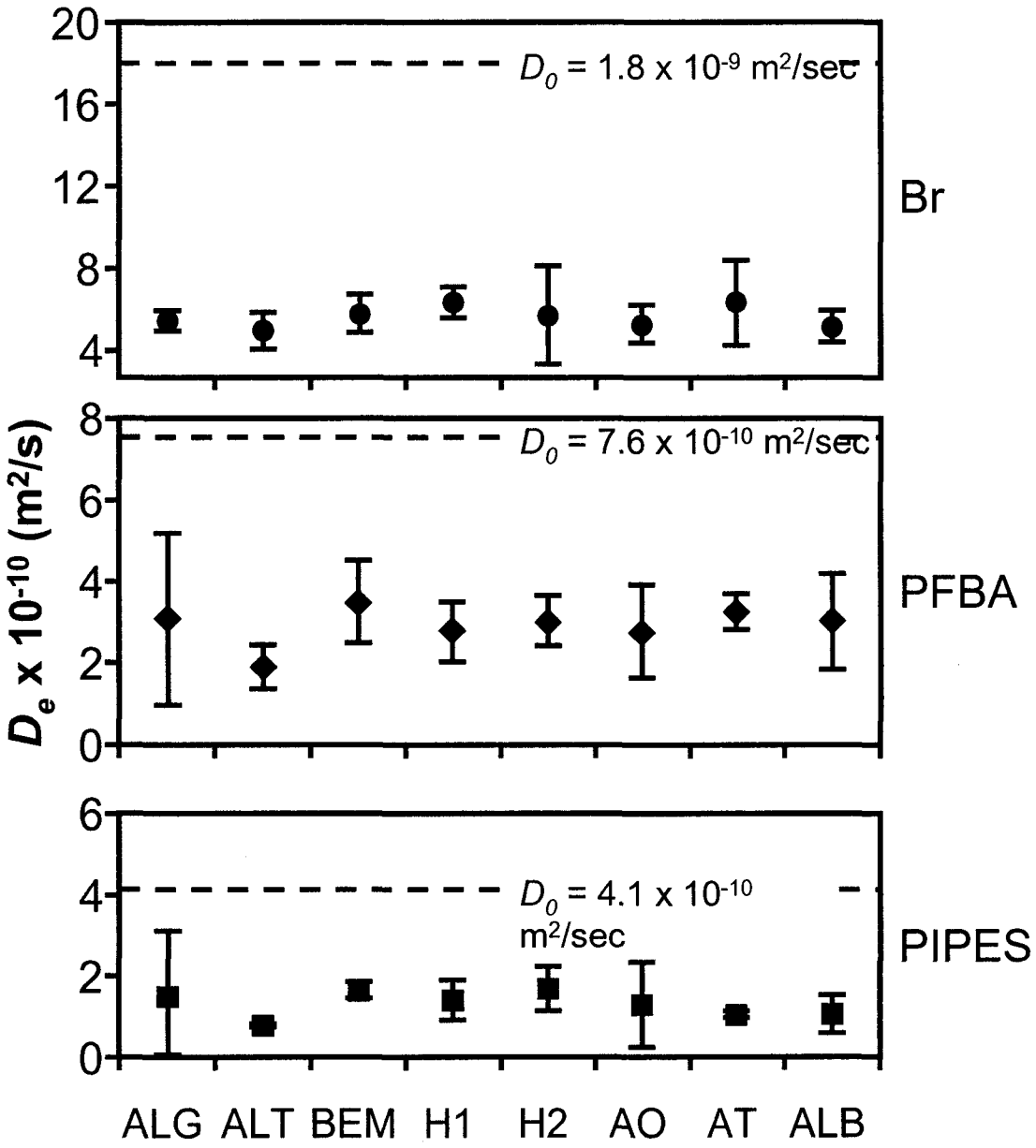

Figure 5. Effective diffusion coefficients (D_e) for Br, PFBA, and PIPES plotted against sample name. Each point represents the mean of 3 replicates, and the bars indicate 95 percent confidence intervals of the mean. The aqueous diffusion coefficient (D_0) for each compound is shown as a dashed line.

Table 1. Location, depth, stratigraphic classification, status of till weathering, bulk density (ρ_b), total porosity (θ_T), and texture of the eight soils evaluated by this study.

Sample name	Site†	Sample depth (m)	Formation	Member	Status of till weathering	ρ_b (kg/m^3)	θ_T (percent)	Sand (percent)	Silt (percent)	Clay (percent)
ALG	DML	1.0	Dows	Alden	weathered	1,670	29.8	46.8	37.8	15.5
ALT	DML	2.0	Dows	Alden	weathered	1,840	30.5	49.6	36.0	14.4
BEM	DML	3.3	Dows	Alden	partially weathered	1,830	29.6	48.2	37.0	14.8
H1	IS	1.3	Wolf Creek	Hickory Hills	weathered	1,820	31.2	38.7	33.8	27.5
H2	IS	1.5	Wolf Creek	Hickory Hills	weathered	1,860	30.7	44.1	33.2	22.8
AO	IDP	10.5	Wolf Creek	Aurora	weathered	1,820	30.5	37.4	38.1	24.6
AT	IDP	16.5	Wolf Creek	Aurora	partially weathered	1,890	28.8	31.0	41.6	27.4
ALB	IDP	27.5	Alburnett	N/A	unweathered	2,010	28.6	31.0	45.6	23.4

† DML = Des Moines Lobe; IES = Iowan Erosion Surface; SIDP = Southern Iowa Drift Plain

Table 2. Total (θ_T) and effective diffusive (θ_{De}) porosities for Br, PFBA, and PIPES. Each value is a mean that represents 3 replicates. The 95-percent confidence intervals of the mean are shown in parentheses.

Sample name	θ_T (percent)	Br θ_{De} (percent)	PFBA θ_{De} (percent)	PIPES θ_{De} (percent)
ALG	29.9 (29.0 to 30.7)	30.0 (28.2 to 31.8)	28.5 (26.4 to 30.6)	24.6 (21.6 to 27.6)
ALT	30.6 (28.5 to 32.7)	29.1 (25.8 to 32.3)	29.2 (28.9 to 29.6)	22.9 (22.8 to 23.1)
BEM	29.6 (28.1 to 31.1)	26.9 (24.4 to 29.4)	25.2 (20.3 to 30.1)	21.5 (20.2 to 22.7)
H1	31.2 (30.2 to 32.2)	29.1 (28.3 to 30.0)	29.8 (24.9 to 34.7)	23.7 (17.7 to 29.7)
H2	30.4 (28.4 to 32.4)	26.5 (23.4 to 29.6)	24.5 (22.3 to 26.7)	18.9 (17.0 to 20.7)
AO	30.7 (29.0 to 32.4)	31.1 (29.5 to 32.8)	29.4 (27.7 to 31.1)	24.1 (22.0 to 26.2)
AT	28.9 (28.5 to 29.3)	24.4 (22.6 to 26.2)	21.3 (20.0 to 22.5)	18.4 (17.5 to 19.4)
ALB	28.6 (28.4 to 28.9)	28.3 (26.3 to 30.4)	25.6 (22.7 to 28.4)	19.9 (17.7 to 22.0)
sample mean	30.0 (29.6 to 30.5)	28.3 (27.4 to 29.2)	26.5 (25.2 to 27.9)	21.6 (20.5 to 22.7)
sample std. dev.	1.1	2.2	3.2	2.6

Table 3. Measured fracture spacing ($2B$) and calculated first-order exchange coefficients (α) for Br, PFBA, and PIPES in the eight soil samples. The 95-percent confidence intervals of the mean are shown in parentheses.

Sample name	$2B$ (cm)	Br $\alpha \times 10^{-7}$ 1/s	PFBA $\alpha \times 10^{-7}$ 1/s	PIPES $\alpha \times 10^{-7}$ 1/s
ALG	4.3	10.5 (9.3 to 11.8)	5.6 (1.7 to 9.6)	2.4 (0.0 to 5.1)
ALT	4.6	8.2 (6.4 to 9.9)	3.1 (2.3 to 4.0)	1.0 (0.96 to 1.1)
BEM	4.3	10.0 (8.2 to 11.9)	5.7 (3.7 to 7.6)	2.3 (2.0 to 2.6)
H1	3.8	13.7 (10.9 to 16.5)	6.7 (3.8 to 9.5)	2.5 (0.4 to 4.6)
H2	6.8	4.1 (2.6 to 5.5)	1.8 (1.5 to 2.1)	0.51 (0.45 to 0.57)
AO	3.4	15.3 (12.3 to 18.2)	7.8 (4.3 to 11.3)	2.2 (1.1 to 3.2)
AT	17.8	0.70 (0.61 to 0.79)	0.31 (0.21 to 0.41)	0.13 (0.07 to 0.18)
ALB	10.4	1.7 (0.9 to 2.5)	0.81 (0.60 to 1.01)	0.35 (0.22 to 0.48)
sample mean	6.9 (2.8 to 11.1)	4.0 (3.7 to 4.3)	1.9 (1.7 to 2.1)	0.93 (0.80 to 1.05)
sample std. dev.	5.0	0.57	0.45	0.30

EFFECT OF FRACTURES ON HYDRAULIC CONDUCTIVITY OF TILL UNITS IN IOWA

A paper to be submitted to Environmental and Engineering Geoscience

M. F. Helmke and W. W. Simpkins

Abstract

Fractures can have a large effect on hydraulic conductivity of geologic materials. The purpose of this paper is to quantify fracture distributions in till units in Iowa, and to relate these distributions to fracture genesis; to measure K_b in large till columns from different depths and till units; and to demonstrate the effect of fracture geometry and genesis on K_b and advective velocity. Till units were studied at three landform regions to evaluate the potential for fracture flow and its effect on hydraulic conductivity and advective velocity. The till units ranged in age from 12.5 to >730 ka and were taken from depths of 1 to 27.5 m. Fractures were mapped in the field to document their density per m^2 and orientation. Clast fabric was measured to determine ice-flow direction. Fractures were present at all study locations and at all depths, including one site where fractures intersected an aquifer at 30 m depth. Fractures at the Des Moines Lobe site had a spacing of 4.3 cm at 3.3 m and a fracture density of 260 fractures/m^2. Two subvertical fracture sets at 56.0° and 214.5° were oriented perpendicular to ice-flow direction as indicated by clast fabric. These fractures probably formed by tension caused during or after glaciation. Fracture spacing at the Iowa Erosion Surface site was 3.8 cm at 1.6 m depth, density was 145 fractures/m^2, and there is no preferred orientation. Clast fabric was weak and these fractures were probably formed by desiccation. Fractures at the Southern Iowa Drift Plain site formed large distinct polygons that were primarily vertical and had no preferred strike orientation. Fracture spacing was 10.4 cm and fracture density was 221 fractures/m^2 at a depth of 27.5 m. Clast fabric

indicated an ice-flow direction from northwest to southeast, but there was no relationship between that and the fracture orientation; hence, these fractures were probably formed by desiccation.

Laboratory experiments using eight large (0.40 to 0.45 m in length and 0.43 m in diameter), undisturbed columns of till from these sites showed bulk hydraulic conductivity (K_b) ranging from 7.7×10^{-10} to 3.8×10^{-5} m/s, which is generally greater than the matrix hydraulic conductivity (K_m) reported in the literature. K_b was not related to the landform region, till unit, or to fracture origin. Instead, values of K_b decreased with depth at all sites as a log-log function. This suggests that lithostatic stress reduces fracture apertures with depth. Calculated advective velocities range from 0.88 to 658 m/d under a unit gradient. Higher velocities occur in till nearest the land surface, while lowest velocities occur at depth, which effectively increases the residence time for sorption and microbial processes to retard or degrade chemicals. The higher velocities in shallow till units suggest that the concept of till aquitards protecting shallow aquifers requires re-evaluation.

Introduction

Till units of Pre-Illinoian through late Wisconsinan age have been assumed to protect aquifers in Iowa from surficial contaminants. In Iowa, like other states in the Midwestern U.S., contaminant sources include nutrients and herbicides applied to fields, landfill leachate, effluent from swine manure lagoons, and toxic compounds from hazardous waste sites. Consultants and regulators have traditionally assumed that till acts as a barrier to contaminant migration, particularly nonpoint source contaminants. Studies in Iowa indicate that widespread nitrate and herbicide contamination of aquifers has occurred despite being

overlain by till (Kross et al., 1994), and that fractures allow contaminants to migrate rapidly through these units (Helmke et al., 2003).

It is well documented that fractures increase solute transport velocity. Fractures increase bulk hydraulic conductivity (K_b) and reduce effective porosity (n_e). The bulk hydraulic conductivity of a fractured till is typically one to 3 orders of magnitude greater than K_b for an unfractured till (Freeze and Cherry, 1979; Keller et al., 1989). Fracture porosity (n_f) is often one to 4 orders of magnitude less than the total porosity (n_T) of till (Jørgensen and Spliid, 1992; McKay et al., 1993a). Advective velocity of solutes may be estimated using the average linear velocity equation

$$V = \frac{K_b i}{n_e} \tag{1}$$

where V is velocity, and i is the hydraulic gradient. By Equation 1, the combined effects of increased K_b and decreased n_e result in a great increase in velocity. Using this equation, fluid velocities up to 200 m/day have been calculated for fractured till (Jørgensen et al., 1998). Processes of matrix diffusion, sorption, and degradation retard contaminant transport through fractured till, allowing only a small percentage of a solute to travel at velocities calculated by Equation 1 (Freeze and Cherry, 1979).

We hypothesize that fractures in till are the primary cause of the increase in hydraulic conductivity above cited values for the till matrix. Furthermore, we hypothesize that the type of fracture distribution and the genesis of those fractures may affect K_b and increase advective velocities. The purpose of this paper is to quantify fracture distributions in till units in Iowa, and to relate these distributions to fracture genesis; to measure K_b in large till

columns from different depths and till units; and to demonstrate the effect of fracture geometry and genesis on K_b and advective velocity.

Methods

Study Sites

Three study sites, each representing a different till unit and a different Iowa landform region, were investigated (Figure 1). The sites were chosen because they represent some of Iowa's youngest and oldest till units (ranging in age from 12.5 to >730 ka), because they allowed access to depths up to 30 m, and because previous studies had established the glacial stratigraphy and hydrogeology at each site. The three sites were named after their respective landform regions: the Des Moines Lobe site (DML), the Iowa Erosion Surface site (IES), and the Southern Iowa Drift Plain site (SIDP).

The DML site is located within the Walnut Creek Watershed, 7 km south of Ames, Iowa. The Quaternary stratigraphy and hydrogeology of the Walnut Creek Watershed was previously investigated as part of the Management Systems Evaluation Area (MSEA) program (Seo, 1996; Eidem et al., 1999). The surficial deposit at the DML site is the Alden Member till of the Dows Formation, deposited 14 to 12.5 ka during the late Wisconsinan (Prior, 1991; Eidem et al., 1999). The Alden Member is a massive, basal till with a bulk density of approximately 1,700 kg/m^3. The texture of the Alden Member is typically 40 percent sand, 45 percent silt, and 15 percent clay and is classified as a loam (Kemmis et al., 1981). Unlike older tills in Iowa, the clay mineralogy of the Alden Member has a high smectite content (69%, Kemmis et al., 1981).

The IES site is located 6 km southwest of Nashua, Iowa. Previous studies established the glacial stratigraphy and hydrogeology at the site (Weis and Simpkins, 1996). The surficial deposit at the site is a 1.1-m thick section of late Wisconsinan- to Holocene-aged pedisediment (Pisgah Formation) above the Hickory Hills Member till of the Wolf Creek Formation, which is Pre-Illinoian in age (approximately 500 ka, Kemmis et al., 1992). Thus, at this site, the columns were taken from till that was just below till-pedisediment interface. The Hickory Hill Member is a loam with 45 percent sand, 35 percent silt, and 20 percent clay with a bulk density ranging between 1,760 and 1,880 kg/m^3 (Kemmis et al., 1992).

The third site (the SIDP site) lies near Coralville, Iowa on the Southern Iowa Drift Plain landform region. At the SIDP site, a 30 m sequence of unlithified deposits had recently been removed to provide quarry access to limestone. Stratigraphic studies at the site (Kemmis et al., 1992) reported the presence of the Hickory Hills, Aurora, and Winthrop till Members of the Wolf Creek Formation (500 to 730 ka), and the Alburnett Formation till (>730 ka). The till units are loams with 30 to 50 percent sand, 30 to 45 percent silt, and 20 to 25 percent clay. Bulk densities range from 1,760 to 2,110 kg/m^3. The deepest and oldest till is the Alburnett Formation, which has a higher bulk density (1.97 to 2.11 kg/m^3, Kemmis at al., 1992).

Fracture Mapping

Fractures were mapped at each site to document their occurrence and to assess any patterns present that would elucidate their genesis. A backhoe was used to excavate soil pits at the DML and IES sites, which were 3.9 and 2.3 m deep, respectively. Active quarry operations at the SIDP site allowed convenient access to fresh till faces to a depth of 30 m.

The walls of the excavation pits were constructed using a bench and tier system, which increased the stability of the walls and provided multiple dihedral faces for mapping fractures and collecting samples. Till exposures were further prepared using a hand trowel and putty knife to ensure that exposed till was fresh and undisturbed by backhoe excavation. Fractures were identified by iron-stained halos or evidence of leaching along fracture surfaces. Fractures from both horizontal and vertical faces were traced onto sheets of clear acetate and later digitized. Fracture spacing ($2B$) was measured at the depth of each column using a measuring tape.

The strike and dip of fractures were measured using a Brunton compass. Strike and dip measurements were transformed to vectors normal to the fracture plane, then plotted on a stereonet. Fracture sets were identified by fitting the Fisher distribution (a 3-dimensional extension to the normal distribution; Fisher, 1953) to the observed data using the software program FracMan/ISIS (Dershowitz et al., 1994). The Kolmogorov-Smirnof method (Conover, 1980) was used to determine statistical confidence that sets were properly represented by the Fisher distribution. The orientation (trend and plunge) of elongate clasts (fabric) was recorded at each site to assist in the determination of ice-flow direction. Eigenvectors and eigenvalues of fabric were calculated using principal component analysis (Mark, 1973). Geomorphic evidence was also evaluated for evidence of ice-flow direction.

Column Preparation

Soil was removed from benches in the soil pits using hand trowels and putty knives to exhume free-standing columns of intact till, 43 cm in diameter and approximately 50 cm in length. The columns were collected from depths between 1.0 and 27.5 m (Table 1). The

cylindrical shape of each column was maintained using a level and a section of polyvinyl chloride (PVC) pipe as a guide. A 61-cm-long piece of PVC with an interior diameter (ID) of 46 cm was placed over each column, leaving a 1-cm void between the column and the pipe. This annulus between the till and the casing was sealed with paraffin wax, a technique that has been demonstrated to prevent sidewall flow (Grisak et al., 1980; Kluitenberg et al., 1991). After the wax cooled (approximately 8 hours), a putty knife was used to separate each column from its in-situ base, after which each column was lifted from the excavation trench. Disks made of high-density polyethylene (HDPE) with a thickness of 3 mm were placed at the column ends and sealed with wax to prevent moisture loss during transport to the laboratory.

Laboratory Methods

After being transported to the laboratory, the column ends were carefully scraped with a putty knife to minimize smearing of the till. Ottawa sand was placed in 5-mm-thick layers at the column ends and held in place by the HDPE disks. Perforated HDPE tubes of 3-mm ID were pressed into the sand to provide fluid access to the sand packs. Pistons of 19-mm-thick plywood were added to the column ends and sealed with silicone caulking. The ends and the walls of the columns were mechanically compressed to a pressure approximately equal to in-situ lithostatic conditions. A pressure of 60 kPa, equivalent to a depth of approximately 3.5 m, was the maximum pressure that could be obtained by this method. Although great care was exercised to minimize desaturation of the columns, it is possible that some of the larger pores drained during excavation and transport. Each column

was slowly re-saturated from beneath by upward flow during a period of at least 7 days to reduce the chance of entrapped air within pores.

Groundwater collected from each site was induced to flow through each column under a constant upward gradient. A unit hydraulic gradient was applied to the ALT, BEM, H1, H2, AO, AT, and ALB columns. A gradient of 0.021 was applied to the ALG column (the most conductive column collected) to reduce the flow rate from 330 mL/min to 6.93 mL/min. Although upward gradients were applied (to prevent desaturation at the column base), groundwater flow was downward with respect to each column because they were inverted in the laboratory. Column temperature was maintained at a constant 12°C to simulate in-situ conditions. Flow rates were monitored and calculation of K_b was performed using the Darcy equation.

Soil texture was determined using the sieve and pipette method (Walter et al., 1978). Sand, silt, and clay particle sizes used in this study were 2 to 0.063 mm, 0.063 to 0.002 mm, and <0.002 mm, respectively. Bulk density (ρ_b) was determined by collecting soil samples in cylinders of known volume and weighing them after being dried for 24 hours at 104°C. Total porosity was determined gravimetrically by weighing saturated samples, oven-drying them, dividing the difference by the density of water, then dividing this by the original volume of each sample. Pore volume (PV) was determined as the product of θ_T and the volume of each column.

Calculation of Fracture Aperture (2b)

Because fractures are planar features, they are commonly considered as parallel plates that are separated by a fracture aperture (2b). By representing fractures as vertical, equally

spaced, and orthogonal plates, the aperture may be estimated using the Cubic Law (Snow, 1969):

$$2b = \left(\frac{K_b 6\mu 2B}{\rho g} \right)^{\frac{1}{3}} \tag{2}$$

where μ is fluid viscosity, ρ is fluid density, and g is the acceleration due to gravity. It is clear by Equation 2 that K_b is a function of the cube of 2b. Therefore, K_b is highly sensitive to aperture. Aperture may in turn be used to estimate n_f by (Sudicky, 1990):

$$n_f = 2\frac{2b}{2B} \tag{3}$$

Velocity may be estimated by substituting n_f for n_e in Equation 1, if the hydraulic gradient is known.

Results and Discussion

Characterization of Materials

Despite the wide range of till these columns represented, the textures of the till units are relatively similar. Soil texture was determined using the sieve and pipette method (Walter et al., 1978). Sand, silt, and clay particle sizes used in this study were 2 to 0.063 mm, 0.063 to 0.002 mm, and <0.002 mm, respectively. Till samples from the DML site had a mean texture of 48 percent sand, 37 percent silt, and 15 percent clay (Table 1). Till units at the IES and SIDP sites were more fine-grained, with mean textures of 36.5 percent sand, 38.5 percent silt, and 25 percent clay (Table 1).

Fracture Mapping

Fractures were encountered at all three study sites and at all depths, although the fracture patterns and the density of fractures were different at the sites. The abundance of fractures at each site suggests that these fractures are ubiquitous in till units in Iowa. The deepest fractures were observed in the Alburnett Formation at the SIDP site (30 m depth) where they intersected the till/limestone contact.

The fractures observed near the base of the DML excavation trench were dense, subvertical, and oriented in a northeast/southwest pattern (Figure 2). The average fracture spacing at this site was 4.3 cm at a depth of 3.3 m with a fracture density of 260 fractures/m^2. The fracture orientations at this depth were plotted on a stereonet of vectors normal to each fracture plane (Figure 2b). Statistical analysis of fracture orientation revealed two nearly vertical fracture sets, with strikes of 56.0° and 214.5° (Kolmogorov-Smirnof confidence of 98.5 percent). This preferential orientation indicates that the fractures did not form randomly as would be expected if they were formed by desiccation (Connell, 1984). Till clasts displayed a fabric of moderate strength (Figure 2c). Principal component analysis of the fabric at this site yielded a principle eigenvector (s_1) with a trend of 323.4°, a plunge of 18.1°, and an eigenvalue of 0.741. Strong till fabrics have been shown to point in the up-ice direction (Mark, 1973), and are used routinely to indicate ice-flow direction. The fabric and the orientation of minor moraine features at the site (Stewart et al., 1988) indicate that ice flow was from the northwest towards the southeast (143°). Ice-flow direction is perpendicular to the orientation of the fractures, which suggests that the fractures formed by tensile stress in the direction of ice flow. Tensile stress (extending ice-flow) could have been present in the glacier at this location if the ice were accelerating, possibly because of local

topography at the base of the ice, or surging. Fracture orientation measurements near the DML site conducted by Lee (1991) showed a preferred orientation approximately 30 to 45 degrees from the ice-flow direction. This suggests that fracture genesis may be influenced by local stresses in the till, and that one mode of genesis may not be appropriate for all fractures. Future work is needed, however, to further investigate how fractures form in till deposited by active glaciers.

In contrast to the fractures observed at the DML site, fractures at the IES lacked a preferred orientation (Figure 3). Fracture spacing at the 1.6 m depth at the IES site was 3.8 cm and fracture density was 145 fractures/m^2. No preferred fracture orientation (Figure 3b) was present vertically or horizontally. Clast fabric at the IES site was weak (Figure 3c), with a principal eigenvector trend and plunge of 357.3° and 11.9°, and an eigenvalue of 0.461. A weak fabric was expected because the shallow sediments (diamicton) at the site are composed of reworked pedisediment (Weis and Simpkins, 1996). Their polygonal pattern and lack of preferential orientation suggest that the fractures were produced primarily by desiccation.

The fractures at the SIDP site form large, distinct polygons (Figure 4). At the sample depth of 27.5 m, average fracture spacing was 10.4 cm and fracture density was 221 fractures/m^2. The fractures were predominantly vertical with a random strike (Figure 4b). Clast fabric at this site was strong, with a principle eigenvector trend of 306.7°, plunge of 11.4°, and an eigenvalue of 0.863, which suggests an ice-flow direction from northwest to southeast. However, there was no apparent correlation between ice-flow direction and fracture strike. The polygonal, vertical and random nature of the fractures indicates that these fractures formed primarily from desiccation, perhaps overprinting stress-related

fratures. Previous investigations of fractures at the SIDP site reported similar polygonal fracture patterns within the Aurora Member till of the Wolf Creek Formation (Hallberg, 1986; Kemmis et al., 1992). They attributed their genesis to desiccation and weathering of paleosurfaces. The fracture spacing reported by these previous studies ranged between 37 and 109 cm with a mean of 68.8 cm (Kemmis et al., 1992).

Bulk Hydraulic Conductivity (K_b)

The results of this study compare well with values of K_b reported for fractured till in the literature. The K_b of the columns spanned 5 orders of magnitude, from 7.7 x 10^{-10} m/s for the deepest column to 3.8 x 10^{-5} m/s for the shallowest column (Figure 5 and Table 2). These values are similar to K_b values determined from slug tests conducted at the DML site (8 x 10^{-8} to 3 x 10^{-5} m/s from late Wisconsinan till at 4.7 to 1.6 m depth, respectively, and 6 x 10^{-10} m/s for unweathered pre-Illinoian till at 15.3 m depth (Seo, 1996). The results are also similar to K_b values derived from slug-tests in Canada (Keller et al., 1988) and large-column tests in Denmark (Jørgensen et al., 1998).

The values of K_b confirm the influence of fractures in these till units. Studies in Canada (Keller et al., 1988; Keller et al., 1989) and Denmark (Fredericia, 1990; Jørgensen et al., 1998) reported that K of unfractured till (determined by permeameter tests) ranges from 1 x 10^{-11} to 7 x 10^{-10} m/s. The texture of the till evaluated in this paper is similar to the texture of till reported in the literature (20 percent clay, 40 percent silt, and 40 percent clay); however, some of the studies evaluated till with a clay percentage up to 40 percent, which represent the lower end of the K spectrum. Using these K values as a proxy for K of the till matrix (K_m), all measured K_b values in this study were greater than K_m (Figure 5). This

provides additional evidence that the fractures increased K beyond what would be expected from the matrix alone.

Elevated values of K_b combined with low estimates of n_f result in rapid transport velocities. Calculated values of n_f ranged from 7.6 x 10^{-3} to 0.5 percent, which were lower than estimates of n_T (28.6 to 31.2 percent, Table 2). Similar low values of n_f were reported by McKay et al. (1993a, n_f 0.03 to 01 percent) and Jørgensen et al. (1998, n_f 0.053 to 0.28 percent) for fractured till in Canada and Denmark, respectively. Estimates of V using Equation 1 with a unit hydraulic gradient range from 0.88 m/d at 27.5 m depth to 658 m/d at 1 m depth (Table 2). The most rapid velocities (greater than 10 m/d) were calculated for shallow till (less than 3 m depth). At depths greater than 3 m, velocities were slower, which would allow processes such as sorption and degradation to retard the movement of contaminants.

Additional evidence of fracture flow is provided by the decrease of K_b with depth. K_b decreased as a log-log function with depth according to the following equation:

$$\text{Log}[K_b \text{ (m/s)}] = -3.2 \text{ Log}[\text{depth (m)}] - 4.7 \quad (4)$$

The coefficient of determination (R^2) of Equation 4 is 0.96 (level of significance > 99 percent). This phenomenon suggests control of K_b by fractures, because K_m should be independent of depth (Keller et al., 1989). The reduction of K_b with depth is well documented for till units in Iowa (Seo, 1996; Eidem et al., 1999), Canada (McKay and Fredericia, 1995), and Denmark (Fredericia, 1990). With all fractures closed, K_b would reduce to K_m. Because fracture density (Table 2) also does not decrease with depth, we

conclude that the reduction of K_b must be due to a reduction in fracture aperture with depth. This is corroborated by estimates of fracture aperture (Table 2). A mechanism for reducing fracture aperture is increased lithostatic stress with depth (Handy and Wang, 1990). However, fractures may still be active regardless of lithostatic stress if they are filled with silt, sand, or other permeable material.

Conclusions

Fractures were present in till at all three study sites and at all depths evaluated, which suggests that till in Iowa is pervasively fractured. Differences in fracture morphology and density indicates that the fractures may have formed by a variety of processes, including stress during or after glaciation, desiccation, or a combination of both.

Results from laboratory experiments using large columns show that the fractures were hydraulically conductive regardless of the particular fracture pattern present or the origin of the fracture. Hydraulic conductivity of the columns was greater than would be expected if the fractures were not present. Values of K_b decreased with depth as a log-log function, suggesting that lithostatic stress reduces fracture apertures and K_b with depth. Fractures found in thin till units play an important role in the transport of chemicals in glaciated regions and should be considered in studies of point and non-point source pollution and assessments of aquifer vulnerability.

Acknowledgements

This research was funded by grants from the American Geophysical Union (Horton Grant), the Association of Ground Water Scientists and Engineers, the Geological Society of

America, Sigma Xi, and the USEPA through an Interagency Agreement DW12036252 to the Agricultural Research Service. The authors wish to thank T. Doe and W. Dershowitz at Golder Associates for providing access to the FracMan/ISIS software package.

References

Conover, W. J. 1980. Practical Nonparametric Statistics (Second Edition). John Wiley and Sons, New York, New York, 493 pp.

Connell, D. E. 1984. Distribution, characteristics, and genesis of joints in fine-grained till and lacustrine sediments, eastern and northwestern Wisconsin. Master's Thesis, University of Wisconsin, Madison. 443 p.

Dershowitz, W., G. Lee, J. Geier, S. Hitchcock, and P. R. La Plointe. 1994. FracMan version 2.4 – Interactive discrete feature data analysis, geometric modeling and exploration simulation. Golder Associates, Inc., Redmond, Washington. 171 p.

Eidem, J. M., W. W. Simpkins, and M. R. Burkart. 1999. Geology, groundwater flow, and water quality in the Walnut Creek watershed. Journal of Environmental Quality. v. 28, pp. 60-69.

Fisher, R. A. 1953. Dispersion on a sphere. Proceedings fromt the Royal Society of London. A217, pp. 295-305.

Fredericia, J. 1990. Saturated hydraulic conductivity of clayey tills and the role of fractures. Nordic Hydrology. v. 21, pp. 119-132.

Freeze, R. A. and J. A. Cherry. 1979. Groundwater. Prentice Hall Pub. 604 p.

Grisak, G. E. and J. F. Pickens. 1980. Solute transport through fractured media: 1. The effect of matrix diffusion. Water Resources Research. v. 16, pp. 719-730.

Grisak, G. E., J. F. Pickens, and J. A. Cherry. 1980. Solute transport through fractured media: 2. Column study of fractured till. Water Resources Research. v. 16, pp. 731-739.

Hallberg, G. R. 1986. Pre-Wisconsinan glacial stratigraphy of the central plains region in Iowa, Nebraska, Kansas, and Missouri. *In* V. Sibrava et al. (ed.) Quaternary glaciations of the Northern Hemisphere. Quat. Sci. Rev. v. 6, pp. 11-16.

Handy, R. L. and H. Y. Wang. 1990. Geotechnical Evaluation of Glacial Till Properties. In Annual Progress Report to the Iowa DNR-GSB, Aquitard Hydrology Project, Ames Research Site, pp. 145-160.

Helmke, M. F., W. W. Simpkins, and R. Horton. 2003. Chapter 1: Fracture-dominated transport of nitrate and atrazine through till in Iowa. In unpub. Ph.D. dissertation, Iowa State University, pp. 5-37.

Jørgensen, P. R. and J. Fredericia. 1992. Migration of nutrients, pesticides and heavy metals in fractured clayey till. Geotechnique. v. 42, pp. 67-77.

Jørgensen, P. R., L. D. McKay, and N. ZH. Spliid. 1998. Evaluation of chloride and pesticide transport in a fractured clayey till using large undisturbed columns and numerical modeling. Water Resources Research. v. 34, pp. 539-553.

Jørgensen, P. R. and N. H. Spliid. 1992. Mechanisms and rates of pesticide leaching in shallow clayey till. European Conference on Integrated Research for Soil and Sediment Protection and Remediation. MECC, Maastricht, the Netherlands. 11 p.

Keller, C. K., G. van der Kamp, and J. A. Cherry. 1988. Hydrogeology of two Saskatchewan tills, I. Fractures, bulk permeability, and special variability of downward flow. Journal of Hydrology. v. 101, pp. 97-121.

Keller, C. K., G. van der Kamp, and J. A. Cherry. 1989. A multiscale study of the permeability of a thick clayey till. Water Resources Research. v. 25, n. 11. pp. 2299-2317.

Kemmis, T. J., E. A. Bettis III, and G. R. Hallberg. 1992. Quaternary geology of Conklin Quarry. Guidebook Series no. 13. Iowa Department of Natural Resources. 41 p.

Kemmis, T. J., G. R. Hallberg, and A. J. Lutenegger. 1981. Depositional environments of glacial sediments and landforms on the Des Moines Lobe, Iowa. Guidebook Series no. 6. Iowa Department of Natural Resources. 132 p.

Kluitenberg, G. L., J. R. Bilskie, and R. Horton. 1991. Rubberized asphalt for sealing cores of shrinking soil. Soil Science Society of America Journal. v. 55, pp. 1504-1507.

Kross, B. C., G. R. Hallberg, D. R. Bruner, R. D. Libra, K. D. Rex, L. M. B. Weih, M. E. Vermace, L. F. Burmeister, N. H. Hall, K. L. Cherryhomes, J. K. Johnson, M. I. Selim, B. K. Nations, L. S. Seigley, D. J. Quaide, A. G. Dudler, K. D. Sesker, M. A. Culp, C. F. Lynch, H. F. Nicholson, and J. Hughes. 1990. *The Iowa State-Wide Rural Well-Water Survey, Water Quality Data: Initial Analysis*, Iowa Department of Natural Resources Technical Information Series 19, 142 p.

Lee, S. H. 1991. Genesis and distribution of fractures in late-Wisconsinan till of the Des Moines Lobe in central Iowa. Unpublished M.S. thesis, Department of Geological and Atmospheric Sciences, Iowa State University, 85 p.

Mark, D. M. 1973. Analysis of axial orientation data, including till fabrics. Geological Society of America Bulletin. v. 84, pp. 1369-1374.

McKay, L. D., D. J. Balfour, and J. A. Cherry. 1998. Lateral chloride migration from a landfill in a fractured clay-rich glacial deposit. Ground Water. v. 36, pp. 988-999.

McKay, L. D., J. A. Cherry, and R. W. Gillham. 1993a. Field experiments in a fractured clay till: 1. Hydraulic conductivity and fracture aperture. Water Resources Research. v. 29, pp. 1149-1162.

McKay, L. D., J. A. Cherry, and R. W. Gillham. 1993b. Field experiments in a fractured clay till: 2. Solute and colloid transport. Water Resources Research. v. 29, pp. 3879-3890.

McKay, L. D. and J. Fredericia. 1995. Distribution, origin, and hydraulic influence of fractures in a clay-rich glacial deposit. Canadian Geotechnical Journal. v. 32, pp. 957-975.

Prior, J. C. 1991. Landforms of Iowa. University of Iowa Press, Iowa City, Iowa. 154 p.

Seo, H. H. 1996. Hydraulic properties of Quaternary stratigraphic units in the Walnut Creek watershed. Master's Thesis. Iowa State University. 145 p.

Snow, D. T. 1969. Anisotropic permeability of fractured media. Water Resources Research. v. 5, pp. 1273-1289.

Stewart, R. A., D. Bryant, and M. J. Sweat. 1988. Nature and origin of corrugated ground moraine of the Des Moines Lobe, Story County, Iowa. Geomorphology. v. 1, pp. 111-130.

Sudicky, E. A. 1990. The Laplace transform Galerkin technique for efficient time-continuous solution of solute transport in double-porosity media. Geoderma. v. 46, pp. 209-232.

Weis, M. R. and W. W. Simpkins. 1996. Nitrate and herbicide transport in groundwater within fractured, pre-Illinoian till units near Nashua, Iowa. Abstracts with Programs, Geological Society of America. v. 28, n. 6, pp. 70.

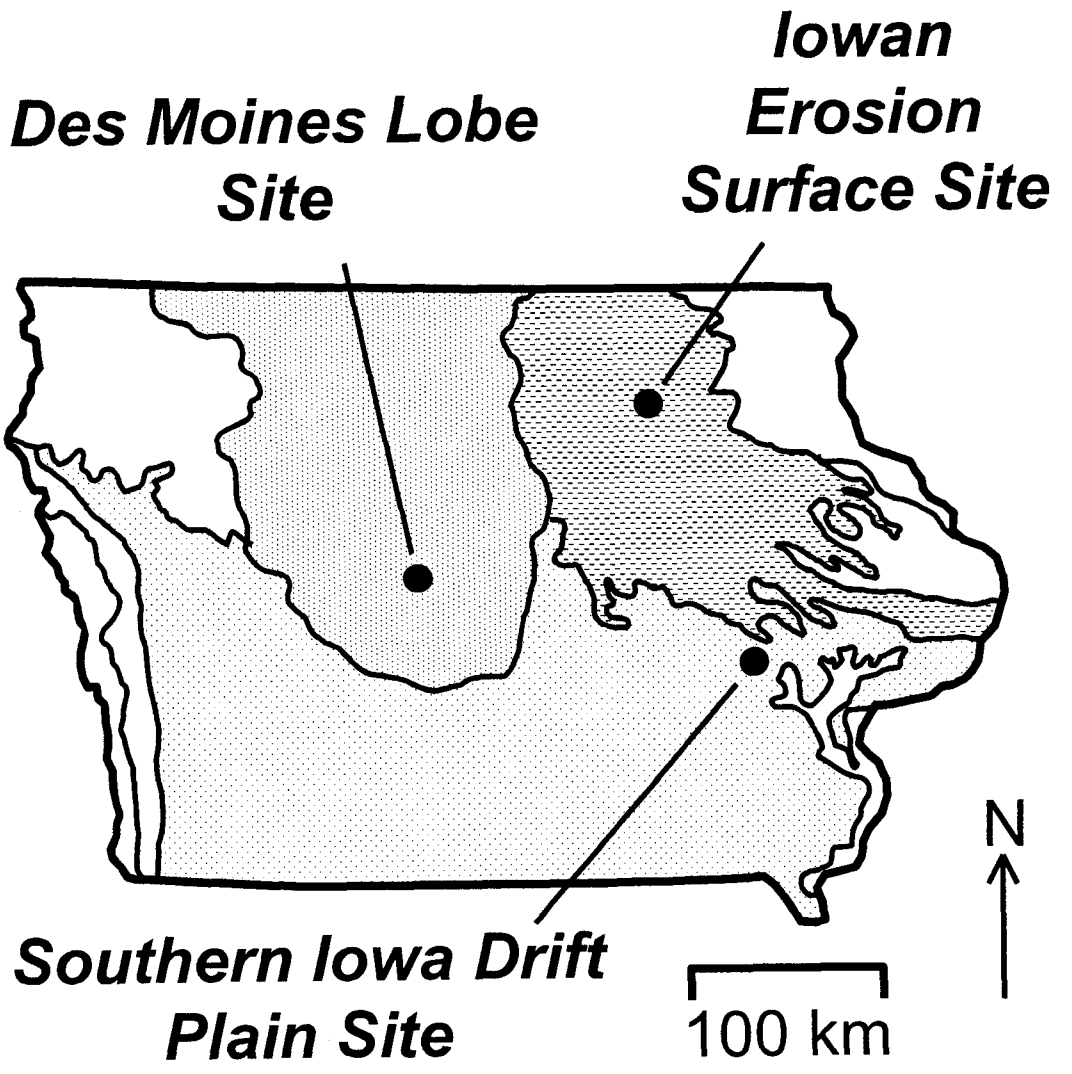

Figure 1. Map showing the locations of the three study sites on the Des Moines Lobe (DML), Iowan Erosion Surface (IES), and Southern Iowa Drift Plain (SIDP) landform regions of Iowa. Other landform regions given in Prior (1991).

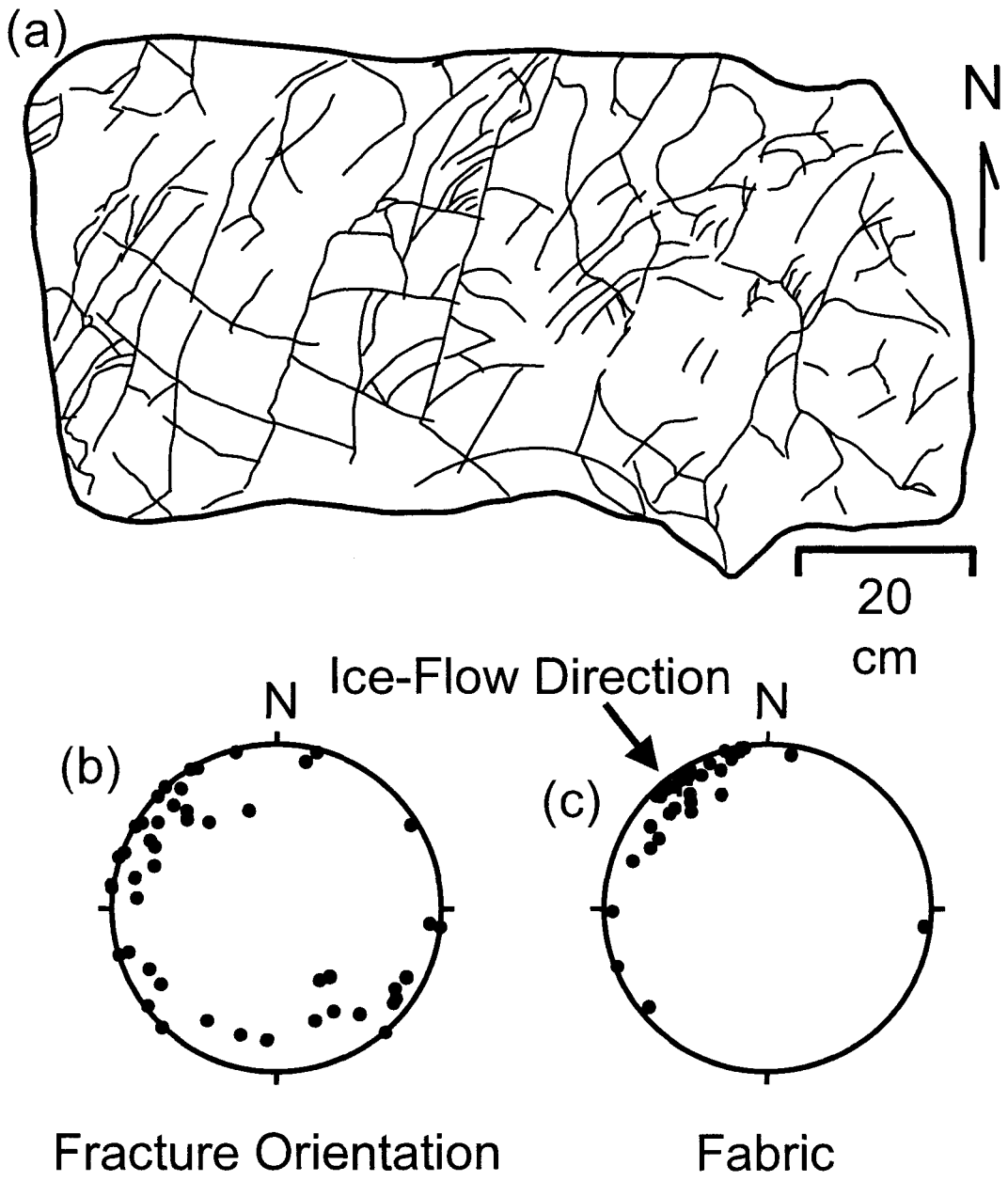

Figure 2. Plan-view fracture map (a), fracture orientation stereonet (b), and till fabric (c) recorded at the DML site at a depth of 3.3 m.

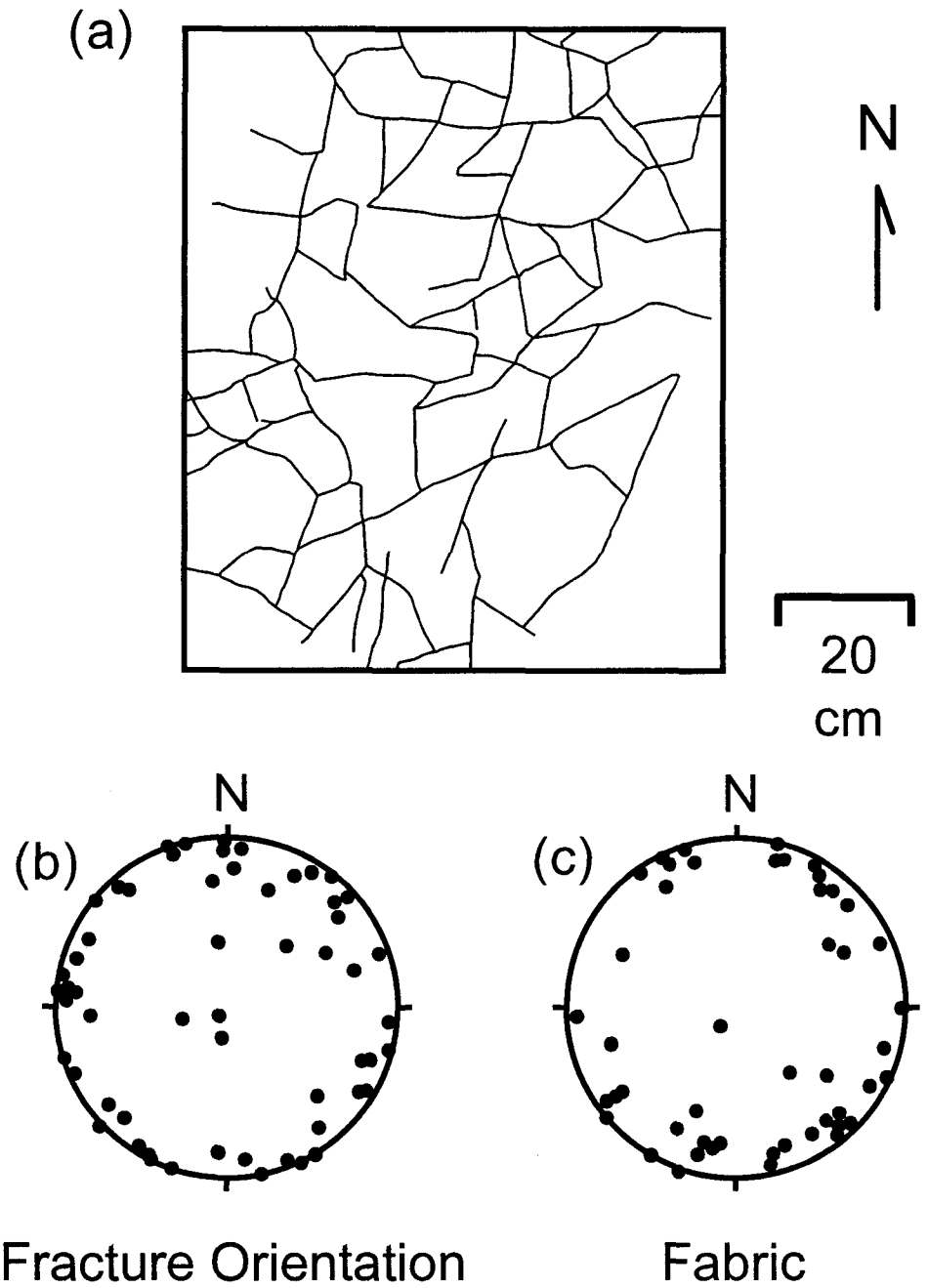

Figure 3. Plan-view fracture map (a), fracture orientation stereonet (b), and till fabric (c) recorded at the IES site at a depth of 1.6 m.

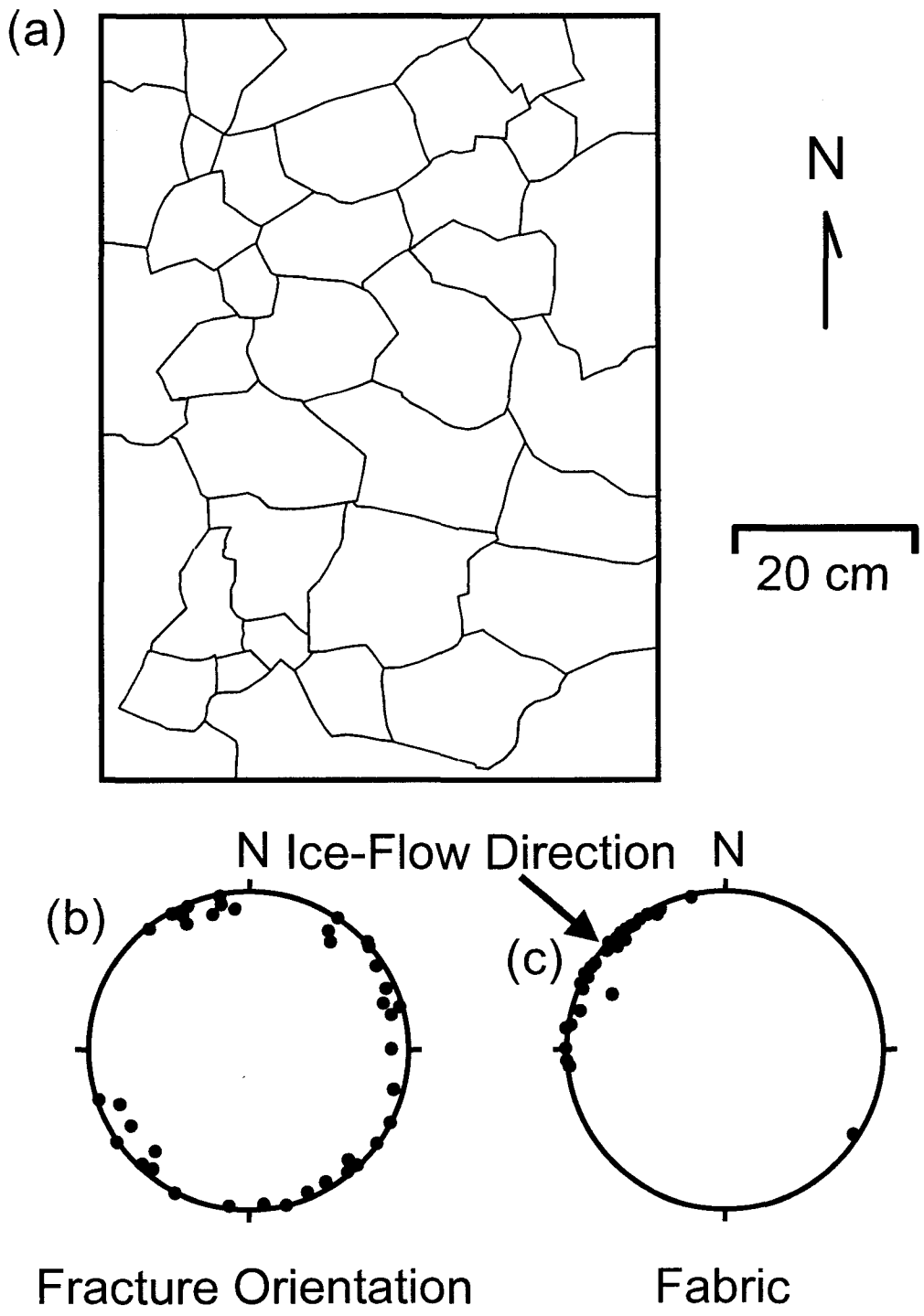

Figure 4. Plan-view fracture map (a), fracture orientation stereonet (b), and till fabric (c) recorded at the IDP site at a depth of 27.5 m.

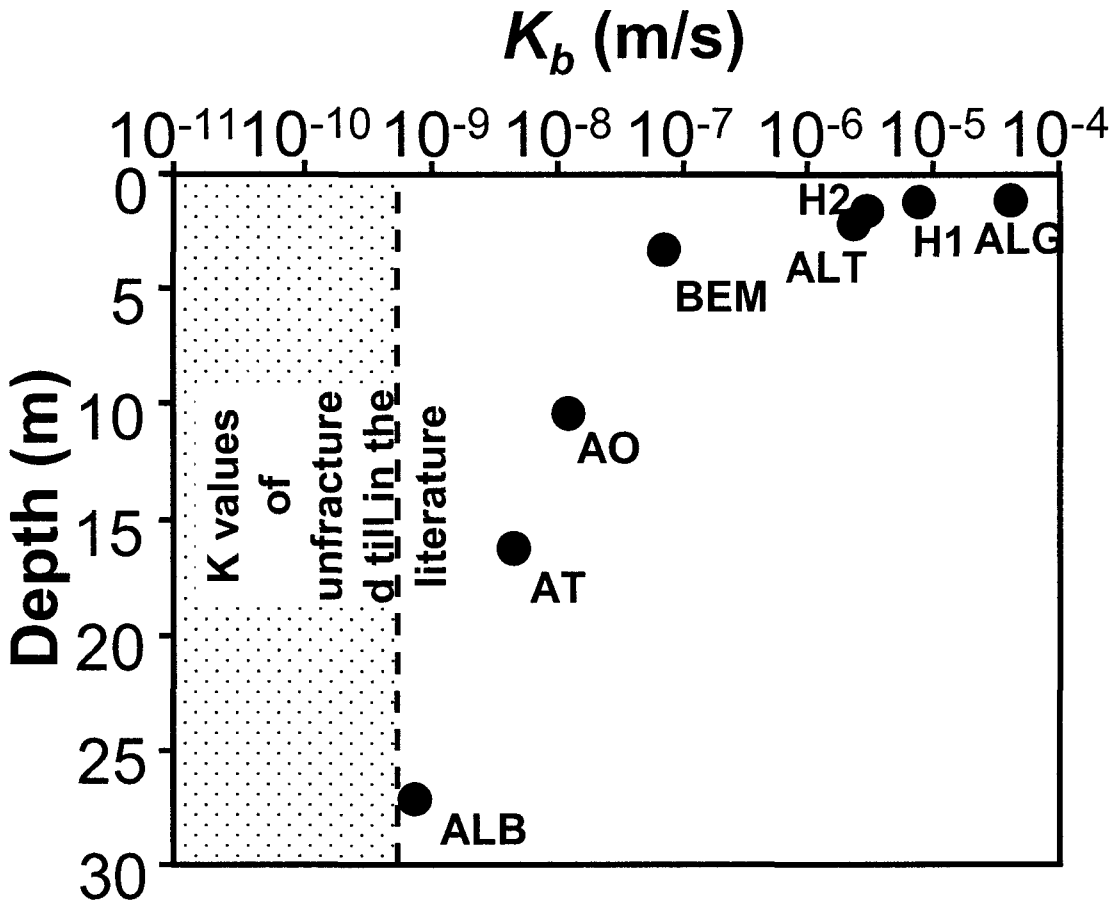

Figure 5. Plot of bulk hydraulic conductivity (K_b) and depth for the eight columns evaluated in this study (note K_b is plotted on a log scale).

Table 1. Location, depth, stratigraphic classification, status of till weathering, bulk density (ρ_b), total porosity (n_T), and texture of the eight columns collected for this study.

Column name	Site†	Sample Depth (m)	Formation	Member	Status of till weathering	ρ_b (kg/m^3)	n_T (percent)	Sand (percent)	Silt (percent)	Clay (percent)
ALG	DML	1.0 to 1.45	Dows	Alden	weathered	1,670	29.8	46.8	37.8	15.5
ALT	DML	2.0 to 2.45	Dows	Alden	weathered	1,840	30.5	49.6	36.0	14.4
BEM	DML	3.3 to 3.7	Dows	Alden	partially weathered	1,830	29.6	48.2	37.0	14.8
H1	IES	1.25 to 1.7	Wolf Creek	Hickory Hills	weathered	1,820	31.2	38.7	33.8	27.5
H2	IES	1.5 to 1.9	Wolf Creek	Hickory Hills	weathered	1,860	30.7	44.1	33.2	22.8
AO	SIDP	10.5 to 10.95	Wolf Creek	Aurora	weathered	1,820	30.5	37.4	38.1	24.6
AT	SIDP	16.5 to 16.95	Wolf Creek	Aurora	partially weathered	1,890	28.8	31.0	41.6	27.4
ALB	SIDP	27.5 to 27.95	Alburnett	N/A	unweathered	2,010	28.6	31.0	45.6	23.4

† DML = Des Moines Lobe; IES = Iowan Erosion Surface; SIDP = Southern Iowa Drift Plain

Table 2. Measured fracture spacing ($2B$), fracture density, bulk hydraulic conductivity (K_b), total porosity (n_T); and calculated fracture aperture ($2b$), fracture porosity (n_f), and advective velocity (V) estimated by Equations 2, 3, and 1, respectively.

Column name	$2B$ (cm)	*Density* (frac./m^2)	K_b (m/s)	n_T (percent)	$2b$ (m)	n_f (percent)	V *(m/d)*
ALG	4.3	292	3.8×10^{-5}	29.8	1.1×10^{-4}	5.0×10^{-1}	658
ALT	4.6	275	2.3×10^{-6}	30.5	4.3×10^{-5}	1.9×10^{-1}	106
BEM	4.3	260	6.8×10^{-8}	29.6	1.3×10^{-5}	6.1×10^{-2}	9.7
H1	3.8	145	7.1×10^{-6}	31.2	5.9×10^{-5}	3.1×10^{-1}	198
H2	6.8	108	2.8×10^{-6}	30.7	5.3×10^{-5}	1.6×10^{-1}	158
AO	3.4	630	1.3×10^{-8}	30.5	6.9×10^{-6}	4.1×10^{-2}	2.7
AT	17.8	124	4.7×10^{-9}	28.8	8.6×10^{-6}	1.0×10^{-2}	4.2
ALB	10.4	221	7.7×10^{-10}	28.6	4.0×10^{-6}	7.6×10^{-3}	0.88

GENERAL SUMMARY

This study demonstrates that tills in Iowa are pervasively fractured, and that these fractures have a controlling influence on solute transport. Fractures were present at all three study sites and at all depths evaluated. The deepest recorded fractures were at the Southern Iowa Drift Plain (SIDP) site, where fractures intersected the till/limestone contact at a depth of 30 m. Differences in fracture morphology suggested that the fractures might have formed by a variety of processes, including stress during or after glaciation, desiccation, or a combination of both.

Results from laboratory experiments using large columns demonstrate that the fractures were hydraulically conductive regardless of the particular fracture pattern present or the origin of the fractures. The bulk hydraulic conductivity (K_b) of the columns ranged from 7.7×10^{-10} to 3.8×10^{-5} m/s, which was greater than the matrix hydraulic conductivity (K_m) reported in the literature. Values of K_b decreased with depth as a log-log function, suggesting that lithostatic stress may reduce fracture apertures and reduce K_b with depth. A dye-trace test demonstrated that water and dye flowed exclusively through the fracture network, providing additional evidence that they are the primary pathway for water and contaminant transport.

The results from the solute transport experiments demonstrated that solutes passed through the columns rapidly as a result of fractures. The breakthrough curves (BTCs) were characterized by short times of first arrival. First arrival velocities of Br ranged from 0.004 to 64.8 m/d, which were between 10 and 100 times faster than calculated using the equivalent porous medium (EPM) assumption. Similar velocities of NO_3 and atrazine were observed for shallow columns (less than 3 m depth).

An evaluation of BTC morphology revealed that although fractures allow low concentrations of solutes to travel rapidly, processes such as matrix diffusion, sorption, and degradation serve to retard contaminant migration. Separation of conservative tracers with different effective diffusion coefficients (D_es) was observed during the rising and tailing limbs of BTCs, which indicated that matrix diffusion was a controlling process. Diminished amplitudes of NO_3 and atrazine in the BTCs of deeper columns indicated that sorption (atrazine) and degradation (NO_3 and atrazine) served to retard their migration. Nitrate and atrazine were not observed in column effluent during experiments of the two deepest columns. Results of this study indicate that fractures in till may allow NO_3 and atrazine to migrate rapidly through shallow aquitards, but may be retarded or degraded in deeper tills.

Three approaches, the Mobile-Immobile Model (MIM), the Parallel Discrete Fracture Model (PDFM), and the 3-Dimensional Discrete Fracture Model (3-D DFM), were used to simulate solute transport through fractures in till. Each model was run in the forward mode using input parameters determined from independent field and laboratory methods. Model results were tested statistically against breakthrough curves (BTCs) generated from solute transport experiments in a large column of fractured till. The MIM and PDFM models were the simplest to construct, and were the most computationally efficient (run times less than 3 seconds). The 3-D DFM model was more difficult to construct, and took approximately 14 hours to simulate a single BTC. However, the 3-D DFM is a compelling approach because it is capable of simulating realistic fracture geometry.

Goodness-of-fit analysis demonstrated that all three models were reasonable predictors of the BTCs (the modified index of agreement (d_1) ranged from 0.751 to 0.959), yet reflected the apparent differences between the modeling approaches. Differences

between model predictions of Br BTCs were not statistically significant ($\alpha = 0.05$), which indicates that more elaborate models do not necessarily produce results that are more accurate. The 3-D DFM was more accurate than the MIM or PDFM when predicting PFBA and PIPES transport, and suggests that fracture orientation and geometry may have an influence on BTCs for compounds with D_es. The affect of fracture geometry and orientation was minor, however, and would likely become insignificant at larger scales due to the high fracture intensity of these till units.

The implications of this study are that fractures have the ability to rapidly transmit dissolved constituents through tills in Iowa. In at least one instance, fractures extended from ground surface to an aquifer, demonstrating that a complete flow path exists. Fortunately, fracture aperture decreased with depth, which increased the residence time for compounds in deeper tills. This would provide an opportunity for matrix diffusion, sorption, and microbial processes to retard or degrade nitrate, herbicides, or other compounds at depth. Three uniquely different modeling approaches were employed in this study. By demonstrating how input parameters may be obtained to construct such models, it is hoped that more hydrogeologists will use the predictive tools already available to simulate solute transport through fractured till. Moreover, the conclusion that conceptually-simple models (i.e. the MIM or PDFM) may be adequate for most applications will make simulation of solute transport in glacial terrain more practical. Fractures found in shallow till units play a dominant role in the transport of chemicals in glaciated regions and should be considered in studies of point and non-point source pollution and assessments of aquifer vulnerability.

APPENDIX A

BREAKTHROUGH CURVE DATA

Table 1. Breakthrough curve data from the ALG column.

dt (days)	Br (mM)	PFBA (mM)	PIPES (mM)	NO3 (mM)	Br (C/C_0)	PFBA (C/C_0)	PIPES (C/C_0)	NO3 (C/C_0)
0.00	0.000	0.000	0.003	0.003	0.000	0.001	0.006	0.006
0.04	0.005	0.002	0.000	0.006	0.010	0.003	0.000	0.012
0.09	0.003	0.011	0.010	0.006	0.007	0.022	0.021	0.012
0.16	0.033	0.042	0.073	0.042	0.066	0.084	0.146	0.084
0.24	0.097	0.088	0.130	0.095	0.194	0.175	0.261	0.190
0.36	0.143	0.132	0.157	0.144	0.285	0.263	0.314	0.287
0.49	0.184	0.178	0.213	0.203	0.369	0.356	0.425	0.406
0.61	0.211	0.204	0.257	0.226	0.423	0.408	0.514	0.451
0.74	0.233	0.216	0.281	0.237	0.467	0.432	0.563	0.475
0.86	0.250	0.235	0.299	0.250	0.501	0.471	0.598	0.500
1.00	0.253	0.246	0.307	0.249	0.507	0.491	0.615	0.499
1.04	0.248	0.239	0.290	0.248	0.495	0.477	0.581	0.496
1.09	0.240	0.221	0.266	0.223	0.481	0.441	0.532	0.446
1.16	0.239	0.212	0.258	0.213	0.478	0.423	0.516	0.426
1.20	0.230	0.201	0.242	0.206	0.460	0.402	0.484	0.412
1.24	0.190	0.173	0.210	0.182	0.381	0.345	0.419	0.363
1.36	0.157	0.144	0.185	0.151	0.313	0.288	0.371	0.301
1.49	0.126	0.123	0.177	0.137	0.251	0.247	0.355	0.274
1.61	0.108	0.104	0.145	0.121	0.216	0.208	0.290	0.243
1.74	0.099	0.086	0.113	0.101	0.198	0.172	0.226	0.203
1.86	0.085	0.073	0.105	0.092	0.169	0.146	0.210	0.185
1.99	0.086	0.063	0.089	0.083	0.172	0.125	0.177	0.167
2.11	0.080	0.056	0.073	0.079	0.160	0.112	0.145	0.158
2.24	0.074	0.052	0.073	0.077	0.148	0.104	0.145	0.153
2.36	0.060	0.048	0.065	0.068	0.119	0.097	0.129	0.136
2.49	0.046	0.042	0.048	0.059	0.093	0.084	0.097	0.118
2.61	0.046	0.034	0.048	0.052	0.093	0.068	0.097	0.104
2.74	0.043	0.029	0.048	0.043	0.087	0.058	0.097	0.086
2.86	0.033	0.024	0.032	0.037	0.066	0.047	0.065	0.073
2.99	0.033	0.024	0.032	0.037	0.066	0.047	0.065	0.073

Table 1b. Breakthrough curve data from the ALG column.

dt (days)	Atrazine (mg/L)	Atrazine (C/C_0)
0.001	0	0
0.084	0.057	0.057
0.168	0.112	0.112
0.251	0.156	0.156
0.334	0.208	0.208
0.417	0.274	0.274
0.501	0.252	0.252
0.584	0.308	0.308
0.834	0.33	0.33
0.917	0.357	0.357
1.001	0.376	0.376
1.084	0.34	0.34
1.167	0.303	0.303
1.251	0.266	0.266
1.334	0.242	0.242
1.417	0.212	0.212
1.501	0.197	0.197
1.584	0.183	0.183
1.668	0.168	0.168
1.751	0.158	0.158
1.834	0.144	0.144
1.917	0.134	0.134
2.001	0.129	0.129
2.084	0.128	0.128
2.167	0.116	0.116
2.251	0.113	0.113
2.334	0.111	0.111
2.417	0.091	0.091
2.501	0.085	0.085
2.584	0.081	0.081
2.751	0.074	0.074
2.834	0.086	0.086
2.917	0.069	0.069
3.001	0.08	0.08
3.084	0.077	0.077

Table 2. Breakthrough curve data from the ALT column.

dt (days)	Br (mM)	PFBA (mM)	PIPES (mM)	NO3 (mM)	Atrazine (mg/L)	Br (C/C_0)	PFBA (C/C_0)	PIPES (C/C_0)	NO3 (C/C_0)	Atrazine (C/C_0)
0.000	0.000	0.000	0.005	0.000	0.000	0.000	0.000	0.009	0.000	0.000
0.042	0.001	0.001	0.006	0.003		0.001	0.002	0.011	0.006	
0.083	0.066	0.076	0.090	0.072	0.096	0.131	0.151	0.180	0.143	0.096
0.125	0.259	0.268	0.267	0.247		0.517	0.536	0.533	0.493	
0.167	0.303	0.323	0.317	0.292	0.379	0.605	0.646	0.633	0.584	0.379
0.208	0.322	0.341	0.352	0.300		0.644	0.681	0.704	0.600	
0.250	0.340	0.352	0.377	0.332	0.511	0.679	0.703	0.753	0.663	0.511
0.292	0.357	0.364	0.387	0.355		0.713	0.727	0.774	0.710	
0.333	0.369	0.380	0.390	0.367	0.534	0.738	0.760	0.780	0.734	0.534
0.375	0.383	0.383	0.392	0.363		0.765	0.765	0.783	0.725	
0.417	0.386	0.390	0.401	0.378	0.578	0.772	0.780	0.802	0.755	0.578
0.458	0.394	0.398	0.404	0.384		0.787	0.795	0.808	0.768	
0.500	0.398	0.399	0.405	0.382	0.588	0.795	0.797	0.810	0.764	0.588
0.542	0.403	0.403	0.408	0.394		0.806	0.805	0.815	0.787	
0.583	0.407	0.421	0.414	0.402	0.610	0.814	0.842	0.827	0.804	0.610
0.625	0.411	0.410	0.412	0.398		0.822	0.819	0.823	0.795	
0.667	0.416	0.413	0.417	0.404	0.590	0.831	0.825	0.834	0.808	0.590
0.708	0.416	0.420	0.427	0.407		0.831	0.840	0.853	0.813	
0.750	0.259	0.247	0.237	0.242	0.413	0.518	0.493	0.473	0.484	0.413
0.792	0.162	0.160	0.155	0.158		0.324	0.320	0.309	0.316	
0.833	0.124	0.115	0.114	0.110	0.202	0.247	0.230	0.228	0.220	0.202
0.875	0.106	0.097	0.097	0.100		0.212	0.193	0.194	0.200	
0.917	0.087	0.086	0.080	0.081	0.192	0.173	0.171	0.160	0.162	0.192
0.958	0.079	0.078	0.087	0.077		0.158	0.155	0.173	0.154	
1.000	0.073	0.068	0.067	0.065	0.140	0.145	0.135	0.134	0.130	0.140
1.042	0.060	0.060	0.049	0.057		0.120	0.120	0.098	0.113	
1.083	0.057	0.054	0.050	0.047	0.128	0.113	0.107	0.100	0.094	0.128
1.125	0.052	0.049	0.044	0.042		0.104	0.097	0.087	0.083	
1.167	0.048	0.050	0.045	0.046	0.111	0.095	0.100	0.090	0.092	0.111
1.208	0.048	0.050	0.045	0.045		0.095	0.100	0.090	0.090	
1.250	0.044	0.038	0.035	0.040	0.120	0.088	0.075	0.070	0.079	0.120
1.292	0.039	0.030	0.034	0.037		0.078	0.060	0.068	0.073	
1.333	0.038	0.032	0.027	0.035	0.103	0.076	0.064	0.053	0.070	0.103
1.417	0.036	0.029	0.030	0.027		0.071	0.058	0.060	0.053	
1.500	0.033	0.028	0.024	0.027	0.100	0.066	0.055	0.047	0.053	0.100
1.583	0.026	0.027	0.022	0.027		0.052	0.054	0.043	0.053	
1.667	0.026	0.024	0.029	0.026	0.116	0.052	0.048	0.058	0.051	0.116
1.750	0.023	0.020	0.017	0.018		0.045	0.040	0.034	0.036	
1.833	0.024	0.015	0.018	0.023	0.089	0.047	0.030	0.036	0.045	0.089
1.917	0.024	0.020	0.018	0.020		0.047	0.040	0.036	0.040	
2.000	0.022	0.017	0.018	0.022	0.103	0.043	0.034	0.036	0.043	0.103

Table 3. Breakthrough curve data from the BEM column.

dt (days)	Br (mM)	PFBA (mM)	PIPES (mM)	NO3 (mM)	Atrazine (mg/L)	Br (C/C_0)	PFBA (C/C_0)	PIPES (C/C_0)	NO3 (C/C_0)	Atrazine (C/C_0)
0.0	0.000	0.000	0.000	0.000	0.000	0.000	0.000	0.000	0.000	0.000
0.2	0.000	0.000	0.000	0.000	0.000	0.000	0.000	0.000	0.000	0.000
1.0	0.000	0.000	0.000	0.000	0.000	0.000	0.000	0.000	0.000	0.000
1.3	0.003	0.000	0.000	0.000	0.000	0.006	0.000	0.000	0.000	0.000
4.7	0.025	0.037	0.060	0.000	0.000	0.050	0.074	0.120	0.000	0.000
5.8	0.036	0.044	0.077	0.000	0.038	0.072	0.089	0.153	0.000	0.038
7.7	0.059	0.066	0.127	0.015	0.081	0.117	0.133	0.253	0.029	0.081
10.8	0.089	0.100	0.193	0.022	0.100	0.178	0.199	0.387	0.044	0.100
12.7	0.117	0.122	0.233	0.022	0.180	0.233	0.244	0.467	0.044	0.180
14.7	0.159	0.159	0.264	0.015	0.203	0.317	0.317	0.528	0.030	0.203
17.2	0.197	0.200	0.301	0.007	0.253	0.394	0.401	0.602	0.015	0.253
19.0	0.241	0.254	0.319	0.021	0.273	0.482	0.508	0.637	0.042	0.273
21.9	0.311	0.290	0.352	0.012	0.326	0.622	0.580	0.704	0.023	0.326
24.9	0.337	0.349	0.380	0.017	0.324	0.674	0.698	0.760	0.035	0.324
27.0	0.390	0.366	0.397	0.016	0.305	0.780	0.732	0.793	0.032	0.305
30.0	0.411	0.412	0.405	0.015	0.350	0.821	0.825	0.810	0.030	0.350
34.0	0.450	0.431	0.430	0.021	0.340	0.900	0.861	0.860	0.042	0.340
37.0	0.478	0.451	0.444	0.017	0.336	0.956	0.902	0.888	0.035	0.336
41.3	0.471	0.477	0.467	0.019	0.341	0.941	0.953	0.933	0.038	0.341
43.9	0.474	0.471	0.472	0.020	0.359	0.948	0.943	0.944	0.040	0.359
46.9	0.490	0.487	0.483	0.022	0.345	0.980	0.973	0.966	0.044	0.345
49.9	0.490	0.501	0.489	0.018	0.379	0.980	1.001	0.978	0.036	0.379
52.9	0.482	0.491	0.486	0.021	0.364	0.965	0.981	0.972	0.042	0.364
56.0	0.495	0.495	0.486	0.017	0.375	0.990	0.990	0.973	0.034	0.375
59.0	0.494	0.505	0.489	0.025	0.361	0.987	1.010	0.978	0.050	0.361
62.0	0.490	0.500	0.497	0.013	0.378	0.980	1.000	0.994	0.026	0.378
65.0	0.505	0.486	0.485	0.021	0.363	1.010	0.973	0.970	0.041	0.363
68.0	0.502	0.487	0.481	0.007	0.369	1.004	0.974	0.962	0.015	0.369
70.0	0.497	0.508	0.489	0.013	0.370	0.995	1.016	0.978	0.027	0.370

Table 4. Breakthrough curve data from the H1 column.

dt (days)	Br (mM)	PFBA (mM)	PIPES (mM)	NO3 (mM)	Br (C/C_0)	PFBA (C/C_0)	PIPES (C/C_0)	NO3 (C/C_0)
0.00	0.012	0.000	0.000	0.000	0.024	0.000	0.000	0.000
0.01	0.053	0.066	0.063	0.047	0.107	0.132	0.126	0.093
0.01	0.148	0.157	0.178	0.147	0.296	0.313	0.357	0.295
0.02	0.225	0.228	0.243	0.225	0.450	0.456	0.487	0.450
0.03	0.260	0.261	0.290	0.256	0.521	0.522	0.580	0.512
0.03	0.290	0.283	0.305	0.283	0.580	0.566	0.610	0.566
0.04	0.305	0.297	0.323	0.302	0.609	0.593	0.647	0.605
0.05	0.320	0.308	0.333	0.314	0.639	0.615	0.665	0.628
0.06	0.328	0.321	0.346	0.326	0.657	0.643	0.691	0.651
0.07	0.340	0.330	0.349	0.337	0.680	0.659	0.699	0.674
0.08	0.349	0.338	0.353	0.345	0.698	0.676	0.706	0.690
0.10	0.361	0.343	0.361	0.364	0.722	0.687	0.721	0.729
0.11	0.367	0.349	0.366	0.353	0.734	0.698	0.732	0.705
0.12	0.373	0.354	0.374	0.364	0.746	0.709	0.747	0.729
0.14	0.376	0.354	0.377	0.364	0.751	0.709	0.755	0.729
0.15	0.379	0.360	0.381	0.368	0.757	0.720	0.762	0.736
0.17	0.385	0.363	0.381	0.372	0.769	0.725	0.762	0.744
0.17	0.320	0.299	0.314	0.314	0.639	0.599	0.628	0.628
0.18	0.228	0.203	0.203	0.217	0.456	0.407	0.405	0.434
0.19	0.169	0.151	0.154	0.159	0.337	0.302	0.309	0.318
0.19	0.130	0.118	0.125	0.120	0.260	0.236	0.249	0.240
0.20	0.104	0.096	0.095	0.093	0.207	0.192	0.190	0.186
0.21	0.089	0.085	0.082	0.078	0.178	0.170	0.164	0.155
0.23	0.056	0.050	0.058	0.043	0.112	0.100	0.116	0.086
0.25	0.036	0.040	0.051	0.034	0.071	0.080	0.101	0.067
0.27	0.036	0.036	0.041	0.023	0.071	0.071	0.082	0.045
0.29	0.036	0.034	0.041	0.020	0.071	0.067	0.082	0.040
0.31	0.026	0.030	0.036	0.019	0.052	0.060	0.071	0.037
0.33	0.020	0.026	0.040	0.013	0.040	0.052	0.080	0.026
0.35	0.026	0.025	0.032	0.006	0.052	0.049	0.063	0.011
0.38	0.020	0.028	0.028	0.006	0.040	0.056	0.056	0.011
0.40	0.020	0.023	0.028	0.010	0.040	0.045	0.056	0.019
0.42	0.017	0.017	0.030	0.004	0.034	0.034	0.060	0.007
0.44	0.017	0.023	0.026	0.013	0.034	0.045	0.052	0.026
0.46	0.020	0.019	0.032	0.010	0.040	0.037	0.063	0.019
0.48	0.020	0.019	0.023	0.011	0.040	0.037	0.045	0.022
0.50	0.015	0.023	0.028	0.004	0.030	0.045	0.056	0.007

Table 4b. Breakthrough curve data from the H1 column.

dt (days)	Atrazine (mg/L)	Atrazine (C/C_0)
0.00	0.105	0.105
0.01	0.122	0.122
0.01	0.164	0.164
0.02	0.257	0.257
0.03	0.333	0.333
0.03	0.403	0.403
0.04	0.433	0.433
0.05	0.455	0.455
0.06	0.495	0.495
0.07	0.502	0.502
0.08	0.520	0.520
0.10	0.538	0.538
0.11	0.554	0.554
0.13	0.570	0.570
0.14	0.573	0.573
0.15	0.584	0.584
0.17	0.597	0.597
0.17	0.572	0.572
0.18	0.297	0.297
0.19	0.232	0.232
0.19	0.225	0.225
0.20	0.225	0.225
0.21	0.215	0.215
0.22	0.207	0.207
0.24	0.178	0.178
0.25	0.154	0.154
0.27	0.141	0.141
0.29	0.126	0.126
0.31	0.131	0.131
0.33	0.116	0.116
0.35	0.120	0.120
0.38	0.120	0.120
0.40	0.120	0.120
0.42	0.104	0.104
0.44	0.082	0.082
0.46	0.097	0.097
0.48	0.075	0.075
0.50	0.080	0.080

Table 5. Breakthrough curve data from the H2 column.

dt (days)	Br (mM)	PFBA (mM)	PIPES (mM)	NO3 (mM)	Atrazine (mg/L)	Br (C/C_0)	PFBA (C/C_0)	PIPES (C/C_0)	NO3 (C/C_0)	Atrazine (C/C_0)
0.000	0.002	0.002	0.004	0.005	0.000	0.005	0.004	0.008	0.010	0.000
0.028	0.044	0.050	0.067	0.053	0.000	0.089	0.101	0.135	0.106	0.000
0.056	0.159	0.180	0.182	0.175	0.245	0.318	0.359	0.365	0.350	0.245
0.083	0.280	0.292	0.319	0.289	0.407	0.560	0.584	0.639	0.579	0.407
0.111	0.317	0.324	0.344	0.326	0.512	0.633	0.647	0.688	0.653	0.512
0.139	0.347	0.364	0.371	0.364	0.586	0.694	0.728	0.741	0.728	0.586
0.194	0.371	0.392	0.401	0.392	0.612	0.743	0.785	0.801	0.785	0.612
0.250	0.391	0.415	0.426	0.409	0.638	0.781	0.830	0.851	0.818	0.638
0.306	0.407	0.426	0.432	0.424	0.646	0.815	0.852	0.864	0.849	0.646
0.361	0.410	0.432	0.434	0.426	0.683	0.820	0.863	0.868	0.852	0.683
0.417	0.429	0.442	0.455	0.445	0.696	0.859	0.884	0.910	0.890	0.696
0.472	0.442	0.464	0.465	0.452	0.690	0.883	0.929	0.929	0.904	0.690
0.500	0.365	0.369	0.387	0.381	0.594	0.730	0.737	0.773	0.762	0.594
0.528	0.250	0.212	0.238	0.248	0.405	0.500	0.425	0.477	0.496	0.405
0.556	0.150	0.128	0.141	0.163	0.243	0.299	0.256	0.282	0.326	0.243
0.583	0.101	0.079	0.088	0.104	0.210	0.202	0.157	0.175	0.209	0.210
0.611	0.078	0.057	0.062	0.082	0.134	0.155	0.114	0.125	0.165	0.134
0.639	0.058	0.045	0.053	0.066	0.122	0.116	0.090	0.105	0.132	0.122
0.667	0.052	0.036	0.052	0.055	0.122	0.104	0.072	0.104	0.109	0.122
0.722	0.046	0.029	0.037	0.048	0.109	0.093	0.058	0.073	0.095	0.109
0.778	0.038	0.028	0.025	0.044	0.095	0.077	0.056	0.050	0.088	0.095
0.833	0.035	0.026	0.022	0.039	0.090	0.070	0.051	0.044	0.078	0.090
0.889	0.028	0.022	0.023	0.033	0.104	0.055	0.045	0.045	0.067	0.104
0.944	0.023	0.021	0.021	0.025		0.047	0.042	0.042	0.050	
1.000	0.021	0.018	0.018	0.025	0.070	0.042	0.036	0.036	0.051	0.070
1.056	0.020	0.013	0.017	0.025		0.039	0.027	0.034	0.050	
1.111	0.019	0.012	0.014	0.020	0.091	0.037	0.024	0.028	0.040	0.091
1.167	0.015	0.012	0.014	0.014		0.029	0.024	0.028	0.028	
1.222	0.015	0.011	0.015	0.014	0.088	0.029	0.022	0.029	0.028	0.088
1.278	0.014	0.012	0.015	0.015		0.027	0.024	0.029	0.030	
1.333	0.015	0.013	0.014	0.014	0.073	0.029	0.027	0.028	0.028	0.073
1.417	0.013	0.011	0.011	0.012	0.060	0.026	0.022	0.023	0.024	0.060

Table 6. Breakthrough curve data from the AO column.

dt (days)	Br (mM)	PFBA (mM)	PIPES (mM)	NO3 (mM)	Atrazine (mg/L)	Br (C/C_0)	PFBA (C/C_0)	PIPES (C/C_0)	NO3 (C/C_0)	Atrazine (C/C_0)
0.0	0.000	0.000	0.000	0.000	0.011	0.000	0.000	0.000	0.000	0.011
5.0	0.000	0.000	0.000	0.000	0.012	0.000	0.000	0.000	0.000	0.012
9.0	0.006	0.019	0.016	0.000	0.000	0.012	0.039	0.032	0.000	0.000
11.8	0.012	0.021	0.031	0.000	0.000	0.024	0.041	0.062	0.000	0.000
14.0	0.024	0.037	0.044	0.000	0.020	0.047	0.073	0.088	0.000	0.020
16.6	0.024	0.038	0.046	0.000	0.018	0.048	0.076	0.091	0.000	0.018
18.6	0.035	0.046	0.057	0.000	0.016	0.070	0.091	0.114	0.000	0.016
22.0	0.052	0.062	0.073	0.000	0.029	0.103	0.123	0.145	0.000	0.029
24.9	0.067	0.077	0.096	0.000	0.035	0.134	0.154	0.192	0.000	0.035
27.4	0.087	0.106	0.116	0.000	0.037	0.174	0.212	0.232	0.000	0.037
30.0	0.100	0.110	0.128	0.000	0.039	0.200	0.220	0.255	0.000	0.039
32.7	0.117	0.125	0.140	0.000	0.045	0.235	0.250	0.279	0.000	0.045
34.6	0.123	0.111	0.147	0.000	0.028	0.246	0.221	0.293	0.000	0.028
37.1	0.137	0.147	0.162	0.000	0.057	0.273	0.293	0.323	0.000	0.057
42.0	0.151	0.161	0.181	0.000	0.054	0.302	0.322	0.362	0.000	0.054
44.0	0.162	0.172	0.179	0.000	0.063	0.324	0.344	0.358	0.000	0.063
47.4	0.179	0.190	0.208	0.000	0.058	0.357	0.380	0.415	0.000	0.058
55.8	0.197	0.209	0.235	0.000	0.050	0.394	0.418	0.470	0.000	0.050
58.0	0.216	0.226	0.244	0.000	0.061	0.432	0.452	0.487	0.000	0.061
64.0	0.228	0.238	0.268	0.000	0.042	0.455	0.475	0.535	0.000	0.042
68.0	0.243	0.255	0.283	0.000	0.062	0.486	0.509	0.566	0.000	0.062
73.0	0.252	0.267	0.297	0.000	0.058	0.504	0.533	0.594	0.000	0.058
78.0	0.258	0.272	0.303	0.000	0.042	0.516	0.544	0.606	0.000	0.042
82.0	0.266	0.280	0.312	0.000	0.055	0.532	0.559	0.623	0.000	0.055
88.0	0.270	0.286	0.323	0.000		0.540	0.571	0.645	0.000	
92.9	0.285	0.298	0.332	0.000	0.064	0.570	0.595	0.664	0.000	0.064
98.8	0.297	0.309	0.343	0.000		0.593	0.618	0.685	0.000	
102.8	0.304	0.316	0.349	0.000	0.061	0.607	0.631	0.697	0.000	0.061
110.0	0.314	0.326	0.359	0.000		0.627	0.652	0.717	0.000	
117.0	0.320	0.333	0.365	0.000	0.068	0.640	0.666	0.729	0.000	0.068

Table 7. Breakthrough curve data from the AT column.

dt (days)	Br (mM)	PFBA (mM)	PIPES (mM)	NO3 (mM)	Atrazine (mg/L)	Br (C/C_0)	PFBA (C/C_0)	PIPES (C/C_0)	NO3 (C/C_0)	Atrazine (C/C_0)
0.0	0.000	0.000	0.000	0.000	0.000	0.000	0.000	0.000	0.000	0.000
5.0	0.000	0.000	0.000	0.000	0.000	0.000	0.000	0.000	0.000	0.000
9.0	0.000	0.000	0.000	0.000	0.000	0.000	0.000	0.000	0.000	0.000
11.8	0.000	0.001	0.003	0.000	0.000	0.000	0.002	0.006	0.000	0.000
16.6	0.001	0.002	0.002	0.000	0.000	0.002	0.003	0.004	0.000	0.000
18.6	0.001	0.001	0.005	0.000	0.000	0.001	0.002	0.009	0.000	0.000
22.0	0.002	0.004	0.005	0.000	0.000	0.004	0.008	0.010	0.000	0.000
24.9	0.002	0.005	0.007	0.000	0.000	0.003	0.009	0.013	0.000	0.000
27.4	0.002	0.005	0.007	0.000	0.000	0.004	0.010	0.014	0.000	0.000
30.0	0.003	0.005	0.007	0.000	0.000	0.005	0.009	0.014	0.000	0.000
34.6	0.003	0.006	0.010	0.000	0.000	0.007	0.012	0.019	0.000	0.000
37.1	0.003	0.007	0.010	0.000	0.000	0.006	0.013	0.020	0.000	0.000
42.0	0.007	0.009	0.014	0.000	0.000	0.013	0.017	0.027	0.000	0.000
47.4	0.006	0.010	0.018	0.000	0.000	0.013	0.020	0.035	0.000	0.000
51.8	0.011	0.015	0.021	0.000	0.000	0.023	0.030	0.042	0.000	0.000
58.0	0.014	0.020	0.026	0.000	0.000	0.028	0.039	0.051	0.000	0.000
64.0	0.016	0.022	0.030	0.000	0.000	0.033	0.043	0.059	0.000	0.000
68.0	0.019	0.023	0.031	0.000	0.000	0.038	0.046	0.061	0.000	0.000
73.0	0.023	0.029	0.034	0.000	0.000	0.046	0.058	0.067	0.000	0.000
78.0	0.026	0.032	0.039	0.000	0.000	0.052	0.064	0.078	0.000	0.000
82.0	0.031	0.036	0.043	0.000	0.000	0.061	0.072	0.087	0.000	0.000
85.1	0.032	0.038	0.047	0.000	0.000	0.065	0.075	0.093	0.000	0.000
89.9	0.036	0.040	0.049	0.000	0.000	0.071	0.079	0.098	0.000	0.000

Table 8. Breakthrough curve data from the ALB column.

dt (days)	Br (mM)	PFBA (mM)	PIPES (mM)	NO3 (mM)	Atrazine (mg/L)	Br (C/C_0)	PFBA (C/C_0)	PIPES (C/C_0)	NO3 (C/C_0)	Atrazine (C/C_0)
0.0	0.000	0.000	0.000	0.000	0.000	0.000	0.000	0.000	0.000	0.000
5.0	0.000	0.000	0.000	0.000	0.000	0.000	0.000	0.000	0.000	0.000
9.0	0.000	0.000	0.000	0.000	0.000	0.000	0.000	0.000	0.000	0.000
14.0	0.000	0.000	0.000	0.000	0.000	0.000	0.000	0.000	0.000	0.000
18.6	0.000	0.000	0.000	0.000	0.000	0.000	0.000	0.000	0.000	0.000
24.9	0.000	0.000	0.000	0.000	0.000	0.000	0.000	0.000	0.000	0.000
30.0	0.000	0.000	0.000	0.000	0.000	0.000	0.000	0.000	0.000	0.000
34.6	0.000	0.000	0.000	0.000	0.000	0.000	0.000	0.000	0.000	0.000
42.0	0.000	0.000	0.001	0.000	0.000	0.000	0.000	0.002	0.000	0.000
47.4	0.000	0.000	0.001	0.000	0.000	0.000	0.001	0.003	0.000	0.000
55.8	0.000	0.001	0.002	0.000	0.000	0.000	0.001	0.003	0.000	0.000
64.0	0.000	0.001	0.002	0.000	0.000	0.000	0.002	0.004	0.000	0.000
68.0	0.000	0.001	0.002	0.000	0.000	0.000	0.002	0.005	0.000	0.000
73.0	0.001	0.002	0.003	0.000	0.000	0.001	0.003	0.006	0.000	0.000
78.0	0.002	0.002	0.003	0.000	0.000	0.003	0.004	0.007	0.000	0.000
82.0	0.002	0.002	0.005	0.000	0.000	0.003	0.005	0.009	0.000	0.000
88.0	0.001	0.003	0.004	0.000	0.000	0.002	0.006	0.008	0.000	0.000
92.9	0.002	0.003	0.005	0.000	0.000	0.004	0.005	0.011	0.000	0.000
98.8	0.002	0.003	0.005	0.000	0.000	0.004	0.006	0.011	0.000	0.000
102.8	0.003	0.004	0.006	0.000	0.000	0.006	0.008	0.013	0.000	0.000
110.0	0.003	0.005	0.008	0.000	0.000	0.006	0.009	0.015	0.000	0.000
117.0	0.005	0.007	0.009	0.000	0.000	0.011	0.015	0.018	0.000	0.000
128.0	0.008	0.010	0.011	0.000	0.000	0.017	0.019	0.021	0.000	0.000
138.0	0.010	0.011	0.012	0.000	0.000	0.020	0.022	0.024	0.000	0.000
145.0	0.011	0.012	0.013	0.000	0.000	0.021	0.024	0.025	0.000	0.000

APPENDIX B

FRACTURE ORIENTATION DATA

Table 1. Till orientation data collected from the DML Site, 3.3 m depth.

Strike (°)	Dip (°)	Strike (°)	Dip (°)	Strike (°)	Dip (°)
185	81	46	66	335	73
219	79	286	68	208	76
314	89	104	88	327	72
48	70	241	59	28	72
53	57	52	83	229	89
37	78	21	88	19	90
61	88	232	69	323	86
20	67	147	85		
344	88	214	74		
9	90	46	78		
48	90	251	60		
13	76	101	81		
33	86	239	41		
29	76	232	43		
31	89	76	89		
274	68	302	68		
344	81	5	73		
44	89	217	78		
59	90	8	89		
75	53	186	88		

Table 2. Till orientation data collected from the IES Site, 1.5 to 2.0 m depth.

Strike (°)	Dip (°)	Strike (°)	Dip (°)	Strike (°)	Dip (°)
275	72	322	78	135	75
92	70	150	54	6	89
116	74	224	61	88	87
94	81	239	87	121	81
264	76	164	64	18	82
298	90	140	71	128	86
81	32	7	85	160	81
133	40	303	85	211	82
343	89	357	69	298	88
108	62	348	23	70	84
88	81	323	6	290	87
4	84	194	85	249	84
259	87	137	82	299	86
69	90	39	89	75	88
83	64	48	84	245	87
314	76	50	79	11	88
338	88	6	79	200	75
201	72	337	86	185	82
212	78	318	90	70	85
233	74	284	14	26	80

Table 3. Till orientation data collected from the SIDP Site, 27.5 m depth.

Strike (°)	Dip (°)	Strike (°)	Dip (°)
231	86	328	76
123	90	67	89
137	90	342	89
215	87	179	77
257	89	207	87
155	82	160	77
338	76	146	84
61	89	240	83
265	85	126	74
64	79	216	87
314	86	163	86
64	84	75	78
310	84	123	79
326	90	84	79
227	86	138	89
278	86	248	84
298	90	228	80
79	84	195	81
51	89	314	74
165	80	79	89

APPENDIX C

TILL FABRIC DATA

Table 1. Till fabric data collected from the DML Site, 3-4 m depth.

Trend (°)	Plunge (°)
310	13
315	12
348	10
315	17
323	20
298	7
290	24
305	32
310	12
327	9
300	39
330	27
15	24
358	48
10	25
343	24
215	11
347	4
286	6
324	2
308	22
2	14
330	27
328	4
55	1
108	47
288	4
315	9
321	47
308	16

Table 2. Till fabric data collected from the DML Site, 1.5-4 m depth.

Trend (°)	Plunge (°)
95°	12°
315°	2°
325°	15°
350°	0°
270°	15°
325°	30°
340°	25°
325°	4°
290°	26°
250°	6°
305°	26°
337°	40°
314°	31°
298°	34°
303°	35°
316°	14°
337°	14°
9°	17°
328°	16°
317°	31°
333°	22°
346°	17°
351°	6°
322°	16°
344°	1°
319°	11°
324°	35°
232°	19°
321°	39°
330°	7°

Table 3. Till fabric data collected from the IES Site, 1-1.5 m depth.

Trend (°)	Plunge (°)
28	16
140	61
202	51
32	23
55	48
115	16
140	19
234	21
194	37
210	9
200	3
105	27
120	26
18	23
62	44
342	11
47	26
65	23
149	31
35	30
296	42
334	3
325	9
224	82
335	20
28	16
140	61
202	51
32	23
55	48

Table 4. Till fabric data collected from the IES Site, 1.5-2.0 m depth.

Trend (°)	Plunge (°)
165	29
141	33
135	20
139	25
126	49
135	31
167	22
188	38
90	15
230	10
160	31
15	27
136	7
206	39
234	30
195	26
234	35
190	35
330	34
255	41
344	26
14	6
267	22
39	27
28	16
140	61
202	51
32	23
55	48
115	16

Table 5. Till fabric data collected from the SIDP Site, 27.5 m depth.

Trend (°)	Plunge (°)
297	39
325	11
123	13
304	13
278	5
294	16
299	15
323	10
314	6
271	11
295	10
280	17
286	21
279	9
264	14
303	12
305	13
349	1
311	14
321	3
322	1
318	9
337	11
331	10
335	15
319	10
315	19
319	20
299	6
328	10
302	2

APPENDIX D

DIFFUSION CELL DATA

Table 1. Diffusion cell results from the ALG sample.

Radial Diffusion Cell A

time (days)	Br (C/C_0)	PFBA (C/C_0)	PIPES (C/C_0)	NO_3 (C/C_0)
0.25	0.53	0.62	0.80	0.56
0.90	0.30	0.37	0.53	0.32
2.15	0.17	0.24	0.33	0.17
5.36	0.08	0.14	0.19	0.01
9.29	0.06	0.08	0.13	0.01
13.29	0.07	0.09	0.12	0.01
17.15	0.06	0.07	0.09	0.00
21.00	0.06	0.06	0.08	0.00
28.00	0.06	0.06	0.07	0.00

Radial Diffusion Cell B

time (days)	Br (C/C_0)	PFBA (C/C_0)	PIPES (C/C_0)	NO_3 (C/C_0)
0.25	0.53	0.62	0.80	0.56
0.90	0.30	0.37	0.53	0.32
2.15	0.17	0.24	0.33	0.17
5.36	0.08	0.14	0.19	0.01
9.29	0.06	0.08	0.13	0.01
13.29	0.07	0.09	0.12	0.01
17.15	0.06	0.07	0.09	0.00
21.00	0.06	0.06	0.08	0.00
28.00	0.06	0.06	0.07	0.00

Radial Diffusion Cell C

time (days)	Br (C/C_0)	PFBA (C/C_0)	PIPES (C/C_0)	NO_3 (C/C_0)
0.25	0.53	0.62	0.82	0.56
0.90	0.30	0.37	0.53	0.32
2.15	0.17	0.25	0.37	0.15
5.36	0.09	0.13	0.22	0.03
9.29	0.06	0.08	0.14	0.01
13.29	0.06	0.08	0.12	0.01
17.15	0.06	0.07	0.09	0.00
21.00	0.06	0.07	0.08	0.00
28.00	0.06	0.06	0.07	0.00

Table 2. Diffusion cell results from the ALT sample.

Radial Diffusion Cell A

time (days)	Br (C/C_0)	PFBA (C/C_0)	PIPES (C/C_0)	NO_3 (C/C_0)
0.25	0.51	0.63	0.84	0.64
0.90	0.35	0.50	0.72	0.37
2.15	0.21	0.40	0.52	0.11
5.36	0.10	0.23	0.37	0.03
9.29	0.07	0.13	0.27	0.01
13.29	0.07	0.12	0.21	0.01
17.15	0.07	0.09	0.17	0.00
21.00	0.07	0.08	0.15	0.00
28.00	0.07	0.07	0.11	0.00

Radial Diffusion Cell B

time (days)	Br (C/C_0)	PFBA (C/C_0)	PIPES (C/C_0)	NO_3 (C/C_0)
0.25	0.53	0.64	0.82	0.57
0.90	0.33	0.47	0.71	0.35
2.15	0.20	0.35	0.56	0.18
5.36	0.10	0.21	0.33	0.01
9.29	0.07	0.13	0.27	0.01
13.29	0.07	0.10	0.21	0.00
17.15	0.06	0.09	0.18	0.00
21.00	0.07	0.08	0.15	0.00
28.00	0.07	0.07	0.13	0.00

Radial Diffusion Cell C

time (days)	Br (C/C_0)	PFBA (C/C_0)	PIPES (C/C_0)	NO_3 (C/C_0)
0.25	0.54	0.66	0.84	0.59
0.90	0.33	0.47	0.69	0.31
2.15	0.19	0.34	0.54	0.18
5.36	0.08	0.18	0.35	0.02
9.29	0.08	0.10	0.29	0.02
13.29	0.07	0.09	0.21	0.00
17.15	0.07	0.08	0.19	0.00
21.00	0.07	0.07	0.17	0.00
28.00	0.07	0.07	0.13	0.00

Table 3. Diffusion cell results from the BEM sample.

Radial Diffusion Cell A

time (days)	Br (C/C_0)	PFBA (C/C_0)	PIPES (C/C_0)	NO_3 (C/C_0)
0.25	0.58	0.65	0.87	0.59
0.90	0.30	0.42	0.69	0.27
2.15	0.16	0.27	0.36	0.05
5.36	0.08	0.13	0.21	0.00
9.29	0.07	0.09	0.16	0.00
13.29	0.06	0.07	0.13	0.00
17.15	0.07	0.07	0.10	0.00
21.00	0.07	0.07	0.09	0.00
28.00	0.07	0.07	0.08	0.00

Radial Diffusion Cell B

time (days)	Br (C/C_0)	PFBA (C/C_0)	PIPES (C/C_0)	NO_3 (C/C_0)
0.25	0.59	0.71	0.82	0.62
0.90	0.29	0.39	0.58	0.28
2.15	0.17	0.25	0.40	0.10
5.36	0.08	0.14	0.26	0.02
9.29	0.07	0.09	0.17	0.01
13.29	0.05	0.07	0.13	0.01
17.15	0.07	0.07	0.11	0.00
21.00	0.06	0.07	0.10	0.00
28.00	0.07	0.07	0.09	0.00

Radial Diffusion Cell C

time (days)	Br (C/C_0)	PFBA (C/C_0)	PIPES (C/C_0)	NO_3 (C/C_0)
0.25	0.60	0.71	0.83	0.62
0.90	0.30	0.39	0.59	0.28
2.15	0.17	0.25	0.43	0.11
5.36	0.08	0.14	0.26	0.03
9.29	0.07	0.09	0.16	0.02
13.29	0.07	0.07	0.13	0.01
17.15	0.07	0.07	0.11	0.00
21.00	0.07	0.07	0.09	0.00
28.00	0.07	0.07	0.09	0.00

Table 4. Diffusion cell results from the H1 sample.

Radial Diffusion Cell A

time (days)	Br (C/C_0)	PFBA (C/C_0)	PIPES (C/C_0)	NO_3 (C/C_0)
0.25	0.52	0.65	0.79	0.55
0.90	0.29	0.43	0.58	0.32
2.15	0.15	0.27	0.43	0.17
5.36	0.08	0.14	0.27	0.08
9.29	0.07	0.09	0.20	0.04
13.29	0.07	0.07	0.16	0.02
17.15	0.07	0.07	0.14	0.01
21.00	0.06	0.07	0.11	0.00
28.00	0.07	0.06	0.09	0.00

Radial Diffusion Cell B

time (days)	Br (C/C_0)	PFBA (C/C_0)	PIPES (C/C_0)	NO_3 (C/C_0)
0.25	0.52	0.64	0.81	0.56
0.90	0.29	0.42	0.57	0.31
2.15	0.16	0.29	0.44	0.16
5.36	0.09	0.13	0.28	0.06
9.29	0.07	0.09	0.17	0.03
13.29	0.06	0.07	0.16	0.01
17.15	0.08	0.06	0.12	0.00
21.00	0.05	0.06	0.10	0.00
28.00	0.06	0.06	0.08	0.00

Radial Diffusion Cell C

time (days)	Br (C/C_0)	PFBA (C/C_0)	PIPES (C/C_0)	NO_3 (C/C_0)
0.25	0.50	0.62	0.77	0.55
0.90	0.26	0.43	0.58	0.28
2.15	0.16	0.24	0.45	0.14
5.36	0.08	0.13	0.26	0.07
9.29	0.06	0.08	0.20	0.02
13.29	0.05	0.07	0.14	0.02
17.15	0.07	0.06	0.11	0.00
21.00	0.07	0.07	0.10	0.00
28.00	0.06	0.06	0.09	0.00

Table 5. Diffusion cell results from the H2 sample.

Radial Diffusion Cell A

time (days)	Br (C/C_0)	PFBA (C/C_0)	PIPES (C/C_0)	NO_3 (C/C_0)
0.25	0.55	0.69	0.91	0.58
0.90	0.31	0.45	0.61	0.34
2.15	0.16	0.28	0.46	0.18
5.36	0.12	0.18	0.28	0.08
9.29	0.07	0.10	0.20	0.04
13.29	0.07	0.08	0.18	0.02
17.15	0.07	0.07	0.13	0.01
21.00	0.07	0.07	0.11	0.00
28.00	0.07	0.07	0.11	0.00

Radial Diffusion Cell B

time (days)	Br (C/C_0)	PFBA (C/C_0)	PIPES (C/C_0)	NO_3 (C/C_0)
0.25	0.56	0.71	0.85	0.60
0.90	0.32	0.46	0.63	0.35
2.15	0.15	0.28	0.47	0.17
5.36	0.09	0.16	0.29	0.08
9.29	0.07	0.09	0.18	0.04
13.29	0.05	0.08	0.15	0.03
17.15	0.06	0.07	0.10	0.00
21.00	0.07	0.08	0.10	0.00
28.00	0.06	0.07	0.09	0.00

Radial Diffusion Cell C

time (days)	Br (C/C_0)	PFBA (C/C_0)	PIPES (C/C_0)	NO_3 (C/C_0)
0.25	0.57	0.70	0.82	0.58
0.90	0.33	0.48	0.63	0.30
2.15	0.18	0.28	0.46	0.15
5.36	0.09	0.14	0.30	0.07
9.29	0.08	0.11	0.20	0.03
13.29	0.05	0.08	0.13	0.03
17.15	0.06	0.08	0.11	0.00
21.00	0.07	0.07	0.10	0.00
28.00	0.07	0.07	0.10	0.00

Table 6. Diffusion cell results from the AO sample.

Radial Diffusion Cell A

time (days)	Br (C/C_0)	PFBA (C/C_0)	PIPES (C/C_0)	NO_3 (C/C_0)
0.25	0.51	0.59	0.72	0.53
0.90	0.30	0.41	0.54	0.29
2.15	0.17	0.26	0.41	0.10
5.36	0.08	0.16	0.26	0.00
9.29	0.06	0.09	0.15	0.01
13.29	0.07	0.08	0.12	0.01
17.15	0.06	0.07	0.09	0.00
21.00	0.06	0.06	0.08	0.00
28.00	0.06	0.06	0.07	0.00

Radial Diffusion Cell B

time (days)	Br (C/C_0)	PFBA (C/C_0)	PIPES (C/C_0)	NO_3 (C/C_0)
0.25	0.51	0.70	0.86	0.35
0.90	0.31	0.45	0.74	0.32
2.15	0.17	0.31	0.52	0.17
5.36	0.09	0.18	0.34	0.01
9.29	0.06	0.10	0.26	0.01
13.29	0.06	0.09	0.21	0.01
17.15	0.06	0.07	0.17	0.00
21.00	0.07	0.07	0.15	0.00
28.00	0.06	0.07	0.13	0.00

Radial Diffusion Cell C

time (days)	Br (C/C_0)	PFBA (C/C_0)	PIPES (C/C_0)	NO_3 (C/C_0)
0.25	0.51	0.59	0.75	0.53
0.90	0.30	0.41	0.59	0.26
2.15	0.16	0.26	0.44	0.09
5.36	0.08	0.16	0.29	0.01
9.29	0.07	0.10	0.21	0.01
13.29	0.07	0.08	0.14	0.01
17.15	0.06	0.07	0.12	0.00
21.00	0.06	0.07	0.11	0.00
28.00	0.07	0.07	0.09	0.00

Table 7. Diffusion cell results from the AT sample.

Radial Diffusion Cell A

time (days)	Br (C/C_0)	PFBA (C/C_0)	PIPES (C/C_0)	NO_3 (C/C_0)
0.25	0.58	0.74	0.86	0.59
0.90	0.29	0.49	0.71	0.31
2.15	0.16	0.29	0.55	0.15
5.36	0.09	0.17	0.38	0.02
9.29	0.08	0.11	0.28	0.01
13.29	0.07	0.09	0.22	0.00
17.15	0.08	0.07	0.17	0.00
21.00	0.07	0.07	0.16	0.00
28.00	0.07	0.08	0.12	0.00

Radial Diffusion Cell B

time (days)	Br (C/C_0)	PFBA (C/C_0)	PIPES (C/C_0)	NO_3 (C/C_0)
0.25	0.58	0.72	0.86	0.58
0.90	0.33	0.47	0.69	0.33
2.15	0.19	0.32	0.54	0.14
5.36	0.08	0.17	0.38	0.01
9.29	0.07	0.10	0.27	0.01
13.29	0.07	0.11	0.23	0.01
17.15	0.07	0.08	0.19	0.00
21.00	0.07	0.08	0.15	0.00
28.00	0.07	0.08	0.12	0.00

Radial Diffusion Cell C

time (days)	Br (C/C_0)	PFBA (C/C_0)	PIPES (C/C_0)	NO_3 (C/C_0)
0.25	0.58	0.75	0.89	0.56
0.90	0.31	0.50	0.67	0.33
2.15	0.18	0.29	0.56	0.12
5.36	0.10	0.17	0.39	0.03
9.29	0.07	0.12	0.25	0.00
13.29	0.07	0.09	0.21	0.01
17.15	0.07	0.09	0.16	0.00
21.00	0.07	0.07	0.13	0.00
28.00	0.07	0.08	0.12	0.00

Table 8. Diffusion cell results from the ALB sample.

Radial Diffusion Cell A

time (days)	Br (C/C_0)	PFBA (C/C_0)	PIPES (C/C_0)	NO_3 (C/C_0)
0.25	0.56	0.67	0.90	0.57
0.90	0.33	0.47	0.68	0.27
2.15	0.17	0.30	0.57	0.04
5.36	0.10	0.15	0.34	0.00
9.29	0.07	0.10	0.29	0.00
13.29	0.06	0.09	0.19	0.01
17.15	0.07	0.07	0.18	0.00
21.00	0.07	0.07	0.16	0.00
28.00	0.07	0.07	0.13	0.00

Radial Diffusion Cell B

time (days)	Br (C/C_0)	PFBA (C/C_0)	PIPES (C/C_0)	NO_3 (C/C_0)
0.25	0.56	0.65	0.87	0.57
0.90	0.33	0.45	0.73	0.28
2.15	0.18	0.30	0.53	0.06
5.36	0.10	0.14	0.31	0.02
9.29	0.07	0.10	0.26	0.01
13.29	0.06	0.10	0.19	0.01
17.15	0.07	0.09	0.17	0.00
21.00	0.07	0.08	0.14	0.00
28.00	0.07	0.07	0.11	0.00

Radial Diffusion Cell C

time (days)	Br (C/C_0)	PFBA (C/C_0)	PIPES (C/C_0)	NO_3 (C/C_0)
0.25	0.54	0.66	0.66	0.57
0.90	0.34	0.45	0.45	0.26
2.15	0.19	0.30	0.30	0.05
5.36	0.09	0.14	0.14	0.03
9.29	0.07	0.10	0.10	0.01
13.29	0.06	0.08	0.08	0.01
17.15	0.06	0.07	0.07	0.00
21.00	0.07	0.08	0.08	0.00
28.00	0.07	0.07	0.07	0.00

APPENDIX E

MIM (CXTFIT 2.1) INPUT FILES

Table 1. CXTFIT 2.1 input file for simulation of the Br BTC of the BEM column.

```
  1
*** BLOCK A: MODEL DESCRIPTION *****************************************
BEM Column Br Forward Mode
(Kd=0.0, unit, m, s, kg)
INVERSE    MODE      NREDU
   0         2         0
 MODC       ZL
   1       0.4
*** BLOCK B: INVERSE PROBLEM ********************************************
  MIT       ILMT     MASS
  50         0         0
  MNEQ      MDEG
   0         0
*** BLOCK C: TRANSPORT PARAMETERS ***************************************
    V        D        R       Beta     omega      Mu1       Mu2
   2.28e-7    1.35e-9    1.0     0.00205     4.46        0.        0.
     0        0        0       0         0          0         0
*** BLOCK D: BVP; MODB=0 ZERO; =1 DIRAC; =2 STEP; =3 A PULSE  ************
  MODB (Reduced Conc.& time) =4 MULTIPLE; =5 EXPONENTIAL; =6 ARBITRARY
   3
   1.0     6.05e+6
*** BLOCK E: IVP; MODI=0 ZERO; =1 CONSTANT; =2 STEPWISE; =3 EXPONENTIAL **
  MODI
    0
*** BLOCK F: PVP; MODP=0 ZERO; =1 CONSTANT; =2 STEPWISE; =3 EXPONENTIAL **
  MODP
    0
*** BLOCK G: DATA FOR INVERSE PROBLEM ***********************************
INPUTM =0; Z,T,C  =1; T,C FOR SAME Z  =2; Z,C FOR SAME T
   1
   0.4
        TIME        CONC     (Give "0 0 0" after last data set.)
       0.000           0.000
       19800.000       0.000
       86400.000       0.000
       113340.000      0.006
       408600.000      0.050
       502200.000      0.072
       661200.000      0.117
       930600.000      0.178
       1094400.000     0.233
       1266900.000     0.317
       1485000.000     0.394
       1639800.000     0.482
       1895400.000     0.622
       2154600.000     0.674
       2331000.000     0.780
       2590200.000     0.821
       2939400.000     0.900
       3198600.000     0.956
       3565800.000     0.941
       3790800.000     0.948
       4051800.000     0.980
       4312800.000     0.980
       4573800.000     0.965
       4834800.000     0.990
       5095800.000     0.987
       5356800.000     0.980
       5617800.000     1.010
       5877000.000     1.004
       6049800.000     0.995
       0           0
```

Table 2. CXTFIT 2.1 input file for simulation of the PFBA BTC of the BEM column.

```
  1
*** BLOCK A: MODEL DESCRIPTION *****************************************
BEM Column PFBA Forward Mode
(Kd=0.0, unit, m, s, kg)
INVERSE    MODE      NREDU
   0         2         0
 MODC       ZL
   1       0.4
*** BLOCK B: INVERSE PROBLEM ********************************************
  MIT       ILMT    MASS
  50         0        0
  MNEQ      MDEG
   0         0
*** BLOCK C: TRANSPORT PARAMETERS ***************************************
    V        D        R       Beta     omega      Mu1       Mu2
   2.28e-7    5.7e-10    1.0     0.00205     2.51        0.        0.
     0        0        0       0         0          0         0
*** BLOCK D: BVP; MODB=0 ZERO; =1 DIRAC; =2 STEP; =3 A PULSE  ************
  MODB (Reduced Conc.& time) =4 MULTIPLE; =5 EXPONENTIAL; =6 ARBITRARY
   3
   1.0     6.05e+6
*** BLOCK E: IVP; MODI=0 ZERO; =1 CONSTANT; =2 STEPWISE; =3 EXPONENTIAL **
  MODI
    0
*** BLOCK F: PVP; MODP=0 ZERO; =1 CONSTANT; =2 STEPWISE; =3 EXPONENTIAL **
  MODP
    0
*** BLOCK G: DATA FOR INVERSE PROBLEM ***********************************
INPUTM =0; Z,T,C  =1; T,C FOR SAME Z  =2; Z,C FOR SAME T
   1
   0.4
        TIME        CONC     (Give "0 0 0" after last data set.)
       0.000          0.000
       19800.000      0.000
       86400.000      0.000
       113340.000     0.000
       408600.000     0.074
       502200.000     0.089
       661200.000     0.133
       930600.000     0.199
       1094400.000    0.244
       1266900.000    0.317
       1485000.000    0.401
       1639800.000    0.508
       1895400.000    0.580
       2154600.000    0.698
       2331000.000    0.732
       2590200.000    0.825
       2939400.000    0.861
       3198600.000    0.902
       3565800.000    0.953
       3790800.000    0.943
       4051800.000    0.973
       4312800.000    1.001
       4573800.000    0.981
       4834800.000    0.990
       5095800.000    1.010
       5356800.000    1.000
       5617800.000    0.973
       5877000.000    0.974
       6049800.000    1.016
       0           0
```

Table 3. CXTFIT 2.1 input file for simulation of the PIPES BTC of the BEM column.

```
  1
*** BLOCK A: MODEL DESCRIPTION *********************************************
BEM Column PIPES Forward Mode
(Kd=0.0, unit, m, s, kg)
INVERSE    MODE      NREDU
   0         2         0
 MODC       ZL
   1       0.4
*** BLOCK B: INVERSE PROBLEM ***********************************************
  MIT       ILMT    MASS
  50        0        0
  MNEQ      MDEG
   0         0
*** BLOCK C: TRANSPORT PARAMETERS ******************************************
    V       D       R       Beta    omega     Mu1      Mu2
   2.28e-7    3.1e-10    1.0     0.00205     1.02        0.       0.
     0       0       0       0       0         0        0
*** BLOCK D: BVP; MODB=0 ZERO; =1 DIRAC; =2 STEP; =3 A PULSE  ************
  MODB (Reduced Conc.& time) =4 MULTIPLE; =5 EXPONENTIAL; =6 ARBITRARY
   3
   1.0     6.05e+6
*** BLOCK E: IVP; MODI=0 ZERO; =1 CONSTANT; =2 STEPWISE; =3 EXPONENTIAL **
  MODI
    0
*** BLOCK F: PVP; MODP=0 ZERO; =1 CONSTANT; =2 STEPWISE; =3 EXPONENTIAL **
  MODP
    0
*** BLOCK G: DATA FOR INVERSE PROBLEM **********************************
INPUTM =0; Z,T,C  =1; T,C FOR SAME Z  =2; Z,C FOR SAME T
   1
   0.4
        TIME       CONC     (Give "0 0 0" after last data set.)
       0.000   0.000
       19800.000       0.000
       86400.000       0.000
       113340.000      0.000
       408600.000      0.120
       502200.000      0.153
       661200.000      0.253
       930600.000      0.387
       1094400.000     0.467
       1266900.000     0.528
       1485000.000     0.602
       1639800.000     0.637
       1895400.000     0.704
       2154600.000     0.760
       2331000.000     0.793
       2590200.000     0.810
       2939400.000     0.860
       3198600.000     0.888
       3565800.000     0.933
       3790800.000     0.944
       4051800.000     0.966
       4312800.000     0.978
       4573800.000     0.972
       4834800.000     0.973
       5095800.000     0.978
       5356800.000     0.994
       5617800.000     0.970
       5877000.000     0.962
       6049800.000     0.978
       0           0
```

APPENDIX F

PDFM (FRACTRAN 5.01) INPUT FILES

Table 1. FRACTRAN 5.01 input file for simulation of the Br BTC for the BEM Column.

```
Br BTC, BEM Column
.FALSE.                 LDIFF  diffusion only
.TRUE.                  LFLOW  flow solution
.TRUE.                  LTRANS transport solution
.TRUE.                  LFRAC  fractured/porous media
.TRUE.                  LKFDM  finite element/finite difference
.TRUE.                  LPMSH  print mesh data
.TRUE.                  LPVEL  print darcy flux data
.TRUE.                  LPHED  print head data
.TRUE.                  LDVEL  write darcy flux data
.TRUE.                  LDHED  write head data
.TRUE.                  LMBAL  mass balance calculation
.FALSE.                 LPERM  element/zoned hydraulic conductivity
.TRUE.                  LSLICE flux crossing a plane
.FALSE.                 LRSTRT restart
.FALSE.                 LTHICK read thickness file
0.0   1.0               XMIN, XMAX  Overall
0.0   0.043             ZMIN, ZMAX  Overall
0.01 0.0043             DXMAX, DZMAX maximum element size
Done grid refinement
Matrix block
0.0   1.00              XBMIN, XBMAX  X-range
0.0   0.043             ZBMIN, ZBMAX  Z-range
1.0e-11 1.0e-11         CKXX, CKZZ  Hydraulic conductivity
0.0  0.0                AL, AT  Dispersivity
4.3e-10 0.268 1.0       DSTAR, POR, RETARD
1830.0 0.00             RHOB GSOURCE  Bulk Density, source generation term
0.0 0.0 0.0             THETAIM, RIM, ALPHAIM Double-porosity parameters
Done porous media zones
-100                    SEED for random number generator, frac location
-100                    SEED for random number generator, frac aperture
Done vertical fracture zones
0.01                    FXMIN  min spacing between rand. vert. frac.
3                       NNXM   min nodes between rand. vert. frac.
Done random vertical fracture zones
Horizontal fracture
0.0 1.0                 XHFMIN, XHFMAX  X-range
0.0215 0.0215           ZHFMIN, ZHFMAX  Z-range
0.1                     HSPACE  Fracture spacing
0.00                    ALFRACH Dispersivity
1.0                     RFRACH  Retardation
1.3e-5    0.0           APH     Aperture
.false.
Done horizontal fracture zones
10.0                    FZMIN  min spacing between rand. horiz. frac.
3                       NNZM   min nodes between rand. horiz. frac.
Done random horizontal fracture zones
Done specified head points
Left end of system - specified head
0.0 0.043               HSMIN, HSMAX  Range
1.0 1.0                 HSSTRT, HSEND Head values
Right end of system - specified head
0.0 0.043               HSMIN, HSMAX Range
```

```
0.0 0.0                 HSSTRT, HSEND Head values
Done specified head fill segments
Done specified head regions
Done specified fluid flux points
Done specified fluid flux fill segments
Done specified fluid flux regions
0.0                     DECAY_S specified solute flux nodes
0.0                     DECAY_1 specified concentration nodes
0.0                     DECAY_3 Third-type rectangle elements
0.0                     DECAYV3 Third-type vfrac elements
0.0                     DECAYH3 Third-type hfrac elements
Source at left end of fracture
0.0 0.0215              CPX, CPZ Coordinate
1                       CPPANEL Time varying panels
0.0  1.0                CPON Time on  CPVAL  Concentration
Done specified concentration points
Done specified concentration regions
Done third-type concentration fill segments
Done specified solute flux points
Done specified solute flux fill segments
0.0                     CINIT  Default initial concentration
Done different initial concentration zones
1.0                     THK_INIT  Default thickness
Done different thickness
Column
0.40                    XSLICE  Slice column x or row z
1.3e-9                  DIFFUS  Free-solution diffusion coefficient
999.498                 RHO     Fluid density
0.0012363               VISC    Fluid viscosity
0.0000000               CLAMDA  Solute first-order decay constant
9.8100000               GRAV    Gravity constant
1.e-8                   EPSF    Convergence criteria for flow
200                     MAXITF  Maximum # of iterations for flow
1.e-6                   EPS     Convergence criteria for concentration
200                     MAXIT   Maximum # of iterations for concentration
2                       INORM   Convergence test type
1.e-4                   RELERR  Relative error
5                       NTERM   Number of Laplace p-space solutions =
2*NTERM+1
6050000.0               TMAX    Maximum time for inversion
```

Table 2. FRACTRAN 5.01 input file for simulation of the PFBA BTC for the BEM Column.

```
PFBA BTC, BEM Column
.FALSE.                 LDIFF  diffusion only
.TRUE.                  LFLOW  flow solution
.TRUE.                  LTRANS transport solution
.TRUE.                  LFRAC  fractured/porous media
.TRUE.                  LKFDM  finite element/finite difference
.TRUE.                  LPMSH  print mesh data
.TRUE.                  LPVEL  print darcy flux data
.TRUE.                  LPHED  print head data
.TRUE.                  LDVEL  write darcy flux data
.TRUE.                  LDHED  write head data
.TRUE.                  LMBAL  mass balance calculation
.FALSE.                 LPERM  element/zoned hydraulic conductivity
.TRUE.                  LSLICE flux crossing a plane
.FALSE.                 LRSTRT restart
.FALSE.                 LTHICK read thickness file
0.0   1.0               XMIN, XMAX  Overall
0.0   0.043             ZMIN, ZMAX  Overall
0.01 0.0043             DXMAX, DZMAX maximum element size
Done grid refinement
Matrix block
0.0   1.00              XBMIN, XBMAX  X-range
0.0   0.043             ZBMIN, ZBMAX  Z-range
1.0e-11 1.0e-11         CKXX, CKZZ  Hydraulic conductivity
0.0  0.0                AL, AT  Dispersivity
2.6e-10 0.252 1.0       DSTAR, POR, RETARD
1830.0 0.00             RHOB GSOURCE  Bulk Density, source generation term
0.0 0.0 0.0             THETAIM, RIM, ALPHAIM Double-porosity parameters
Done porous media zones
-100                    SEED for random number generator, frac location
-100                    SEED for random number generator, frac aperture
Done vertical fracture zones
0.01                    FXMIN  min spacing between rand. vert. frac.
3                       NNXM   min nodes between rand. vert. frac.
Done random vertical fracture zones
Horizontal fracture
0.0 1.0                 XHFMIN, XHFMAX  X-range
0.0215 0.0215           ZHFMIN, ZHFMAX  Z-range
0.1                     HSPACE  Fracture spacing
0.00                    ALFRACH Dispersivity
1.0                     RFRACH  Retardation
1.3e-5    0.0           APH     Aperture
.false.
Done horizontal fracture zones
10.0                    FZMIN  min spacing between rand. horiz. frac.
3                       NNZM   min nodes between rand. horiz. frac.
Done random horizontal fracture zones
Done specified head points
Left end of system - specified head
0.0 0.043               HSMIN, HSMAX  Range
1.0 1.0                 HSSTRT, HSEND Head values
Right end of system - specified head
0.0 0.043               HSMIN, HSMAX Range
```

```
0.0 0.0                 HSSTRT, HSEND Head values
Done specified head fill segments
Done specified head regions
Done specified fluid flux points
Done specified fluid flux fill segments
Done specified fluid flux regions
0.0                     DECAY_S specified solute flux nodes
0.0                     DECAY_1 specified concentration nodes
0.0                     DECAY_3 Third-type rectangle elements
0.0                     DECAYV3 Third-type vfrac elements
0.0                     DECAYH3 Third-type hfrac elements
Source at left end of fracture
0.0 0.0215              CPX, CPZ Coordinate
1                       CPPANEL Time varying panels
0.0  1.0                CPON Time on  CPVAL  Concentration
Done specified concentration points
Done specified concentration regions
Done third-type concentration fill segments
Done specified solute flux points
Done specified solute flux fill segments
0.0                     CINIT  Default initial concentration
Done different initial concentration zones
1.0                     THK_INIT  Default thickness
Done different thickness
Column
0.40                    XSLICE  Slice column x or row z
5.7e-10                 DIFFUS  Free-solution diffusion coefficient
999.498                 RHO     Fluid density
0.0012363               VISC    Fluid viscosity
0.0000000               CLAMDA  Solute first-order decay constant
9.8100000               GRAV    Gravity constant
1.e-8                   EPSF    Convergence criteria for flow
200                     MAXITF  Maximum # of iterations for flow
1.e-6                   EPS     Convergence criteria for concentration
200                     MAXIT   Maximum # of iterations for concentration
2                       INORM   Convergence test type
1.e-4                   RELERR  Relative error
5                       NTERM   Number of Laplace p-space solutions =
2*NTERM+1
6050000.0               TMAX    Maximum time for inversion
```

Table 3. FRACTRAN 5.01 input file for simulation of the PIPES BTC for the BEM Column.

```
PIPES BTC, BEM Column
.FALSE.                 LDIFF  diffusion only
.TRUE.                  LFLOW  flow solution
.TRUE.                  LTRANS transport solution
.TRUE.                  LFRAC  fractured/porous media
.TRUE.                  LKFDM  finite element/finite difference
.TRUE.                  LPMSH  print mesh data
.TRUE.                  LPVEL  print darcy flux data
.TRUE.                  LPHED  print head data
.TRUE.                  LDVEL  write darcy flux data
.TRUE.                  LDHED  write head data
.TRUE.                  LMBAL  mass balance calculation
.FALSE.                 LPERM  element/zoned hydraulic conductivity
.TRUE.                  LSLICE flux crossing a plane
.FALSE.                 LRSTRT restart
.FALSE.                 LTHICK read thickness file
0.0   1.0               XMIN, XMAX  Overall
0.0   0.043             ZMIN, ZMAX  Overall
0.01 0.0043             DXMAX, DZMAX maximum element size
Done grid refinement
Matrix block
0.0   1.00              XBMIN, XBMAX  X-range
0.0   0.043             ZBMIN, ZBMAX  Z-range
1.0e-11 1.0e-11         CKXX, CKZZ  Hydraulic conductivity
0.0  0.0                AL, AT  Dispersivity
1.3e-10 0.214 1.0       DSTAR, POR, RETARD
1830.0 0.00             RHOB GSOURCE  Bulk Density, source generation term
0.0 0.0 0.0             THETAIM, RIM, ALPHAIM Double-porosity parameters
Done porous media zones
-100                    SEED for random number generator, frac location
-100                    SEED for random number generator, frac aperture
Done vertical fracture zones
0.01                    FXMIN  min spacing between rand. vert. frac.
3                       NNXM   min nodes between rand. vert. frac.
Done random vertical fracture zones
Horizontal fracture
0.0 1.0                 XHFMIN, XHFMAX  X-range
0.0215 0.0215           ZHFMIN, ZHFMAX  Z-range
0.1                     HSPACE  Fracture spacing
0.00                    ALFRACH Dispersivity
1.0                     RFRACH  Retardation
1.3e-5    0.0           APH     Aperture
.false.
Done horizontal fracture zones
10.0                    FZMIN  min spacing between rand. horiz. frac.
3                       NNZM   min nodes between rand. horiz. frac.
Done random horizontal fracture zones
Done specified head points
Left end of system - specified head
0.0 0.043               HSMIN, HSMAX  Range
1.0 1.0                 HSSTRT, HSEND Head values
```

```
Right end of system - specified head
0.0 0.043                HSMIN, HSMAX Range
0.0 0.0                  HSSTRT, HSEND Head values
Done specified head fill segments
Done specified head regions
Done specified fluid flux points
Done specified fluid flux fill segments
Done specified fluid flux regions
0.0                      DECAY_S specified solute flux nodes
0.0                      DECAY_1 specified concentration nodes
0.0                      DECAY_3 Third-type rectangle elements
0.0                      DECAYV3 Third-type vfrac elements
0.0                      DECAYH3 Third-type hfrac elements
Source at left end of fracture
0.0 0.0215               CPX, CPZ Coordinate
1                        CPPANEL Time varying panels
0.0  1.0                 CPON Time on  CPVAL  Concentration
Done specified concentration points
Done specified concentration regions
Done third-type concentration fill segments
Done specified solute flux points
Done specified solute flux fill segments
0.0                      CINIT  Default initial concentration
Done different initial concentration zones
1.0                      THK_INIT  Default thickness
Done different thickness
Column
0.40                     XSLICE  Slice column x or row z
3.1e-10                  DIFFUS  Free-solution diffusion coefficient
999.498                  RHO     Fluid density
0.0012363                VISC    Fluid viscosity
0.0000000                CLAMDA  Solute first-order decay constant
9.8100000                GRAV    Gravity constant
1.e-8                    EPSF    Convergence criteria for flow
200                      MAXITF  Maximum # of iterations for flow
1.e-6                    EPS     Convergence criteria for concentration
200                      MAXIT   Maximum # of iterations for concentration
2                        INORM   Convergence test type
1.e-4                    RELERR  Relative error
5                        NTERM   Number of Laplace p-space solutions =
2*NTERM+1
6050000.0                TMAX    Maximum time for inversion
```

APPENDIX G

3-D DFM (MAFIC) INPUT FILES

Table 1. MAFIC input file for simulation of the Br BTC for the BEM Column (Stochastic DFM).

```
Bemis Br
      $MAFIC IPART=10000,     $END
      PROJ  IOUT  IPLOT IETYP ISTART      IMTYP ITRANS      I1D
      1     1     0     1     0     3     0     0
TOL   NITMAX
      1.00E-06    100
ETIME IOFLAG      NSTEPS
      1.00E-03    1     1
      20000 2     1
      40000 2     1
      86400 2     1
      864000      2     1
      8640000     7     1
      0     0     0
NUMBER      OF    NODAL GROUPS      (NNGRP)
      3
      Data  Pairs for   Nodal Group 1     BND-TYPE=   1
      0
      BOUNDARY    GROUP #     2:00  Base  BND-TYPE=   1
      0
      BOUNDARY    GROUP #     3:00  Sides BND-TYPE=   -1
      0
SOLUTE      TRANSPORT   MODE
      001
      Seed  LDisp TDisp Diffuse     PMass FDensity    RSink NPTrack
      7     0.00  0.00  4.3e-10     0.005 1000  0     0
      NSource
      1
      NSVal NGrp  Chemical    --    for   source      1
      3     1     Br
      Time  Conc
      0     1
      2592000     0
      8640000     0
***   HEADER      bemisjune
      NODE  X     Y     Z     Type  H     Q     Grp

   1  -2.00E-01   -1.69E-01   2.00E-01 1  4.00E-01 0.00E+00 1
   …
   1028  2.00E-01 -9.13E-02   3.74E-02 -1 0.00E+00 0.00E+00 3  0  0.00E+00
   0.00E+00 0.00E+00 0  0.00E+00 0.00E+00 0  Elem. #  Node1 Node2 Node3
   frac. #  set   #  Trans Stor  Apert Minerals
   1  1  3  4  1  1  5.90E-09 1.00E-06 3.66E-05 …
      1884  981   982   1011  100   2  7.05E-09 1.00E-06 3.88E-05
   0  0  0  0  0  0  0.00E+00 0.00E+00 0.00E+00
   CONDUCTIVITY   STORATIVITY POROSITY HEAD  NMBEL
   3.00E-20 0  0.268 0  1
   RADII OF GENERIC  MATRIX   ELEMENT
   2.15E-02
```

Table 2. MAFIC input file for simulation of the PFBA BTC for the BEM Column (Stochastic DFM).

```
Bemis PFBA
      $MAFIC IPART=10000,     $END
      PROJ  IOUT  IPLOT IETYP ISTART      IMTYP ITRANS      I1D
      1     1     0     1     0     3     0     0
TOL   NITMAX
      1.00E-06    100
ETIME IOFLAG      NSTEPS
      1.00E-03    1     1
      20000 2     1
      40000 2     1
      86400 2     1
      864000      2     1
      8640000     7     1
      0     0     0
NUMBER      OF    NODAL GROUPS      (NNGRP)
      3
      Data  Pairs for   Nodal Group 1     BND-TYPE=   1
      0
      BOUNDARY    GROUP #     2:00  Base  BND-TYPE=   1
      0
      BOUNDARY    GROUP #     3:00  Sides BND-TYPE=   -1
      0
SOLUTE      TRANSPORT   MODE
      001
      Seed  LDisp TDisp Diffuse     PMass FDensity    RSink NPTrack
      7     0.00  0.00  2.6e-10     0.005 1000  0     0
      NSource
      1
      NSVal NGrp  Chemical    --    for   source      1
      3     1     Br
      Time  Conc
      0     1
      2592000     0
      8640000     0
***   HEADER      bemisjune
      NODE  X     Y     Z     Type  H     Q     Grp

   1  -2.00E-01   -1.69E-01   2.00E-01 1  4.00E-01 0.00E+00 1
   …
   1028  2.00E-01 -9.13E-02   3.74E-02 -1 0.00E+00 0.00E+00 3  0  0.00E+00
   0.00E+00 0.00E+00 0  0.00E+00 0.00E+00 0  Elem. #  Node1 Node2 Node3
   frac. #  set   #  Trans Stor  Apert Minerals
   1  1  3  4  1  1  5.90E-09 1.00E-06 3.66E-05 …
      1884  981   982   1011  100   2  7.05E-09 1.00E-06 3.88E-05
   0  0  0  0  0  0  0.00E+00 0.00E+00 0.00E+00
   CONDUCTIVITY   STORATIVITY POROSITY HEAD  NMBEL
   3.00E-20 0  0.252 0  1
   RADII OF GENERIC  MATRIX   ELEMENT
   2.15E-02
```

Table 3. MAFIC input file for simulation of the PIPES BTC for the BEM Column (Stochastic DFM).

```
Bemis PIPES
      $MAFIC IPART=10000,     $END
      PROJ  IOUT  IPLOT IETYP ISTART      IMTYP ITRANS      I1D
      1     1     0     1     0     3     0     0
TOL   NITMAX
      1.00E-06    100
ETIME IOFLAG      NSTEPS
      1.00E-03    1     1
      20000 2     1
      40000 2     1
      86400 2     1
      864000      2     1
      8640000     7     1
      0     0     0
NUMBER      OF    NODAL GROUPS      (NNGRP)
      3
      Data  Pairs for   Nodal Group 1     BND-TYPE=   1
      0
      BOUNDARY    GROUP #     2:00  Base  BND-TYPE=   1
      0
      BOUNDARY    GROUP #     3:00  Sides BND-TYPE=   -1
      0
SOLUTE      TRANSPORT   MODE
      001
      Seed  LDisp TDisp Diffuse     PMass FDensity    RSink NPTrack
      7     0.00  0.00  1.3e-10     0.005 1000  0     0
      NSource
      1
      NSVal NGrp  Chemical    --    for   source      1
      3     1     Br
      Time  Conc
      0     1
      2592000     0
      8640000     0
***   HEADER      bemisjune
      NODE  X     Y     Z     Type  H     Q     Grp

   1  -2.00E-01   -1.69E-01   2.00E-01 1  4.00E-01 0.00E+00 1
   …
   1028  2.00E-01 -9.13E-02   3.74E-02 -1 0.00E+00 0.00E+00 3  0  0.00E+00
   0.00E+00 0.00E+00 0  0.00E+00 0.00E+00 0  Elem. #  Node1 Node2 Node3
   frac. #  set   #  Trans Stor  Apert Minerals
   1  1  3  4  1  1  5.90E-09 1.00E-06 3.66E-05 …
      1884  981   982   1011  100   2  7.05E-09 1.00E-06 3.88E-05
   0  0  0  0  0  0  0.00E+00 0.00E+00 0.00E+00
   CONDUCTIVITY   STORATIVITY POROSITY HEAD  NMBEL
   3.00E-20 0  0.214 0  1
   RADII OF GENERIC  MATRIX   ELEMENT
   2.15E-02
```

Table 4. MAFIC input file for simulation of the Br BTC for the BEM Column (Reconstructed DFM).

```
Bemis Br
      $MAFIC IPART=10000,     $END
      PROJ  IOUT  IPLOT IETYP ISTART      IMTYP ITRANS      I1D
      1     1     0     1     0     3     0     0
TOL   NITMAX
      1.00E-06    100
ETIME IOFLAG      NSTEPS
      1.00E-03    1     1
      20000 2     1
      40000 2     1
      86400 2     1
      864000      2     1
      8640000     7     1
      0     0     0
NUMBER      OF    NODAL GROUPS      (NNGRP)
      3
      Data  Pairs for   Nodal Group 1     BND-TYPE=   1
      0
      BOUNDARY    GROUP #     2:00  Base  BND-TYPE=   1
      0
      BOUNDARY    GROUP #     3:00  Sides BND-TYPE=   -1
      0
SOLUTE      TRANSPORT   MODE
      001
      Seed  LDisp TDisp Diffuse     PMass FDensity    RSink NPTrack
      7     0.00  0.00  4.3e-10     0.005 1000  0     0
      NSource
      1
      NSVal NGrp  Chemical    --    for   source      1
      3     1     Br
      Time  Conc
      0     1
      2592000     0
      8640000     0
***   HEADER
   NODE  X  Y  Z  Type  H  Q  Grp
   1  -2.00E-01   -1.69E-01   2.00E-01 1  4.00E-01 0.00E+00 1
   ...
   1028  2.00E-01 -9.13E-02   3.74E-02 -1 0.00E+00 0.00E+00 3

   0  0.00E+00 0.00E+00 0.00E+00 0  0.00E+00 0.00E+00 0
   Elem. #  Node1 Node2 Node3 frac. #  set   #  Trans Stor  Apert Minerals
   1  1  3  4  1  1  5.90E-09 1.00E-06 3.66E-05 ...
   1884  981   982   1011  100   2  7.05E-09 1.00E-06 3.88E-05
   0  0  0  0  0  0  0.00E+00 0.00E+00 0.00E+00
   CONDUCTIVITY   STORATIVITY POROSITY HEAD  NMBEL
   3.00E-20 0  0.268 0  1
   RADII OF GENERIC  MATRIX   ELEMENT
   2.15E-02
```

Table 5. MAFIC input file for simulation of the PFBA BTC for the BEM Column (Reconstructed DFM).

```
Bemis PFBA
      $MAFIC IPART=10000,     $END
      PROJ  IOUT  IPLOT IETYP ISTART      IMTYP ITRANS      I1D
      1     1     0     1     0     3     0     0
TOL   NITMAX
      1.00E-06    100
ETIME IOFLAG      NSTEPS
      1.00E-03    1     1
      20000 2     1
      40000 2     1
      86400 2     1
      864000      2     1
      8640000     7     1
      0     0     0
NUMBER      OF    NODAL GROUPS      (NNGRP)
      3
      Data  Pairs for   Nodal Group 1     BND-TYPE=   1
      0
      BOUNDARY    GROUP #     2:00  Base  BND-TYPE=   1
      0
      BOUNDARY    GROUP #     3:00  Sides BND-TYPE=   -1
      0
SOLUTE      TRANSPORT   MODE
      001
      Seed  LDisp TDisp Diffuse     PMass FDensity    RSink NPTrack
      7     0.00  0.00  2.6e-10     0.005 1000  0     0
      NSource
      1
      NSVal NGrp  Chemical    --    for   source      1
      3     1     Br
      Time  Conc
      0     1
      2592000     0
      8640000     0
***   HEADER
   NODE  X  Y  Z  Type  H  Q  Grp
   1  -2.00E-01   -1.69E-01   2.00E-01 1  4.00E-01 0.00E+00 1
   ...
   1028  2.00E-01 -9.13E-02   3.74E-02 -1 0.00E+00 0.00E+00 3

   0  0.00E+00 0.00E+00 0.00E+00 0  0.00E+00 0.00E+00 0
   Elem. #  Node1 Node2 Node3 frac. #  set   #  Trans Stor  Apert Minerals
   1  1  3  4  1  1  5.90E-09 1.00E-06 3.66E-05 ...
   1884  981   982   1011  100   2  7.05E-09 1.00E-06 3.88E-05
   0  0  0  0  0  0  0.00E+00 0.00E+00 0.00E+00
   CONDUCTIVITY   STORATIVITY POROSITY HEAD  NMBEL
   3.00E-20 0  0.252 0  1
   RADII OF GENERIC  MATRIX   ELEMENT
   2.15E-02
```

Table 6. MAFIC input file for simulation of the PIPES BTC for the BEM Column (Reconstructed DFM).

```
Bemis PIPES
      $MAFIC IPART=10000,     $END
      PROJ  IOUT  IPLOT IETYP ISTART      IMTYP ITRANS      I1D
      1     1     0     1     0     3     0     0
TOL   NITMAX
      1.00E-06    100
ETIME IOFLAG      NSTEPS
      1.00E-03    1     1
      20000 2     1
      40000 2     1
      86400 2     1
      864000      2     1
      8640000     7     1
      0     0     0
NUMBER      OF    NODAL GROUPS      (NNGRP)
      3
      Data  Pairs for   Nodal Group 1     BND-TYPE=   1
      0
      BOUNDARY    GROUP #     2:00  Base  BND-TYPE=   1
      0
      BOUNDARY    GROUP #     3:00  Sides BND-TYPE=   -1
      0
SOLUTE      TRANSPORT   MODE
      001
      Seed  LDisp TDisp Diffuse     PMass FDensity    RSink NPTrack
      7     0.00  0.00  1.3e-10     0.005 1000  0     0
      NSource
      1
      NSVal NGrp  Chemical    --    for   source      1
      3     1     Br
      Time  Conc
      0     1
      2592000     0
      8640000     0
***   HEADER
   NODE  X  Y  Z  Type  H  Q  Grp
   1  -2.00E-01   -1.69E-01   2.00E-01 1  4.00E-01 0.00E+00 1
   ...
   1028  2.00E-01 -9.13E-02   3.74E-02 -1 0.00E+00 0.00E+00 3

   0  0.00E+00 0.00E+00 0.00E+00 0  0.00E+00 0.00E+00 0
   Elem. #  Node1 Node2 Node3 frac. #  set   #  Trans Stor  Apert Minerals
   1  1  3  4  1  1  5.90E-09 1.00E-06 3.66E-05 ...
   1884  981   982   1011  100   2  7.05E-09 1.00E-06 3.88E-05
   0  0  0  0  0  0  0.00E+00 0.00E+00 0.00E+00
   CONDUCTIVITY   STORATIVITY POROSITY HEAD  NMBEL
   3.00E-20 0  0.214 0  1
   RADII OF GENERIC  MATRIX   ELEMENT
   2.15E-02
```

REFERENCES

Brockman, C. S. and J. P. Szabo. 2000. Fractures and their distribution in the tills of Ohio. Ohio Journal of Science. v. 100, n. 3/4, pp. 39-55.

Bruner, D. R. and A. J. Lutenegger. 1993. Measurement of saturated hydraulic conductivity in fine-grained glacial tills in Iowa: Comparison of in situ and laboratory methods. Hydraulic Conductivity and Waste Contaminant Transport in Soils, ASTM STP 1142, David E. Daniel and Stephen J. Trautwein, Eds., American Society for Testing and Materials, Philadelphia.

Connell, D. E. 1984. Distribution, characteristics, and genesis of joints in fine-grained till and lacustrine sediments, eastern and northwestern Wisconsin. Master's Thesis, University of Wisconsin, Madison. 443 p.

Eidem, J. M., W. W. Simpkins, and M. R. Burkart. 1999. Geology, groundwater flow, and water quality in the Walnut Creek watershed. Journal of Environmental Quality. v. 28, pp. 60-69.

Fredericia, J. 1990. Saturated hydraulic conductivity of clayey tills and the role of fractures. Nordic Hydrology. v. 21, pp. 119-132.

Grisak, G. E. and J. F. Pickens. 1980. Solute transport through fractured media: 1. The effect of matrix diffusion. Water Resources Research. v. 16, pp. 719-730.

Helmke, M. F., W. W. Simpkins, and R. Horton. 1998. Genesis, morphology, and contaminant transport potential of till fractures in Iowa, USA. *Abstracts from Mass Transport in Fractured Aquifers and Aquitards, Geological Institute, University of Copenhagen, Denmark*, p. 21.

Jørgensen, P. R. and J. Fredericia. 1992. Migration of nutrients, pesticides and heavy metals in fractured clayey till. Geotechnique. v. 42, pp. 67-77.

Jørgensen, P. R., L. D. McKay, and N. ZH. Spliid. 1998. Evaluation of chloride and pesticide transport in a fractured clayey till using large undisturbed columns and numerical modeling. Water Resources Research. v. 34, pp. 539-553.

Keller, C. K., G. van der Kamp, and J. A. Cherry. 1988. Hydrogeology of two Saskatchewan tills, I. Fractures, bulk permeability, and special variability of downward flow. Journal of Hydrology. v. 101, pp. 97-121.

Keller, C. K., G. van der Kamp, and J. A. Cherry. 1989. A multiscale study of the permeability of a thick clayey till. Water Resources Research. v. 25, n. 11. pp. 2299-2317.

Kemmis, T. J., E. A. Bettis III, and G. R. Hallberg. 1992. Quaternary geology of Conklin Quarry. Guidebook Series no. 13. Iowa Department of Natural Resources. 41 p.

Klint, K. E. S. and P. Gravensen. 1999. Fractures and biopores in Weichselian clayey till Aquitards at Flakkebjerg, Denmark. Nordic Hydrology. v. 30, n. 4/5, pp. 267-284.

Kross, B. C., G. R. Hallberg, D. R. Bruner, R. D. Libra, K. D. Rex, L. M. B. Weih, M. E. Vermace, L. F. Burmeister, N. H. Hall, K. L. Cherryhomes, J. K. Johnson, M. I. Selim, B. K. Nations, L. S. Seigley, D. J. Quaide, A. G. Dudler, K. D. Sesker, M. A. Culp, C. F. Lynch, H. F. Nicholson, and J. Hughes. 1990. The Iowa State-Wide Rural Well-Water Survey, Water Quality Data: Initial Analysis. Iowa Department of Natural Resources Technical Information Series 19. 142 p.

Lee, S. H. 1991. Genesis and distribution of fractures in late-Wisconsinan till of the Des Moines Lobe in central Iowa.

McKay, L. D., J. A. Cherry, and R. W. Gillham. 1993b. Field experiments in a fractured clay till: 2. Solute and colloid transport. Water Resources Research. v. 29, pp. 3879-3890.

McKay, L. D. and J. Fredericia. 1995. Distribution, origin, and hydraulic influence of fractures in a clay-rich glacial deposit. Canadian Journal of Technology. v. 32, pp. 957-975.

Mickelson, D. M., and W. W. Simpkins. 1991. Observations on the origin of fractures in fine-grained lake sediment and till in the Midwestern and Eastern U.S. EOS. v. 72, n. 44, p. 166.

Ruland, W. W., J. A. Cherry, and Stan Feenstra. 1991. The depth of fractures and active ground-water flow in a clayey till plain in southwestern Ontario. Ground Water. V. 29, n. 3, pp. 405-417.

Seo, H. H. 1996. Hydraulic properties of Quaternary stratigraphic units in the Walnut Creek watershed. Master's Thesis. Iowa State University. 145 p.

Simpkins, W. W. and K. R. Bradbury. 1992. Groundwater flow, velocity, and age in a thick, fine-grained till unit in southeastern Wisconsin. Journal of Hydrology. v. 132, pp. 283-319.

U.S. Environmental Protection Agency. 1994. Progress at Region 7 National Priorities List (NPL) Superfund Sites, Iowa. Report published by EPA Region 7, 73 p.

ACKNOWLEDGEMENTS

I would like to thank my committee members for all of their help along the way. Dr. William Simpkins, my advisor, for providing guidance, allowing freedom, having endless patience, and offering encouragement and critical review of this project. Dr. Robert Horton, my former co-major professor, for his guidance and mentorship in the field of soil physics. Dr. Michael Burkart, my co-major professor, for his contributions in the areas of agricultural water quality and hydrology. Dr. Carl Jacobson, for his guidance in the field of structural geology and fracture genesis. Dr. Thomas Moorman, who contributed his knowledge and expertise in the area of agricultural chemical fate and transport. And Dr. Lee Burras for his encouragement and his contributions in the area of geomorphology and soil science. In addition, I wish to thank Beth Douglass and Alissara Reungsang at the National Soil Tilth Laboratory, who analyzed the atrazine samples for this research.

I would like to thank the many students at Iowa State University who provided immeasurable assistance in the field and laboratory for this project, most notably Mark Mathison, Rob Andress, Trenton Twedt, Beth Spear, and Sarah Vlachos.

This research was funded by grants from the American Geophysical Union, the Association of Ground Water Scientists and Engineers, the U.S. EPA through an Interagency Agreement DW12036252 to the Agricultural Research Service, the Geological Society of America, and Sigma Xi. I wish to thank Golder Associates and the University of Waterloo for providing the FracMan/MAFIC and FRACTRAN software packages, respectively.

Most of all, I'd like to thank my wife, Victoria, and my family for their relentless encouragement, patience, and support of this project.